The geochemical formation and evolution of a beryllium-rich, beryl-hosting pegmatite system from Mount Antero, Colorado, USA

by

Logan John Erichsen

B.S., Fort Hays State University, 2024

A THESIS

submitted in partial fulfillment of the requirements for the degree

MASTER OF SCIENCE

Department of Geology
College of Arts and Sciences

KANSAS STATE UNIVERSITY
Manhattan, Kansas

2026

Approved by:

Major Professor
Dr. Matthew E. Brueseke

Abstract

Mount Antero, Colorado (USA) is a known locality for gem-quality beryl (var. aquamarine and goshenite), quartz (var. smoky), fluorite, phenakite, and bertrandite. These minerals primarily occur in and adjacent to pegmatites, hydrothermal veins, and related features within ~30 Ma A-type granites. The pegmatites investigated in this study come from one location on Mt. Antero and occur as spheroids which range from 5 to 75 cm. Two pegmatite compositions exist: beryl-rich and beryl-poor. The beryl-rich pegmatites may contain beryl, bertrandite, quartz, muscovite, biotite, alkali feldspar, and plagioclase feldspar. The beryl-poor pegmatites contain quartz, muscovite, biotite, alkali feldspar, and plagioclase feldspar. Based on this mineralogy, Mt. Antero pegmatites are classified as Residual Melts of Granite Magmatism Group 2 (RMG-2). LA-ICP-MS trace element analyses were performed on beryl and quartz from both pegmatite types. Lithium and Zn are enriched in the cores of euhedral beryls when compared to the rims, while Mg, Sc, V, Mn, Fe, Ga, Rb, and Cs are enriched in the rims when compared to the cores. Anhedral beryl in the pegmatites have a more similar chemical composition to the euhedral beryl rims than the euhedral beryl cores. When examining the Na/Li versus ppm Cs, euhedral beryl cores appear less fractionated than the euhedral rims and anhedral beryl. Thus, we argue that euhedral beryl cores formed first, followed by euhedral beryl rims and anhedral beryl, while crystallizing from a singular evolving melt. LA-ICP-MS quartz data shows that Mt. Antero RMG-2 pegmatites are chemically distinct from other worldwide pegmatite types on bivariate plots of Al versus Li, Be, B, Ti, Ge, Ga, and Rb. The most notable differences between Mt. Antero RMG-2 pegmatites and DPA-1, DPA-2, and RMG-1 pegmatites occur when plotting Al vs Be, B, Ga, and Rb. These plots show that Be, B, Al, Ga, and Rb all have elevated concentrations when compared to other pegmatites. Overall, these results indicate that the

pegmatites on Mt. Antero are classified as RMG-2, crystallized from one evolving melt, and Mt. Antero RMG-2 pegmatites plot distinct from other documented pegmatite types based on quartz trace element geochemistry.

Table of Contents

List of Figures v
List of Appendix Figures xi
List of Tables xxvii
Acknowledgements xxviii
Dedication xxx
Chapter 1 - Introduction 1
Chapter 2 - Background 5
Geologic History 5
Granite Type 9
Recognized Mineralization on Mount Antero 12
Pegmatite Naming Scheme 17
Chapter 3 - Methods 21
Chapter 4 - Results 25
Pegmatite Mineralization on the *Thank You Lord* claim 27
Sample Descriptions 31
Beryl Chemistry 40
Quartz Data 53
Quartz Trace Element Concentrations Through USTs 57
Chapter 5 - Discussion 65
Pegmatite Classification for Mt. Antero 65
Beryl 66
Quartz 68
Chapter 6 - Conclusions 82
Future Work 82
References 84
Appendix A - Thick Sections and Concentration (ppm) Versus Transect Length LA-ICP-MS Graphs 88
Appendix B - Pegmatite Beryl Comparison Graphs 272
Appendix C - Quartz Bivariate Graphs 284

List of Figures

Figure 1: Location of the study area (B. Busse's Claim) on Mount Antero and near Mount White in South Central, Colorado (USA), along with the location of the Mount Princeton Batholith. 6

Figure 2: General geology of the study area along with B. Busse's *Thank You Lord* mining claim and the historic area of the California Mine. Rock formations not necessary for the study were omitted from the key as all formations that begin with Q are quaternary in age. Geologic Map adapted from Kellogg et al. (2017). 8

Figure 3: Discrimination diagram of Whalen et al. (1987) that represents California and Antero granite bulk rock geochemistry data from Shannon (1988) and other references therein. ... 10

Figure 4: Discrimination diagrams of Pearce et al. (1984) represent California and Antero granite bulk rock geochemistry data from Shannon (1988) and other references therein. A) Y versus Nb. B) Y+Nb versus Rb. 11

Figure 5: Drawing of a regular miarolitic cavity which is currently found on Mount Antero within the pegmatites. Common minerals are beryl (var. aquamarine), smoky quartz, quartz, muscovite (musc.), fluorite, and cleavelandite. Sketch after Jacobson (1993). 15

Figure 6: A drawing of a solid pegmatite spheroid ~75 cm across at the *Thank You Lord* claim on Mount Antero, Colorado. Major minerals found in this pegmatite spheroid are beryl, quartz, biotite, muscovite, alkali feldspar, and albite. The pegmatite is surrounded by beryl-bearing California Granite. 16

Figure 7: Images of the California Granite cliffs on the southwest ridge of Mount Antero. A) Southward view of the cliffs jutting out of talus. B) A view looking up at the California Granite cliffs from the base of the talus slope with a vertical relief of ~250 m. 26

Figure 8: Pegmatite spheroids on Mount Antero vary in size but share similar mineralogy. A) A spheroid pegmatite spheroid that is approximately 75 cm in diameter outlined in yellow. B) A spheroid pegmatite spheroid that is approximately 5 cm in diameter outlined in yellow. 28

Figure 9: Common pegmatite unidirectional solidification textures (USTs) from Mount Antero. A) Sample LE25-1: A beryl, quartz, alkali feldspar, and plagioclase feldspar pegmatite UST that contains five zones. B) A quartz, alkali feldspar, and plagioclase feldspar pegmatite UST that contains five zones. 29

Figure 10: Sample LE25-1 is beryl-bearing UST from Mount Antero divided into five zones. Zone 1 granite to aplite transition, with abundant plagioclase feldspar, alkali feldspar, and quartz all ~1-2 mm. Zone 2 aplite zone with finer quartz ~1 mm and plagioclase and alkali feldspar ~100-150 μm. Zone 3 intermediate section made of 5-10 mm quartz grains and interstitial plagioclase and alkali feldspar, quartz, and beryl all ~100-150 μm. Zone 4 aplite with quartz, beryl, and plagioclase and alkali feldspar ~100-150 μm. Zone 5 core zone with 5-10 mm grains of quartz and beryl. 29
Figure 11: A quartz, plagioclase feldspar, and alkali feldspar UST from Mount Antero divided into four zones. Zone 1 granite to aplite transition with abundant plagioclase, alkali feldspar, and quartz with grains ~1-2 mm. Zone 2 aplite with finer quartz, alkali feldspar, and plagioclase feldspar~0.25-0.5 mm. Zone 3 intermediate zone with 1mm grains of alkali feldspar, plagioclase feldspar and quartz. Zone 4 core zone with 5-10 mm grains of quartz, alkali feldspar, and plagioclase feldspar. 30
Figure 12: Sample LE25-1 which is a beryl UST consisting of beryl (Brl), quartz (Qtz), alkali feldspar (Afs), and plagioclase feldspar (Pl) with five distinct zones. A) LE25-1 divided into five zones. Panels B – F are photomicrographs of the various zones in crossed polarized light (XPL). B) Zone 1: Plagioclase feldspar and quartz with grain sizes ~100 μm. C) Zone 2: Quartz grains ~600 μm with interstitial plagioclase ~50 μm. D) Zone 3: Grains of quartz, plagioclase, and beryl ~100-150 μm. E) Zone 4: Grains of quartz, plagioclase, and beryl ~50-100 μm. F) Zone 5: Grains of quartz and beryl (not shown) ~5 mm. 33
Figure 13: Sample LE25-2 is a mass of gem-quality blue beryl (Brl) which is fractured and partially replaced by bertrandite (Btd). A) Sample LE25-2. B) Photomicrograph of sample LE25-2 in XPL showing fractured beryl and elongated laths of bertrandite. 34
Figure 14: Sample LE25-3 California Granite and pegmatite. A) The California Granite is 44% quartz, 44% plagioclase feldspar, 5% beryl, 5% biotite, 1% clay minerals, and 1% bertrandite. Most beryl crystals are partially replaced by bertrandite. The clay minerals are found near the beryl and bertrandite zones. The blue crystals are blue beryl (e.g., “blue granite”. B) Pegmatite core zone with euhedral blue beryl crystal ~1.5 cm across. 34
Figure 15: LE25-2 are 3-cm-wide quartz crystals capped by ~1 mm crystals of bertrandite and beryl. 35

Figure 16: Sample LE25-5L green beryl pegmatite. A) Pegmatite spheroid in situ with the pegmatite outlined in yellow, within California Granite host. B) Sample taken from the field before being sliced by a rock saw. 35
Figure 17: Sample LE25-5C which is a blue beryl pegmatite. A) Pegmatite spheroid in situ with California Granite host rock, where the spheroid is ~5-cm-wide. B) Sample taken from the field before being cut by a rock saw. 36
Figure 18: Sample LE25-5R which is a green and blue pegmatite spheroid. A) Pegmatite spheorid in situ with California Granite host rock. B) Sample taken from the field before being cut by a rock saw. 37
Figure 19: Cluster of single continuous pegmatite that consists of LE25-5L, 5C, and 5R. A) Pegmatite sample LE25-5L outlined in yellow, LE25-5C outlined in green, and LE25-5R outlined in purple. B) A closer picture of pegmatite LE25-5L in yellow and LE25-5C in green. 38
Figure 20: Sample LE25-6 is a pegmatite core zone. This sample consists of 54% quartz, 35% blue beryl, 9% feldspar, 1% muscovite and 1% bertrandite. 38
Figure 21: Sample LE25-8 is a pegmatite core zone which has a vuggy texture. Beryl (~50%) is mostly blue and all of it is anhedral. Also present is quartz (~40%), plagioclase feldspar (~5%), clays (~2%), bertrandite (~2%), and muscovite (~1%). 39
Figure 22: Sample LE25-9 is pegmatite core zone which exhibits a vuggy texture. The beryl (~55%) is anhedral, blue, and green. Also found in the sample is: quartz ~30%, muscovite ~5%, plagioclase feldspar ~5%, clays ~3%, and bertrandite ~2%. 39
Figure 23: Sample LE25-10 is a euhedral gem-quality blue beryl (aquamarine). 40
Figure 24: Sample LE25-3A3, 100 μm double polished thick section of a pegmatite core zone. Blue (beryl transect) lines and numbers correspond to LA-ICP-MS transect lines (e.g., LE25-3A3.6 is the blue line labeled 6). Analyzed beryls are shown outlined in yellow..... 41
Figure 25: Sample LE25-3A3.2 is a euhedral beryl transect from the core zone of pegmatite 3A3 (Fig. 24). Spikes (e.g., abruptly elevated concentrations of Na, K, Mg, Ti) reflect the laser encountering inclusions of other minerals in the host beryl. 42
Figure 26: Sample LE25-3A3.6 in XPL (A) and PPL (B) which shows the LA-ICP-MS transect line..... 43

Figure 27: SEM image of LE25-3A3.6. Upper image is a back-scattered electron (BSE) image, while the Na, Al, Si, K, Fe images are elemental maps obtained via energy dispersive spectrometer. 44
Figure 28: Sample LE25-3A3.4 is a euhedral beryl transect from the core zone of pegmatite 3A3 (Fig. 24). 45
Figure 29: Sample LE25-3A3.7 is an anhedral beryl transect from the core zone of pegmatite 3A3 (Fig. 24). 46
Figure 30: Sample LE25-10, 100 µm double polished thick section of a euhedral beryl. The blue (beryl transect) line labelled 1 corresponds to LA-ICP-MS transect line LE25-10.1. 47
Figure 31: Sample LE25-10.1 is a transect from a euhedral gem-quality beryl crystal. 48
Figure 32: Bivariate graph with beryl averages of Na/Li versus Cs (ppm) representing euhedral beryl rims, euhedral beryl cores, and anhedral beryls. Na/Li calculated from ppm values. . 49
Figure 33: Beryl values of Na/Li versus Cs (Wt %) plotted on fields after Černý (2002). Letter fields refer to: A) Sterile pegmatites and geochemically primitive beryl-type pegmatites; B) Beryl-columbite-type pegmatites and geochemically evolved beryl-columbitephosphate pegmatites, C) Albite-spodumene and complex pegmatites; D) Highly fractionated Li, Cs, Ta-rich complex pegmatites. Na/Li calculated from ppm values. 50
Figure 34: Box and whisker plots representing the concentration changes of Li, Mg, Sc, V, Mn, Fe, Zn, Ga, Rb, and Cs in LE25-3A3.2. 51
Figure 35: Elemental concentrations in beryl from LE25-5L-1A normalized to the Rim (A) and Core (B) of euhedral beryl LE25-3A3.2. 52
Figure 36: Sample LE25-3A1, 100 micron-thick double polished standard size section of California Granite. The yellow (quartz transect) line labelled 6 corresponds to LA-ICP-MS transect line LE25-3A1.6. 54
Figure 37: Sample LE25-3A1.6 is a transect from a quartz crystal within the California Granite proximal to pegmatite 3A5. Uncertainties for the selected transect element concentrations are displayed below. 55
Figure 38: Bivariate plots for trace element concentrations from select Mt. Antero quartz crystals (n=7,139). A) Ti versus Al; B) Li versus Al; C) Ge versus Al; D) B versus Al; E) Ga versus Al; F) Rb versus Al. 56

Figure 39: Bivariate plot of Be versus Al for trace element concentrations from select Mt. Antero quartz crystals (n=7,139). 57
Figure 40: Box plots of Be, B, and Cs concentrations through the wall rock, aplite, intermediate, and core zone of pegmatite UST LE25-7. 58
Figure 41: Box plots of Li, Cr, and Fe concentrations through the wall rock, aplite, intermediate, and core zone of pegmatite UST LE25-7. 59
Figure 42: Box plots of Ge and Ga concentrations through the wall rock, aplite, intermediate, and core zone of pegmatite UST LE25-7. 60
Figure 43: Box plots of Be, B, and Cs concentration through the wall rock, aplite, and core zone of pegmatite LE25-5R. 62
Figure 44: Box plots of Li, Cr, and Fe concentration through the wall rock, aplite, and core zone of pegmatite LE25-5R. 63
Figure 45 Box plots of Ge and Ga concentration through the wall rock, aplite, and core zone of pegmatite LE25-5R. 64
Figure 45: Anhedral beryl from all beryl-rich pegmatites normalized to euhedral beryl core LE25-3A3.2. 68
Figure 46: Bivariate plots for trace element concentrations of quartz from DPA-1, DPA-2, RMG-1, and Mount Antero (RMG-2) pegmatites. A) Ti versus Al; B) Li versus Al; C) Ge versus Al; D) B versus Al; E) Rb versus Al; F) Ga versus Al. 71
Figure 47: Mt. Antero quartz data depicted in Figure 46 with added density contours. Contours represent kernel density estimates (KDE) of the bivariate distribution of Al and Li, calculated in R using a Gaussian smoothing function. Lines show regions of equal point density, highlighting areas of higher sample concentration. Also shown are other pegmatite types for comparison. 72
Figure 48: Selected Mt. Antero quartz data depicted in Figure 46 with added density contours. Contours represent kernel density estimates (KDE) of the bivariate distribution of Al and Be, calculated in R using a Gaussian smoothing function. Lines show regions of equal point density, highlighting areas of higher sample concentration. Also shown are other pegmatite types for comparison. 73
Figure 49: Selected Mt. Antero quartz data depicted in Figure 46 with added density contours. Contours represent kernel density estimates (KDE) of the bivariate distribution of Al and B,

calculated in R using a Gaussian smoothing function. Lines show regions of equal point density, highlighting areas of higher sample concentration. Also shown are other pegmatite types for comparison. 74
Figure 50: Selected Mt. Antero quartz data depicted in Figure 46 with added density contours. Contours represent kernel density estimates (KDE) of the bivariate distribution of Al and Ti, calculated in R using a Gaussian smoothing function. Lines show regions of equal point density, highlighting areas of higher sample concentration. Also shown are other pegmatite types for comparison. 75
Figure 51: Selected Mt. Antero quartz data depicted in Figure 46 with added density contours. Contours represent kernel density estimates (KDE) of the bivariate distribution of Al and Ga, calculated in R using a Gaussian smoothing function. Lines show regions of equal point density, highlighting areas of higher sample concentration. Also shown are other pegmatite types for comparison. 76
Figure 52: Selected Mt. Antero quartz data depicted in Figure 46 with added density contours. Contours represent kernel density estimates (KDE) of the bivariate distribution of Al and Ge, calculated in R using a Gaussian smoothing function. Lines show regions of equal point density, highlighting areas of higher sample concentration. Also shown are other pegmatite types for comparison. 77
Figure 53: Selected Mt. Antero quartz data depicted in Figure 46 with added density contours. Contours represent kernel density estimates (KDE) of the bivariate distribution of Al and Rb, calculated in R using a Gaussian smoothing function. Lines show regions of equal point density, highlighting areas of higher sample concentration. Also shown are other pegmatite types for comparison. 78
Figure 54: Bivariate plots for trace element concentrations of quartz from DPA-1, DPA-2, RMG-1, and Mount Antero (RMG-2) pegmatites with added density contours. Contours represent kernel density estimates (KDE) of the bivariate distribution of Al and Ti, Li, Ge, B, Rb and Ga, calculated in R using a Gaussian smoothing function. Lines show regions of equal point density, highlighting areas of higher sample concentration. A) Ti versus Al; B) Li versus Al; C) Ge versus Al; D) B versus Al; E) Rb versus Al; F) Ga versus Al. 79
Figure 55: RMG-2 Ge versus Al trace element quartz data from Pikes Peak, Colorado and Mt. Antero, Colorado. 81

List of Appendix Figures

Appendix Figure 1: Sample LE25-3A1, 100 micron double polished thick section of California Granite transition zone proximal to pegmatite LE25-3A3. The yellow (quartz transect) line labelled 6 corresponds to LA-ICP-MS transect line LE25-3A1.6. 88
Appendix Figure 2: Concentrations (ppm) versus transect length. Sample LE25-3A1.6 is a quartz transect from the California Granite transition zone proximal to pegmatite LE25-3A3. 89
Appendix Figure 3: Concentrations (ppm) versus transect length. Sample LE25-3A1.7 is a quartz transect from the California Granite transition zone proximal to pegmatite LE25-3A3. 90
Appendix Figure 4: Concentrations (ppm) versus transect length. Sample LE25-3A1.8 is a quartz transect from the California Granite transition zone proximal to pegmatite LE25-3A3. 91
Appendix Figure 5: Concentrations (ppm) versus transect length. Sample LE25-3A1.9 is a quartz transect from the California Granite transition zone proximal to pegmatite LE25-3A3. 92
Appendix Figure 6: Concentrations (ppm) versus transect length. Sample LE25-3A1.10 is a quartz transect from the California Granite transition zone proximal to pegmatite LE25-3A3. 93
Appendix Figure 7: Concentrations (ppm) versus transect length. Sample LE25-3A1.11 is a quartz transect from the California Granite transition zone proximal to pegmatite LE25-3A3. 94
Appendix Figure 8: Concentrations (ppm) versus transect length. Sample LE25-3A1.13 is a quartz transect from the California Granite transition zone proximal to pegmatite LE25-3A3. 95
Appendix Figure 9: Concentrations (ppm) versus transect length. Sample LE25-3A1.14 is a quartz transect from the California Granite transition zone proximal to pegmatite LE25-3A3. 96
Appendix Figure 10: Concentrations (ppm) versus transect length. Sample LE25-3A1.16 is a quartz transect from the California Granite transition zone proximal to pegmatite LE25-3A3. 97
Appendix Figure 11: Concentrations (ppm) versus transect length. Sample LE25-3A1.17 is a quartz transect from the California Granite transition zone proximal to pegmatite LE25-3A3. 98

Appendix Figure 12: Concentrations (ppm) versus transect length. Sample LE25-3A1.19 is a quartz transect from the California Granite transition zone proximal to pegmatite LE25-3A3. 99
Appendix Figure 13: Concentrations (ppm) versus transect length. Sample LE25-3A1.20 is a quartz transect from the California Granite transition zone proximal to pegmatite LE25-3A3. 100
Appendix Figure 14: Sample LE25-3A5, 100 micron double polished thick section of a pegmatite core zone. Blue (beryl transect) and yellow (quartz transect) lines and numbers correspond to LA-ICP-MS transect lines (e.g., LE25-3A5.1 is the blue line labelled 1). .. 101
Appendix Figure 15: Concentrations (ppm) versus transect length. Sample LE25-3A5.1 is a beryl transect from pegmatite LE25-3A5. 102
Appendix Figure 16: Concentrations (ppm) versus transect length. Sample LE25-3A5.2 is a beryl transect from pegmatite LE25-3A5. 103
Appendix Figure 17: Concentrations (ppm) versus transect length. Sample LE25-3A5.7 is a beryl transect from pegmatite LE25-3A5. 104
Appendix Figure 18: Concentrations (ppm) versus transect length. Sample LE25-3A5.10 is a quartz transect from pegmatite LE25-3A5. 105
Appendix Figure 19: Sample LE25-5L-1A, 100 micron double polished thick section of a pegmatite core zone. Blue (beryl transect) lines and numbers correspond to LA-ICP-MS transect lines (e.g., LE25-5L-1A.1 is the blue line labelled 1). 106
Appendix Figure 20: Concentrations (ppm) versus transect length. Sample LE25-5L-1A.1 is a beryl transect from pegmatite LE25-5L. 107
Appendix Figure 21: Concentrations (ppm) versus transect length. Sample LE25-5L-1A.2 is a beryl transect from pegmatite LE25-5L. 108
Appendix Figure 22: Concentrations (ppm) versus transect length. Sample LE25-5L-1A.3 is a beryl transect from pegmatite LE25-5L. 109
Appendix Figure 23: Concentrations (ppm) versus transect length. Sample LE25-5L-1A.4 is a beryl transect from pegmatite LE25-5L. 110
Appendix Figure 24: Concentrations (ppm) versus transect length. Sample LE25-5L-1A.7 is a beryl transect from pegmatite LE25-5L. 111

Appendix Figure 25: Concentrations (ppm) versus transect length. Sample LE25-5L-1A.8 is a beryl transect from pegmatite LE25-5L. 112
Appendix Figure 26: Concentrations (ppm) versus transect length. Sample LE25-5L-1A.9 is a beryl transect from pegmatite LE25-5L. 113
Appendix Figure 27: Concentrations (ppm) versus transect length. Sample LE25-5L-1A.10 is a beryl transect from pegmatite LE25-5L. 114
Appendix Figure 28: Concentrations (ppm) versus transect length. Sample LE25-5L-1A.11 is a beryl transect from pegmatite LE25-5L. 115
Appendix Figure 29: Concentrations (ppm) versus transect length. Sample LE25-5L-1A.12 is a beryl transect from pegmatite LE25-5L. 116
Appendix Figure 30: Concentrations (ppm) versus transect length. Sample LE25-5L-1A.13 is a beryl transect from pegmatite LE25-5L. 117
Appendix Figure 31: Concentrations (ppm) versus transect length. Sample LE25-5L-1A.14 is a beryl transect from pegmatite LE25-5L. 118
Appendix Figure 32: Concentrations (ppm) versus transect length. Sample LE25-5L-1A.15 is a beryl transect from pegmatite LE25-5L. 119
Appendix Figure 33: Concentrations (ppm) versus transect length. Sample LE25-5L-1A.17 is a beryl transect from pegmatite LE25-5L. 120
Appendix Figure 34: Concentrations (ppm) versus transect length. Sample LE25-5L-1A.18 is a beryl transect from pegmatite LE25-5L. 121
Appendix Figure 35: Concentrations (ppm) versus transect length. Sample LE25-5L-1A.19 is a beryl transect from pegmatite LE25-5L. 122
Appendix Figure 36: Concentrations (ppm) versus transect length. Sample LE25-5L-1A.20 is a beryl transect from pegmatite LE25-5L. 123
Appendix Figure 37: Sample LE25-5L-1B, 100 micron double polished thick section of pegmatite transition zone proximal to pegmatite LE25-5L. The yellow (quartz transect) line labelled 6 corresponds to LA-ICP-MS transect line LE25-5L-1B.6. 124
Appendix Figure 38: Concentrations (ppm) versus transect length. Sample LE25-5L-1B.4 is a quartz transect from pegmatite LE25-5L. 125
Appendix Figure 39: Concentrations (ppm) versus transect length. Sample LE25-5L-1B.6 is a quartz transect from pegmatite LE25-5L. 126

Appendix Figure 40: Concentrations (ppm) versus transect length. Sample LE25-5L-1B.8 is a quartz transect from pegmatite LE25-5L. 127
Appendix Figure 41: Sample LE25-5L-1B, 100 micron double polished thick section of pegmatite core zone LE25-5L. The blue (beryl transect) line labelled 1 corresponds to LA-ICP-MS transect line LE25-5L-2A.1. 128
Appendix Figure 42: Concentrations (ppm) versus transect length. Sample LE25-5L-2A.1 is a beryl transect from pegmatite LE25-5L. 129
Appendix Figure 43: Concentrations (ppm) versus transect length. Sample LE25-5L-2A.2 is a beryl transect from pegmatite LE25-5L. 130
Appendix Figure 44: Concentrations (ppm) versus transect length. Sample LE25-5L-2A.3 is a beryl transect from pegmatite LE25-5L. 131
Appendix Figure 45: Concentrations (ppm) versus transect length. Sample LE25-5L-2A.4 is a beryl transect from pegmatite LE25-5L. 132
Appendix Figure 46: Concentrations (ppm) versus transect length. Sample LE25-5L-2A.5 is a beryl transect from pegmatite LE25-5L. 133
Appendix Figure 47: Concentrations (ppm) versus transect length. Sample LE25-5L-2A.6 is a beryl transect from pegmatite LE25-5L. 134
Appendix Figure 48: Concentrations (ppm) versus transect length. Sample LE25-5L-2A.7 is a beryl transect from pegmatite LE25-5L. 135
Appendix Figure 49: Concentrations (ppm) versus transect length. Sample LE25-5L-2A.8 is a beryl transect from pegmatite LE25-5L. 136
Appendix Figure 50: Concentrations (ppm) versus transect length. Sample LE25-5L-2A.9 is a beryl transect from pegmatite LE25-5L. 137
Appendix Figure 51: Concentrations (ppm) versus transect length. Sample LE25-5L-2A.10 is a beryl transect from pegmatite LE25-5L. 138
Appendix Figure 52: Concentrations (ppm) versus transect length. Sample LE25-5L-2A.12 is a beryl transect from pegmatite LE25-5L. 139
Appendix Figure 53: Concentrations (ppm) versus transect length. Sample LE25-5L-2A.13 is a beryl transect from pegmatite LE25-5L. 140
Appendix Figure 54: Concentrations (ppm) versus transect length. Sample LE25-5L-2A.14 is a beryl transect from pegmatite LE25-5L. 141

Appendix Figure 55: Sample LE25-5C-1A, 100 micron double polished thick section of a pegmatite core zone. Blue (beryl transect) and yellow (quartz transect) lines and numbers correspond to LA-ICP-MS transect lines (e.g., LE25-5C-1A.5 is the blue line labelled 5). 142
Appendix Figure 56: Concentrations (ppm) versus transect length. Sample LE25-5C-1A.1 is a beryl transect from pegmatite LE25-5C..... 143
Appendix Figure 57: Concentrations (ppm) versus transect length. Sample LE25-5C-1A.2 is a beryl transect from pegmatite LE25-5C..... 144
Appendix Figure 58: Concentrations (ppm) versus transect length. Sample LE25-5C-1A.3 is a beryl transect from pegmatite LE25-5C..... 145
Appendix Figure 59: Concentrations (ppm) versus transect length. Sample LE25-5C-1A.4 is a beryl transect from pegmatite LE25-5C..... 146
Appendix Figure 60: Concentrations (ppm) versus transect length. Sample LE25-5C-1A.5 is a beryl transect from pegmatite LE25-5C..... 147
Appendix Figure 61: Concentrations (ppm) versus transect length. Sample LE25-5C-1A.6 is a beryl transect from pegmatite LE25-5C..... 148
Appendix Figure 62: Concentrations (ppm) versus transect length. Sample LE25-5C-1A.7 is a beryl transect from pegmatite LE25-5C..... 149
Appendix Figure 63: Concentrations (ppm) versus transect length. Sample LE25-5C-1A.8 is a beryl transect from pegmatite LE25-5C..... 150
Appendix Figure 64: Concentrations (ppm) versus transect length. Sample LE25-5C-1A.9 is a beryl transect from pegmatite LE25-5C..... 151
Appendix Figure 65: Concentrations (ppm) versus transect length. Sample LE25-5C-1A.10 is a beryl transect from pegmatite LE25-5C..... 152
Appendix Figure 66: Concentrations (ppm) versus transect length. Sample LE25-5C-1A.12 is a beryl transect from pegmatite LE25-5C..... 153
Appendix Figure 67: Concentrations (ppm) versus transect length. Sample LE25-5C-1A.13 is a beryl transect from pegmatite LE25-5C..... 154
Appendix Figure 68: Concentrations (ppm) versus transect length. Sample LE25-5C-1A.15 is a beryl transect from pegmatite LE25-5C..... 155

Appendix Figure 69: Concentrations (ppm) versus transect length. Sample LE25-5C-1A.17 is a quartz transect from pegmatite LE25-5C. 156
Appendix Figure 70: Sample LE25-5C-1B, 100 micron double polished thick section of pegmatite transition zone proximal to pegmatite LE25-5L. The yellow (quartz transect) line labelled 2 corresponds to LA-ICP-MS transect line LE25-5C-1B.2. 157
Appendix Figure 71: Concentrations (ppm) versus transect length. Sample LE25-5C-1B.2 is a quartz transect from pegmatite LE25-5C. 158
Appendix Figure 72: Concentrations (ppm) versus transect length. Sample LE25-5C-1B.6 is a quartz transect from pegmatite LE25-5C. 159
Appendix Figure 73: Concentrations (ppm) versus transect length. Sample LE25-5C-1B.7 is a quartz transect from pegmatite LE25-5C. 160
Appendix Figure 74: Concentrations (ppm) versus transect length. Sample LE25-5C-1B.8 is a quartz transect from pegmatite LE25-5C. 161
Appendix Figure 75: Concentrations (ppm) versus transect length. Sample LE25-5C-1B.12 is a quartz transect from pegmatite LE25-5C. 162
Appendix Figure 76: Concentrations (ppm) versus transect length. Sample LE25-5C-1B.14 is a quartz transect from pegmatite LE25-5C. 163
Appendix Figure 77: Concentrations (ppm) versus transect length. Sample LE25-5C-1B.17 is a quartz transect from pegmatite LE25-5C. 164
Appendix Figure 78: Concentrations (ppm) versus transect length. Sample LE25-5C-1B.18 is a quartz transect from pegmatite LE25-5C. 165
Appendix Figure 79: Concentrations (ppm) versus transect length. Sample LE25-5C-1B.19 is a quartz transect from pegmatite LE25-5C. 166
Appendix Figure 80: Concentrations (ppm) versus transect length. Sample LE25-5C-1B.20 is a quartz transect from pegmatite LE25-5C. 167
Appendix Figure 81: Sample LE25-5R-1A, 100 micron double polished thick section of a pegmatite core zone. Blue (beryl transect) and yellow (quartz transect) lines and numbers correspond to LA-ICP-MS transect lines (e.g., LE25-5R-1A.1 is the blue line labelled 1). 168
Appendix Figure 82: Concentrations (ppm) versus transect length. Sample LE25-5R-1A.1 is a beryl transect from pegmatite LE25-5R. 169

Appendix Figure 83: Concentrations (ppm) versus transect length. Sample LE25-5R-1A.2 is a beryl transect from pegmatite LE25-5R. 170
Appendix Figure 84: Concentrations (ppm) versus transect length. Sample LE25-5R-1A.7 is a quartz transect from pegmatite LE25-5R. 171
Appendix Figure 85: Concentrations (ppm) versus transect length. Sample LE25-5R-1A.9 is a quartz transect from pegmatite LE25-5R. 172
Appendix Figure 86: Concentrations (ppm) versus transect length. Sample LE25-5R-1A.10 is a quartz transect from pegmatite LE25-5R. 173
Appendix Figure 87: Concentrations (ppm) versus transect length. Sample LE25-5R-1A.11 is a quartz transect from pegmatite LE25-5R. 174
Appendix Figure 88: Sample LE25-5R-1B, 100 micron double polished thick section of pegmatite transition zone proximal to pegmatite LE25-5L. The yellow (quartz transect) line labelled 2 corresponds to LA-ICP-MS transect line LE25-5R-1B.2. 175
Appendix Figure 89: Concentrations (ppm) versus transect length. Sample LE25-5R-1B.1 is a quartz transect from pegmatite LE25-5R. 176
Appendix Figure 90: Concentrations (ppm) versus transect length. Sample LE25-5R-1B.2 is a quartz transect from pegmatite LE25-5R. 177
Appendix Figure 91: Concentrations (ppm) versus transect length. Sample LE25-5R-1B.4 is a quartz transect from pegmatite LE25-5R. 178
Appendix Figure 92: Concentrations (ppm) versus transect length. Sample LE25-5R-1B.4 is a quartz transect from pegmatite LE25-5R. 179
Appendix Figure 93: Concentrations (ppm) versus transect length. Sample LE25-5R-1B.8 is a quartz transect from pegmatite LE25-5R. 180
Appendix Figure 94: Concentrations (ppm) versus transect length. Sample LE25-5R-1B.11 is a quartz transect from pegmatite LE25-5R. 181
Appendix Figure 95: Concentrations (ppm) versus transect length. Sample LE25-5R-1B.12 is a quartz transect from pegmatite LE25-5R. 182
Appendix Figure 96: Concentrations (ppm) versus transect length. Sample LE25-5R-1B.14 is a quartz transect from pegmatite LE25-5R. 183
Appendix Figure 97: Concentrations (ppm) versus transect length. Sample LE25-5R-1B.17 is a quartz transect from pegmatite LE25-5R. 184

Appendix Figure 98: Concentrations (ppm) versus transect length. Sample LE25-5R-1B.20 is a quartz transect from pegmatite LE25-5R. 185
Appendix Figure 99: Sample LE25-6-1, 100 micron double polished thick section of a pegmatite core zone. Blue (beryl transect) and yellow (quartz transect) lines and numbers correspond to LA-ICP-MS transect lines (e.g., LE25-6-1.3 is the blue line labelled 3). 186
Appendix Figure 100: Concentrations (ppm) versus transect length. Sample LE25-6-1.3 is a beryl transect from pegmatite LE25-6. 187
Appendix Figure 101: Concentrations (ppm) versus transect length. Sample LE25-6-1.4 is a beryl transect from pegmatite LE25-6. 188
Appendix Figure 102: Concentrations (ppm) versus transect length. Sample LE25-6-1.5 is a quartz transect from pegmatite LE25-6. 189
Appendix Figure 103: Concentrations (ppm) versus transect length. Sample LE25-6-1.6 is a quartz transect from pegmatite LE25-6. 190
Appendix Figure 104: Concentrations (ppm) versus transect length. Sample LE25-6-1.7 is a beryl transect from pegmatite LE25-6. 191
Appendix Figure 105: Concentrations (ppm) versus transect length. Sample LE25-6-1.8 is a beryl transect from pegmatite LE25-6. 192
Appendix Figure 106: Concentrations (ppm) versus transect length. Sample LE25-6-1.12 is a beryl transect from pegmatite LE25-6. 193
Appendix Figure 107: Concentrations (ppm) versus transect length. Sample LE25-6-1.13 is a beryl transect from pegmatite LE25-6. 194
Appendix Figure 108: Concentrations (ppm) versus transect length. Sample LE25-6-1.14 is a beryl transect from pegmatite LE25-6. 195
Appendix Figure 109: Concentrations (ppm) versus transect length. Sample LE25-6-1.15 is a beryl transect from pegmatite LE25-6. 196
Appendix Figure 110: Concentrations (ppm) versus transect length. Sample LE25-6-1.16 is a quartz transect from pegmatite LE25-6. 197
Appendix Figure 111: Concentrations (ppm) versus transect length. Sample LE25-6-1.17 is a quartz transect from pegmatite LE25-6. 198
Appendix Figure 112: Concentrations (ppm) versus transect length. Sample LE25-6-1.18 is a quartz transect from pegmatite LE25-6. 199

Appendix Figure 113: Concentrations (ppm) versus transect length. Sample LE25-6-1.19 is a beryl transect from pegmatite LE25-6. 200
Appendix Figure 114: Concentrations (ppm) versus transect length. Sample LE25-6-1.19 is a quartz transect from pegmatite LE25-6. 201
Appendix Figure 115: Concentrations (ppm) versus transect length. Sample LE25-6-1.20 is a quartz transect from pegmatite LE25-6. 202
Appendix Figure 116: Sample LE25-6-2, 100 micron double polished thick section of a pegmatite core zone. Blue (beryl transect) and yellow (quartz transect) lines and numbers correspond to LA-ICP-MS transect lines (e.g., LE25-6-2.1 is the blue line labelled 1)..... 203
Appendix Figure 117: Concentrations (ppm) versus transect length. Sample LE25-6-2.0 is a beryl transect from pegmatite LE25-6. 204
Appendix Figure 118: Concentrations (ppm) versus transect length. Sample LE25-6-2.1 is a beryl transect from pegmatite LE25-6. 205
Appendix Figure 119: Concentrations (ppm) versus transect length. Sample LE25-6-2.3 is a quartz transect from pegmatite LE25-6. 206
Appendix Figure 120: Concentrations (ppm) versus transect length. Sample LE25-6-2.6 is a quartz transect from pegmatite LE25-6. 207
Appendix Figure 121: Concentrations (ppm) versus transect length. Sample LE25-6-2.8 is a quartz transect from pegmatite LE25-6. 208
Appendix Figure 122: Sample LE25-7-1A, 100 micron double polished thick section of pegmatite LE25-7 core zone. The yellow (quartz transect) line labelled 1 corresponds to LA-ICP-MS transect line LE25-7-1A.1. 209
Appendix Figure 123: Concentrations (ppm) versus transect length. Sample LE25-7-1A.1 is a quartz transect from pegmatite LE25-7. 210
Appendix Figure 124: Concentrations (ppm) versus transect length. Sample LE25-7-1A.3 is a quartz transect from pegmatite LE25-7. 211
Appendix Figure 125: Concentrations (ppm) versus transect length. Sample LE25-7-1A.7 is a quartz transect from pegmatite LE25-7. 212
Appendix Figure 126: Concentrations (ppm) versus transect length. Sample LE25-7-1A.10 is a quartz transect from pegmatite LE25-7. 213

Appendix Figure 127: Concentrations (ppm) versus transect length. Sample LE25-7-1A.11 is a quartz transect from pegmatite LE25-7. 214
Appendix Figure 128: Sample LE25-7-1B, 100 micron double polished thick section of pegmatite transition zone proximal to pegmatite LE25-7. The yellow (quartz transect) line labelled 2 corresponds to LA-ICP-MS transect line LE25-7-1B. 215
Appendix Figure 129: Concentrations (ppm) versus transect length. Sample LE25-7-1B.1 is a quartz transect from pegmatite LE25-7. 216
Appendix Figure 130: Concentrations (ppm) versus transect length. Sample LE25-7-1B.5 is a quartz transect from pegmatite LE25-7. 217
Appendix Figure 131: Concentrations (ppm) versus transect length. Sample LE25-7-1B.7 is a quartz transect from pegmatite LE25-7. 218
Appendix Figure 132: Concentrations (ppm) versus transect length. Sample LE25-7-1B.10 is a quartz transect from pegmatite LE25-7. 219
Appendix Figure 133: Sample LE25-7-2A, 100 micron double polished thick section of pegmatite LE25-7 core zone. The yellow (quartz transect) line labelled 1 corresponds to LA-ICP-MS transect line LE25-7-2A.1. 220
Appendix Figure 134: Concentrations (ppm) versus transect length. Sample LE25-7-2A.1 is a quartz transect from pegmatite LE25-7. 221
Appendix Figure 135: Concentrations (ppm) versus transect length. Sample LE25-7-2A.5 is a quartz transect from pegmatite LE25-7. 222
Appendix Figure 136: Concentrations (ppm) versus transect length. Sample LE25-7-2A.10 is a quartz transect from pegmatite LE25-7. 223
Appendix Figure 137: Concentrations (ppm) versus transect length. Sample LE25-7-2A.12 is a quartz transect from pegmatite LE25-7. 224
Appendix Figure 138: Concentrations (ppm) versus transect length. Sample LE25-7-2A.14 is a quartz transect from pegmatite LE25-7. 225
Appendix Figure 139: Concentrations (ppm) versus transect length. Sample LE25-7-2A.15 is a quartz transect from pegmatite LE25-7. 226
Appendix Figure 140: Sample LE25-7-2B, 100 micron double polished thick section of pegmatite transition zone proximal to pegmatite LE25-7. The yellow (quartz transect) line labelled 3 corresponds to LA-ICP-MS transect line LE25-7-2B.3. 227

Appendix Figure 141: Concentrations (ppm) versus transect length. Sample LE25-7-2B.1 is a quartz transect from pegmatite LE25-7. 228
Appendix Figure 142: Concentrations (ppm) versus transect length. Sample LE25-7-2B.3 is a quartz transect from pegmatite LE25-7. 229
Appendix Figure 143: Concentrations (ppm) versus transect length. Sample LE25-7-2B.6 is a quartz transect from pegmatite LE25-7. 230
Appendix Figure 144: Concentrations (ppm) versus transect length. Sample LE25-7-2B.8 is a quartz transect from pegmatite LE25-7. 231
Appendix Figure 145: Concentrations (ppm) versus transect length. Sample LE25-7-2B.10 is a quartz transect from pegmatite LE25-7. 232
Appendix Figure 146: Concentrations (ppm) versus transect length. Sample LE25-7-2B.13 is a quartz transect from pegmatite LE25-7. 233
Appendix Figure 147: Concentrations (ppm) versus transect length. Sample LE25-7-2B.14 is a quartz transect from pegmatite LE25-7. 234
Appendix Figure 148: Concentrations (ppm) versus transect length. Sample LE25-7-2B.16 is a quartz transect from pegmatite LE25-7. 235
Appendix Figure 149: Concentrations (ppm) versus transect length. Sample LE25-7-2B.17 is a quartz transect from pegmatite LE25-7. 236
Appendix Figure 150: Concentrations (ppm) versus transect length. Sample LE25-7-2B.18 is a quartz transect from pegmatite LE25-7. 237
Appendix Figure 151: Concentrations (ppm) versus transect length. Sample LE25-7-2B.20 is a quartz transect from pegmatite LE25-7. 238
Appendix Figure 152: Concentrations (ppm) versus transect length. Sample LE25-7-2B.21 is a quartz transect from pegmatite LE25-7. 239
Appendix Figure 153: Sample LE25-8-1, 100 micron double polished thick section of a pegmatite core zone LE25-8. Blue (beryl transect) and yellow (quartz transect) lines and numbers correspond to LA-ICP-MS transect lines (e.g., LE25-8-1.1 is the blue line labelled 1). 240
Appendix Figure 154: Concentrations (ppm) versus transect length. Sample LE25-8-1.1 is a beryl transect from pegmatite LE25-8. 241

Appendix Figure 155: Concentrations (ppm) versus transect length. Sample LE25-8-1.2 is a beryl transect from pegmatite LE25-8. 242
Appendix Figure 156: Concentrations (ppm) versus transect length. Sample LE25-8-1.4 is a beryl transect from pegmatite LE25-8. 243
Appendix Figure 157: Concentrations (ppm) versus transect length. Sample LE25-8-1.8 is a beryl transect from pegmatite LE25-8. 244
Appendix Figure 158: Concentrations (ppm) versus transect length. Sample LE25-8-1.17 is a quartz transect from pegmatite LE25-8. 245
Appendix Figure 159: Sample LE25-8-2, 100 micron double polished thick section of a pegmatite core zone. Blue (beryl transect) and yellow (quartz transect) lines and numbers correspond to LA-ICP-MS transect lines (e.g., LE25-8-2.6 is the blue line labelled 6)..... 246
Appendix Figure 160: Concentrations (ppm) versus transect length. Sample LE25-8-2.2 is a quartz transect from pegmatite LE25-8. 247
Appendix Figure 161: Concentrations (ppm) versus transect length. Sample LE25-8-2.5 is a quartz transect from pegmatite LE25-8. 248
Appendix Figure 162: Concentrations (ppm) versus transect length. Sample LE25-8-2.6 is a beryl transect from pegmatite LE25-8. 249
Appendix Figure 163: Concentrations (ppm) versus transect length. Sample LE25-8-2.8 is a beryl transect from pegmatite LE25-8. 250
Appendix Figure 164: Concentrations (ppm) versus transect length. Sample LE25-8-2.10 is a beryl transect from pegmatite LE25-8. 251
Appendix Figure 165: Concentrations (ppm) versus transect length. Sample LE25-8-2.13 is a beryl transect from pegmatite LE25-8. 252
Appendix Figure 166: Sample LE25-9-1, 100 micron double polished thick section of pegmatite LE25-9 core zone. Blue (beryl transect) and yellow (quartz transect) lines and numbers correspond to LA-ICP-MS transect lines (e.g., LE25-9-1.3 is the blue line labelled 3)..... 253
Appendix Figure 167: Concentrations (ppm) versus transect length. Sample LE25-9-1.3 is a beryl transect from pegmatite LE25-9. 254
Appendix Figure 168: Concentrations (ppm) versus transect length. Sample LE25-9-1.4 is a beryl transect from pegmatite LE25-9. 255

Appendix Figure 169: Concentrations (ppm) versus transect length. Sample LE25-9-1.5 is a quartz transect from pegmatite LE25-9. 256
Appendix Figure 170: Concentrations (ppm) versus transect length. Sample LE25-9-1.6 is a beryl transect from pegmatite LE25-9. 257
Appendix Figure 171: Concentrations (ppm) versus transect length. Sample LE25-9-1.7 is a beryl transect from pegmatite LE25-9. 258
Appendix Figure 172: Concentrations (ppm) versus transect length. Sample LE25-9-1.8 is a beryl transect from pegmatite LE25-9. 259
Appendix Figure 173: Concentrations (ppm) versus transect length. Sample LE25-9-1.10 is a beryl transect from pegmatite LE25-9. 260
Appendix Figure 174: Concentrations (ppm) versus transect length. Sample LE25-9-1.11 is a beryl transect from pegmatite LE25-9. 261
Appendix Figure 175: Concentrations (ppm) versus transect length. Sample LE25-9-1.12 is a beryl transect from pegmatite LE25-9. 262
Appendix Figure 176: Concentrations (ppm) versus transect length. Sample LE25-9-1.13 is a beryl transect from pegmatite LE25-9. 263
Appendix Figure 177: Concentrations (ppm) versus transect length. Sample LE25-9-1.14 is a beryl transect from pegmatite LE25-9. 264
Appendix Figure 178: Sample LE25-9-2, 100 micron double polished thick section of pegmatite LE25-9 core zone. Blue (beryl transect) lines and numbers correspond to LA-ICP-MS transect lines (e.g., LE25-9-2.1 is the blue line labelled 1). 265
Appendix Figure 179: Concentrations (ppm) versus transect length. Sample LE25-9-2.1 is a beryl transect from pegmatite LE25-9. 266
Appendix Figure 180: Concentrations (ppm) versus transect length. Sample LE25-9-2.5 is a beryl transect from pegmatite LE25-9. 267
Appendix Figure 181: Concentrations (ppm) versus transect length. Sample LE25-9-2.8 is a beryl transect from pegmatite LE25-9. 268
Appendix Figure 182: Concentrations (ppm) versus transect length. Sample LE25-9-2.9 is a beryl transect from pegmatite LE25-9. 269
Appendix Figure 183: Concentrations (ppm) versus transect length. Sample LE25-9-2.10 is a beryl transect from pegmatite LE25-9. 270

Appendix Figure 184: Concentrations (ppm) versus transect length. Sample LE25-9-2.12 is a beryl transect from pegmatite LE25-9. 271
Appendix Figure 185: Beryl concentrations from LE25-3A3 normalized to the rim (A) and core (B) of euhedral beryl LE25-3A3.2. 272
Appendix Figure 186: Beryl concentrations from LE25-3A5 normalized to the rim (A) and core (B) of euhedral beryl LE25-3A3.2. 273
Appendix Figure 187: Beryl concentrations from LE25-5C-1A normalized to the rim (A) and core (B) of euhedral beryl LE25-3A3.2. 274
Appendix Figure 188: Beryl concentrations from LE25-5L-2A normalized to the rim (A) and core (B) of euhedral beryl LE25-3A3.2. 275
Appendix Figure 189: Beryl concentrations from LE25-5R-1A normalized to the rim (A) and core (B) of euhedral beryl LE25-3A3.2. 276
Appendix Figure 190: Beryl concentrations from LE25-6-1 normalized to the rim (A) and core (B) of euhedral beryl LE25-3A3.2. 277
Appendix Figure 191: Beryl concentrations from LE25-6-2 normalized to the rim (A) and core (B) of euhedral beryl LE25-3A3.2. 278
Appendix Figure 192: Beryl concentrations from LE25-8-1 normalized to the rim (A) and core (B) of euhedral beryl LE25-3A3.2. 279
Appendix Figure 193: Beryl concentrations from LE25-8-2 normalized to the rim (A) and core (B) of euhedral beryl LE25-3A3.2. 280
Appendix Figure 194: Beryl concentrations from LE25-9-1 normalized to the rim (A) and core (B) of euhedral beryl LE25-3A3.2. 281
Appendix Figure 195: Beryl concentrations from LE25-9-2 normalized to the rim (A) and core (B) of euhedral beryl LE25-3A3.2. 282
Appendix Figure 196: Beryl concentrations from LE25-10 normalized to the rim (A) and core (B) of euhedral beryl LE25-3A3.2. 283
Appendix Figure 197: Bivariate plots for trace element concentrations from Mt. Antero quartz crystal LE25-3A1.6 (n=101). A) Al versus Ti; B) Al versus Li; C) Al versus Ge; D) Al versus B; E) Al versus Ga; F) Al versus Rb. 284

Appendix Figure 198: Bivariate plots for trace element concentrations from Mt. Antero quartz crystal LE25-3A1.17 (n=110). A) Al versus Ti; B) Al versus Li; C) Al versus Ge; D) Al versus B; E) Al versus Ga; F) Al versus Rb. 285
Appendix Figure 199: Bivariate plots for trace element concentrations from Mt. Antero quartz crystal LE25-5C-1A.17 (n=166). A) Al versus Ti; B) Al versus Li; C) Al versus Ge; D) Al versus B; E) Al versus Ga; F) Al versus Rb. 286
Appendix Figure 200: Bivariate plots for trace element concentrations from Mt. Antero quartz crystals LE25-5C-1B.14 (n=120). A) Al versus Ti; B) Al versus Li; C) Al versus Ge; D) Al versus B; E) Al versus Ga; F) Al versus Rb. 287
Appendix Figure 201: Bivariate plots for trace element concentrations from Mt. Antero quartz crystal LE25-5L-1B.4 (n=174). A) Al versus Ti; B) Al versus Li; C) Al versus Ge; D) Al versus B; E) Al versus Ga; F) Al versus Rb. 288
Appendix Figure 202: Bivariate plots for trace element concentrations from Mt. Antero quartz crystal LE25-5R-1A.7 (n=55). A) Al versus Ti; B) Al versus Li; C) Al versus Ge; D) Al versus B; E) Al versus Ga; F) Al versus Rb. 289
Appendix Figure 203: Bivariate plots for trace element concentrations from Mt. Antero quartz crystal LE25-5R-1B.7 (n=55). A) Al versus Ti; B) Al versus Li; C) Al versus Ge; D) Al versus B; E) Al versus Ga; F) Al versus Rb. 290
Appendix Figure 204: Bivariate plots for trace element concentrations from Mt. Antero quartz crystal LE25-6-1.19 (n=427). A) Al versus Ti; B) Al versus Li; C) Al versus Ge; D) Al versus B; E) Al versus Ga; F) Al versus Rb. 291
Appendix Figure 205: Bivariate plots for trace element concentrations from Mt. Antero quartz crystal LE25-6-2.3 (n=910). A) Al versus Ti; B) Al versus Li; C) Al versus Ge; D) Al versus B; E) Al versus Ga; F) Al versus Rb. 292
Appendix Figure 206: Bivariate plots for trace element concentrations from Mt. Antero quartz crystal LE25-7-1A.11 (n=345). A) Al versus Ti; B) Al versus Li; C) Al versus Ge; D) Al versus B; E) Al versus Ga; F) Al versus Rb. 293
Appendix Figure 207: Bivariate plots for trace element concentrations from Mt. Antero quartz crystal LE25-7-1B.1 (n=67). A) Al versus Ti; B) Al versus Li; C) Al versus Ge; D) Al versus B; E) Al versus Ga; F) Al versus Rb. 294

Appendix Figure 208: Bivariate plots for trace element concentrations from Mt. Antero quartz crystal LE25-7-2A.1 (n=2,755). A) Al versus Ti; B) Al versus Li; C) Al versus Ge; D) Al versus B; E) Al versus Ga; F) Al versus Rb. 295
Appendix Figure 209: Bivariate plots for trace element concentrations from Mt. Antero quartz crystal LE25-7-2A.15 (n=340). A) Al versus Ti; B) Al versus Li; C) Al versus Ge; D) Al versus B; E) Al versus Ga; F) Al versus Rb. 296
Appendix Figure 210: Bivariate plots for trace element concentrations from Mt. Antero quartz crystal LE25-7-2B.1 (n=827). A) Al versus Ti; B) Al versus Li; C) Al versus Ge; D) Al versus B; E) Al versus Ga; F) Al versus Rb. 297
Appendix Figure 211: Bivariate plots for trace element concentrations from Mt. Antero quartz crystal LE25-7-2B.10 (n=249). A) Al versus Ti; B) Al versus Li; C) Al versus Ge; D) Al versus B; E) Al versus Ga; F) Al versus Rb. 298
Appendix Figure 212: Bivariate plots for trace element concentrations from Mt. Antero quartz crystal LE25-8-2.5 (n=337). A) Al versus Ti; B) Al versus Li; C) Al versus Ge; D) Al versus B; E) Al versus Ga; F) Al versus Rb. 299

List of Tables

Table 1: Pegmatite, hydrothermal veins, aplites, and greisen differences on Mt. Antero 13
Table 2: Typical Examples of Accessory Mineral Assemblages in Pegmatite Groups (Wise et al. 2022) 18
Table 3: General Characteristics of RMG and DPA Type Pegmatites from Wise et al. (2022) .. 19
Table 4: LA-ICP-MS Reproducibility and Detection Limits Based on NIST 610 and 612 Glass 23

Acknowledgements

I would like to express my appreciation and gratitude to all who made this project possible. Firstly, thank you my family for being supportive of my dreams, pushing me to continue, and always letting me talk about my ongoing research. I always remember the vacations we took to the Colorado mountains and the abandoned mines that my brother and I so wished we could break into.

Thank you to my thesis advisor, Dr. Matt Brueseke, for taking a chance on this project when I walked into your office and suggested a change of research plans. Your guidance has honed my geology and research skills. I will always remember our time together and hope to continue working together in the future.

Thank you to Brian Busse for letting us conduct research on his claim. Without you the project would not have been possible. I have enjoyed getting to know a legend that I grew up watching on TV and who also influenced my love for geology. I look forward to working with you more in the future.

Thank you to Dr. Pamela Kempton, the committee member and the teacher I took the most classes from here at K-State. Thank you for pushing me and making me want to continue learning. Each class I took from you added to my geological skills and I know I will continue using many things you taught me in the coming future.

Thank you to my committee member, Dr. Mike Wise. Thank you for guiding my project and introducing me to the world of pegmatology. Your knowledge has been invaluable for this project and for my education. I hope to work more with you in the future on more pegmatite systems.

To my undergraduate advisor and friend, Dr. Jon Sumrall, thank you for teaching me the fundamentals of geology. I have learned to hone these skills and apply them to complex problems. I enjoy all our talks and your willingness to discuss any topic has greatly contributed to my success. I look forward to catching up when you return home from being deployed.

Thank you to all my friends here at K-State. A special thank you to Quillen, Levi, James, and Wyatt. I enjoyed our many lunches, evenings, and study sessions hanging out, completing homework, and harassing each other about our theses being done. I can finally tell you all that mine is done.

Thank you to all the organizations that funded this research: The Houston Geological Society, Geological Society of America, the Wyoming Geological Association, and the Colorado Scientific Society. Thank you also to the Maine Mineral and Gem Museum who sponsored my attendance at their pegmatite workshop which greatly increased my knowledge of pegmatites. Without you all this research would not have been possible.

Dedication

I dedicate this thesis to my two biggest supporters: my Mom and Dad. Words will never describe how thankful I am for all you have done for me over the years. Thank you for pushing me to be the best person I can be and for always checking in on me to make sure school is going well. Over our many years of camping trips, I was convinced to be a geologist. Thank you for always letting me go check out the old mine tailings in the mountains and for letting me put rocks in your garden when I cannot find enough room for them in my room.

To my Dad, thank you for talking to Brian in the jeep shop that day. I will never forget when he poured about 15 perfect euhedral beryls in my hand and offered to let me do research on his claim. Without you driving the conversation none of this would have happened.

To my Mom, thank you for always calling to talk to me and for checking up to make sure everything is okay. Thank you for the proofreading that you have always done and the many suggestions you have given me.

I love you both and I am very thankful that you are my parents.

Chapter 1 - Introduction

Granitic pegmatites are a complicated igneous phenomena characterized by their large crystal size compared to the surrounding rocks. Incompatible elements are concentrated in pegmatites within rare silicate minerals, such as spodumene, beryl, and tourmaline, which crystallize from the pegmatitic melt. Thus, pegmatites are often sought after for their economic significance, based on critical mineral potential and how they host colorful gem-quality minerals.

Pegmatite nomenclature varies widely because multiple classifications are used to interpret pegmatitic bodies with some classifications containing many subclasses. Other confusion about pegmatites comes from the diverse textures, mineralogy, and chemical compositions that pegmatites represent (Wise et al. 2022). Pegmatites generally are thought to represent the last stage of a hydrous granitic melt or form directly from anatexis, which is why they are enriched in incompatible elements and volatiles excluded from the crystallization of the parental granitoid (Černý and Ercit 2005; London and Morgan 2012).

Magmatic, hydrothermal, and metasomatic processes can all occur in a single granite-pegmatite system and the driver(s) for which mechanism dominates remains debated (Müller et al. 2022). Pegmatites are generally thought to form via extensive magmatic differentiation (Jahns and Burnham 1969; Müller et al. 2022; Simmons et al. 2022). Hydrothermal processes transport dissolved ions in aqueous solutions which then precipitate out of the fluid and form minerals. Metasomatic processes chemically alter and replace minerals in pegmatites and surrounding rock with aqueous fluids enriched in trace elements (Lindgren 1925). Jacobson (1993) showed that the Mt. Antero pegmatites in this study crystallized from the California and Antero Granites, but as will be discussed below, some pegmatite core zones were altered by hydrothermal and metasomatic processes related to the final cooling of the pegmatites.

In a “typical” granitoid, crystallization of igneous minerals like feldspars, quartz, and mafic minerals leaves behind, in the residual melt, incompatible elements like B, P, Li, and F (Simmons et al. 2012; Dharmapriya et al. 2025). These elements, along with residual water, lower the melt viscosity and crystallization temperature (Jahns and Burnham 1969; London 2008; Simmons et al. 2012). When water exceeds the solubility limit of the melt, an aqueous fluid can form which will potentially allow for a volatile-rich pocket to form in the granitoid crystal-rich mush (Simmons et al. 2012; Troch et al. 2022). In these miarolitic cavities (pockets), gem-quality Be-, Li-, B-, and F- silicate minerals grow, along with other minerals which might not be of gem quality (Simmons et al. 2012). The pocket represents the final product of crystallization of the highly evolved, genetically related granitoid (Jahns and Brunham 1969; London 2008; Simmons et al. 2012).

As stated previously, pegmatites incorporate residual incompatible elements. The United States Geological Survey has designated sixty elements and minerals as critical minerals as of the Fall of 2025 (U. S. Geological Survey 2025). Several critical elements are found in pegmatites and include Be, Li, Nb and Ta. Lithium’s utility in the twenty-first century is arguably one of the greatest with it being the main metal in lithium-ion batteries (Balaram et al., 2024; Dharmapriya et al. 2025). Tantalum and Nb are almost always found together (Schulz et al. 2017). Niobium is used for anticorrosion properties in alloys and Ta is used for electronic capacitors (Schulz et al. 2017).

Beryllium-rich pegmatites are often significant because they yield colorful gem-quality minerals (London 2008; McLemore 2010; Simmons et al. 2012) and while there is still robust interest for gem-quality beryl, Be is now used in metal alloys which can be found in various

applications, such as lightweight alloys used in aerospace and defense industries (McLemore 2010; Lederer et al. 2016).

Beryl, a beryllium aluminum silicate, with a formula of $Be_3Al_2Si_6O_{18}$, commonly occurs in granitic pegmatites and can be of gem quality or opaque (London and Morgan 2012; Simmons et al. 2012; Simmons et al. 2022; Wise et al. 2022). Common gem-beryl varieties that occur in pegmatites are aquamarine, heliodor, morganite, and goshenite, with a much less common variety being emerald (Shigley and Kampf 1984; Simmons et al. 2012; Simmons et al. 2022). These varieties are differentiated based on color, which is caused by trace elements being incorporated into the octahedral and channel sites of the crystal structure. Emeralds reflect impurities of Cr and V (Simmons et al. 2012). Aquamarines, which are most commonly blue but can be green, are caused by impurities of Fe^{2+} (Wood and Nassau 1968). Heliodor, which is yellow, is caused by impurities of Fe^{3+} (Wood and Nassau 1968). Morganites, which are pink, are caused by impurities of Mn^{2+} (Wood and Nassau 1968). If beryl is colorless then it is referred to as goshenite. If the beryl is opaque then it is referred to as its observed color (e.g., beryl that appears opaque blue is blue beryl).

Notable blue beryl-bearing systems in North America include the Maine pegmatite field (Simmons et al. 2012), the Sawtooth Range, Idaho (Reid 1963), and in pegmatites on Mt. Antero, Colorado, in the Sawatch Range (Jacobson 1993, Simmons et al. 2012). While beryllium mining does not occur at Mt. Antero, gem-quality minerals are routinely extracted from the veins and pegmatites on the mountain. Aquamarine was chosen as Colorado's state gemstone in 1971 due to the exquisite crystals found on Mt. Antero (Jacobson 1993). Mount Antero beryls are the focus of this study.

At Mt. Antero, the differences in crystal quality (e.g., color, size, and shape) have not been documented between pegmatites and related geological features (Table 1), all producing gem-quality specimens of beryl and smoky quartz (Jacobson, 1993). The trace element geochemical signatures of the beryl and quartz have also not been documented. The formation temperature and characteristics of the melt and fluids (e.g., homogenization temperature (T_h) and salinity) that formed the pegmatites and related geological features of different localities are unknown. This study aims to compare the trace element geochemistry in different spheroid pegmatites on Mt. Antero using quartz and beryl trace element geochemistry to better understand the melts and fluids which formed this pegmatite system. These results give insights into the geochemical differences of the system through formation.

Chapter 2 - Background

Geologic History

Mount Antero is in the north-south trending Sawatch Range in South Central, Colorado (Fig 1). The range lies on the western side of the Arkansas River valley, adjacent to the basin-bounding fault of the Rio Grande Rift (Mills and Coleman 2013) and has been exposed due to post-Laramide extension along the northern Rio Grande Rift (McIntosh and Chapin 2004). This region is broadly part of the middle Tertiary (38-29 Ma) Central Colorado Volcanic Field and contains eruptive centers (e.g., primarily felsic calderas and interspersed andesite volcanoes) and exhumed batholiths (McIntosh and Chapin 2004). These volcanoes are also associated with the western Cordillera ignimbrite flare-up (McIntosh and Chapin 2004) and the greater southern Rocky Mountain volcanic field.

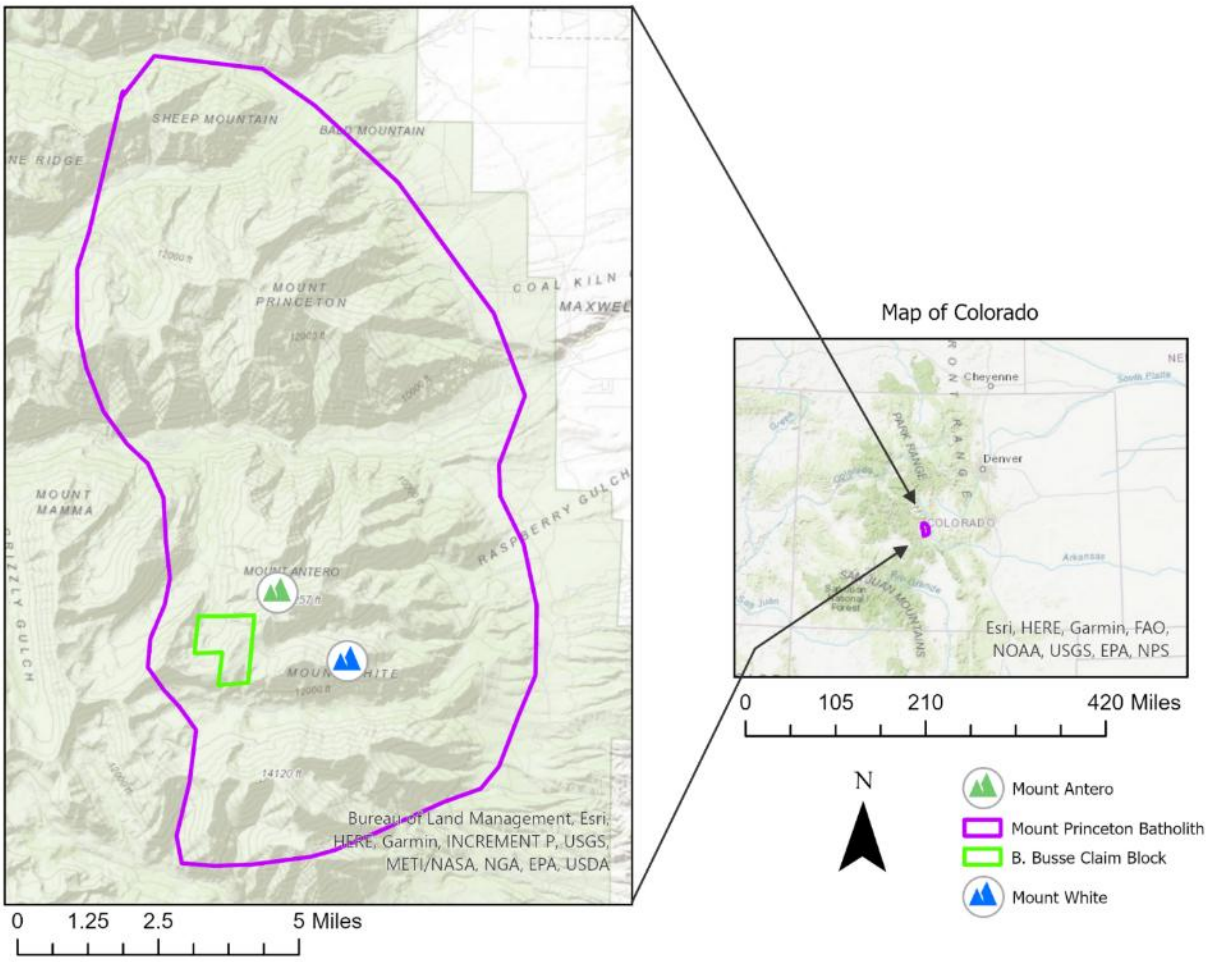


Figure 1: Location of the study area (B. Busse's Claim) on Mount Antero and near Mount White in South Central, Colorado (USA), along with the location of the Mount Princeton Batholith.

The region of Mt. Antero, Mt. White, and Mt. Princeton consists of a sequence of granitoid plutons that make up the Mount Princeton Batholith (Fig.1; Mills and Coleman 2013). The main unit consists of the ~36 Ma Mt. Princeton quartz monzonite (Mills and Coleman 2013), which is most recently mapped as the equigranular biotite-hornblende monzogranite interior facies ($P_E$mpm) by Kellogg et al. (2017). The composition of the main unit in the pluton is variable as shown by the differences in names used by the above references. This main unit

encompasses much of Mt. Princeton to the north and extends to the Mt. Antero area. The southern end of the main unit is intruded by younger, ~30 Ma, leucogranites once called the Antero, California, and North Fork, but is now considered the leucogranite suite of Mt. Antero (Fig. 2) (Kellogg et al. 2017). Kellog et al. (2017) further split this temporally coeval suite into the main phase Antero leucogranite ($P_E$ag) and the leucogranite of the California Mine ($P_E$cg). Previous research in the area (Shannon 1988, Jacobson 1993, Mills and Coleman 2013) considered the Antero, North Fork, and California granitoids as three separate intrusions and sometimes lumped them into one collective unit of young granites for mapping purposes. These granites are all exposed near the summits of Mounts White and Antero at or above an elevation of 3657 m.

The three young granites, or leucogranite suite of Mt. Antero, originate from a silicic crustal melt associated with the Rio Grande Rift (McIntosh and Chapin 2004), which post-dates the main phase of ignimbrite-flare-up volcanism in the Central Colorado Volcanic Field (Zimmer and McIntosh 2013). Shannon (1988) speculated that these intrusions signaled the beginning of magmatism related to local opening of the Rio Grande Rift at ca. ~30 Ma. They overlap spatially with a series of A-type topaz rhyolite domes across the Arkansas River valley (e.g., Nathrop domes; Wegert et al. 2013); thus, there does seem to be a localized period of crustal melting, extension, and magmatism coincident with granite pluton generation at ca. ~30 Ma. Inside these granite plutons are where the beryl-bearing pegmatites, dikes, and veins hosting mineralization are found. The mining claim *Thank You Lord,* owned by B. Busse, where the research was focused, includes part of the California Granite (Fig. 2).

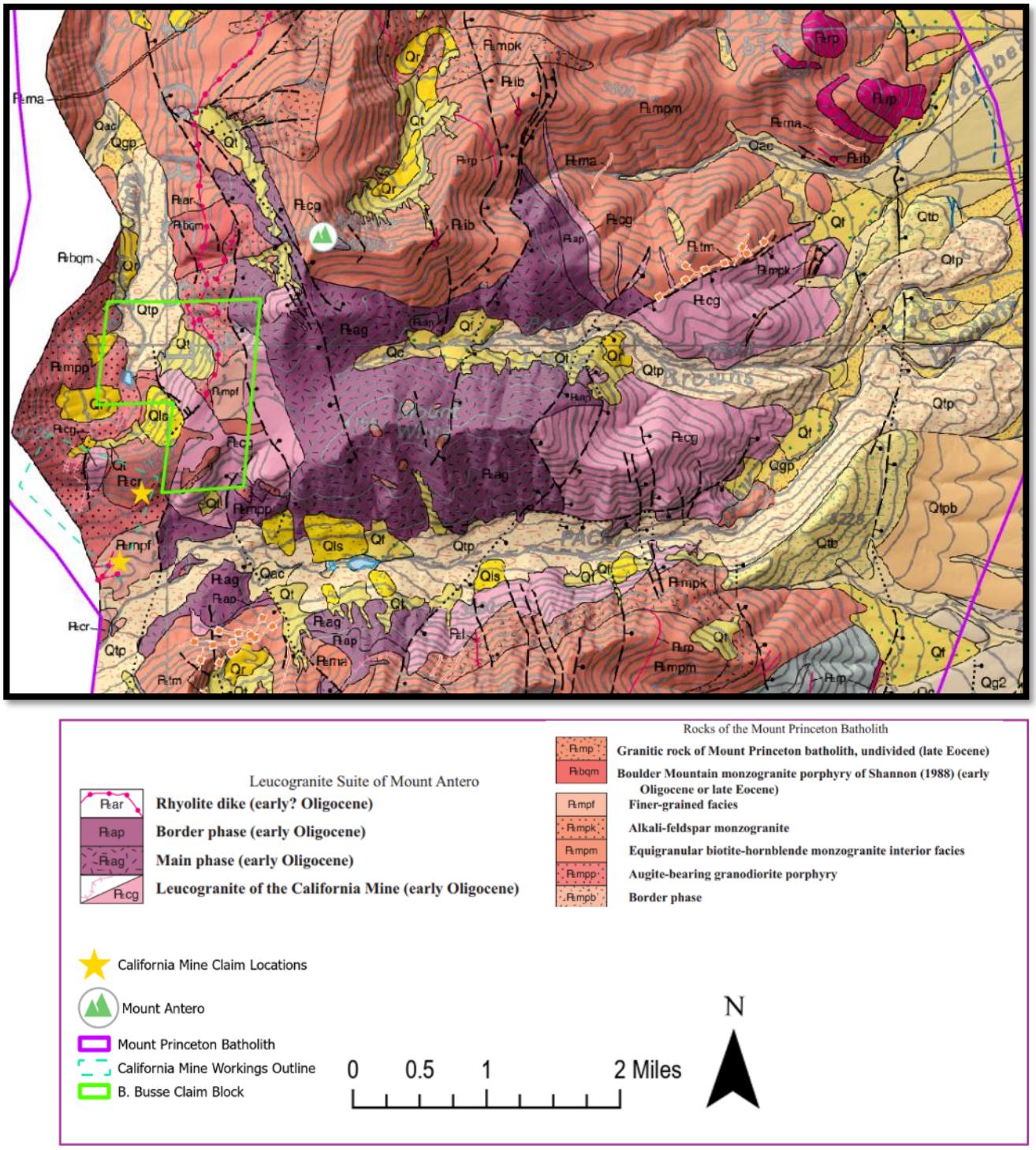


Figure 2: General geology of the study area along with B. Busse's *Thank You Lord* mining claim and the historic area of the California Mine. Rock formations not necessary for the study were omitted from the key as all formations that begin with Q are quaternary in age. Geologic Map adapted from Kellogg et al. (2017).

Granite Type

Shannon (1988) proclaimed the California and Antero Granites A-type based on the following findings from his research. These granites are subalkaline and like Climax-type molybdenum deposits (e.g., Climax, Red Mountain, and Mount Emmons) (Shannon 1988). The California and Antero granites are higher in Al_2O_3 than other A-type granites from other localities, and are enriched in Rb, Nb, Ga, and Th and lower in Sr, Ba, Y, Zr, and REEs (Shannon 1988). This suite of granites represents a geochemical subgroup of A-type granites associated with the northern Rio Grande Rift and are similar composition to the Nathrop topaz rhyolites (Shannon 1988).

Bulk rock geochemistry of different facies of both the California and Antero Granite exists from Shannon (1988) and other references therein. Some discrepancies exist when these data are plotted on a Whalen et al. (1987) discrimination diagram (Fig. 3). As shown, all points representing the California and Antero Granites fall within a wide range of the I- and S-type granite and A-type granite fields. When these data are plotted on the Pearce et al. (1984) discrimination diagram Nb versus Y (Fig. 4a), the data plot as a mix of A-type and I- and S-type. When the data are plotted on the Pearce et al. (1984) discrimination diagram Rb versus Y+Nb (Fig. 4B), the data once again plot along the I-, S-, and A-type boundary with most points lying within the S-type field. While the granite originated from an "anorogenic" environment, the source rock was most likely metasediments, as Shannon (1988) concluded. Based on Figures 3 and 4, this granite is an A-type hybrid granite encompassing characteristics of both S- and A-type granite.

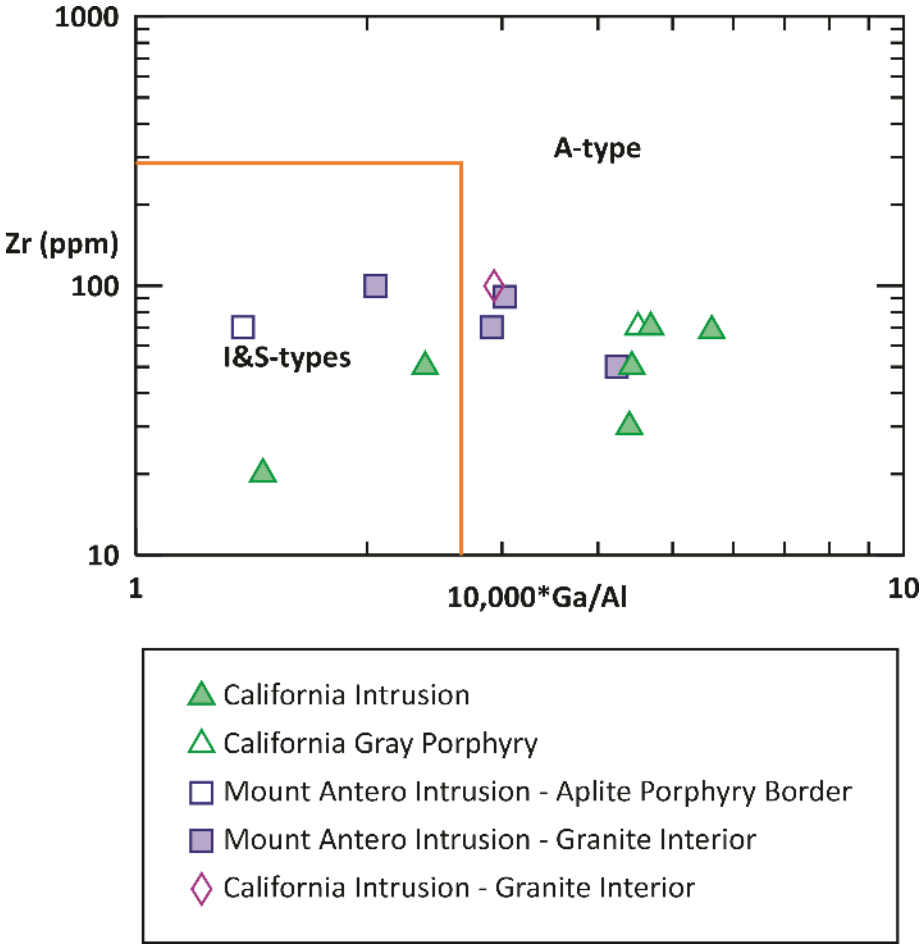


Figure 3: Discrimination diagram of Whalen et al. (1987) that represents California and Antero granite bulk rock geochemistry data from Shannon (1988) and other references therein.

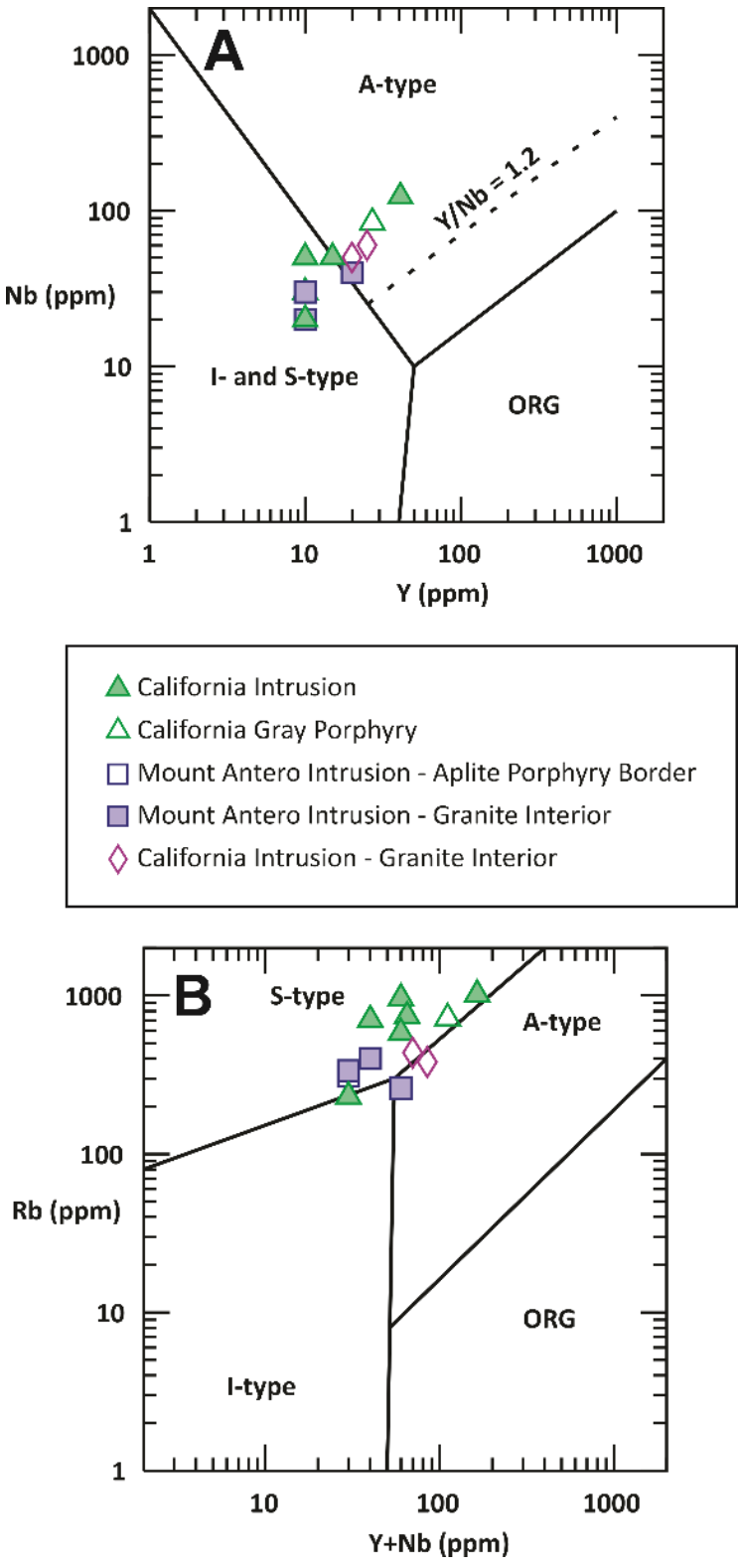


Figure 4: Discrimination diagrams of Pearce et al. (1984) represent California and Antero granite bulk rock geochemistry data from Shannon (1988) and other references therein. A) Y versus Nb. B) Y+Nb versus Rb.

Recognized Mineralization on Mount Antero

The three granites that make up the leucogranite suite of Mt. Antero are known to contain pegmatites and related features that are beryllium-rich in composition and yield gem-quality minerals (Jacobson 1993). Although leucogranites, these are referred to as the California, Antero, and North Fork granites. The California granite, which exists on Mt. Antero and Mt. White, is known for its molybdenum-rich veins that also bear smoky quartz and beryl (Jacobson 1993). The molybdenum was once mined at the California Mine (Fig. 2, Jacobson 1993). Sharp (1976) mapped the Antero, California, and North Fork granites as the Mt. Antero fine-grained granite and porphyritic granite variants (Jacobson 1993). The California granite is slightly more evolved than the Antero granite and is thought to have originated from the same source at depth (Shannon 1988; Jacobson 1993). The California and Antero Granites are associated with pegmatites, hydrothermal veins, quartz-beryl-topaz greisens, and layered aplites containing miarolitic cavities (Jacobson, 1993). Pegmatites are found as oblate to spheroid bodies and are found within the upper parts of both the California and Antero Granites (Switzer 1939; Jacobson 1993, Erichsen et al. 2025). Jacobson further split pegmatites into the following: injected pegmatite veins and miarolitic cavity pegmatites. Jacobson (1993) also commented on miarolitic layered-albitite veins, pegmatoid-aplite veins, hydrothermal veins, and greisens. Table 1 shows the differences between each.

Table 1: Pegmatite, hydrothermal veins, aplites, and greisen differences on Mt. Antero

Geologic Feature	Structure Description	References
Spheroid Pegmatites	Spheroid pegmatites range from 5 to 75 cm. Can contain USTs with zones of granite, aplite, intermediate, and core. Are contained within parental granite. Can contain miarolitic cavities.	Erichsen et al. 2025 Jacobson 1993
Injected Pegmatite Veins	Veins with a clearly defined border zone due to being injected within or out of the parental granite. These occur as pods, ribbons, bulbs, or bean shapes. Can contain miarolitic cavities.	Jacobson 1993
Miarolitic Layered-Albitite Veins	Pegmatite-like veins which are elliptical to circular in cross sections and pinch and swell along their lengths. These fill fractures within the granite and are considered transitional between true hydrothermal and pegmatite. Neither a well-defined border zone nor graphic granite exists on the edges.	Jacobson 1993
Pegmatoid-Aplite Veins (Dikes)	Pegmatoid-aplite veins are aplite injections that occasionally contain a miarolitic cavity.	Jacobson 1993
Hydrothermal Veins	Hydrothermal veins are veins with predominantly quartz or beryl and can include sulfides. The California Mine contains a quartz-beryl-molybdenite vein.	Adams 1953 Jacobson 1993
Greisens	These rocks are gray to tan, fine to coarse-grained and composed of quartz and mica. Greisens in the area appear as altered and strongly fractured granite.	Jacobson 1993

The pegmatites on Mt. Antero also bear pockets in which gem-quality minerals have crystallized (Switzer 1939). Mount Antero pegmatites occur as cylindrical bodies that crosscut through granite plutons (Jacobson 1993). Field observations on Mt. Antero have also shown that

pegmatites can occur as spheroids within the granite (Erichsen et al. 2025). Jacobson (1993) presents evidence of a 2.5 by 1 m oblate pocket that yielded smoky quartz crystals up to 25 by 5 cm in size. Switzer (1939) observed a wide range in the size of pegmatites with a notable one being ~30 cm across with a cylindrical cavity extending back ~120 cm while others were 5 to 10 cm in diameter.

Mount Antero miarolitic cavities can contain several mineral assemblages. One assemblage is smoky quartz, microcline, beryl, fluorite, and muscovite (Jacobson 1993). Switzer (1939) originally classified the pegmatites into four groups: (i) beryl-smoky quartz (Fig. 3), (ii) phenakite (a beryllium orthosilicate, Be_2SiO_4), (iii) beryl-quartz-bertrandite (a beryllium sorosilicate hydroxide, $Be_4Si_2O_7(OH)_2$), and (iv) topaz. Switzer (1939) only found one fragmented topaz-bearing pegmatite. Mount Antero aplite dikes can also contain miarolitic cavaties and are potentially the transition between the pegmatite and hydrothermal system (Jacobson 1993). Jacobson (1993) describes hydrothermal veins that primarily contain quartz, but some also contain so much beryl they appear to be ~100% beryl in some sections. These veins contain the sulfides molybdenite, pyrite, ferrimolybdite, along with fluorite, adularia, hematite, and phenakite (Jacobson 1993). The mineralization in the pegmatites and related features described in Table 1 have similarities and differences within their mineral assemblages which raises the question of whether these systems are petrogenetically related and ultimately derived from the same source.

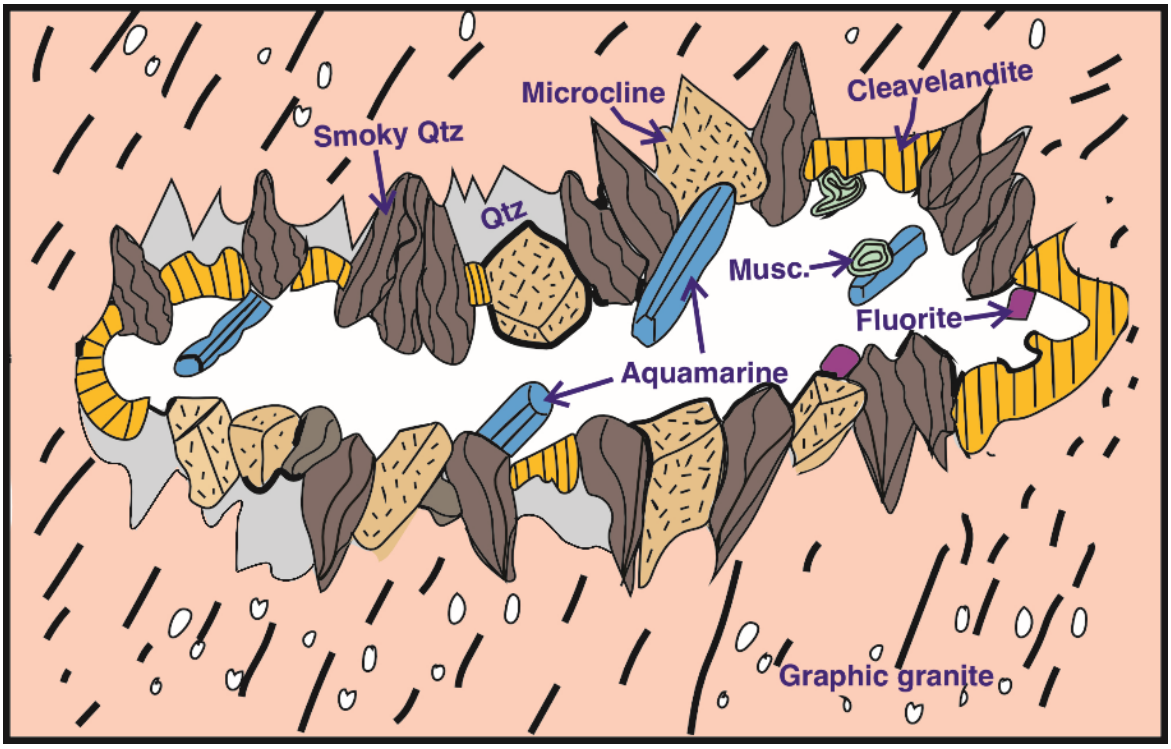


Figure 5: Drawing of a regular miarolitic cavity which is currently found on Mount Antero within the pegmatites. Common minerals are beryl (var. aquamarine), smoky quartz, quartz, muscovite (musc.), fluorite, and cleavelandite. Sketch after Jacobson (1993).

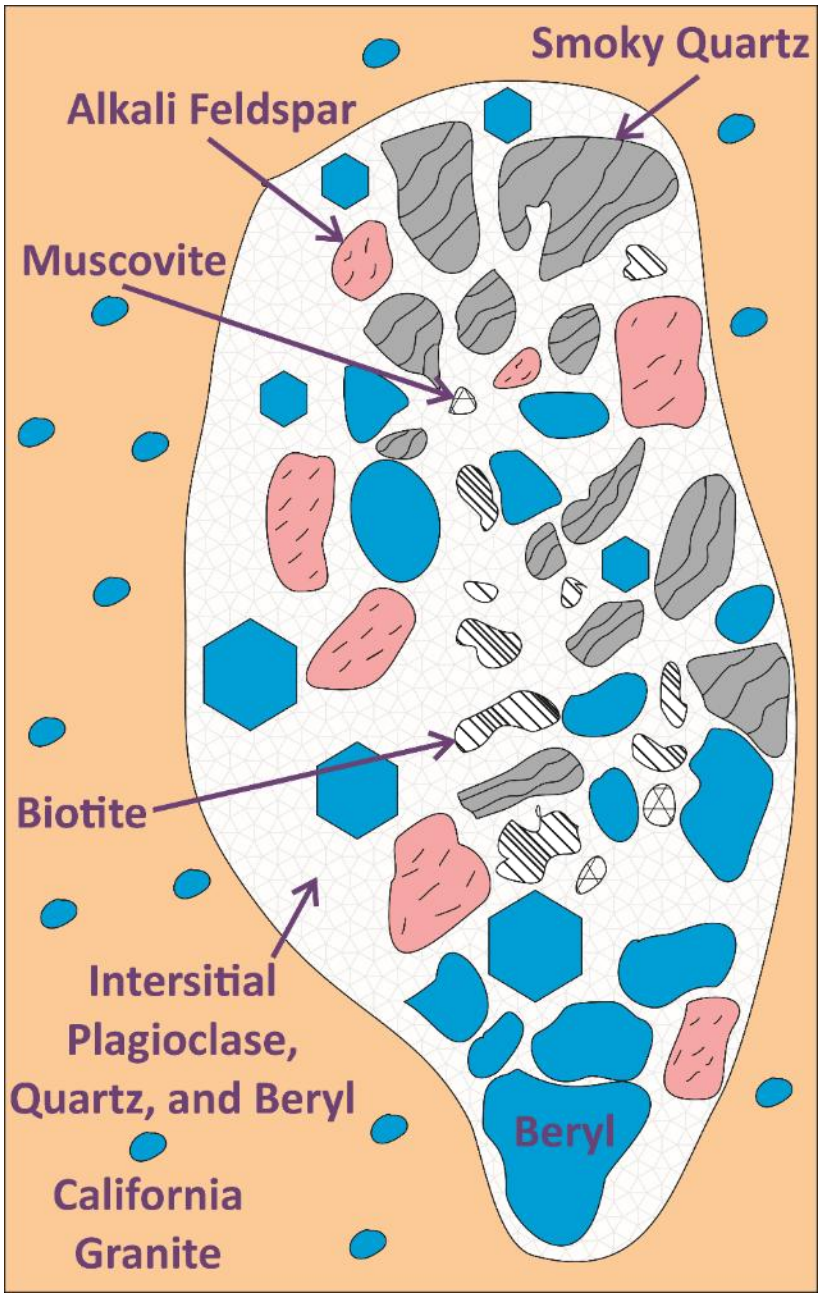


Figure 6: A drawing of a solid pegmatite spheroid ~75 cm across at the *Thank You Lord* claim on Mount Antero, Colorado. Major minerals found in this pegmatite spheroid are beryl, quartz, biotite, muscovite, alkali feldspar, and albite. The pegmatite is surrounded by beryl-bearing California Granite.

The pegmatites in the vicinity of Mt. Antero yield colorful blue gem-quality beryls that are sought after by collectors (Jacobson 1993). Furthermore, the California Granite can be totally blue in areas due to opaque blue beryl clots (Jacobson 1993; Erichsen et al. 2025). This world

class mineral collecting locality has not been adequately studied from a mineralogical perspective. Minimal trace element data exists for beryls in the area. Kar (1991) analyzed beryl from the Mt. Antero and Mt. White areas to determine the concentrations of Na, Mg, K, Fe, and Cs. Kar (1991) also determined fluid inclusion homogenization temperatures of 350 to 360 °C for inclusions within beryls and suggested beryls began growing at ~500 to 600 °C, which shows the beryl formed over a wide range of temperatures. A unique characteristic of the pegmatite system in the Mt. Antero area is that beryls are also found within aplite dikes and hydrothermal veins (Jacobson, 1993).

Pegmatite Naming Scheme

Under the scheme of Wise et al (2022), pegmatites are divided into three main groups (Groups 1, 2, and 3) based on their association of primary rock-forming and rare-element minerals (Table 2). Pegmatites are further distinguishable by the type of granitoid melt or metamorphic facies from which they form (Wise et al. 2022) (Table 3). These three groups are then defined by their source of either residual melts of granite magmatism (RMG) or direct product of anatexis (DPA). Group one pegmatites are formed from either I or S-type granite (RMG) or granulite to amphibolite facies metamorphic rocks (DPA) (Wise et al. 2022). Group two pegmatites are formed from either A or I-type granite (RMG) or granulite to amphibolite facies of metamorphic rocks (DPA) (Wise et al. 2022). Group three pegmatites are formed from granulite to amphibolite facies and are only DPA (Wise et al. 2022). Each group is also geochemically distinct; for example, group two pegmatites are enriched in rare earth elements (REEs), Be, F, and Nb (Wise et al. 2022). As stated above, Wise et al. (2022) has defined the groups based on minerals found within their respective pegmatites. For example, RMG group

two (RMG-2) pegmatites can contain minerals assemblages of beryl ± phenakite and beryl ± topaz ± fluorite (Wise et al. 2022).

Table 2: Typical Examples of Accessory Mineral Assemblages in Pegmatite Groups (Wise et al. 2022)

Group 1	**Group 2**	**Group 3**
Beryl ± Columbite ± Triphylite ± Graftonite	Magnetite ± Epidote ± Titanite	Andalusite ± Sillimanite ± Corundum
Beryl + Amblygonite + Columbite	Uraninite ± Magnetite	Kyanite ± Rutile
Amblygonite + Spodumene	Fayalite ± Magnetite	Cordierite ± Beryl
Spodumene ± Elbaite	Arfvedsonite-riebeckite ± Fayalite	Sapphirine ± Sillimanite
Spodumene ± Petalite	Arfvedsonite-riebeckite ± Aegirine ± Fluorite	Chrysoberyl ± Beryl ± Schorl
Spodumene + Lepidolite + Elbaite	Allanite ± Gadolinite	Dumortierite ± Grandidierite ± Borasilite
Spodumene + Albite	Allanite ± Monazite ± Euxenite	Dumortierite ± Schorl
Lepidolite + Elbaite	Allanite ± Beryl ± Columbite	
Elbaite ± Danburite ± Hambergite ± Zeolites	Gadolinite ± Euxenite ± Fergusonite	
	Beryl ± Topaz ± Fluorite	
	Beryl ± Phenakite	
	Microcline (var. Amazonite) ± Fluorite	
	Micocline (var. Amazonite) ± Topaz ± Fluorite	

Table 3: General Characteristics of RMG and DPA Type Pegmatites from Wise et al. (2022)

RMG (Residual Melts of Granite Magmatism)			
Typical Source Rock	S-Type Granite	A-Type Granite	I-Type Granite
Granite Chemistry	Peraluminous	Peralkaline and Metaluminous to Mildly Peraluminous	Peraluminous to Metaluminous
Relation of Pegmatites to Source	Interior to Marginal	Interior to Marginal	Interior to Marginal
Pegmatite Type	Group 1	Group 2	Groups 1 & 2
Typical Geochemical Signatures	Be, Nb, Ta, Pm Sn, Li, Cs, B	REE, Be, Nb, F	B, Be, REE, Nb, Ti, Li, Ca
Examples	Winnipeg River, MB, Canada; Canada pegmatite, Spain; Kalba Field, Kazakhstan; Malkhan Field, Russia	Pikes Peak, CO, USA; Mt. Perdosa, Italy; Amis complex, Namibia; Luumaki, Finland	Třebič pluton, Czech Republic; Stzegom granite, Poland; O'Grady batholith, NWT, Canada; Greer Lake, MB, Canada
DPA (Direct Products of Anatexis)			
Typical Source Rock	Granulite to Amphibolite Facies	Granulite to Amphibolite Facies Metamorphic Rocks	Granulite to Amphibolite Facies Metamorphic rocks
Relation of Pegmatites to Source	Segregations of Anatectic Melts	Segregations of Anatectic Melts	Segregations of Anatectic Melts
Pegmatite Type	Group 1	Group 2	Group 3
Typical Geochemical Signatures	Be, B, Ta, P, Li, B	REE, U, Be	Al, Be, B
Examples	Góry Sowie. Poland; Oxford field, ME, USA; Cape Cross-Uis, Namibia; Leinster pegmatite belt, Ireland	Evje-Iveland, Norway; Lewisian Gneiss Complex, Scotland; Fraser Lake, SK, Canada; Ploskaya Kola Peninsula, Russia	East Antarctica, Antarctica; Thomas mine, NC, USA; Dolní Bory, Czech Republic; Batchellerville, NY, USA

This naming scheme is validated by recent trace element studies. For example, Müller et al. (2021) used LA-ICP-MS analyses of pegmatite-hosted quartz to determine the geochemical

classification of pegmatites based on their Al, Ti, Li, and Ge concentrations. Müller et al. (2021) also documented that Be, Rb, and B values of quartz also help distinguish these pegmatite groups; thus, pegmatite source rock chemistry seems to control pegmatite quartz trace element chemistry, which allows for the determination of region-specific Li, Ge, and Al contents (Müller et al. 2021).

Chapter 3 - Methods

Pegmatite samples were collected from the southwest ridge of Mt. Antero (Fig. 2) from the *Thank You Lord* mining claim which is shown as the B. Busse Claim Block. This claim is ~1 km south of the Antero four-wheel drive road. Sampling was focused on collecting pegmatites that displayed differences in textures, mineralogy, and beryl color. Overall, ten pegmatite samples were collected from Mt. Antero. Twenty-one double-polished thick sections, twenty-six traditional thin sections, and two single polished thin sections were produced from the samples. The traditional thin sections were primarily used to identify beryl targets for laser ablation-inductively coupled-mass spectrometry (LA-ICP-MS) and secondarily were used to characterize the mineralogy and textural relationships of the rocks. The thick sections were used to obtain LA-ICP-MS trace element transect lines across beryl and quartz crystals. The single-polished thin sections were also used to characterize the mineralogy and textural relationships of the rocks but were obtained in case Raman spectroscopy needed to be utilized on unknown minerals. All thin and thick sections were observed using a Nikon Eclipse 6600 POL petrographic microscope. Select thick sections were also analyzed using a JEOL JCM-7000 Benchtop Scanning Electron Microscope (SEM) at Kansas State University. The SEM analyses were conducted at a landing voltage of 15.0 kV and a working distance of 13.1 mm. The detector was set at 0% dead time (DT) and an average of 29 counts per second (cps) was recorded. Energy dispersive spectrometry was also applied via the SEM to identify any possible geochemical zonation across beryl crystals.

A comprehensive suite of trace elements was obtained using LA-ICP-MS. Transect lines along beryl and quartz were obtained using a Thermo Icap Q ICP-MS with an ESI NWR 193 laser attachment at the University of Arkansas Trace Element and Radiogenic Isotope Lab.

Transect lines are 30 microns wide and variable in length due to variation of grain size. The repetition rate was 10 Hz, raster speed 10 μm/sec, and fluence is ~4.5 J/cm^2. A NIST 610 and 612 glass standard (Jochum et al. 2011) was used to quantify elements into counts per second (cps) and parts per million (ppm). Fifty-three elements were analyzed and are: ^{3}Li, ^{4}Be, ^{5}B, ^{11}Na, ^{12}Mg, ^{13}Al, ^{15}P, ^{19}K, ^{20}Ca, ^{21}Sc, ^{22}Ti, ^{23}V, ^{24}Cr, ^{25}Mn, ^{26}Fe, ^{28}Ni, ^{29}Cu, ^{30}Zn, ^{31}Ga, ^{32}Ge, ^{37}Rb, ^{38}Sr, ^{39}Y, ^{40}Zr, ^{41}Nb, ^{42}Mo, ^{47}Ag, ^{50}Sn, ^{51}Sb, ^{55}Cs, ^{56}Ba, ^{57}La, ^{58}Ce, ^{59}Pr, ^{60}Nd, ^{62}Sm, ^{63}Eu, ^{64}Gd, ^{65}Tb, ^{66}Dy, ^{67}Ho, ^{68}Er, ^{69}Tm, ^{70}Yb, ^{71}Lu, ^{72}Hf, ^{73}Ta, ^{74}W, ^{79}Au, ^{82}Pb, ^{83}Bi, ^{90}Th and ^{92}U. Other pegmatites, greisen, and granite literature formed the rationale for elements chosen. Normalization of the elements to SiO_2 used ^{29}Si. A complete data set of the performed LA-ICP-MS analyses is available in the Supplemental Files.

The analyses took 25 hours and ablation of 512 transect lines of varying lengths were completed. Data reduction was performed using the Iolite Software Program (Paton et al. 2011). Quartz was normalized to 99.9% ^{29}Si and beryl was normalized to 65% ^{29}Si. Standard errors were calculated for each element over each transect line. The standard error for some elements from some transects were <5% of the mean, which indicates homogenous concentrations within the mineral along that transect. However, the standard errors for some elements can be ~200% of the mean, which suggests the minerals can contain zones of differing concentrations. Given that the LA-ICP-MS data were collected along line scans, each data point represents an independent analysis location on the line. Therefore, relative standard deviation (RSD) and RD (relative difference) cannot be used to identify data points that might reflect inclusions of non-target minerals or fractures.

Detection limits and reproducibility values are listed in Table 4. The values are based on 106 laser ablation analyses of both the NIST 610 and NIST 612 glasses. Reproducibility is

expressed as relative standard deviation % (RSD%), which is calculated from 2 standard errors (2SE). The detection limits were calculated by the Iolite Software Program (Paton et al. 2011) and used the Longerich et al. (1996) method.

Table 4: LA-ICP-MS Reproducibility and Detection Limits Based on NIST 610 and 612 Glass

	NIST 610		NIST 612	
Element	**Reproducibility %**	**Detection Limit (ppm)**	**Reproducibility %**	**Detection Limit (ppm)**
Li	7.53	0.18	9.23	0.19
Be	11.12	0.53	40.56	0.52
B	9.74	1.91	27.12	2.04
Na	7.07	3.43	5.98	3.57
Mg	7.21	0.27	14.74	0.27
Al	6.93	0.31	5.99	0.35
P	11.24	5.79	26.12	6.04
K	31.6	2.07	84.89	2.21
Ca	7.28	41.55	6.53	43.35
Sc	7.2	0.09	8.39	0.1
Ti	14.67	0.54	34.26	0.53
V	7.14	0.11	8.49	0.11
Cr	6.92	1.09	9.56	1.12
Mn	6.64	0.21	8.39	0.23
Fe	11.95	2.36	31.13	2.49
Ni	7.38	0.17	13.89	0.18
Cu	6.9	0.36	17.9	0.38
Zn	8.26	0.39	19.11	0.43
Ga	7.09	0.02	8.76	0.02
Ge	8.37	0.79	17.76	0.49
Rb	7.07	0.07	8.59	0.07
Sr	7.27	0	7.02	0.01
Y	7.25	0	7.38	0
Zr	7.43	0	16.46	0
Nb	6.59	0	9.73	0
Mo	7.73	0	12.85	0
Ag	7.57	0.06	10.28	0.05
Sn	7.02	0.37	9.08	0.38
Sb	7.32	0.14	8.66	0.08
Cs	7.53	0.04	9.37	0.04
Ba	7.05	0	11.74	0
La	6.79	0	6.91	0
Ce	6.29	0	6.52	0
Pr	6.54	0	6.29	0
Nd	6.95	0	9.55	0
Sm	7.31	0	10.13	0
Eu	6.92	0	7.4	0

Gd	7.71	0	10.49	0
Tb	7.35	0	7.04	0
Dy	7.71	0	9.11	0
Ho	7.62	0	7.21	0
Er	7.71	0	8.65	0
Tm	7.66	0	7.44	0
Yb	7.75	0	9.19	0
Lu	7.9	0	7.54	0
Hf	8.15	0	9.3	0
Ta	7.8	0	7.53	0
W	7.29	0.02	9.28	0.02
Au	9.35	0.22	16.67	0.22
Pb	7.16	0.02	8.1	0.02
Bi	7.29	0.03	7.33	0.03
Th	7.48	0	7.29	0
U	7.41	0	7.55	0

Chapter 4 - Results

The mineralization on the *Thank You Lord* claim is found within the California Granite first mapped by Shannon (1988) (Fig. 2). Figure 7A shows the California Granite cliffs looking southwest from the four-wheel drive road at the base of the Antero switchbacks. Figure 7B shows the California Granite cliffs looking up from their base. The cliffs are intensely fractured, reflecting the local faulting that was mapped by Sharp (1976). The base of the cliffs occurs at an elevation of approximately 3658 m and the outcrop extends to approximately 3810 m, for an outcrop height of ~150 m.

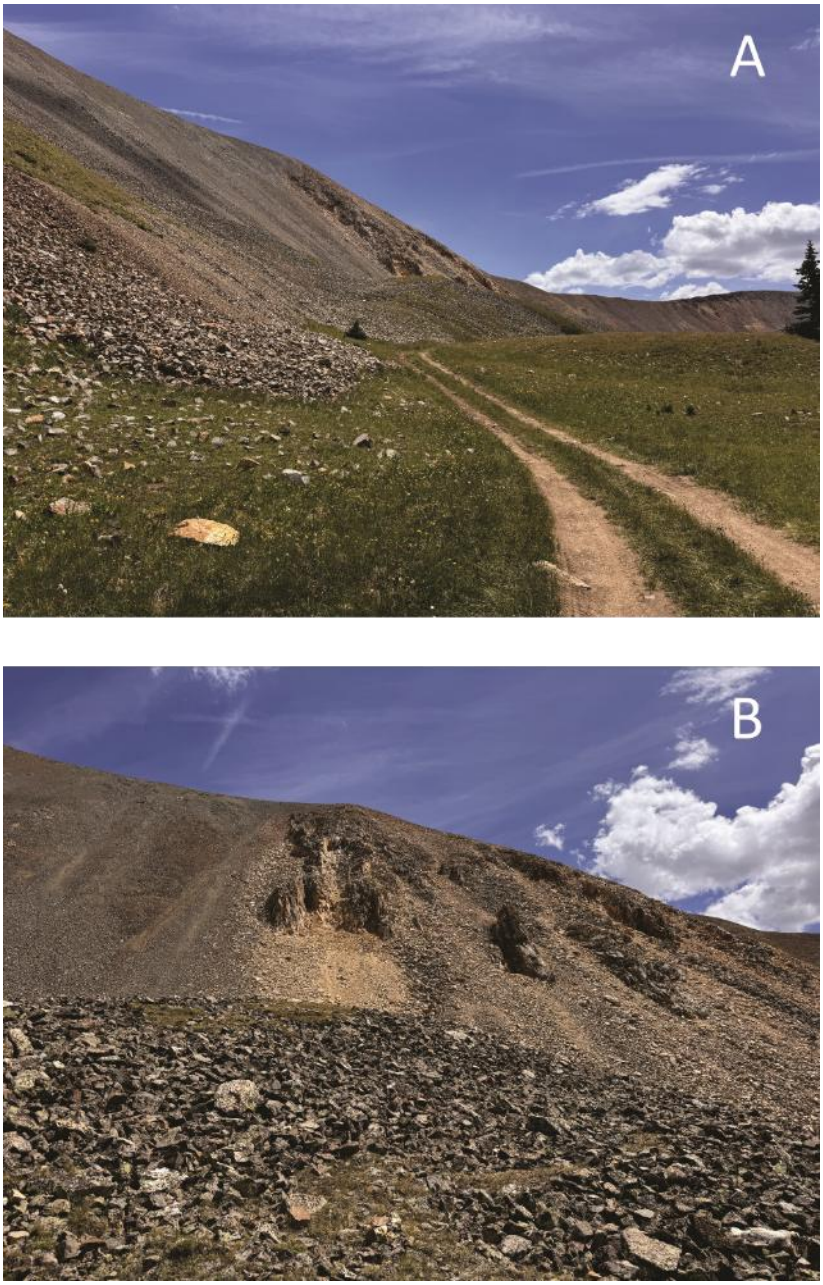


Figure 7: Images of the California Granite cliffs on the southwest ridge of Mount Antero. A) Southward view of the cliffs jutting out of talus. B) A view looking up at the California Granite cliffs from the base of the talus slope with a vertical relief of ~250 m.

Pegmatite Mineralization on the *Thank You Lord* claim

The pegmatites on the *Thank you Lord* mining claim occur as spheroids (Fig. 8). All pegmatites observed have the same primary mineralogy: quartz, plagioclase feldspar, alkali feldspar, muscovite, and sometimes beryl. Accessory minerals in the pegmatites include fluorite, bertrandite, phenakite, and biotite. Biotite is mainly restricted to the California Granite; it occurs only sparsely (<5%) in the pegmatites. The beryl ranges from blue to green and includes some gem-quality blue beryl crystals. The quartz ranges from colorless to smoky to milky. The spatial distribution of the pegmatites on the claim could not be linked to any discernable distribution pattern or structural element that might aid future mineral exploration. The best indicator that a beryl-rich pegmatite is near is finding "blue granite", which is granite that appears blue from the ~5% of beryl occurring alongside the quartz, plagioclase and alkali feldspar, and muscovite. The beryl that occurs in this blue granite is the same crystal size as the other minerals contained in the granite at ~1-2 mm. In contrast, the pegmatite spheroids found range from 5 to 75 cm in diameter and include crystals that range from 5 to 20 mm (Fig. 6).

Antero pegmatites exhibit unidirectional solidification textures (USTs) (Fig. 9) with definitive textural zones caused by areas of different cooling and nucleation within the pegmatite. These textural zones are primarily comprised of alkali feldspar (~2 mm in size) that exhibits perthite textures, plagioclase feldspar (~0.2 mm), and quartz (~1-2 mm), with little beryl until the core zone. An Antero pegmatite UST commonly will have textural areas of aplite, intermediate areas and core areas (Figs. 10 and 11). The intermediate zones lie between the aplite and core and contain crystal sizes roughly the same as the host granite. Figure 9A shows pegmatite sample LE25-1, which has a core zone containing beryl, whereas Figure 9B shows pegmatite sample LE25-7, which contains only quartz, alkali feldspar, and plagioclase feldspar.

The USTs of sample LE25-1 can be divided into five distinct zones (Fig. 10). Sample LE25-7 is divided into four distinct zones (Fig. 11). The beryl-rich USTs observed do not contain more than 5% beryl through the aplite and intermediate zones. The only zone of the UST besides the host granite that contains >5% beryl is the core. Beryl-poor USTs contain no beryl through any part of the USTs.

Samples collected, with brief descriptions, are listed in Table 5. Photos of each sample are provided in Figures 9-23. Other thick section pictures are available in Appendix A.

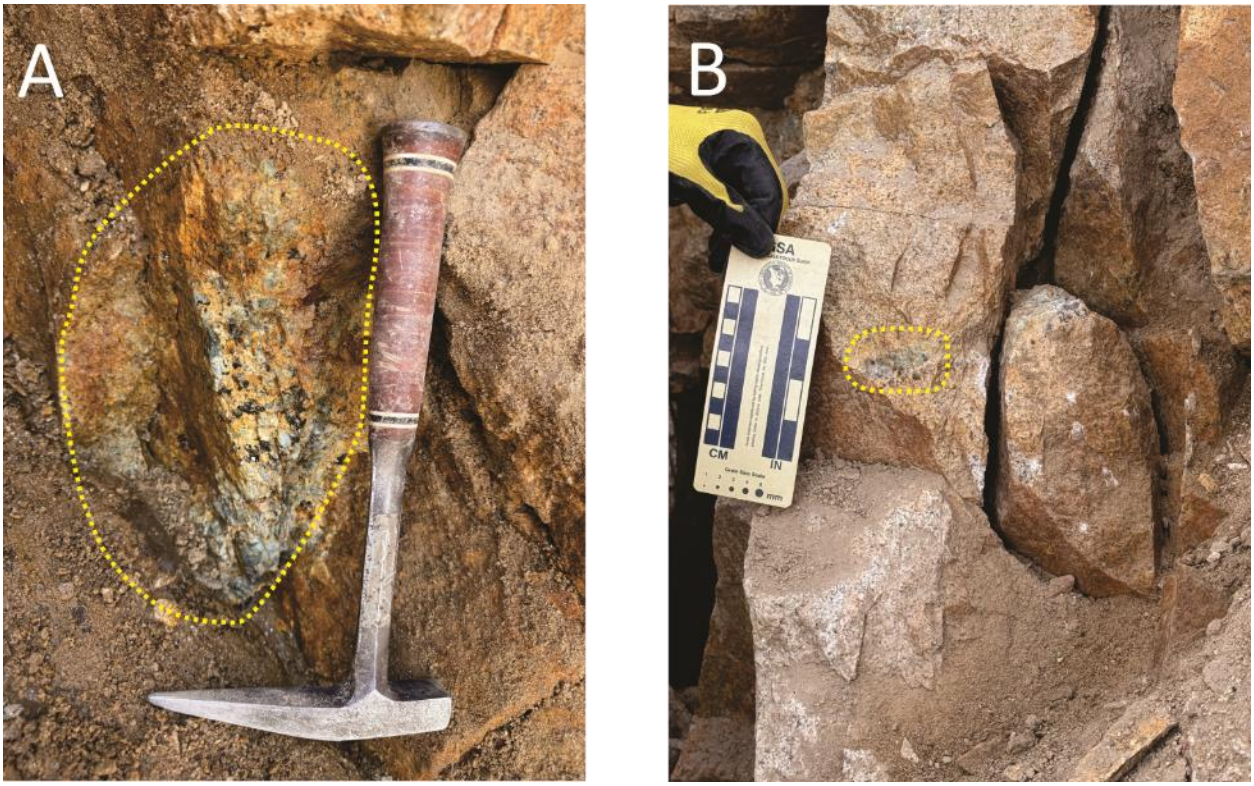


Figure 8: Pegmatite spheroids on Mount Antero vary in size but share similar mineralogy. A) A spheroid pegmatite spheroid that is approximately 75 cm in diameter outlined in yellow. B) A spheroid pegmatite spheroid that is approximately 5 cm in diameter outlined in yellow.

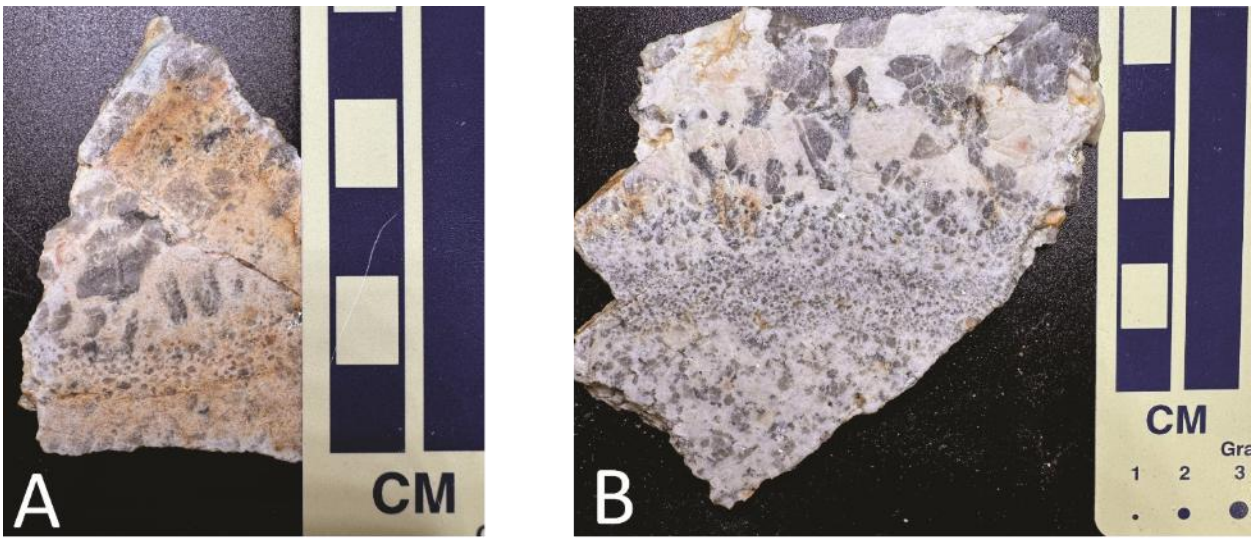


Figure 9: Common pegmatite unidirectional solidification textures (USTs) from Mount Antero. A) Sample LE25-1: A beryl, quartz, alkali feldspar, and plagioclase feldspar pegmatite UST that contains five zones. B) A quartz, alkali feldspar, and plagioclase feldspar pegmatite UST that contains five zones.

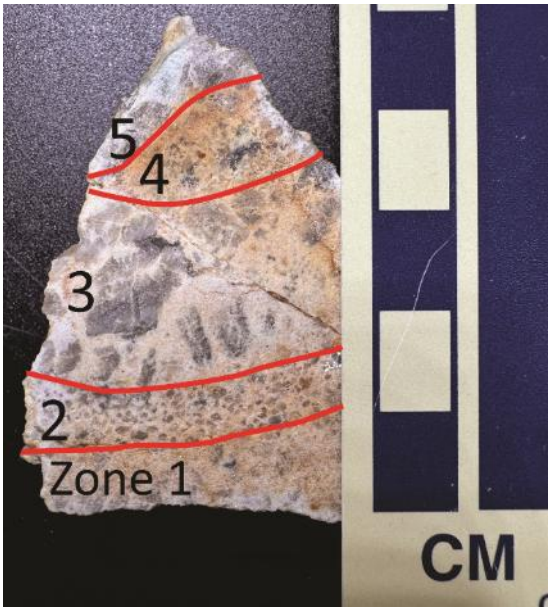


Figure 10: Sample LE25-1 is beryl-bearing UST from Mount Antero divided into five zones. Zone 1 granite to aplite transition, with abundant plagioclase feldspar, alkali feldspar, and quartz all ~1-2 mm. Zone 2 aplite zone with finer quartz ~1 mm and plagioclase and alkali feldspar ~100-150 μm. Zone 3 intermediate section made of 5-10 mm quartz grains and interstitial plagioclase and alkali feldspar, quartz, and beryl all ~100-150 μm. Zone 4 aplite with quartz, beryl, and plagioclase and alkali feldspar ~100-150 μm. Zone 5 core zone with 5-10 mm grains of quartz and beryl.

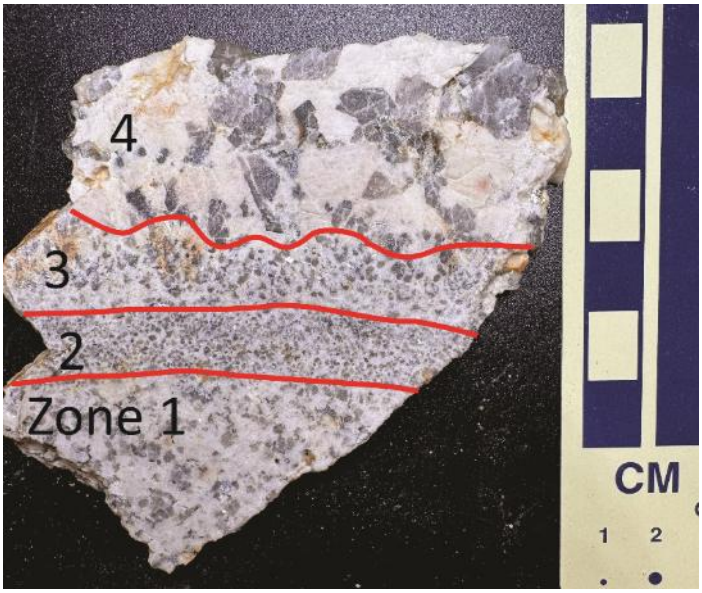


Figure 11: A quartz, plagioclase feldspar, and alkali feldspar UST from Mount Antero divided into four zones. Zone 1 granite to aplite transition with abundant plagioclase, alkali feldspar, and quartz with grains ~1-2 mm. Zone 2 aplite with finer quartz, alkali feldspar, and plagioclase feldspar~0.25-0.5 mm. Zone 3 intermediate zone with 1mm grains of alkali feldspar, plagioclase feldspar and quartz. Zone 4 core zone with 5-10 mm grains of quartz, alkali feldspar, and plagioclase feldspar.

Sample Descriptions

Table 5: Sample numbers, descriptions, and corresponding figures used in this study.

Sample	Description	Designation	Corresponding Figures
LE25-1	Pegmatite UST ~ 6 cm across that contains beryl, plagioclase feldspar, and quartz. Variations in crystal size define different zones including granite, aplite, intermediate, and core. Beryl is not readily evident except in the core zone. The feldspar and quartz are stained orange from oxidation.	Beryl-Rich	Figure 9A Figure 10 Figure 12
LE25-2	Spheroid mass of gem-quality blue beryl ~5 cm across that is fractured by bertrandite laths and interstitial clay minerals. Referred to as "honeycomb" by local prospectors. The blue beryl is fractured to the point that it is friable and produces blue grains ~0.5-1 mm in size. Sample fizzes due to secondary calcareous clays.	Beryl-Rich	Figure 13
LE25-3	Pegmatite and California Granite together. The California Granite within ~1 cm of a pegmatite consists of 44% quartz, 44% plagioclase feldspar, 5% beryl, 5% biotite, 1% clay minerals, and 1% bertrandite. Most beryl crystals are partially replaced by bertrandite. The quartz exhibits both feathery and mosaic textures. The clay minerals are found near the beryl and bertrandite zones. The outside weathering rind is an orange and tan color. All grains range from 0.5-2 mm in length. The pegmatite contains euhedral blue beryl crystals that are up to 1.5 cm across. Quartz and feldspar up to 0.5 cm in size are also present. No USTs exist in this sample.	Beryl-Rich	Figure 14
LE25-4	Pegmatite core zone consisting of large 2-4 cm quartz crystals that transition into fractured blue beryls ~0.5-1 cm in length. Some beryl is partially replaced by bertrandite laths ~1 mm in size.	Beryl-Rich	Figure 15
LE25-5L	Pegmatite spheroid that contains green beryl in the core zone and is also comprised of quartz and feldspar. The entire pegmatite is ~6 cm across. The transition from host California Granite to pegmatite happens over a 2-3 mm boundary. No pegmatite UST zones exist besides granite and core zone.	Beryl-Rich	Figure 16 Figure 19

LE25-5C	Pegmatite spheroid that contains blue-green beryl in the core zone and is also comprised of quartz, alkali feldspar, and plagioclase feldspar. The entire pegmatite is ~5 cm across. The transition from host California Granite to pegmatite occurs over a 2-3 mm boundary. No pegmatite UST zones exist besides granite and core zone.	Beryl-Rich	Figure 17 Figure 19
LE25-5R	Pegmatite spheroid that contains blue beryl in the core zone and is also comprised of quartz, plagioclase, and alkali feldspar. The entire pegmatite is ~5 cm across. The transition from host California Granite to pegmatite happens over a 2-3 mm boundary. No pegmatite UST zones exist besides granite and core zone.	Beryl-Rich	Figure 18 Figure 19
LE25-6	Coarse pegmatite core zone sample that consists of 54% quartz, 35% blue beryl, 9% feldspar, 1% muscovite and 1% bertrandite. Outside of sample appeared to be completely quartz and feldspar and when cut exposed anhedral beryl crystals. Both quartz and beryl crystals in the sample are ~0.5-2 cm in length. Feldspar grew interstitially to the beryl and quartz.	Beryl-Rich	Figure 20
LE25-7	Pegmatite UST consists of quartz, alkali feldspar, and plagioclase feldspar. No beryl exists in this sample. The UST contains four zones: granite, fine aplite, coarse aplite, and a core. Each zone is separated due to a change in crystal size with a distinct boundary that can be seen macroscopically. The UST evolves from granite to the core zone in ~4 cm.	Beryl-Poor	Figure 9B Figure 11
LE25-8	Pegmatite core zone ~6 cm across that contains beryl (~0.5 cm), quartz (~1 cm), plagioclase feldspar (~100-150 μm), bertrandite (~100-150 μm), muscovite (~100-150 μm), and clay minerals (~5-10 μm). This sample contains vugs ~0.5-1 cm in length. A black metallic mineral, likely a sulfide, ~0.5 mm in length was seen by hand lens in a vug while in the field but after cutting the sample for preparation it was unable to be located. Beryl appears blue and green in this sample and is altering to bertrandite.	Beryl-Rich	Figure 21
LE25-9	Pegmatite core zone ~6 cm across that contains beryl (~0.5 cm), quartz (~1 cm), plagioclase feldspar (~100-150 μm), bertrandite (~100-150 μm), muscovite (1 mm), and clay minerals (~5-10 μm). This sample contains vugs but no metallic minerals were noted when collected. Beryl appears blue and green in this sample and is altering to bertrandite.	Beryl-Rich	Figure 22
LE25-10	Single euhedral gem-quality crystal found as float. The crystal is 1-cm-long down the c-axis.	N/A	Figure 23

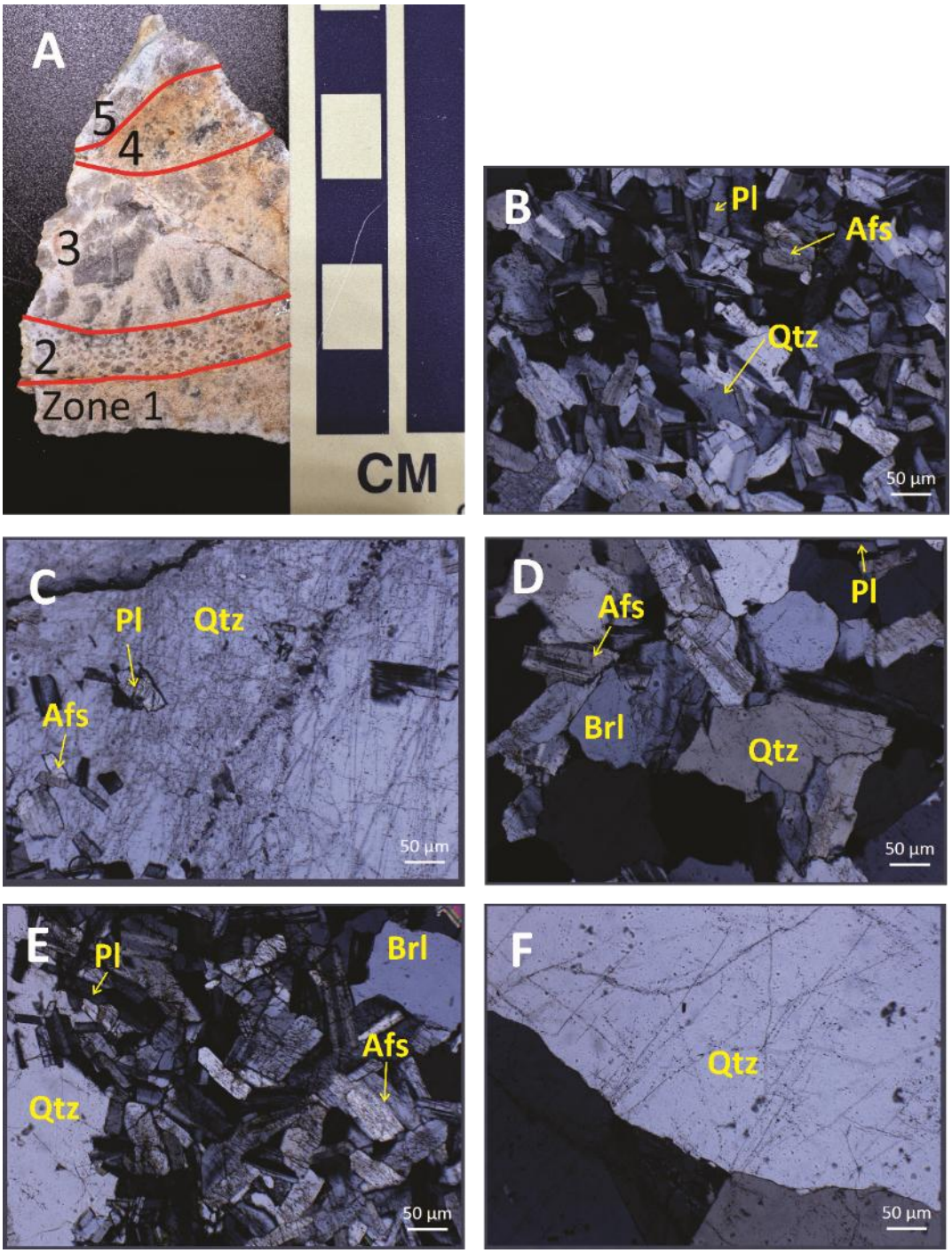


Figure 12: Sample LE25-1 which is a beryl UST consisting of beryl (Brl), quartz (Qtz), alkali feldspar (Afs), and plagioclase feldspar (Pl) with five distinct zones. A) LE25-1 divided into five zones. Panels B – F are photomicrographs of the various zones in crossed polarized light (XPL). B) Zone 1: Plagioclase feldspar and quartz with grain sizes ~100 µm. C) Zone 2: Quartz grains ~600 µm with interstitial plagioclase ~50 µm. D) Zone 3: Grains of quartz, plagioclase, and beryl ~100-150 µm. E) Zone 4: Grains of quartz, plagioclase, and beryl ~50-100 µm. F) Zone 5: Grains of quartz and beryl (not shown) ~5 mm.

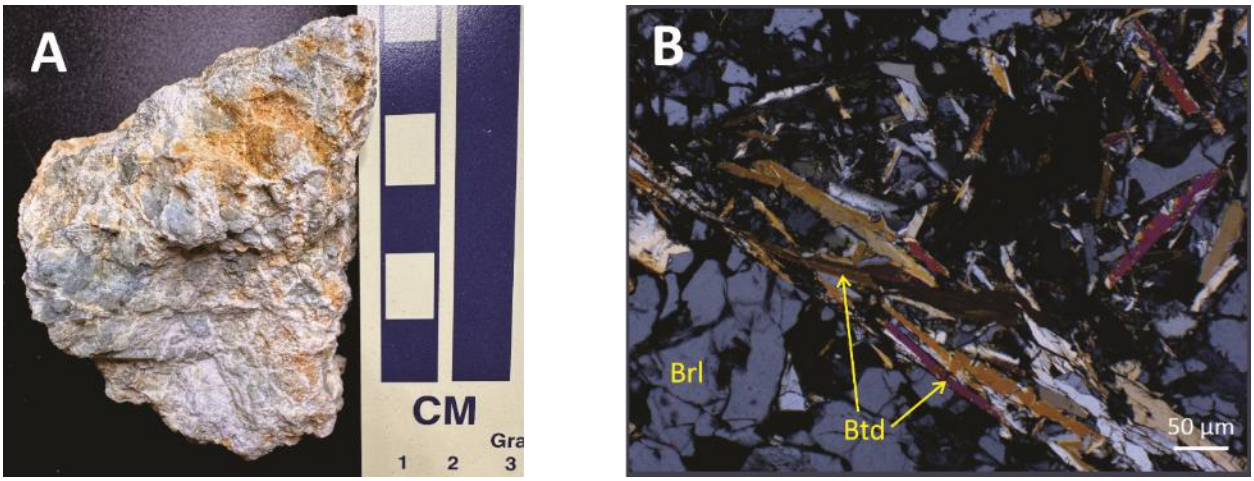


Figure 13: Sample LE25-2 is a mass of gem-quality blue beryl (Brl) which is fractured and partially replaced by bertrandite (Btd). A) Sample LE25-2. B) Photomicrograph of sample LE25-2 in XPL showing fractured beryl and elongated laths of bertrandite.

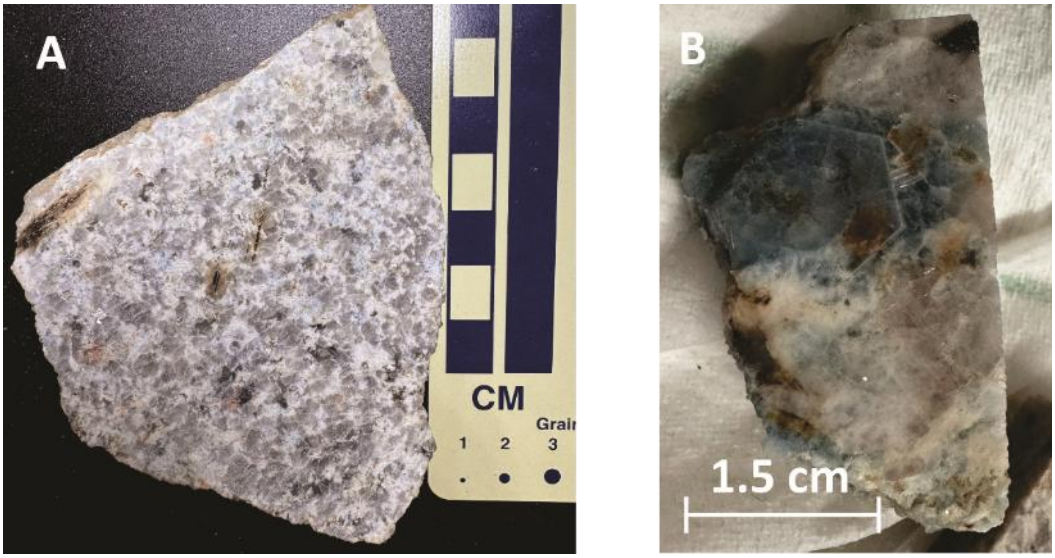


Figure 14: Sample LE25-3 California Granite and pegmatite. A) The California Granite is 44% quartz, 44% plagioclase feldspar, 5% beryl, 5% biotite, 1% clay minerals, and 1% bertrandite. Most beryl crystals are partially replaced by bertrandite. The clay minerals are found near the beryl and bertrandite zones. The blue crystals are blue beryl (e.g., “blue granite”. B) Pegmatite core zone with euhedral blue beryl crystal ~1.5 cm across.



Figure 15: LE25-2 are 3-cm-wide quartz crystals capped by ~1 mm crystals of bertrandite and beryl.

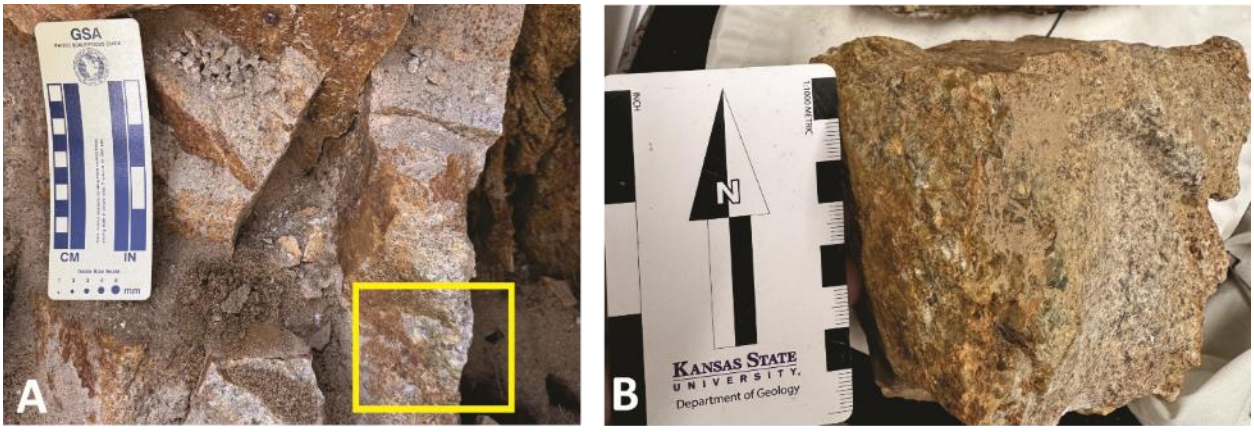


Figure 16: Sample LE25-5L green beryl pegmatite. A) Pegmatite spheroid in situ with the pegmatite outlined in yellow, within California Granite host. B) Sample taken from the field before being sliced by a rock saw.

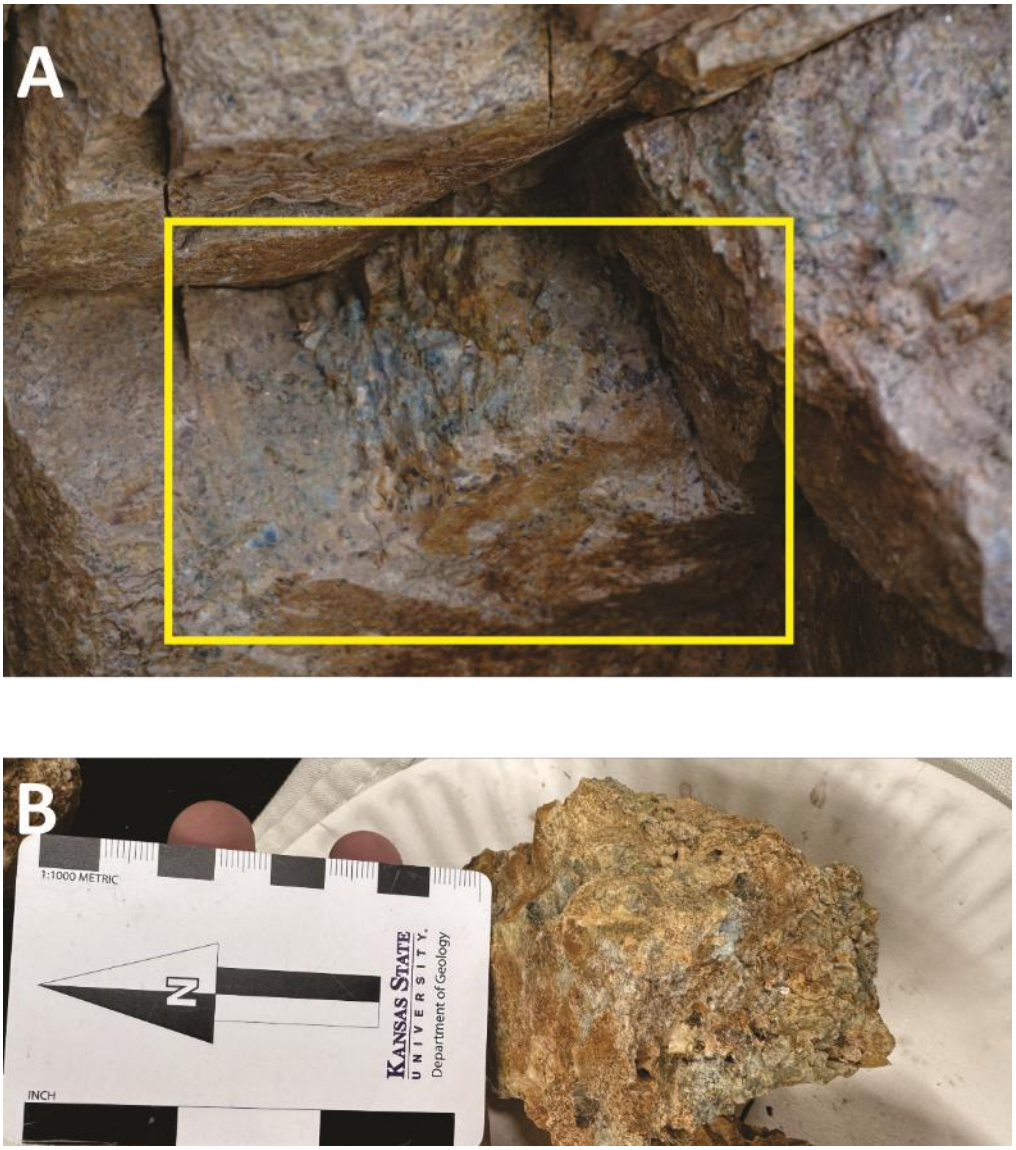


Figure 17: Sample LE25-5C which is a blue beryl pegmatite. A) Pegmatite spheroid in situ with California Granite host rock, where the spheroid is ~5-cm-wide. B) Sample taken from the field before being cut by a rock saw.

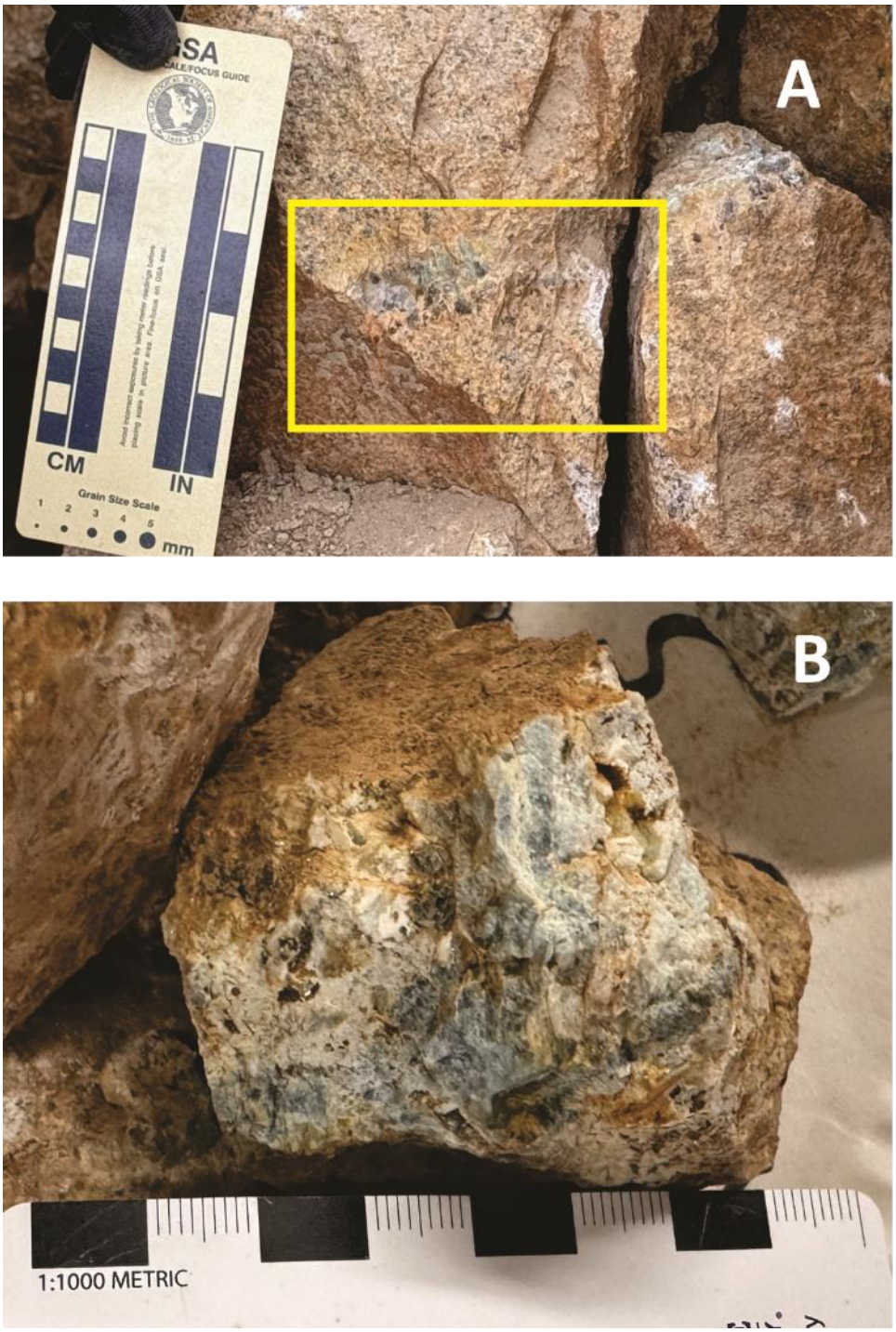


Figure 18: Sample LE25-5R which is a green and blue pegmatite spheroid. A) Pegmatite spheorid in situ with California Granite host rock. B) Sample taken from the field before being cut by a rock saw.

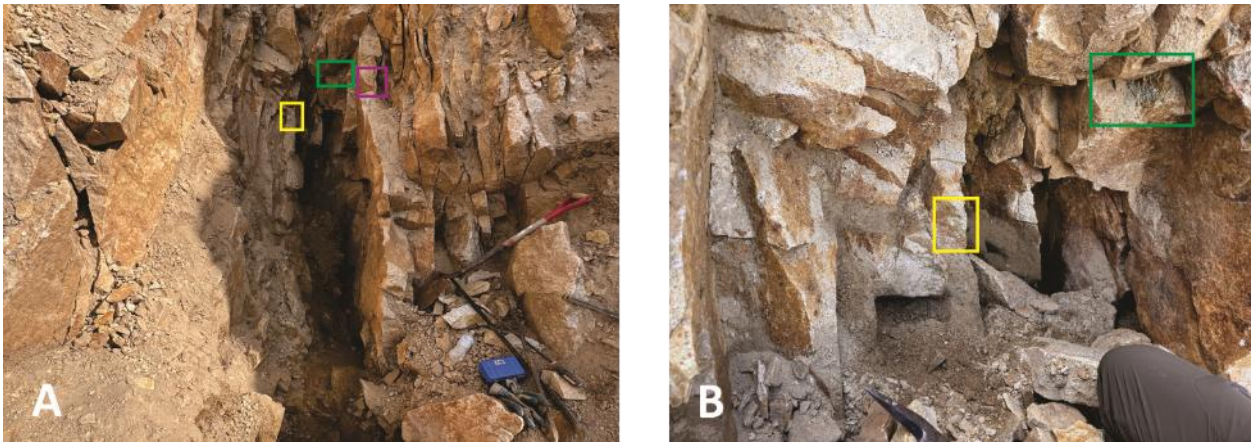


Figure 19: Cluster of single continuous pegmatite that consists of LE25-5L, 5C, and 5R. A) Pegmatite sample LE25-5L outlined in yellow, LE25-5C outlined in green, and LE25-5R outlined in purple. B) A closer picture of pegmatite LE25-5L in yellow and LE25-5C in green.



Figure 20: Sample LE25-6 is a pegmatite core zone. This sample consists of 54% quartz, 35% blue beryl, 9% feldspar, 1% muscovite and 1% bertrandite.



Figure 21: Sample LE25-8 is a pegmatite core zone which has a vuggy texture. Beryl (~50%) is mostly blue and all of it is anhedral. Also present is quartz (~40%), plagioclase feldspar (~5%), clays (~2%), bertrandite (~2%), and muscovite (~1%).

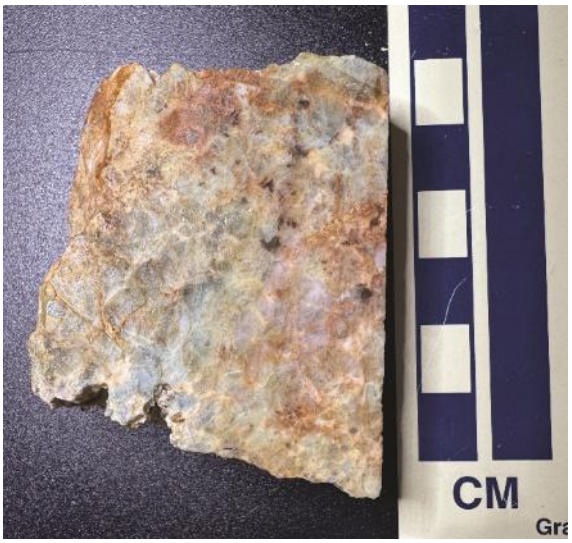


Figure 22: Sample LE25-9 is pegmatite core zone which exhibits a vuggy texture. The beryl (~55%) is anhedral, blue, and green. Also found in the sample is: quartz ~30%, muscovite ~5%, plagioclase feldspar ~5%, clays ~3%, and bertrandite ~2%.

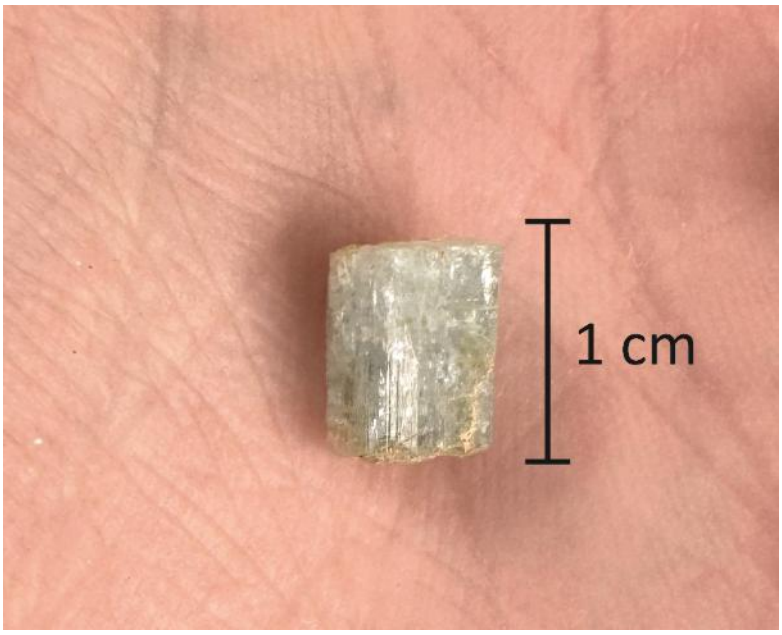


Figure 23: Sample LE25-10 is a euhedral gem-quality blue beryl (aquamarine).

Beryl Chemistry

Plots summarizing the data generated by LA-ICP-MS transects were produced for beryl (Figs. 24 to 31). A complete data set of the following LA-ICP-MS analyses can be found in the Supplemental Files. The chemical variations in the beryls are represented here by 13 elements: Li, Na, Mg, K, Sc, Ti, V, Mn, Fe, Zn, Ga, Rb, and Cs. The elemental transect plots of all measured beryl are displayed in Appendix A.

Euhedral, hexagonal-shaped beryl crystals show elevated levels of Li and Zn within the core of the crystal (Figs. 25, 28, and 31). Beryls that are anhedral show homogenous concentrations of Li and Zn (Fig. 29). Also shown in the plots are increases in Na and K that correlate with Rb spikes, which may indicate inclusions of plagioclase feldspar within the beryl. The anhedral beryls show nearly homogenous concentrations of Li, Mg, Sc, V, Mn, Fe, Zn, Ga, Rb, and Cs. Sample LE25-3A3 (Fig. 24) contains both euhedral and anhedral beryl. Figure 25 shows a photomicrograph of LE25-3A3.6 in both plane and cross polarized light. SEM BSE and

EDS imaging shows no zonation for the euhedral beryl LE25-3A3.6 (Fig. 26). The euhedral beryls show elevated concentrations of Li and Zn within the cores, while anhedral beryl shows more homogenous concentrations across the entire crystal. At the same time, the euhedral beryls have elevated concentrations in the rims of Mg, Sc, Ti, V, Mn, Fe, Ga, Rb, and Cs while the anhedral beryls are again more homogenous. The euhedral gem-quality beryl, LE25-10 (Figs. 30 and 31), also shows an elevated concentration of Li and Zn in the core with an elevated concentration of Mg, Sc, V, Mn, Fe, Ga, Rb, and Cs in the rim. Boron also has a slightly elevated concentration in the core when compared to the rim, in this sample, but data are discontinuous and some are below the detection limits, so B data is not shown on the graphs for any euhedral or anhedral beryls.

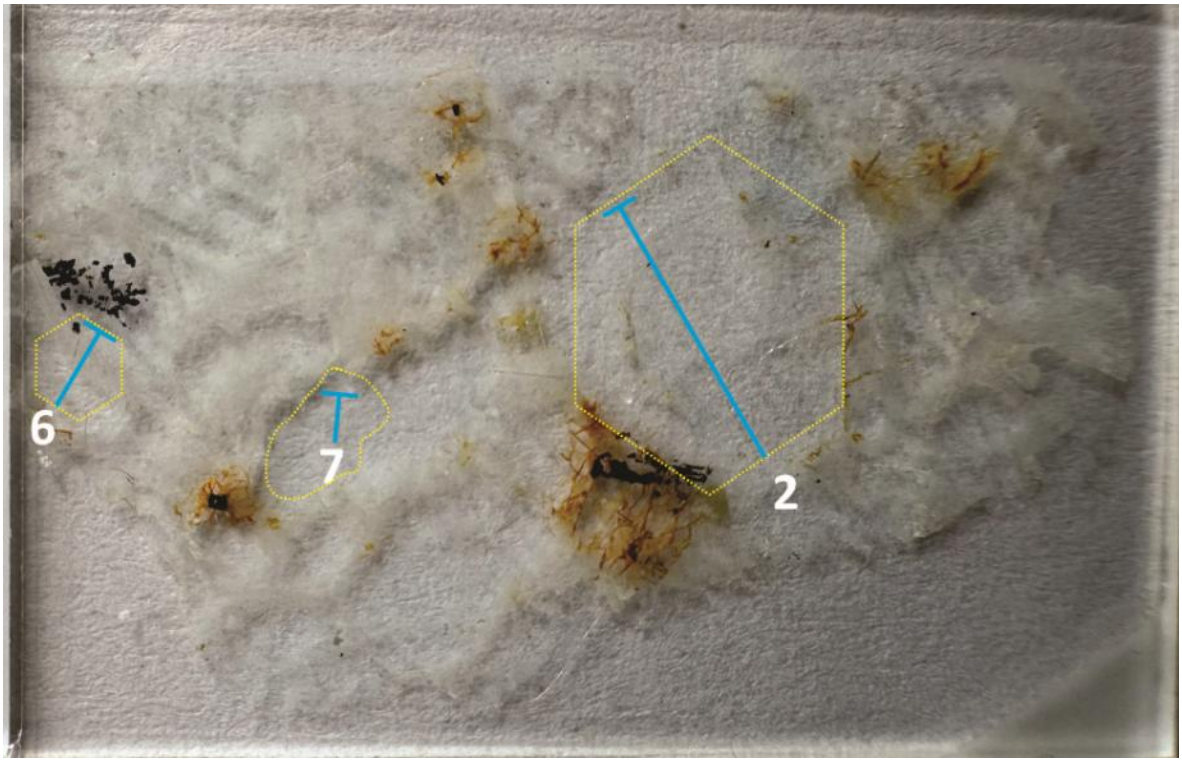


Figure 24: Sample LE25-3A3, 100 µm double polished thick section of a pegmatite core zone. Blue (beryl transect) lines and numbers correspond to LA-ICP-MS transect lines (e.g., LE25-3A3.6 is the blue line labeled 6). Analyzed beryls are shown outlined in yellow.

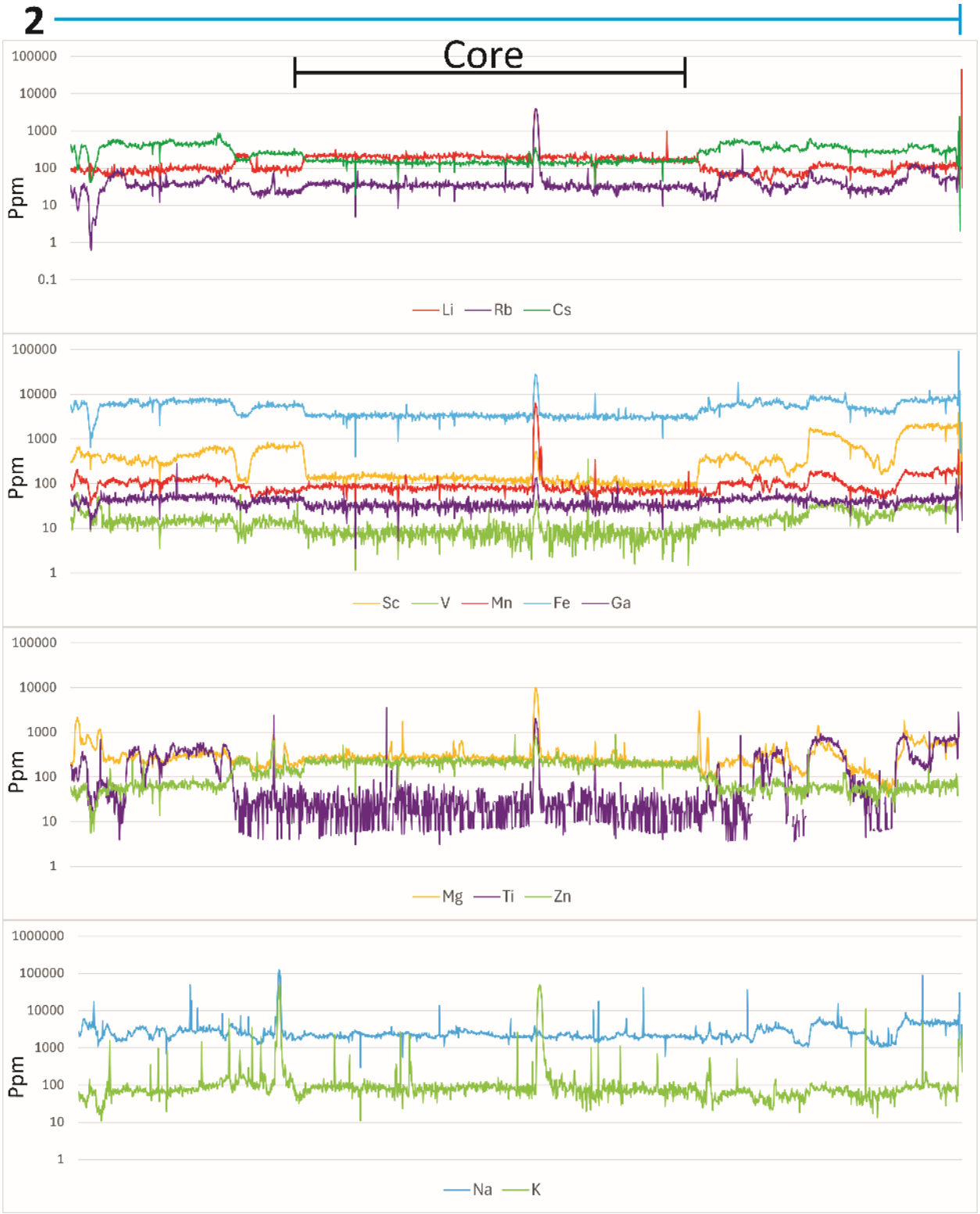


Figure 25: Sample LE25-3A3.2 is a euhedral beryl transect from the core zone of pegmatite 3A3 (Fig. 24). Spikes (e.g., abruptly elevated concentrations of Na, K, Mg, Ti) reflect the laser encountering inclusions of other minerals in the host beryl.

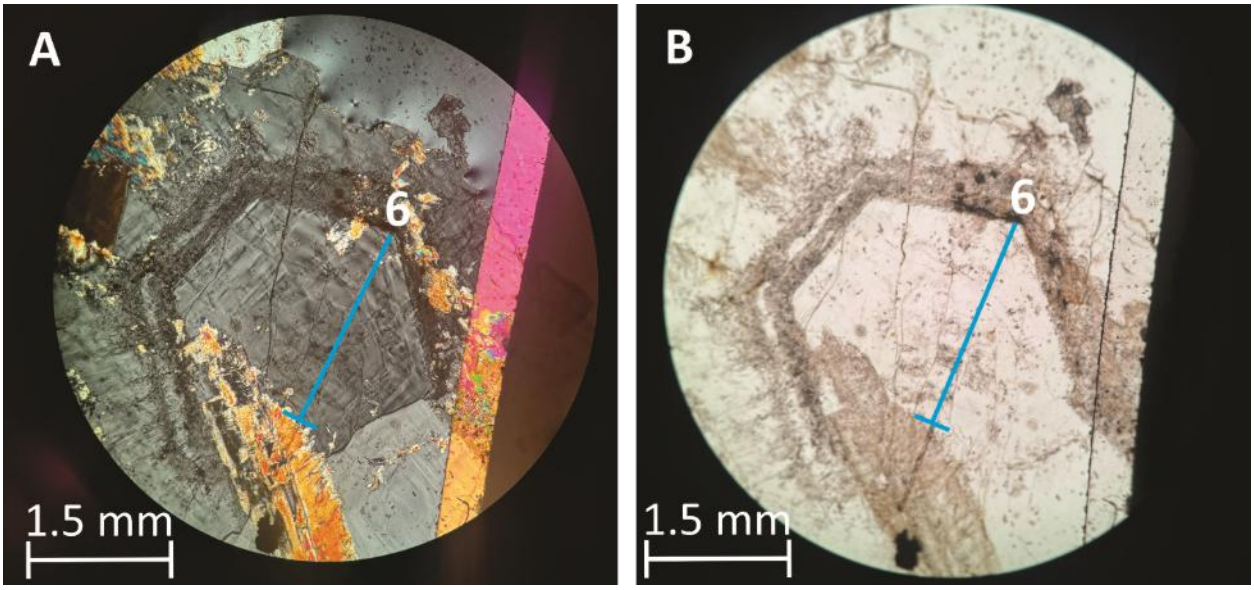


Figure 26: Sample LE25-3A3.6 in XPL (A) and PPL (B) which shows the LA-ICP-MS transect line.

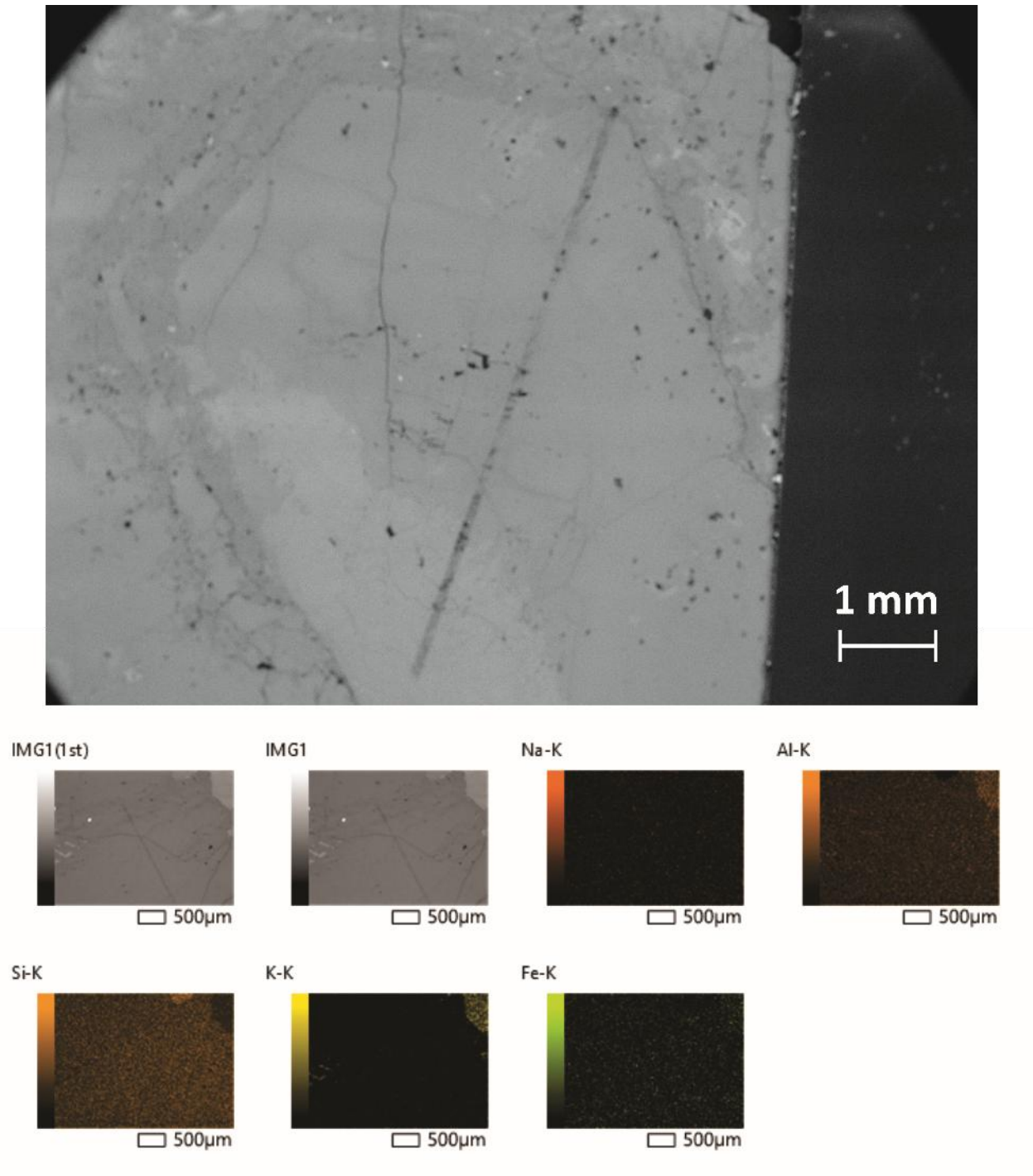


Figure 27: SEM image of LE25-3A3.6. Upper image is a back-scattered electron (BSE) image, while the Na, Al, Si, K, Fe images are elemental maps obtained via energy dispersive spectrometer.

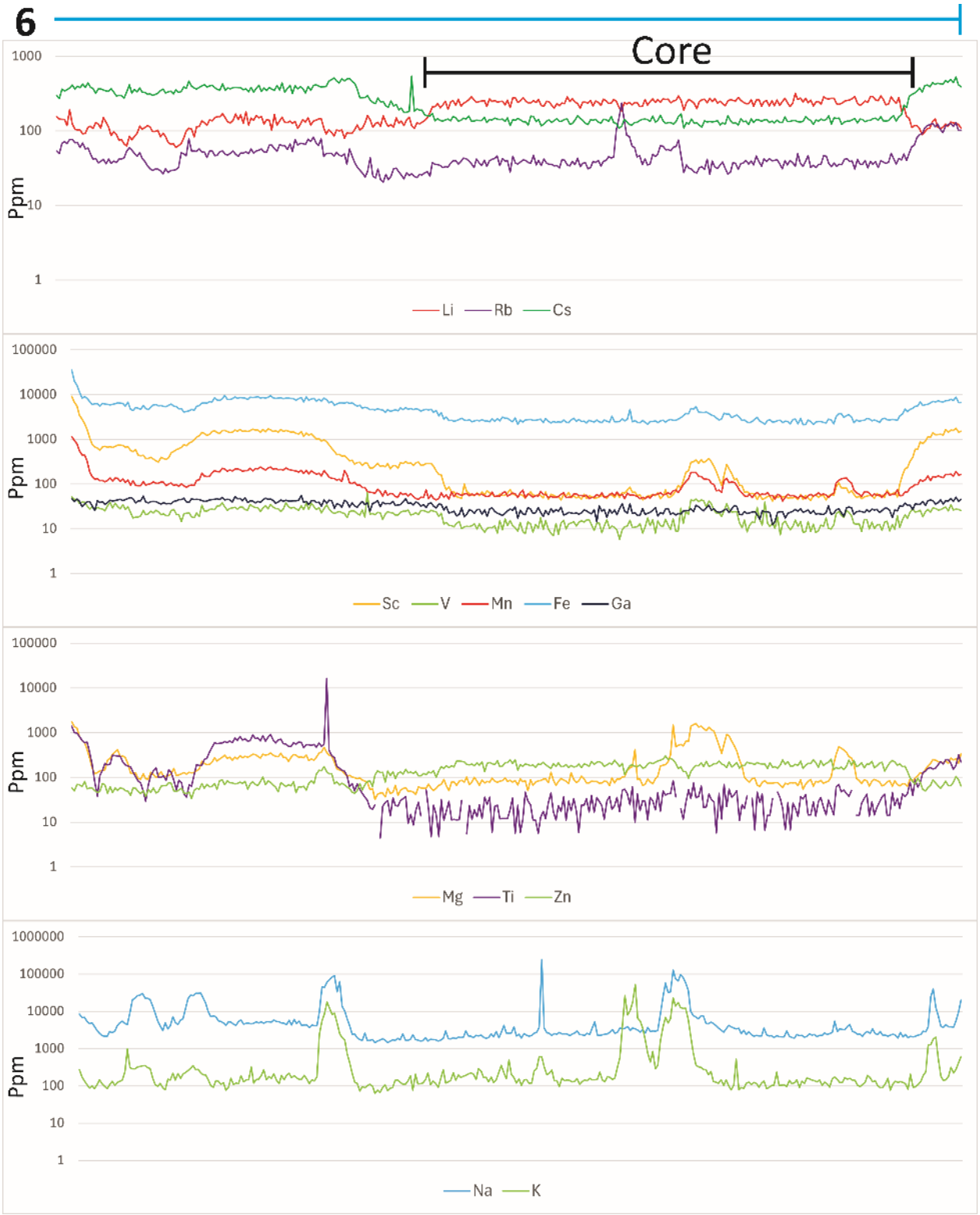


Figure 28: Sample LE25-3A3.4 is a euhedral beryl transect from the core zone of pegmatite 3A3 (Fig. 24).

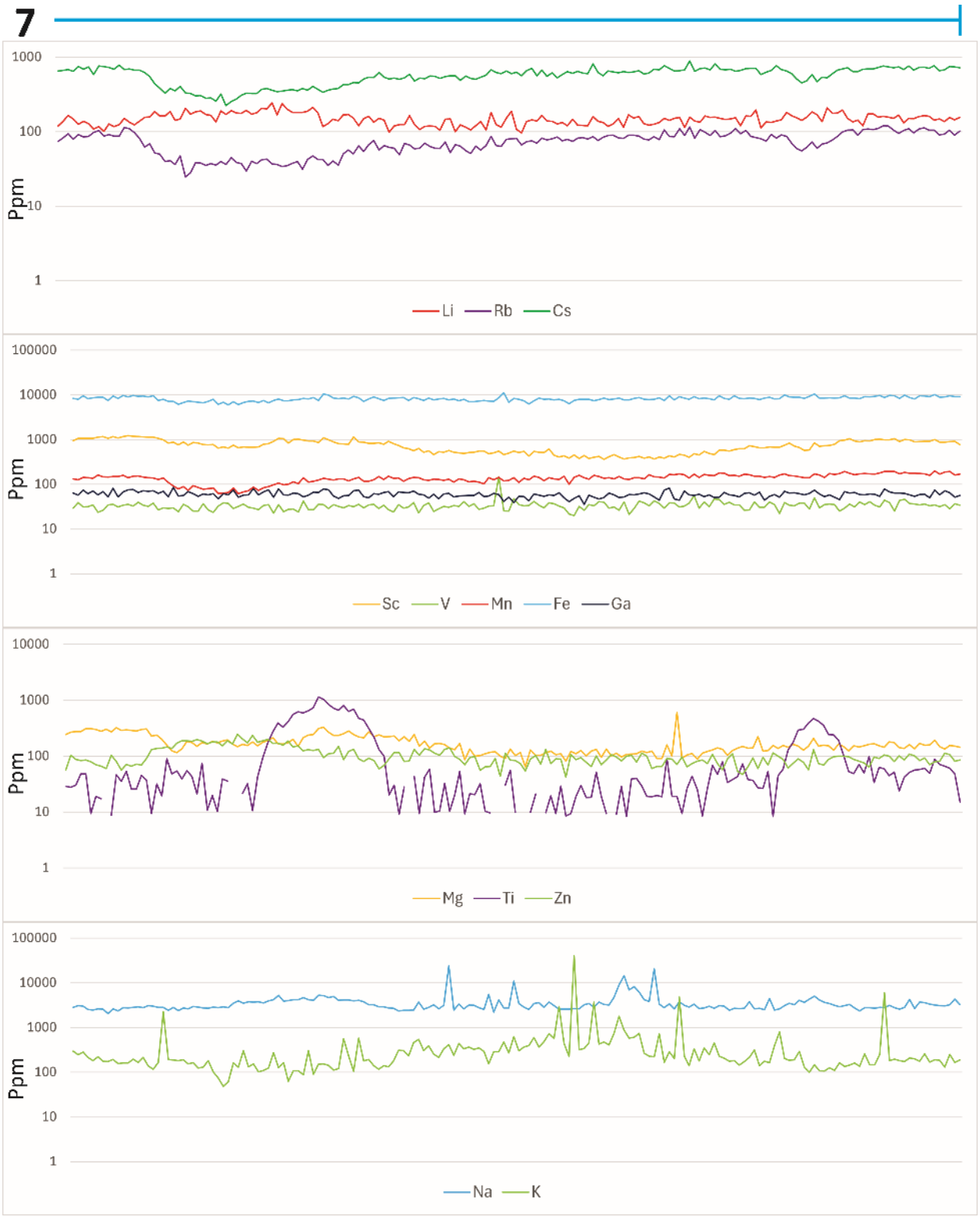


Figure 29: Sample LE25-3A3.7 is an anhedral beryl transect from the core zone of pegmatite 3A3 (Fig. 24).

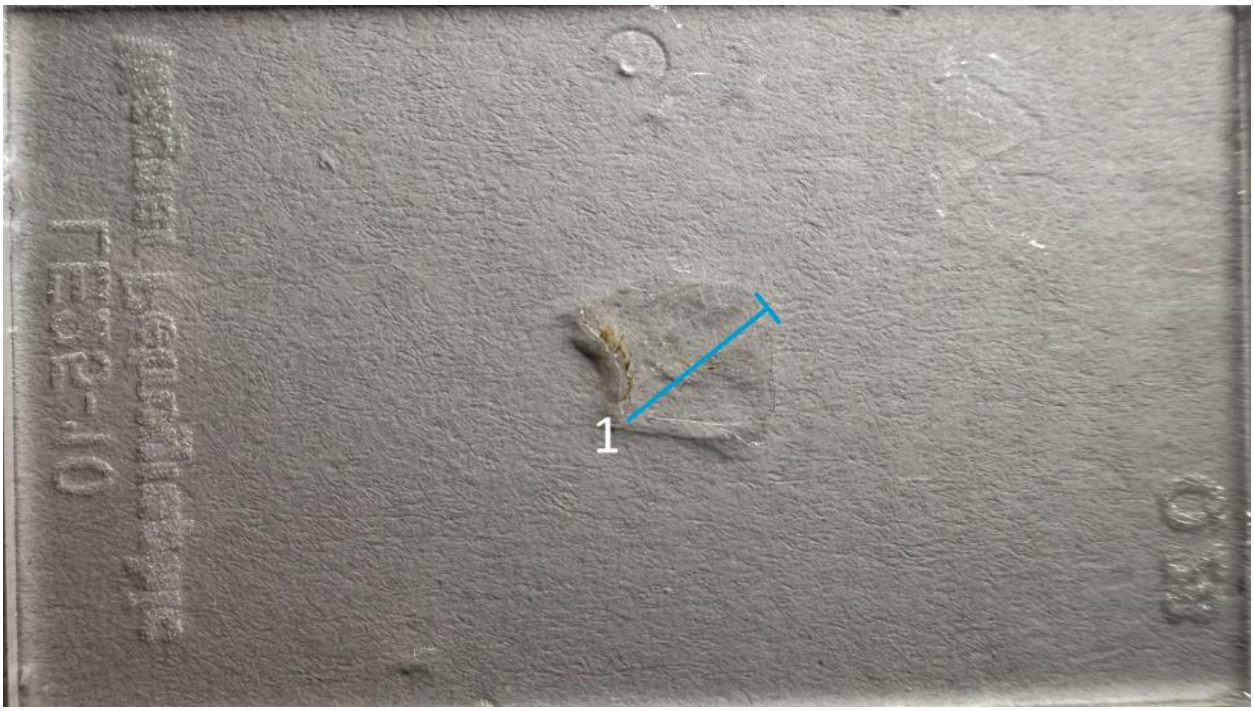


Figure 30: Sample LE25-10, 100 μm double polished thick section of a euhedral beryl. The blue (beryl transect) line labelled 1 corresponds to LA-ICP-MS transect line LE25-10.1.

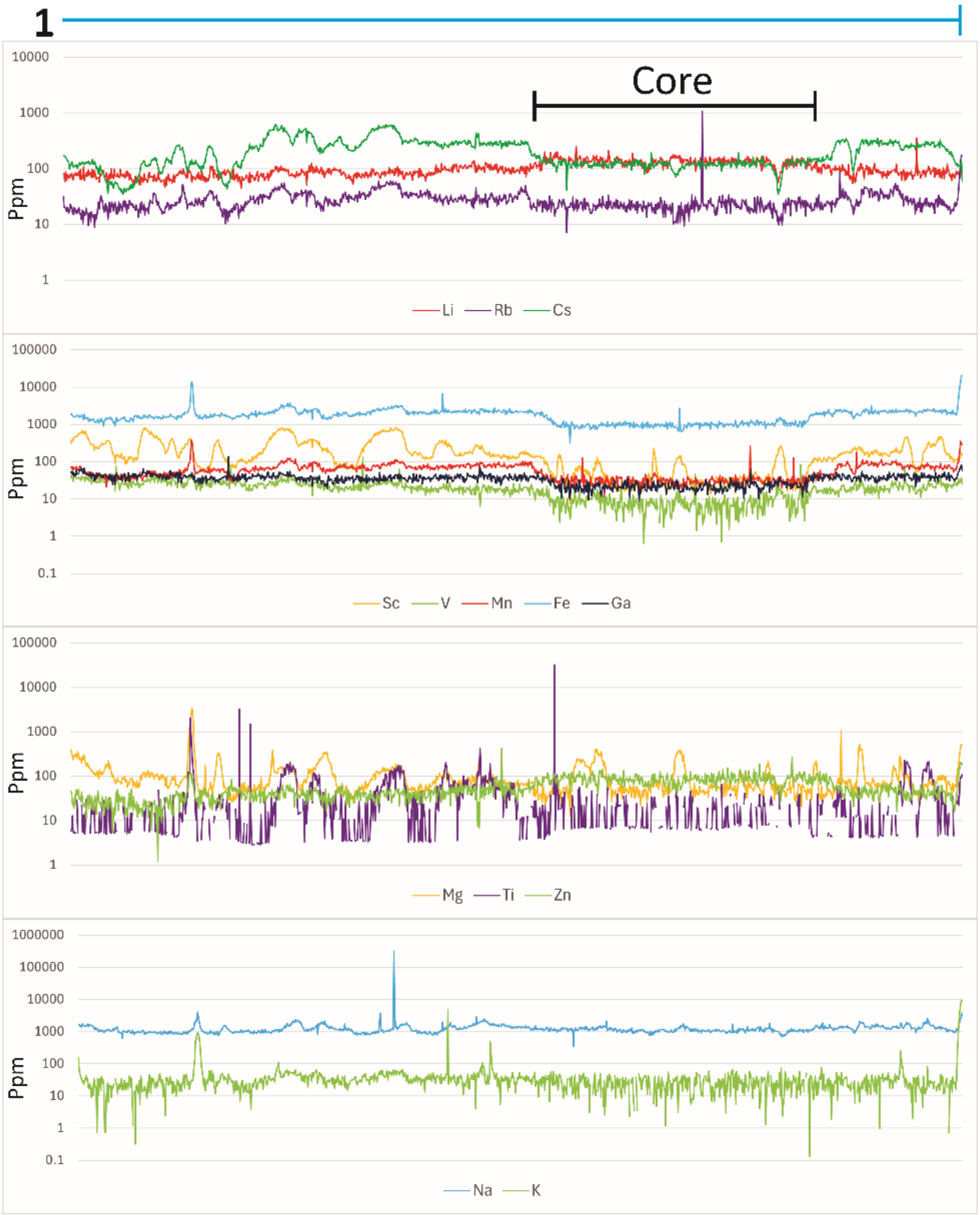


Figure 31: Sample LE25-10.1 is a transect from a euhedral gem-quality beryl crystal.

Na/Li and Cs are commonly used geochemical indicators of magma evolution in pegmatite beryls, where the higher Cs contents and lower Na/Li indicate crystallization of the beryl. When Mt. Antero beryl averages of Na/Li versus Cs are plotted on an X-Y plot (Fig. 32), euhedral beryl cores are the most primitive. The most fractionated beryls (e.g., highest Cs in this case) are the anhedral beryls and euhedral beryl rims. When these values are plotted on the Na/Li versus Cs plot after Černý (2002) (Fig. 33), the Mt. Antero beryls plot within Field A, "geochemically primitive pegmatites."

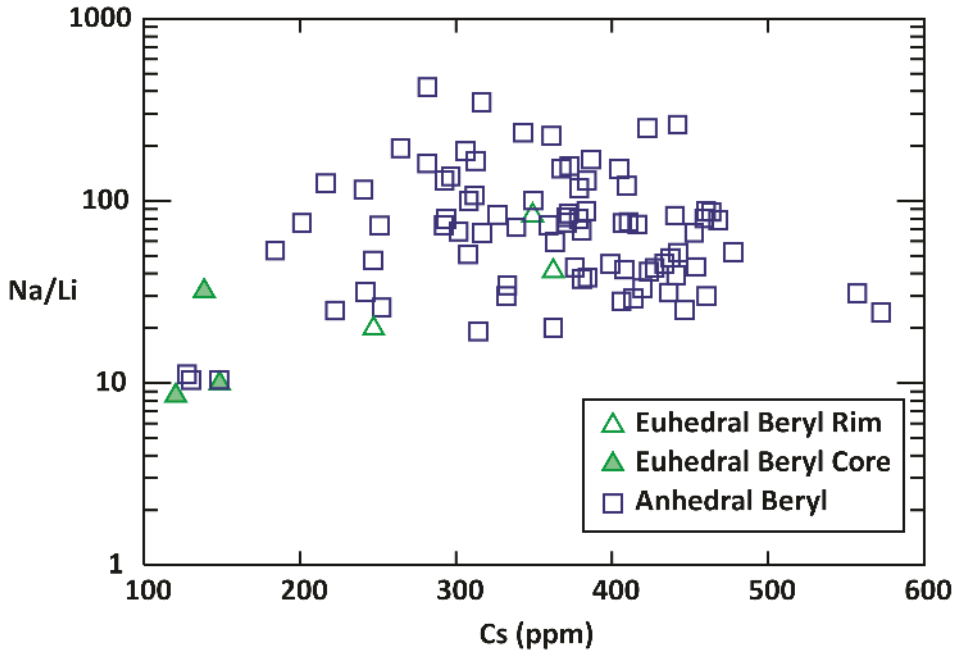


Figure 32: Bivariate graph with beryl averages of Na/Li versus Cs (ppm) representing euhedral beryl rims, euhedral beryl cores, and anhedral beryls. Na/Li calculated from ppm values.

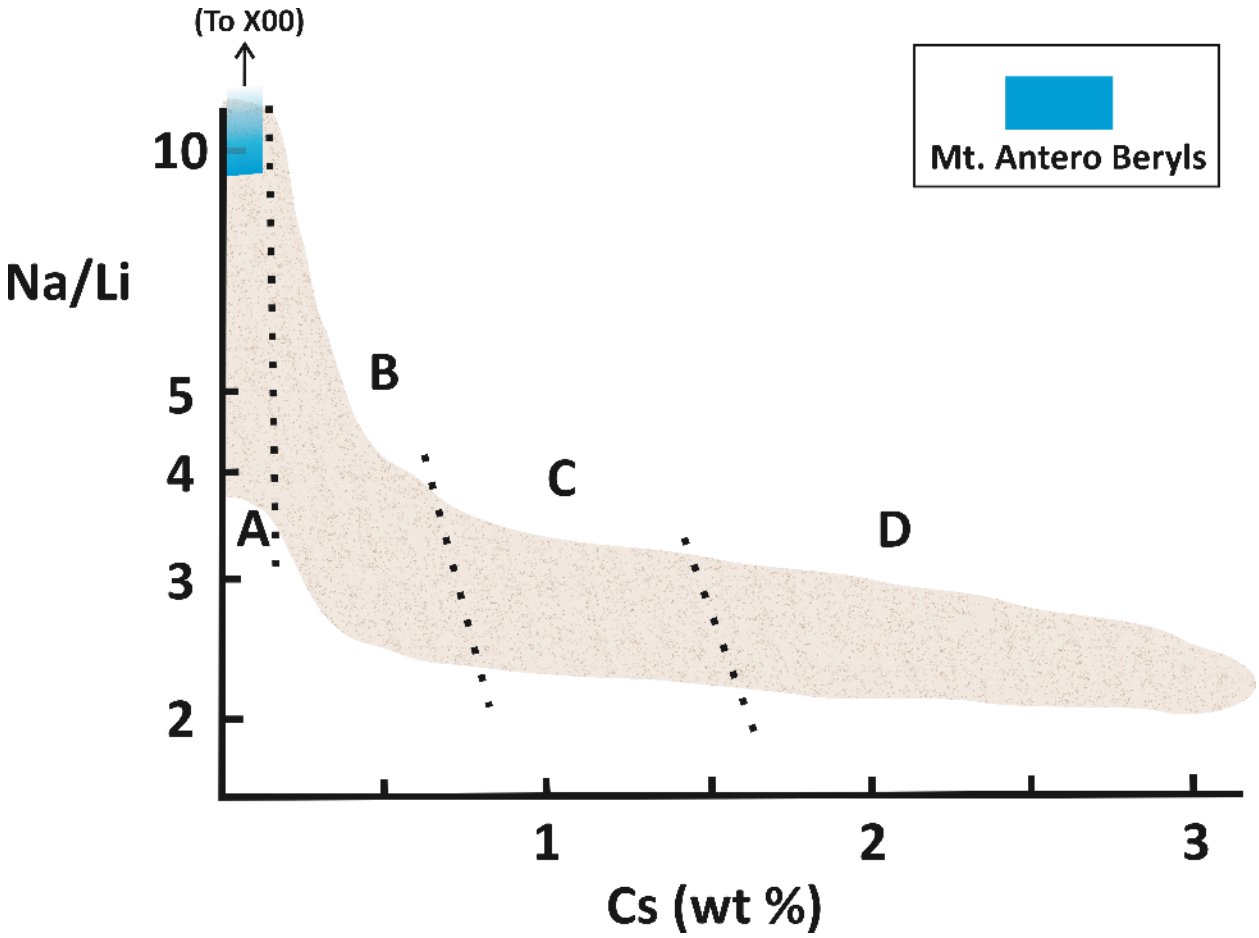


Figure 33: Beryl values of Na/Li versus Cs (Wt %) plotted on fields after Černý (2002). Letter fields refer to: A) Sterile pegmatites and geochemically primitive beryl-type pegmatites; B) Beryl-columbite-type pegmatites and geochemically evolved beryl-columbitephosphate pegmatites, C) Albite-spodumene and complex pegmatites; D) Highly fractionated Li, Cs, Ta-rich complex pegmatites. Na/Li calculated from ppm values.

Figure 34 shows the increase or decrease in concentrations of Li, Mg, Sc, V, Mn, Fe, Zn, Ga, Rb, and Cs between the core and rim of euhedral beryl LE25-3A3.2. The increases and decreases are also shown in the LA-ICP-MS transect graphs of LE25-3A3.2 (Fig. 25). Here, again Li and Zn decrease from core to rim, while Mg, Sc, Ti, V, Mn, Fe, Ga, Rb, and Cs increase from core to rim.

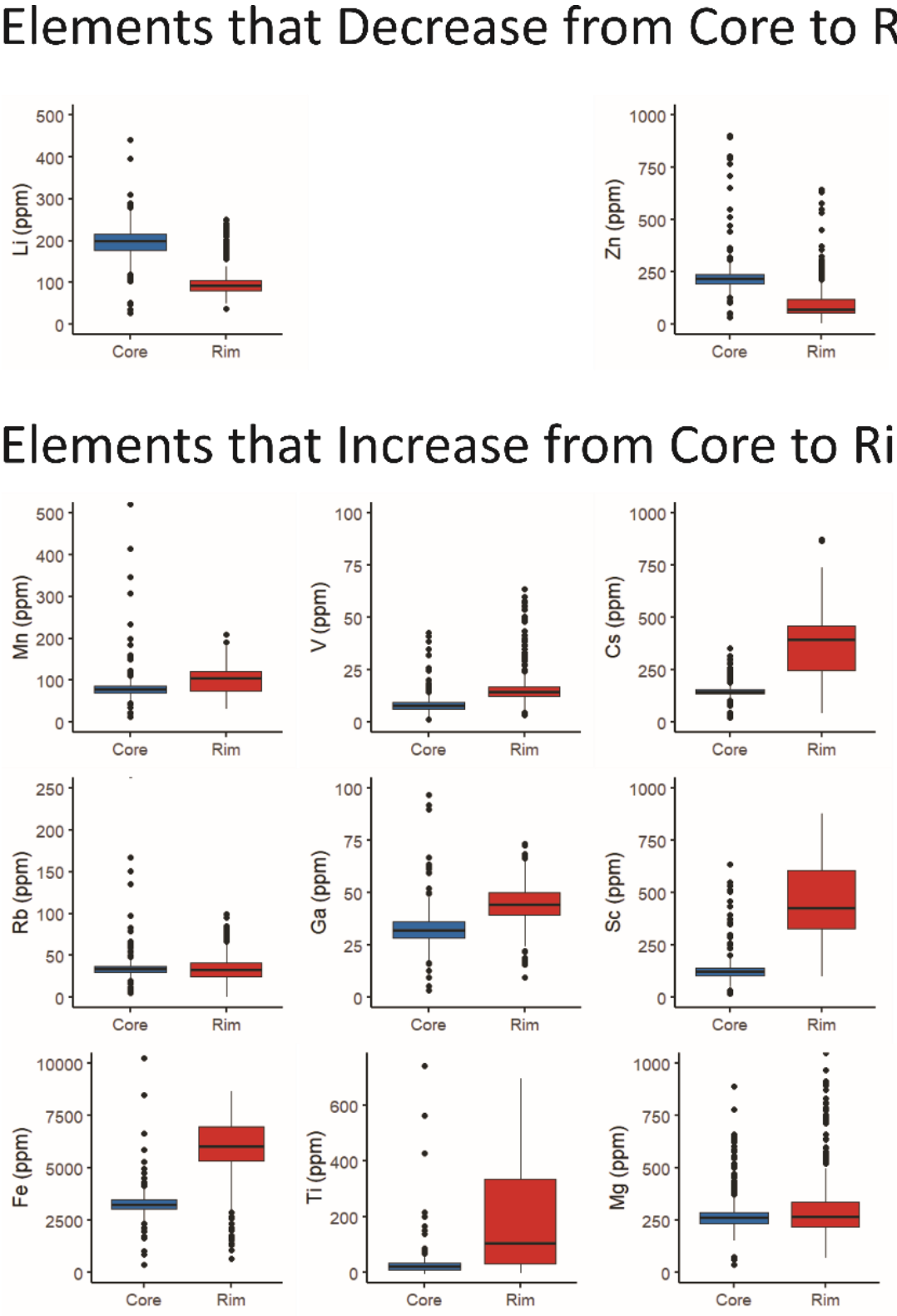


Figure 34: Box and whisker plots representing the concentration changes of Li, Mg, Sc, V, Mn, Fe, Zn, Ga, Rb, and Cs in LE25-3A3.2.

Sample LE25-5L-1A contains 14 anhedral beryls. When the concentration averages of the anhedral beryls in LE25-5L-1A are normalized to the average concentrations of the core (Fig. 35A) and rim (Fig. 35B) of euhedral beryl LE25-3A3.2, the anhedral beryls more closely represent the average concentration of the euhedral beryl rim. Each anhedral beryl shows slight variations but shows the same general trend. Normalized Fe values tend to show the greatest variation while Ga values show the least variation. Other multi-element variation graphs are found in Appendix B. Each pegmatite differs in beryl composition slightly.

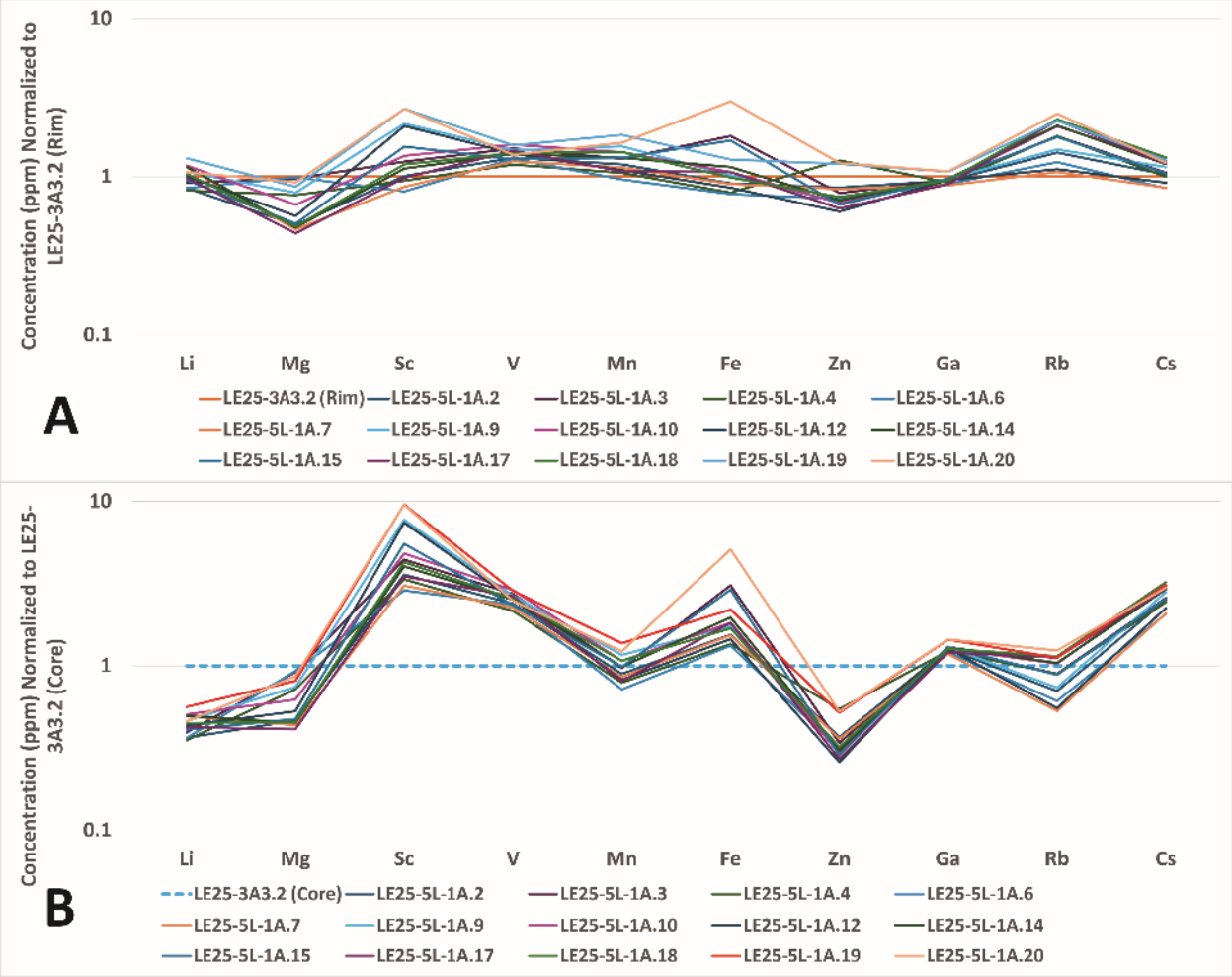


Figure 35: Elemental concentrations in beryl from LE25-5L-1A normalized to the Rim (A) and Core (B) of euhedral beryl LE25-3A3.2.

Quartz Data

All analyzed quartz samples exhibit a wide range of concentrations for each element over the transect lines (Fig. 37). A complete data set of the following LA-ICP-MS analyses can be found in the Supplemental Files. Some elements increased and decreased several orders of magnitude (e.g., titanium ranges from over 10,000 ppm to just above 10 ppm), and no elements were completely homogenous across the quartz crystals. Sodium, Mg, Al, K, Ti, Cr, Cu, and Zn were chosen to depict chemical variations in the quartz transect lines due to continuity of data available from the transects. Figure 36 shows sample LE-3A1 and Figure 37 shows LE-3A1.6. Plots of all other quartz transects can be found in Appendix A.

When depicted on bivariate plots, quartz concentrations of Li, Be, B, Ti, Ga, Ge, and Rb versus Al show distinct groupings in all quartz samples (Fig. 38). Samples LE25-3A1.6, LE25-3A1.17, LE25-5C-1A.17, LE25-5C-1B.4, LE25-5R-1A.7, LE25-6-1.19, LE25-6-2.3, LE25-7-1A.2, LE25-7-2A.1, LE25-7-2A.15, LE25-7-2B.1, LE25-7-2B.10, and LE25-8-2.5 were chosen to represent the Mt. Antero quartz due to Ti data being above detection limits across the entire crystal transect. Other quartz crystals had sections of the transect where Ti concentration was below detection limits. Individual sample plots of each element listed above are included in Appendix C for the listed samples. Figure 38 and 39 shows bivariate diagrams of sample points formatted after Müller et al. (2021) that depict quartz concentrations of select elements versus Al.

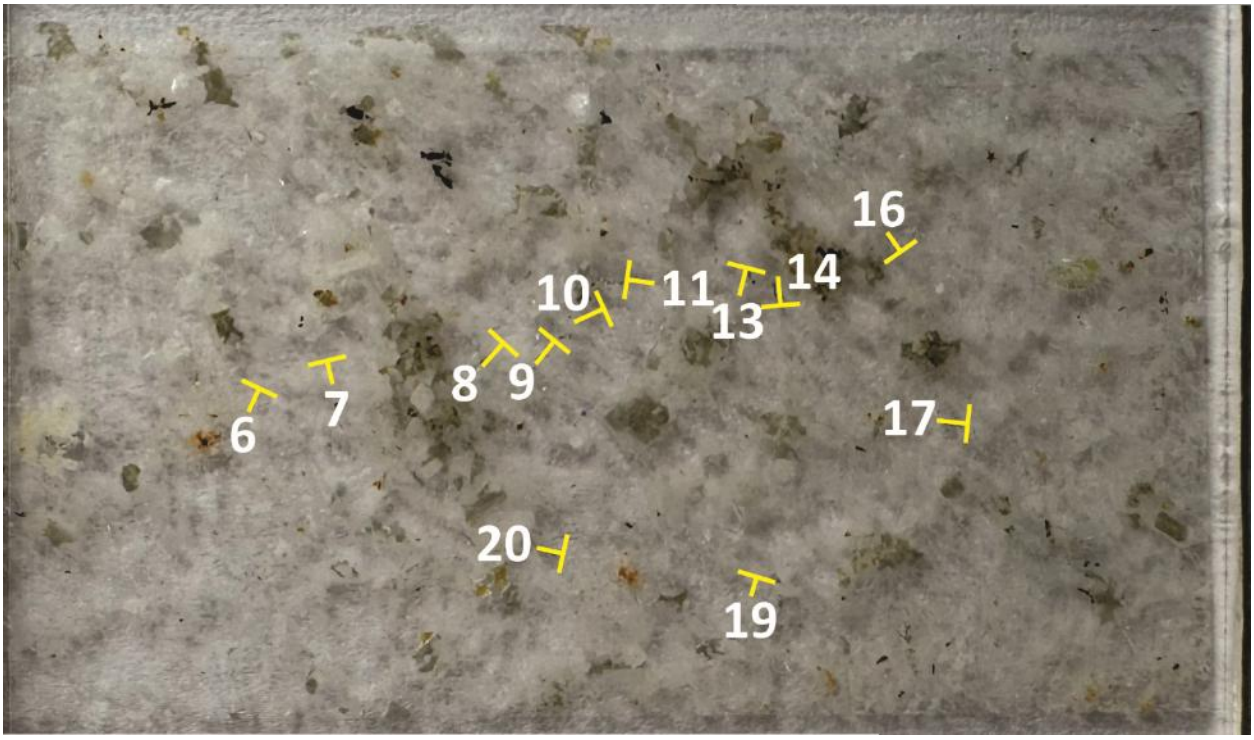


Figure 36: Sample LE25-3A1, 100 micron-thick double polished standard size section of California Granite. The yellow (quartz transect) line labelled 6 corresponds to LA-ICP-MS transect line LE25-3A1.6.

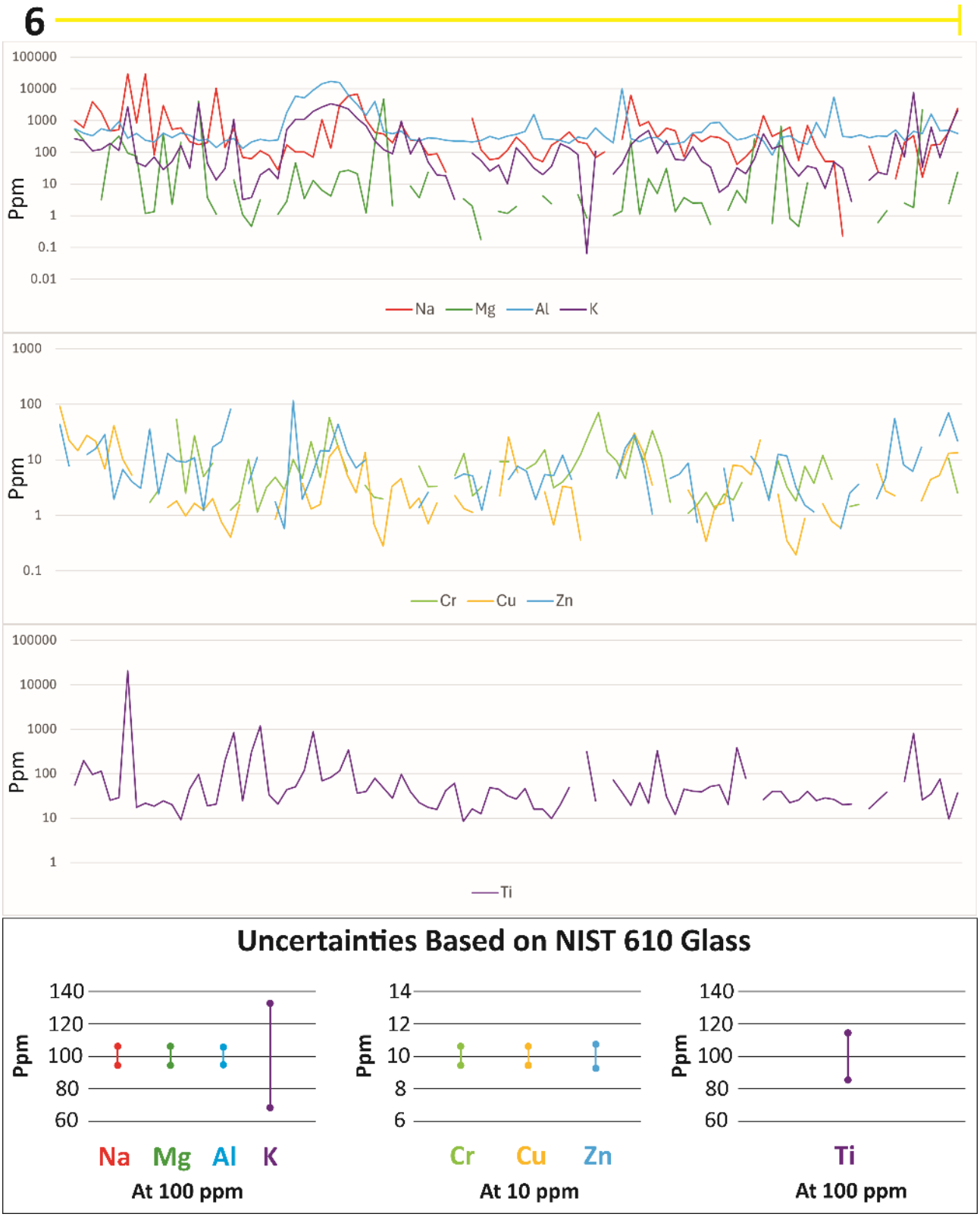


Figure 37: Sample LE25-3A1.6 is a transect from a quartz crystal within the California Granite proximal to pegmatite 3A5. Uncertainties for the selected transect element concentrations are displayed below.

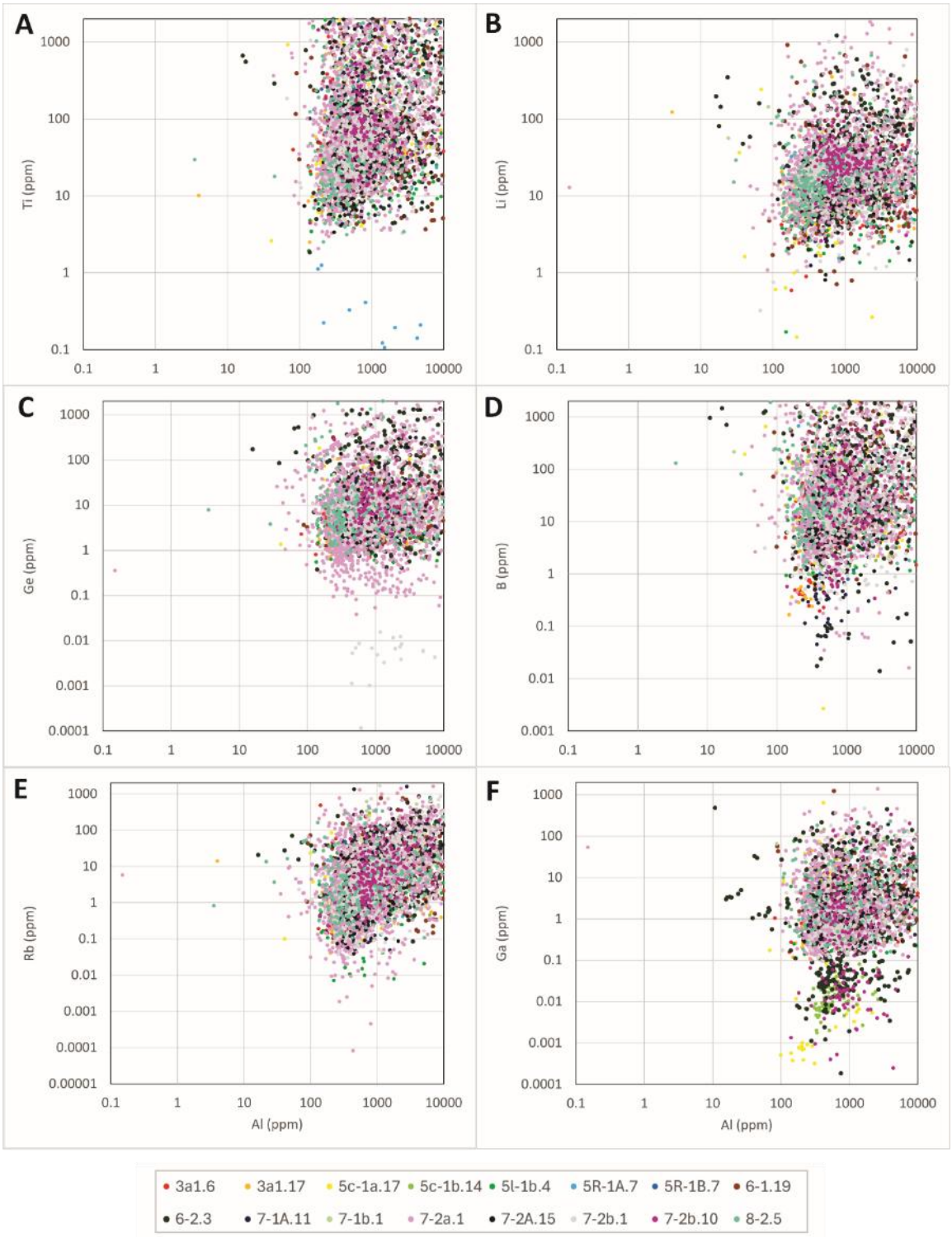


Figure 38: Bivariate plots for trace element concentrations from select Mt. Antero quartz crystals (n=7,139). A) Ti versus Al; B) Li versus Al; C) Ge versus Al; D) B versus Al; E) Ga versus Al; F) Rb versus Al.

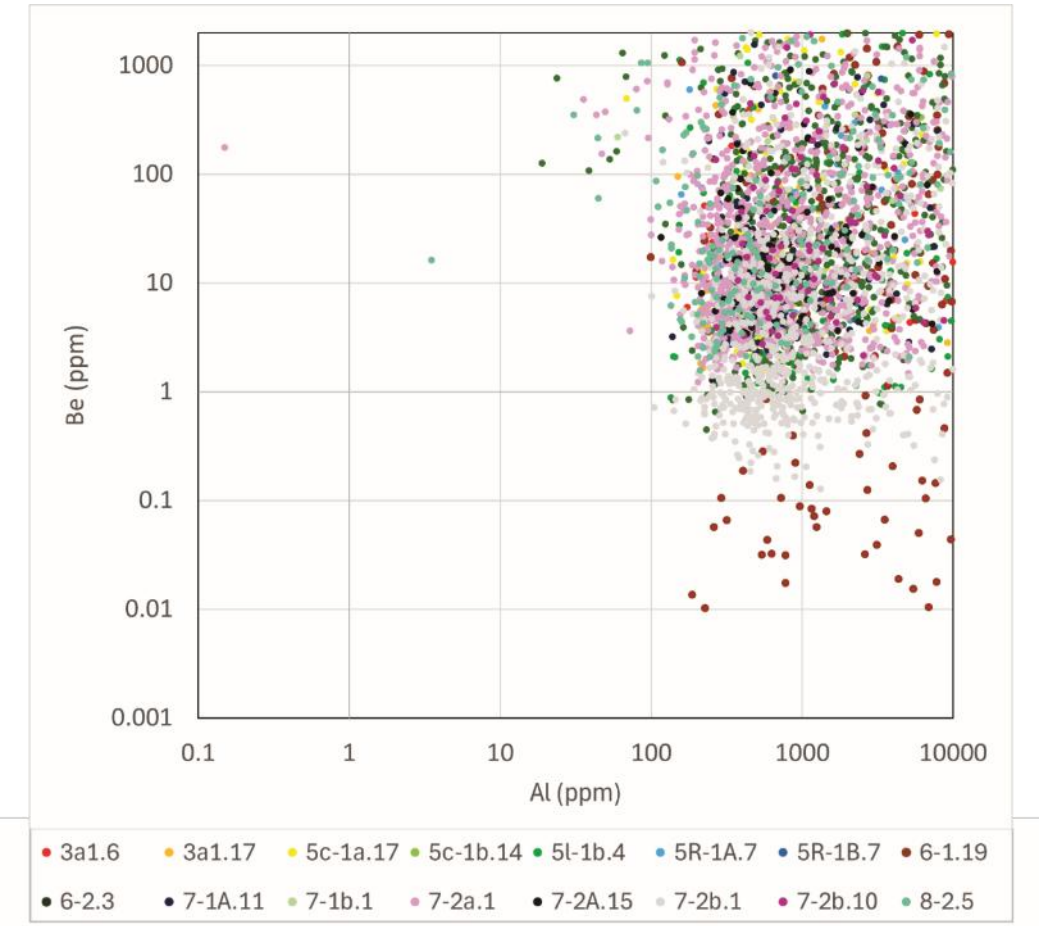


Figure 39: Bivariate plot of Be versus Al for trace element concentrations from select Mt. Antero quartz crystals (n=7,139).

Quartz Trace Element Concentrations Through USTs

Beryl-bearing (Figs. 9A, 10, and 12) and non-beryl-bearing (Figs. 9B and 11) USTs exist on Mt. Antero. Differences in quartz trace element chemistry within the USTs also exist. Non-beryl bearing UST LE25-7 shows that trace element concentrations in quartz tend to decrease through the USTs except for LE25-7-2B.13. Figure 40 shows overall decreasing B, Be, and Cs from wallrock to core. Figure 41 shows overall decreasing Li, Cr, and Fe, and Figure 42 shows overall decreasing Ge and Ga, again, going form wallrock to core.

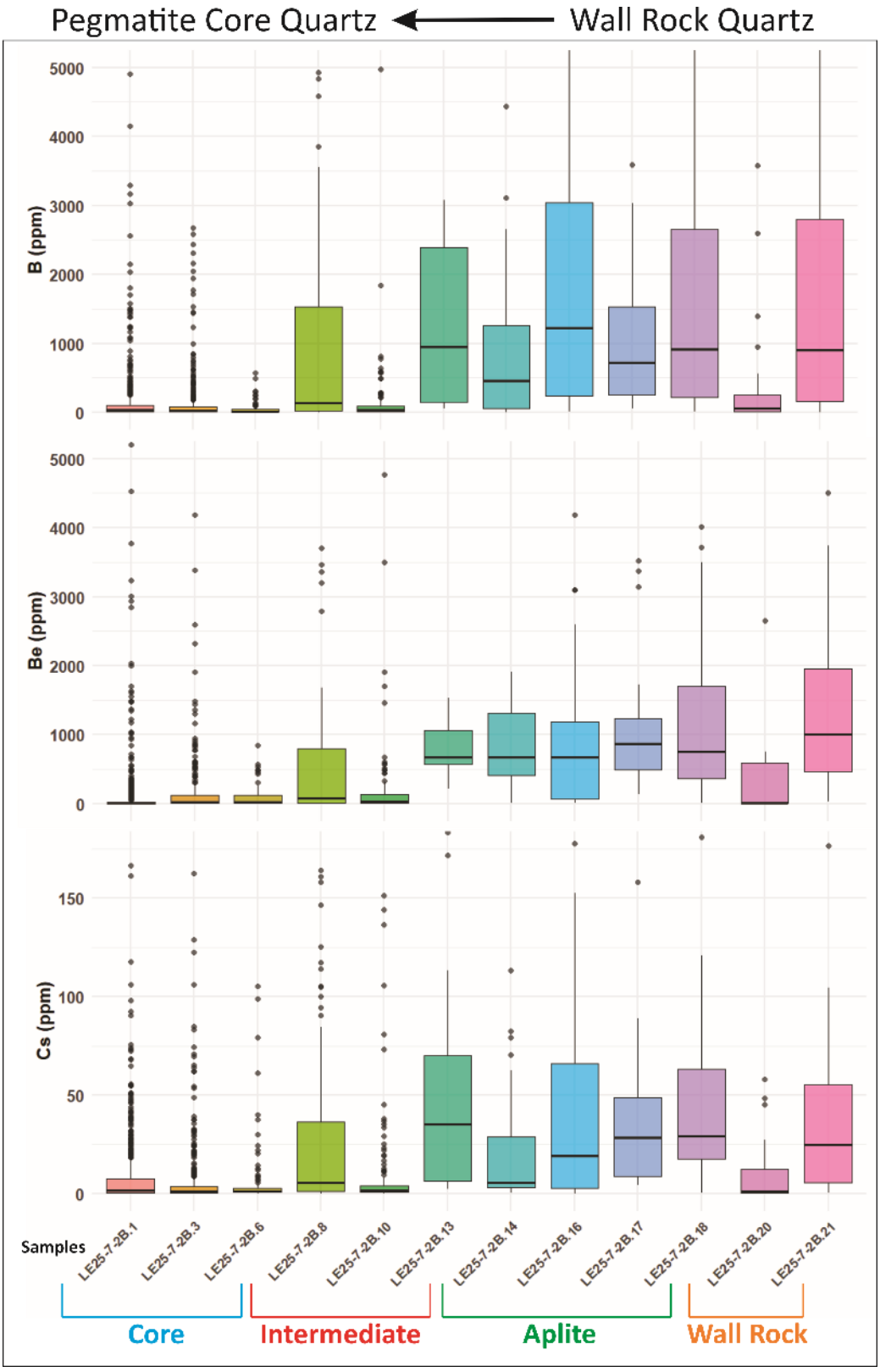


Figure 40: Box plots of Be, B, and Cs concentrations through the wall rock, aplite, intermediate, and core zone of pegmatite UST LE25-7.

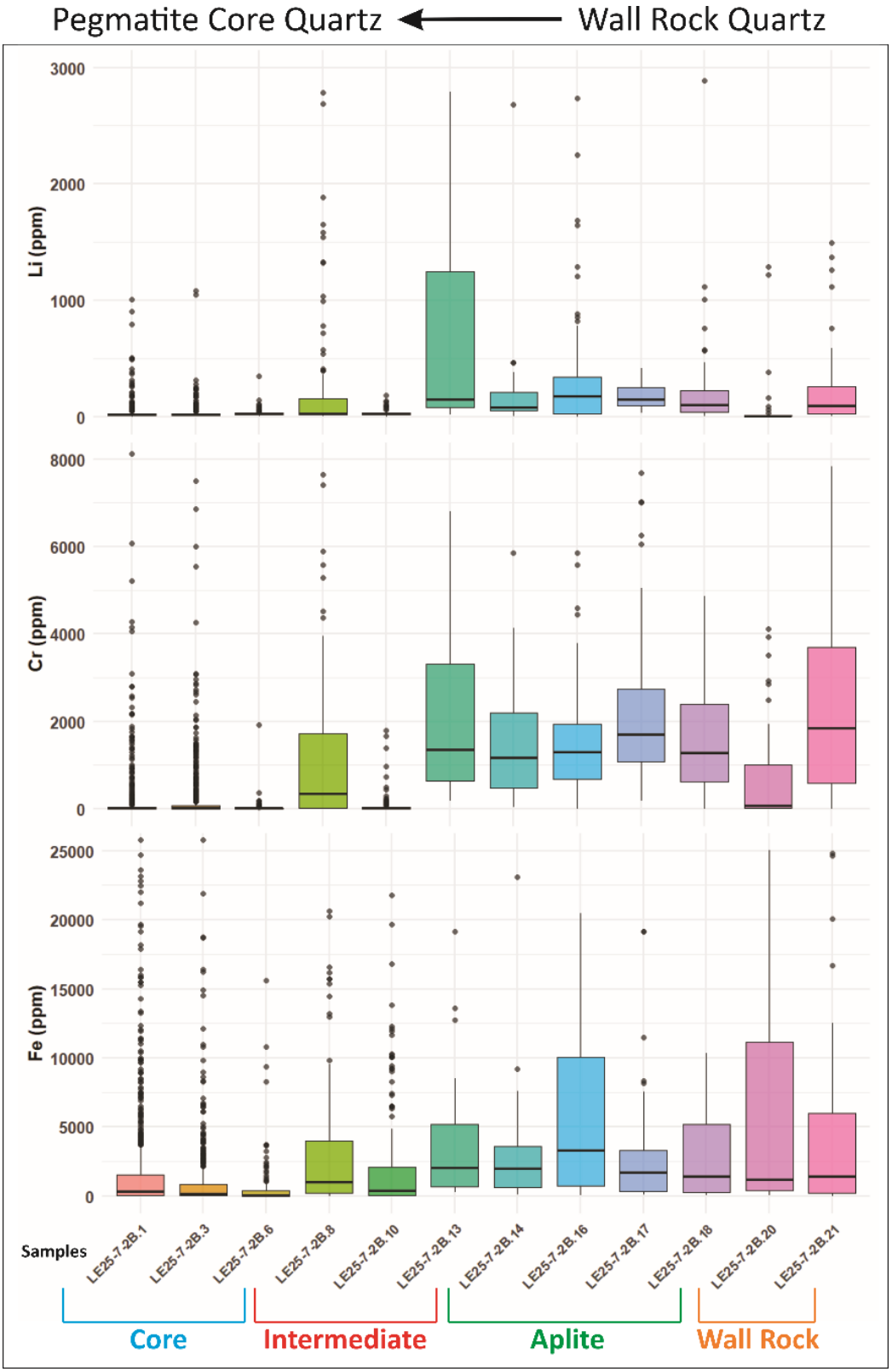


Figure 41: Box plots of Li, Cr, and Fe concentrations through the wall rock, aplite, intermediate, and core zone of pegmatite UST LE25-7.

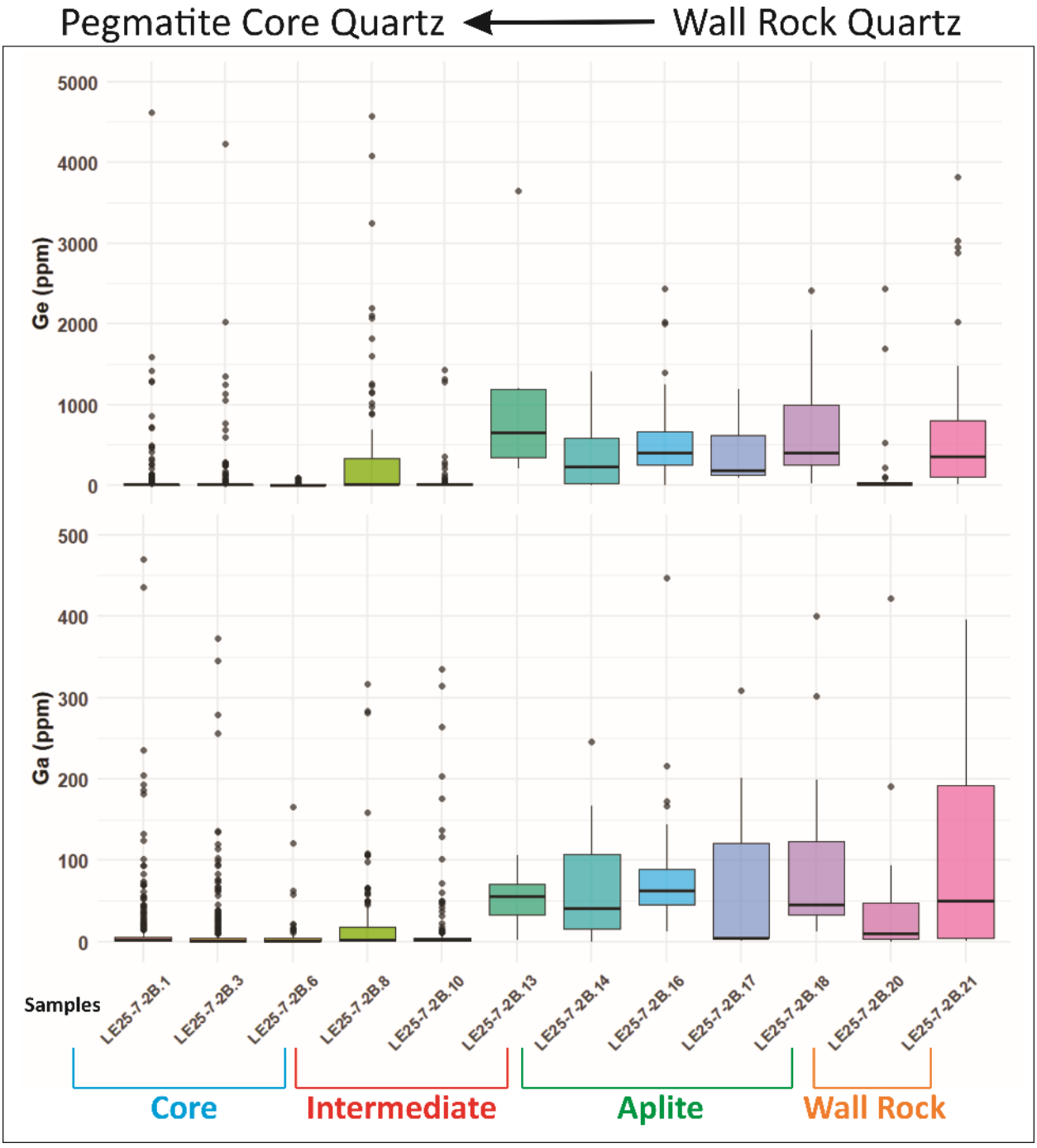


Figure 42: Box plots of Ge and Ga concentrations through the wall rock, aplite, intermediate, and core zone of pegmatite UST LE25-7.

Spheroid beryl-bearing pegmatite LE25-5R contains USTs with a wall rock zone, a transition aplite zone, and core zone. Figure 43 shows the concentration of Be, B, and Cs, while Figures 44 and 45 show the concentrations of Li, Cr, and Fe, and Ge and Ga, respectively. All three figures show how each element decreases from the wall rock into the pegmatite. Once reaching the aplite of the USTs, the concentration of these elements increases then slightly decreases into the pegmatite core.

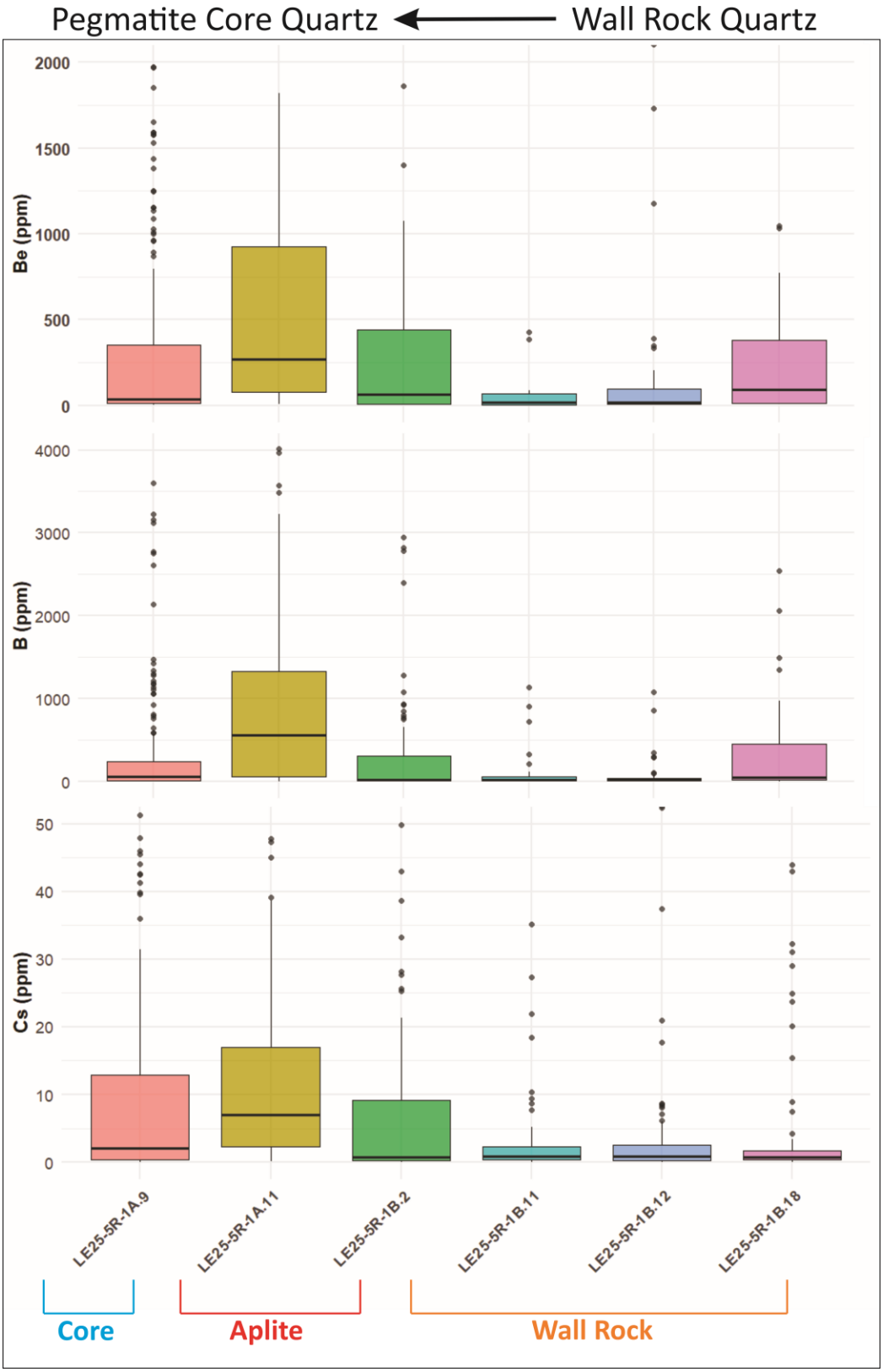


Figure 43: Box plots of Be, B, and Cs concentration through the wall rock, aplite, and core zone of pegmatite LE25-5R.

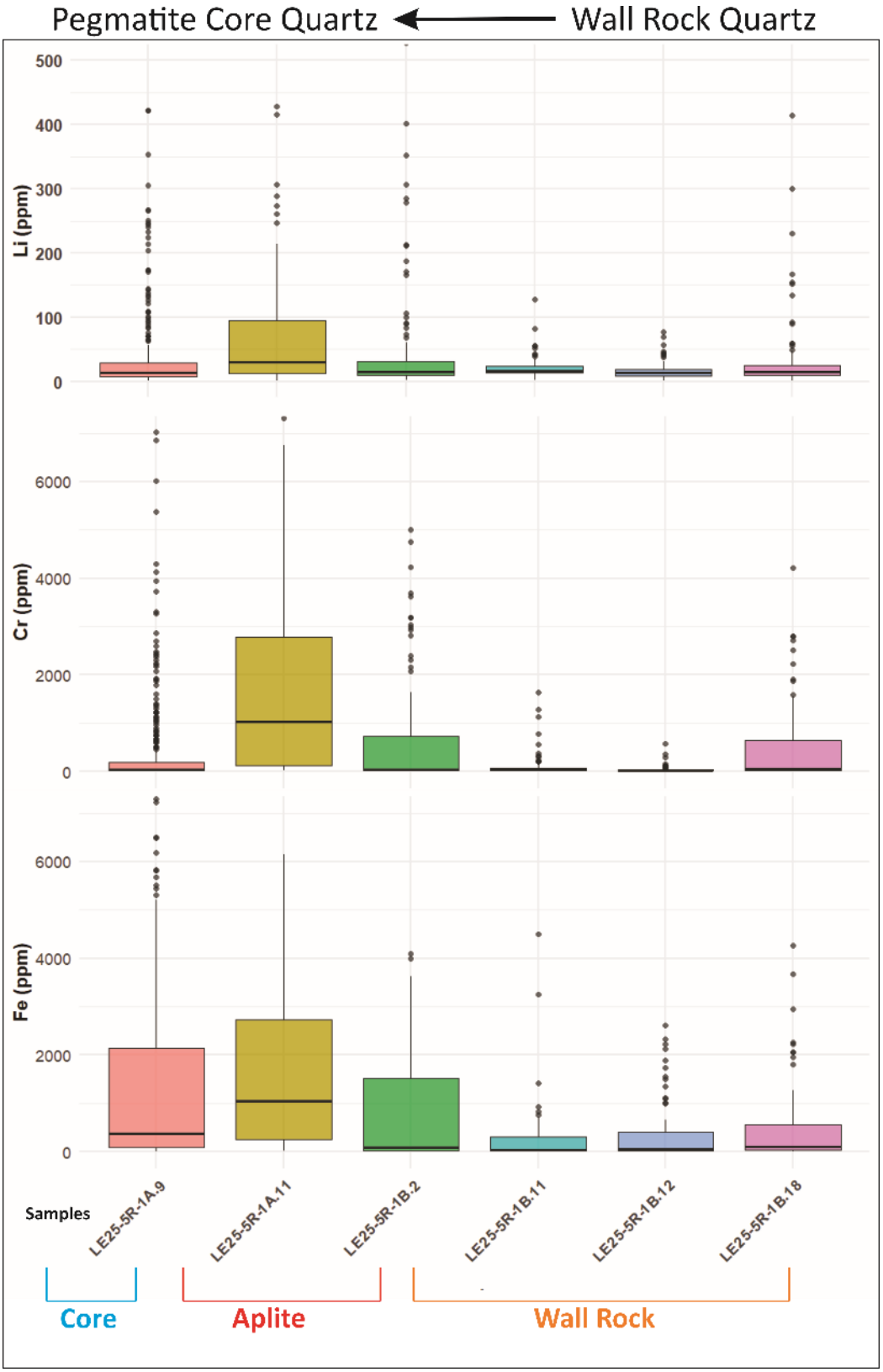


Figure 44: Box plots of Li, Cr, and Fe concentration through the wall rock, aplite, and core zone of pegmatite LE25-5R.

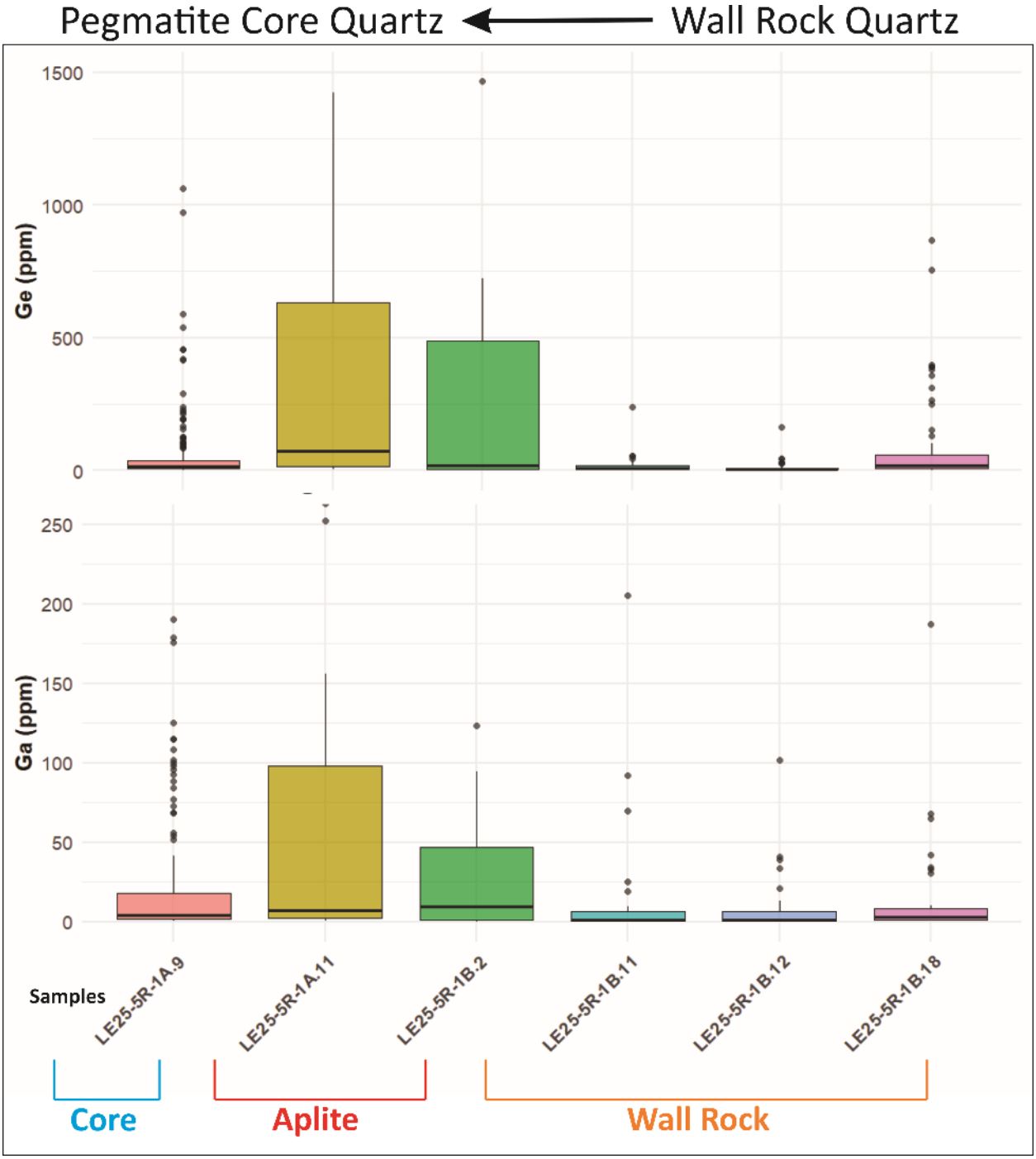


Figure 45 Box plots of Ge and Ga concentration through the wall rock, aplite, and core zone of pegmatite LE25-5R.

Chapter 5 - Discussion

Mt. Antero pegmatites sampled as part of this study are all mineralogically similar, with two distinct types, both of which can exhibit USTs: beryl-rich and beryl-poor pegmatites. We begin by formally classifying the Mt. Antero pegmatites using the pegmatite classification of Wise et al. (2022) using mineralogy and granite type. We then use beryl and quartz trace element geochemistry to better understand the chemistry of the melt and fluid from which the pegmatites formed. This quartz trace element geochemistry is then used to demonstrate that the pegmatite groups of Wise et al. (2022) are chemically distinct from one another.

Pegmatite Classification for Mt. Antero

The spheroidal pegmatites in this study crystallized from within the granite with no fluid pathways from other igneous bodies observed, so therefore are Residual Melts of Granite Magmatism (RMG). The mineralogy of these pegmatites is quartz, alkali and plagioclase feldspar, beryl, bertrandite, biotite, and muscovite. Other researchers have noted topaz, phenakite, and fluorite. Group 2 pegmatites (Table 2) may contain accessory mineral assemblages of both beryl ± topaz ± fluorite and beryl ± phenakite.

Table 3 shows general characteristics of each pegmatite group. Typical source rocks exist for each pegmatite group. Figures 3 and 4 show bulk rock chemistry results from Shannon (1988) (and others therein), which classify the California Granite and Antero Granite, which the pegmatites formed within, as S- or A-type based on Whalen et al (1987) and Pearce et al. (1984) discrimination diagrams. While these results show that the California Granite and Antero Granite are not truly S- or A-type but rather a hybrid, they can still be classified as an A-type granite for the basis of the pegmatite classification scheme due to forming in an extensional tectonic

environment. The S-type signature most likely comes from Precambrian metasediments being melted by the emplacement of the Rio Grande Rift as Shannon (1988) theorized. The Mt. Antero pegmatites are RMG Group 2 (RMG-2) pegmatites based on the classification of Wise et al. (2022). This is based on field observations presented in this thesis, along with previous research stated above.

Beryl

Beryl exists in all pegmatite samples except for LE25-7. The beryl collected and analyzed can be placed into two groups based on crystal habit: euhedral and anhedral. Euhedral beryl had space to form out of a contained melt and is geochemically distinct from anhedral beryl (Fig. 35). Euhedral beryl is enriched in Li and Zn within the core of crystals, compared to rims, whereas rims are enriched in Mg, Sc, V, Mn, Fe, Ga, Rb, and Cs and are depleted within cores (Figs. 25, 28, and 31). The compositional transition between core and rim is sharp, suggesting that the melt evolved over the crystallization period. Thus, the euhedral crystals began to crystallize from a melt which over time became more depleted in Li or Zn when the system began to crystallize out other minerals. Both muscovite and biotite are found within the system and can be possible recipients for Li and Zn. The decrease of Li and Zn in the pegmatite-forming melt was therefore likely caused by other mineral phases joining the crystallization sequence.

When the average trace element compositions of anhedral beryl, euhedral beryl cores, and euhedral beryl rims are depicted on a bivariate diagram showing Na/Li versus Cs concentration (Fig. 32), the anhedral beryls formed from the most evolved portion of the melt (e.g., high Cs indicates the most evolved beryl). The euhedral beryl rims more closely match the anhedral beryl in composition rather than the euhedral beryl cores. Figure 35 also displays the

difference in anhedral beryl vs euhedral cores or rims. The melt composition at the time the anhedral beryl crystallized is more similar to the melt composition that formed the euhedral beryl rims rather than the melt composition that formed the euhedral beryl cores.

Jacobson (1993) documented the occurrence of beryl greisens along the ridge between Baldwin Mountain and Mt. Antero. The ridge runs between the *Thank You Lord* claim block and California Mine locations (Fig. 2). While no hydrothermal veins were observed on the *Thank You Lord* mining claim, it lies within a known beryl greisen area (Adams 1953), which could have affected some of the fluids in the study area. Piranjo (1992) demonstrated that greisens concentrate volatile elements such as F, B, and Li in a cooling body of granite and these greisen systems also are associated with Sn, W, Mo, Be, Bi, Li, and F mineralization. Beryl, molybdenite, and fluorite (rich in Be, Mo, and F, respectively) are all found in the immediate area on Mt. Antero (Adams 1953; Jacobson 1993). Though even while known molybdenum deposits sharing similar mineralogy and age exist within close proximity (~2 km) of the Antero pegmatites (Adams 1953), none were found on the *Thank You Lord* claim.

Kar (1991) also investigated euhedral beryls from the Mt. Antero and Mt. White areas. He found that the concentrations of Fe and Cs increased from core to rim in all crystals, except for one goshenite crystal. Kar (1991) also found that Na and Mg concentrations inversely correlated with Fe enrichments and depletions. However, our results contrast with these findings, as the Na contents of the euhedral beryls we analyzed stayed constant across crystal transects, except for spikes that may represent a Na-rich fluid inclusion or feldspar (Figs. 25, 28, 31). The Na and K staying relatively homogenous throughout the crystallization of the euhedral beryls in our study likely reflects continuous co-crystallization of alkali and plagioclase feldspar.

Available in Appendix B are multi-element plots of anhedral beryl from each beryl-rich pegmatite that are normalized to the rim and core of euhedral beryl LE25-3A3.2. Each multi-element plot shows a near similar pattern as the anhedral beryls represented by Figure 45. Each pegmatite's anhedral beryl differs slightly in concentration of the selected elements but still appears to overlap with anhedral beryl from other pegmatites. The anhedral beryl in each respective pegmatite seems, overall, to be like other anhedral beryl from the same pegmatite. As shown in Figure 45, Fe concentrations in anhedral beryl create the largest range of the depicted elements.

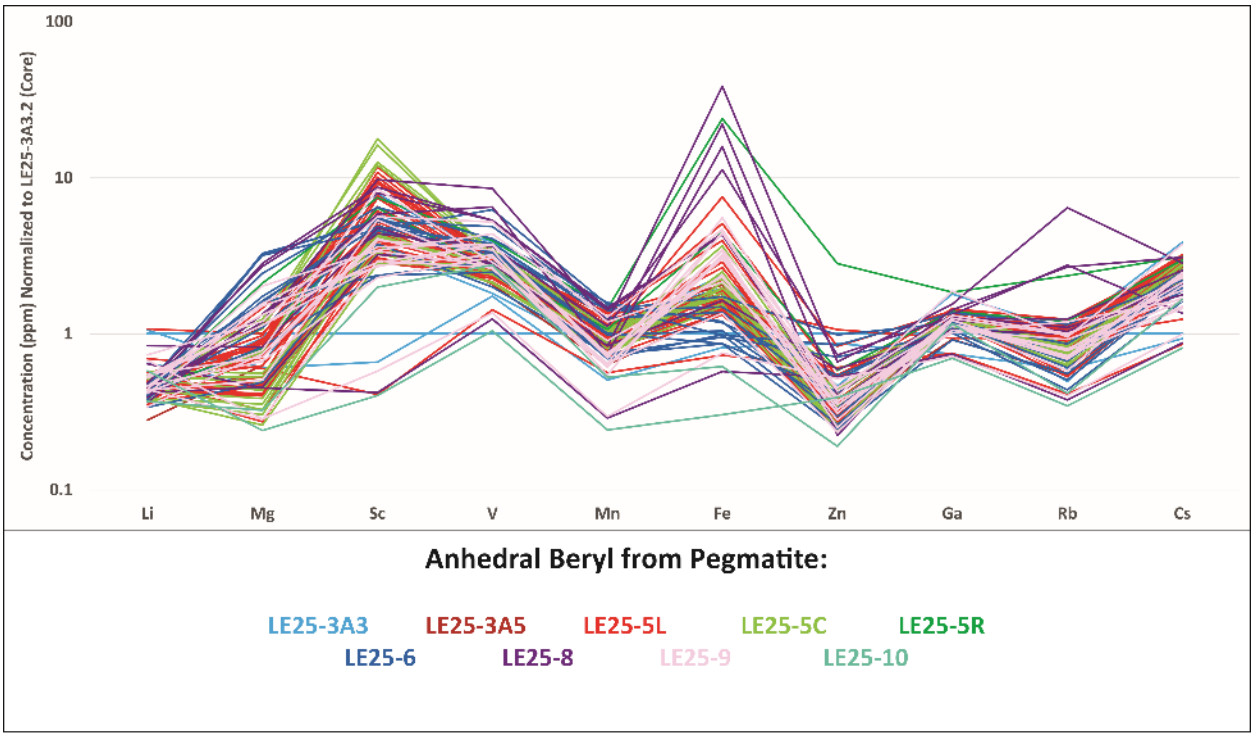


Figure 46: Anhedral beryl from all beryl-rich pegmatites normalized to euhedral beryl core LE25-3A3.2.

Quartz

Quartz trace element chemistry has been recently used to help decipher and classify pegmatite types (Müller et al. 2021), especially those described in the classification scheme of

Wise et al. (2022). The plots of Li, B, Ti, Ga, Ge, and Rb versus Al are shown by Müller et al. (2021) to help distinguish RMG-1, DPA-1, and DPA-2 pegmatites. Our work shows that quartz from Mt. Antero's RMG-2 pegmatites is compositionally distinct from quartz from DPA-1, DPA-2, and RMG-1 pegmatites (Müller et al. 2021) on some of these discrimination diagrams (Figure 46), though overlap exists. Aluminum is elevated in the Mt. Antero quartz data and creates a distinct shift to higher Al concentrations, relative to other pegmatite type quartz data in each of the bivariate plots; these shifts are outside the range of Al analytical uncertainty (Table 4, Fig. 37).

Figures 47 to 53 shows Li, Be, B, Ti, Ga, Ge, and Rb versus Al on bivariate plots and includes contours representing kernel density estimates (KDE) of the bivariate distribution of Al versus each element. Figure 54 is a combined plot of all six plots. The contours have been calculated in R using a Gaussian smoothing function with the ggplot2 package. Lines show regions of equal point density, highlighting areas of higher sample concentration. Müller et al. (2021) lists research conducted to determine that Ge, Rb, B, and Be in quartz increases with fractionation of the melt. While Ge is not distinct, both B and Be concentrations are distinct when plotted against Al, and Rb concentrations are slightly elevated. Ga concentrations from Mt. Antero are also distinct when plotted against Al.

These plots show that the RMG-2 type pegmatites from Mt Antero are chemically distinct from other pegmatite types (e.g., DPA-1, DPA-2, and RMG-1) based on quartz geochemistry. As noted previously, Shannon (1988) determined that the California Granite is higher in wt % Al_2O_3 than other A-type granites from other localities and is also enriched in Rb, Nb, Ga, and Th and lower in Sr, Ba, Y, Zr, and REEs. The studied pegmatites, which originated from the California Granite, also reflect these characteristics with most notable characteristics

being the high amount of aluminum, along with elevated Be, B, Ga, and Rb, which likely reflect high concentrations of these elements in the source rock that melted to form the California (and related), granitoids. Tourmaline is not found within the Mt. Antero RMG-2 pegmatites, so boron that might be incorporated into the crystal structure of tourmaline, is available to be incorporated into Mt. Antero pegmatite quartz.

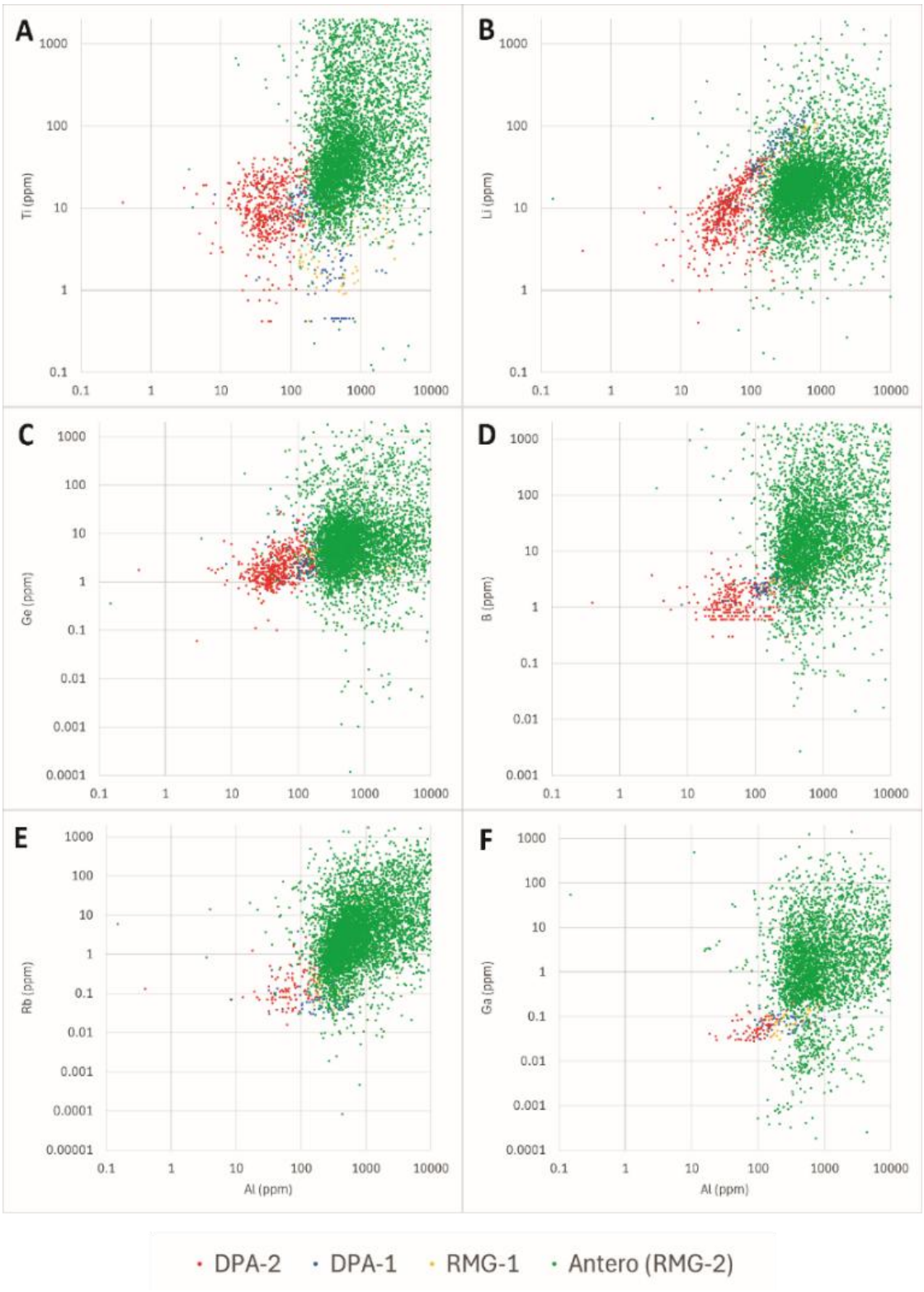


Figure 47: Bivariate plots for trace element concentrations of quartz from DPA-1, DPA-2, RMG-1, and Mount Antero (RMG-2) pegmatites. A) Ti versus Al; B) Li versus Al; C) Ge versus Al; D) B versus Al; E) Rb versus Al; F) Ga versus Al.

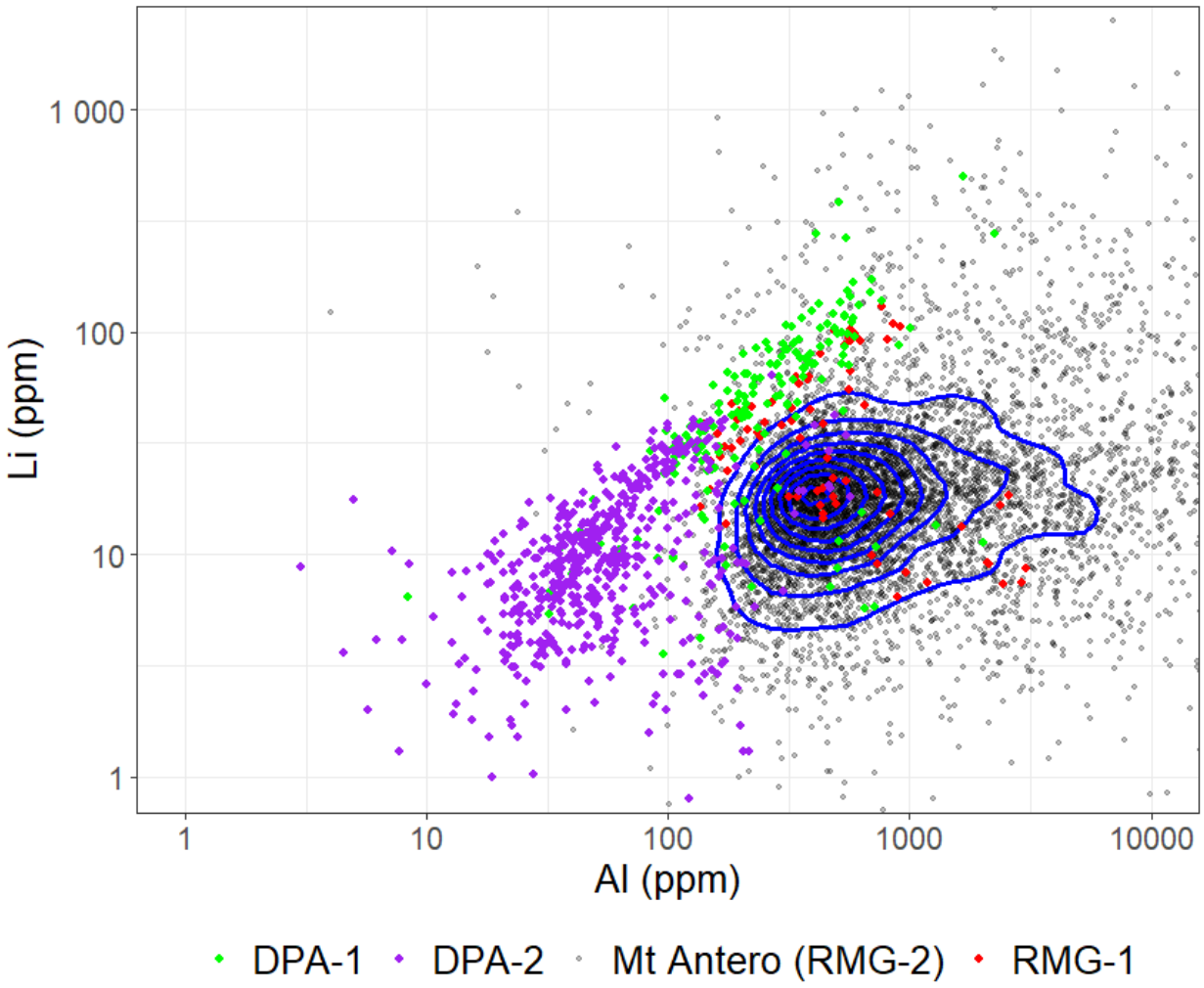


Figure 48: Mt. Antero quartz data depicted in Figure 46 with added density contours. Contours represent kernel density estimates (KDE) of the bivariate distribution of Al and Li, calculated in R using a Gaussian smoothing function. Lines show regions of equal point density, highlighting areas of higher sample concentration. Also shown are other pegmatite types for comparison.

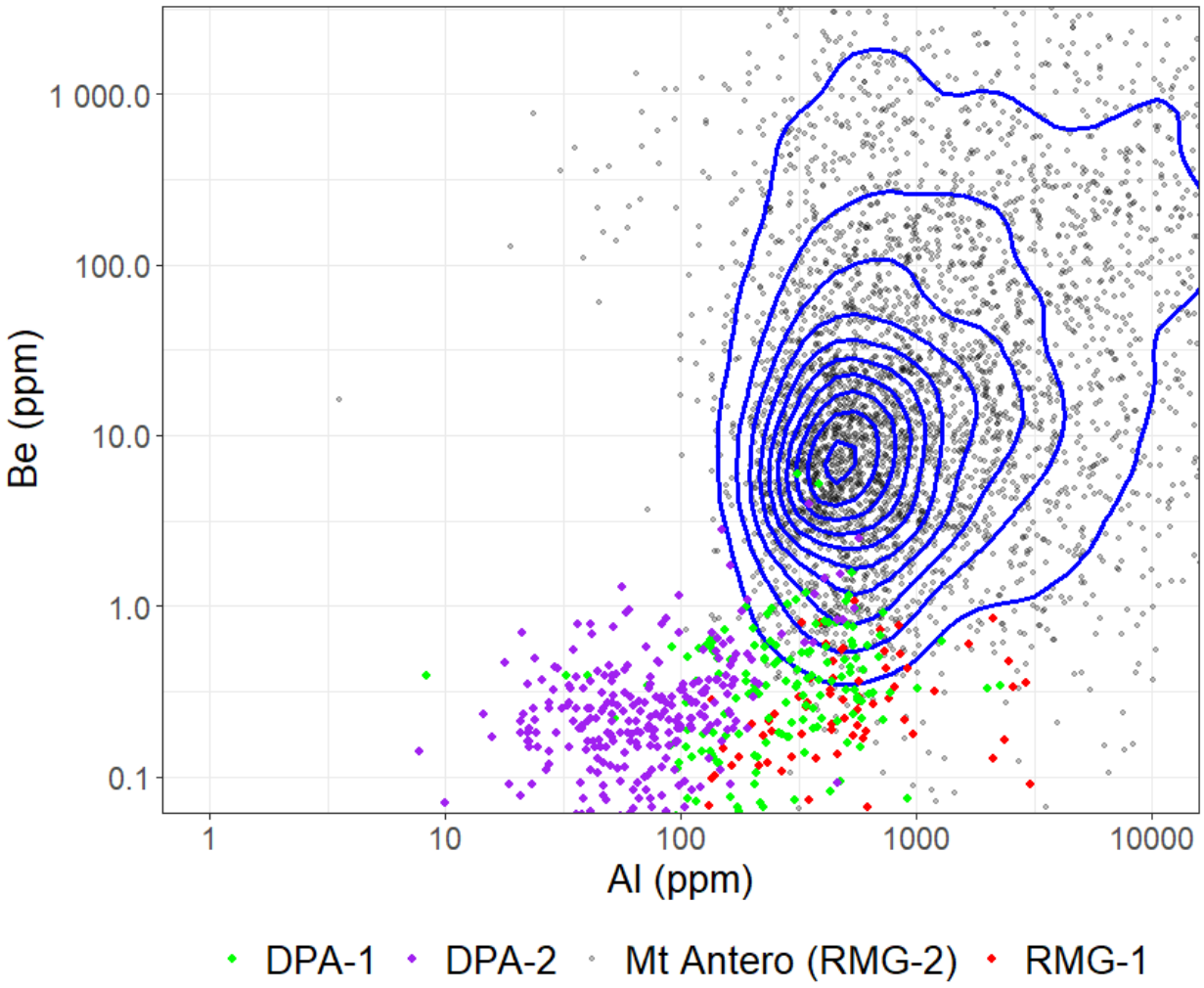


Figure 49: Selected Mt. Antero quartz data depicted in Figure 46 with added density contours. Contours represent kernel density estimates (KDE) of the bivariate distribution of Al and Be, calculated in R using a Gaussian smoothing function. Lines show regions of equal point density, highlighting areas of higher sample concentration. Also shown are other pegmatite types for comparison.

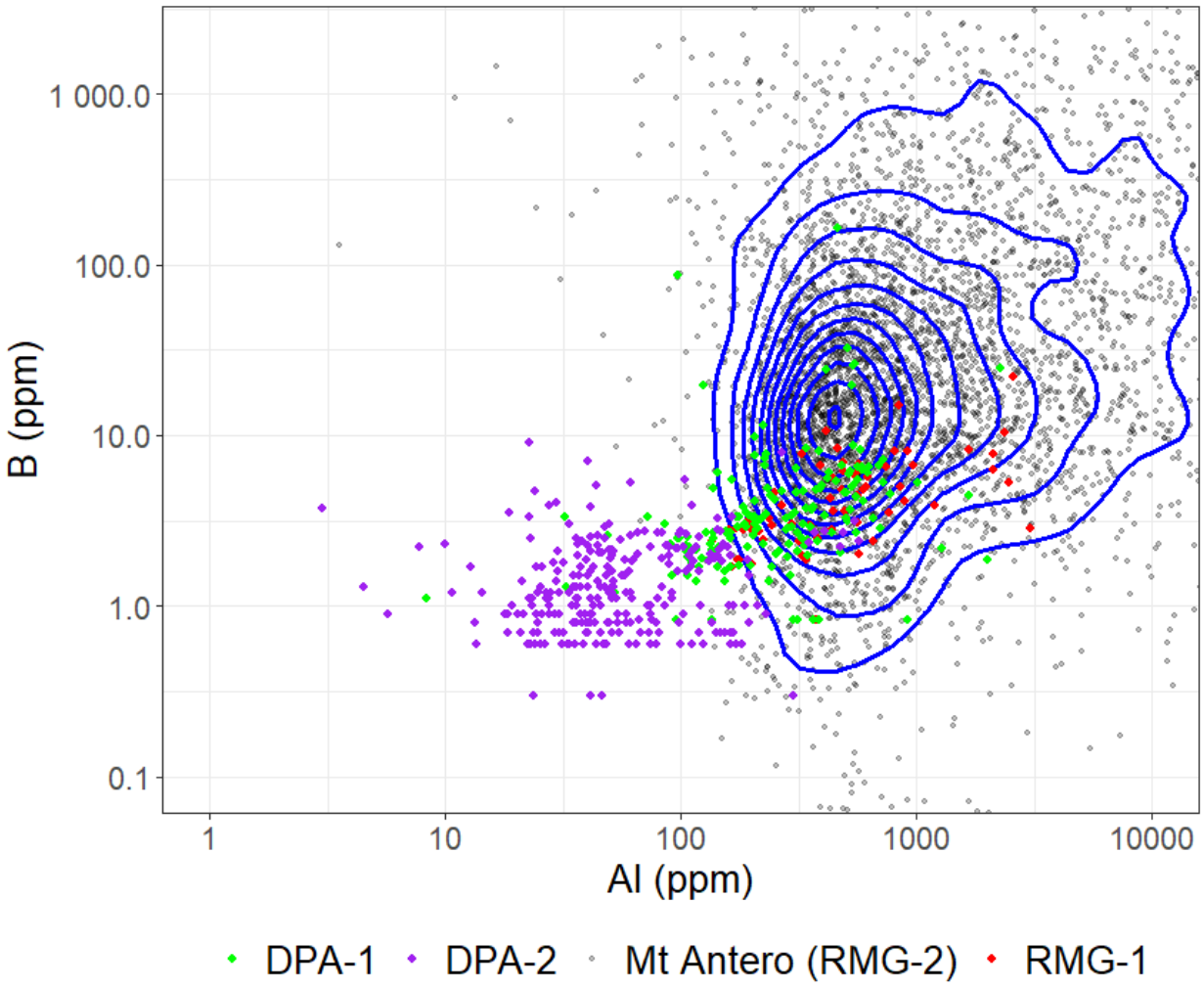


Figure 50: Selected Mt. Antero quartz data depicted in Figure 46 with added density contours. Contours represent kernel density estimates (KDE) of the bivariate distribution of Al and B, calculated in R using a Gaussian smoothing function. Lines show regions of equal point density, highlighting areas of higher sample concentration. Also shown are other pegmatite types for comparison.

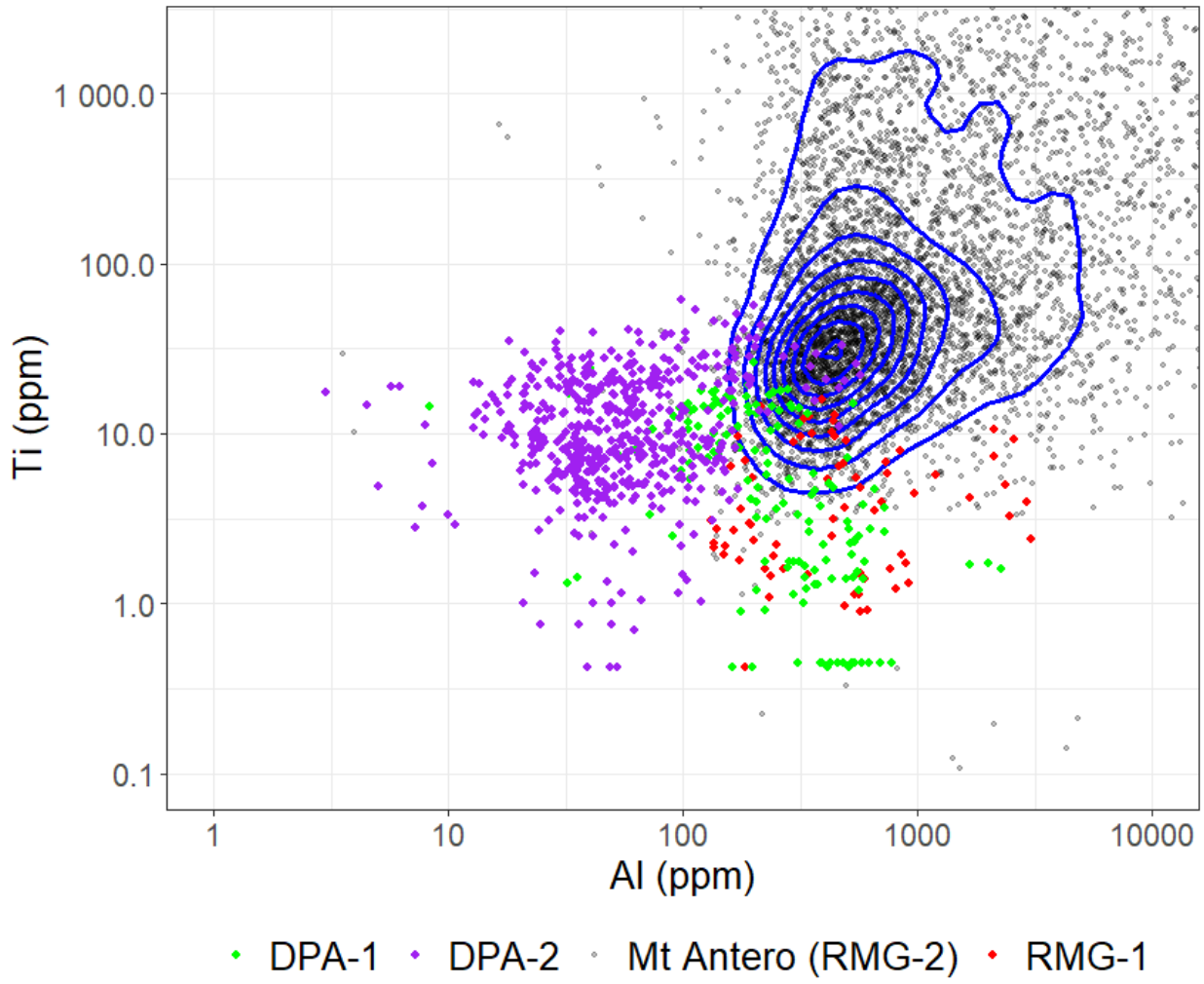


Figure 51: Selected Mt. Antero quartz data depicted in Figure 46 with added density contours. Contours represent kernel density estimates (KDE) of the bivariate distribution of Al and Ti, calculated in R using a Gaussian smoothing function. Lines show regions of equal point density, highlighting areas of higher sample concentration. Also shown are other pegmatite types for comparison.

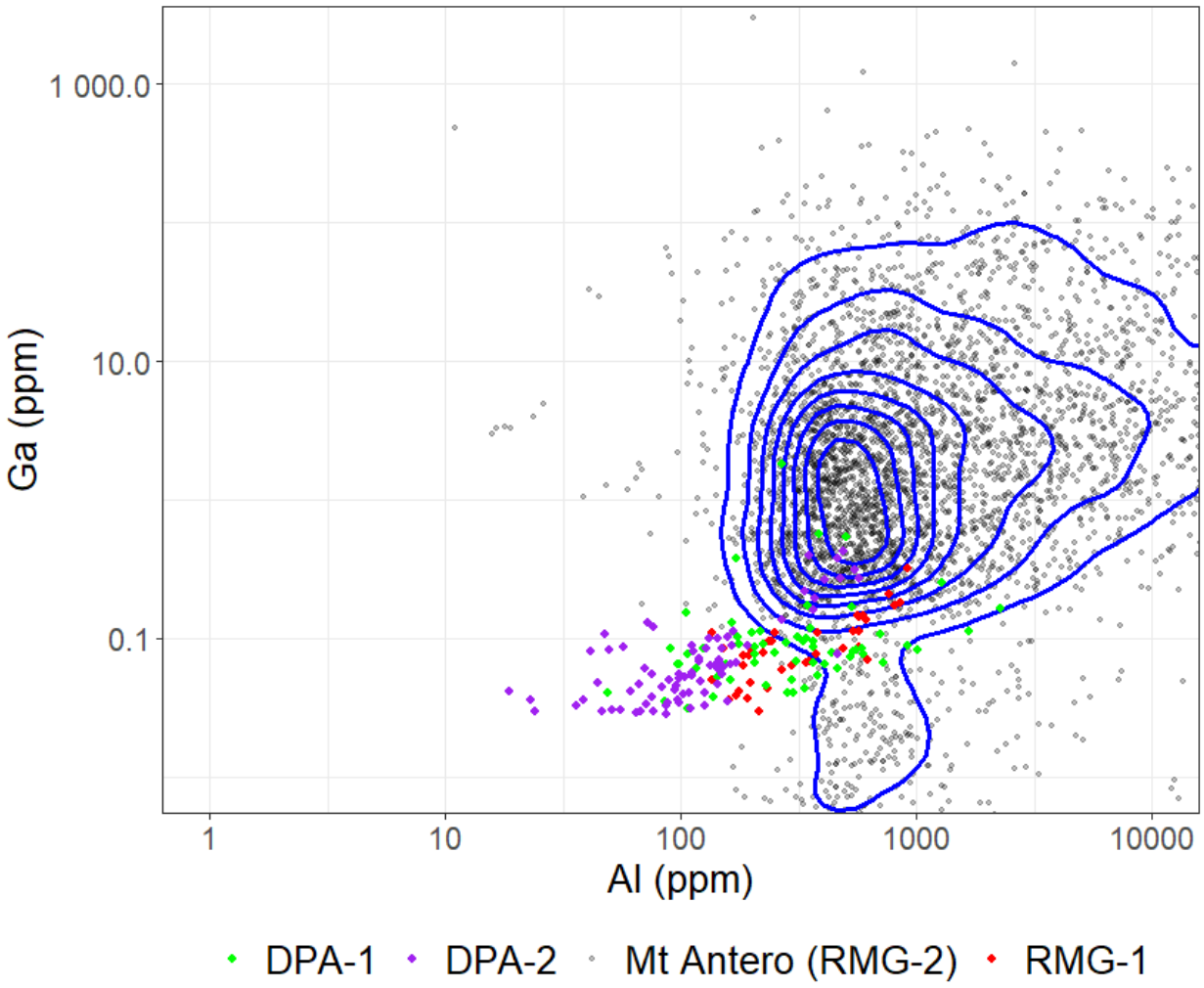


Figure 52: Selected Mt. Antero quartz data depicted in Figure 46 with added density contours. Contours represent kernel density estimates (KDE) of the bivariate distribution of Al and Ga, calculated in R using a Gaussian smoothing function. Lines show regions of equal point density, highlighting areas of higher sample concentration. Also shown are other pegmatite types for comparison.

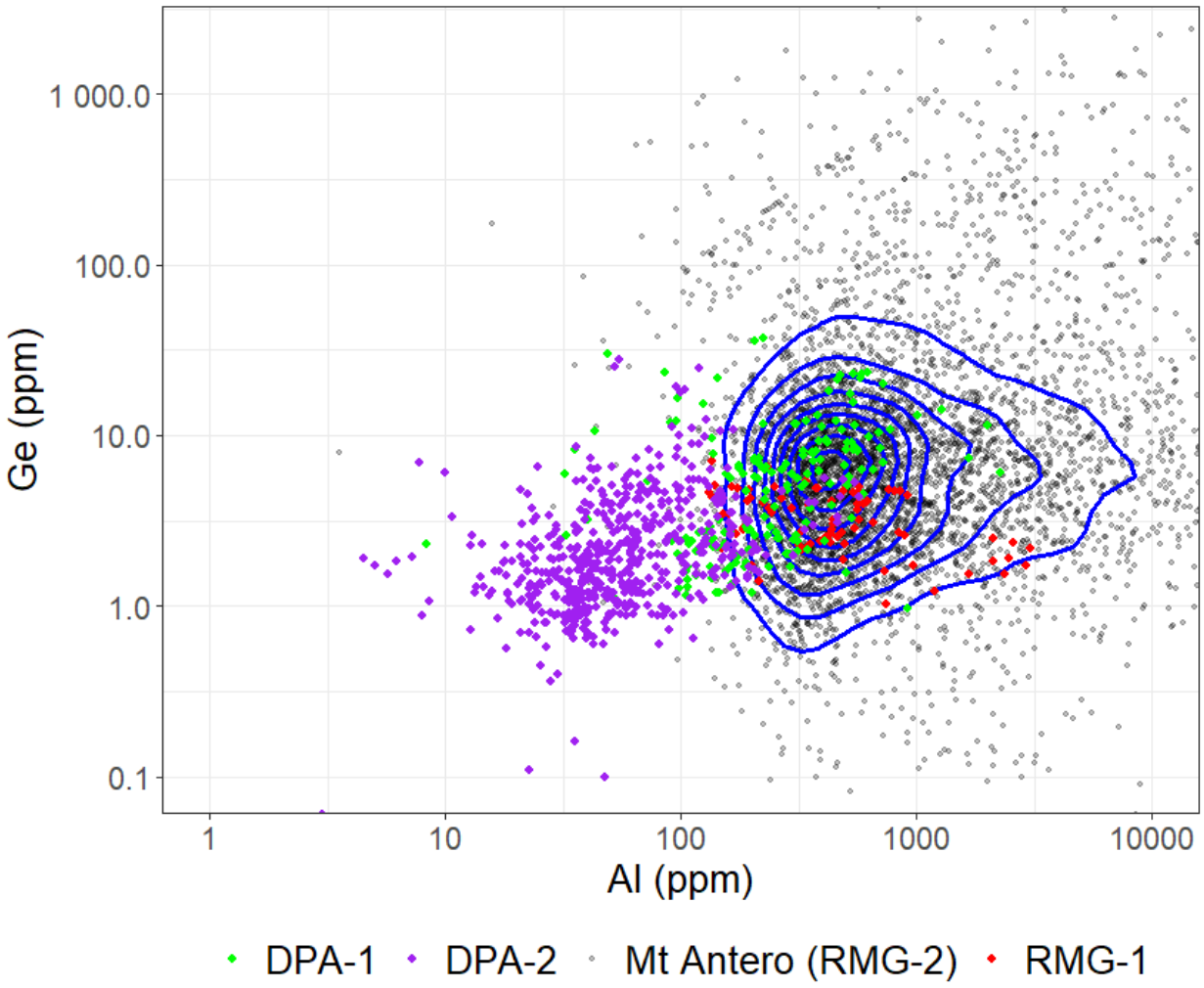


Figure 53: Selected Mt. Antero quartz data depicted in Figure 46 with added density contours. Contours represent kernel density estimates (KDE) of the bivariate distribution of Al and Ge, calculated in R using a Gaussian smoothing function. Lines show regions of equal point density, highlighting areas of higher sample concentration. Also shown are other pegmatite types for comparison.

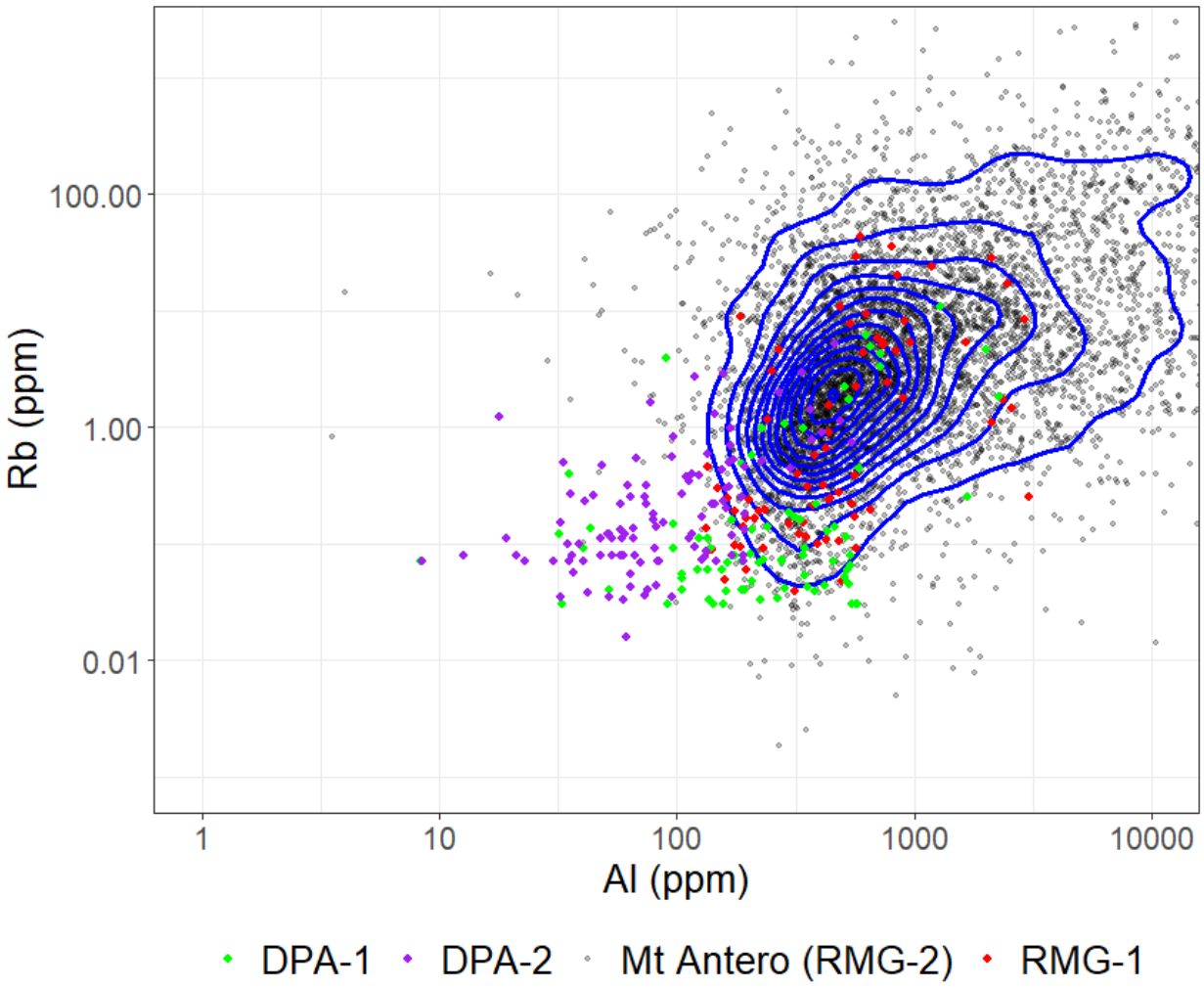


Figure 54: Selected Mt. Antero quartz data depicted in Figure 46 with added density contours. Contours represent kernel density estimates (KDE) of the bivariate distribution of Al and Rb, calculated in R using a Gaussian smoothing function. Lines show regions of equal point density, highlighting areas of higher sample concentration. Also shown are other pegmatite types for comparison.

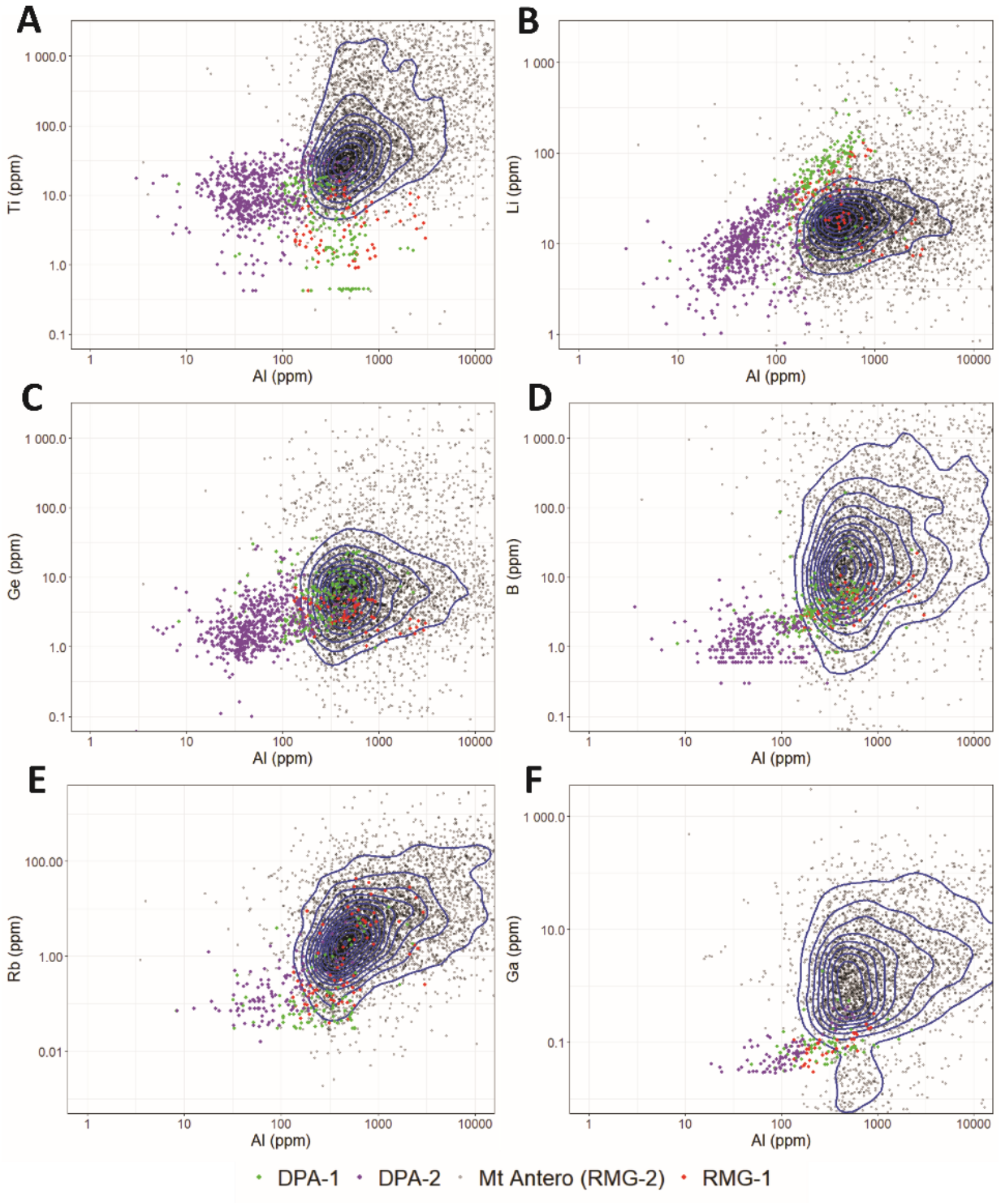


Figure 55: Bivariate plots for trace element concentrations of quartz from DPA-1, DPA-2, RMG-1, and Mount Antero (RMG-2) pegmatites with added density contours. Contours represent kernel density estimates (KDE) of the bivariate distribution of Al and Ti, Li, Ge, B, Rb and Ga, calculated in R using a Gaussian smoothing function. Lines show regions of equal point density, highlighting areas of higher sample concentration. A) Ti versus Al; B) Li versus Al; C) Ge versus Al; D) B versus Al; E) Rb versus Al; F) Ga versus Al.

When compared against RMG-2 pegmatite data from Pikes Peak (Fonseca Teixeira et al. 2022), Mt. Antero's RMG-2 pegmatites are up to two magnitudes higher in Al concentration (Fig. 55). Germanium concentrations for the RMG-2 Pikes Peak pegmatites range from ~1 to 2.5 ppm, while the Ge concentrations of the Mt. Antero RMG-2 pegmatites range from ~1 to 1,000 ppm (Fig. 55). While Mt. Antero and Pikes Peak are both located in Colorado, USA, and both have RMG-2 pegmatites, the pegmatite quartz contains drastically differing Al concentrations. Pikes Peak RMG-2 pegmatites contain mostly <200 ppm of Al, while Mt. Antero RMG-2 pegmatites contain mostly >200 ppm of Al. Mt. Antero RMG-2 pegmatites also contain a higher concentration of Ge, with the majority of data points ranging from 1 to 30 ppm, while Pikes Peak RMG-2 pegmatites contain mostly 1 to 3 ppm Ge.

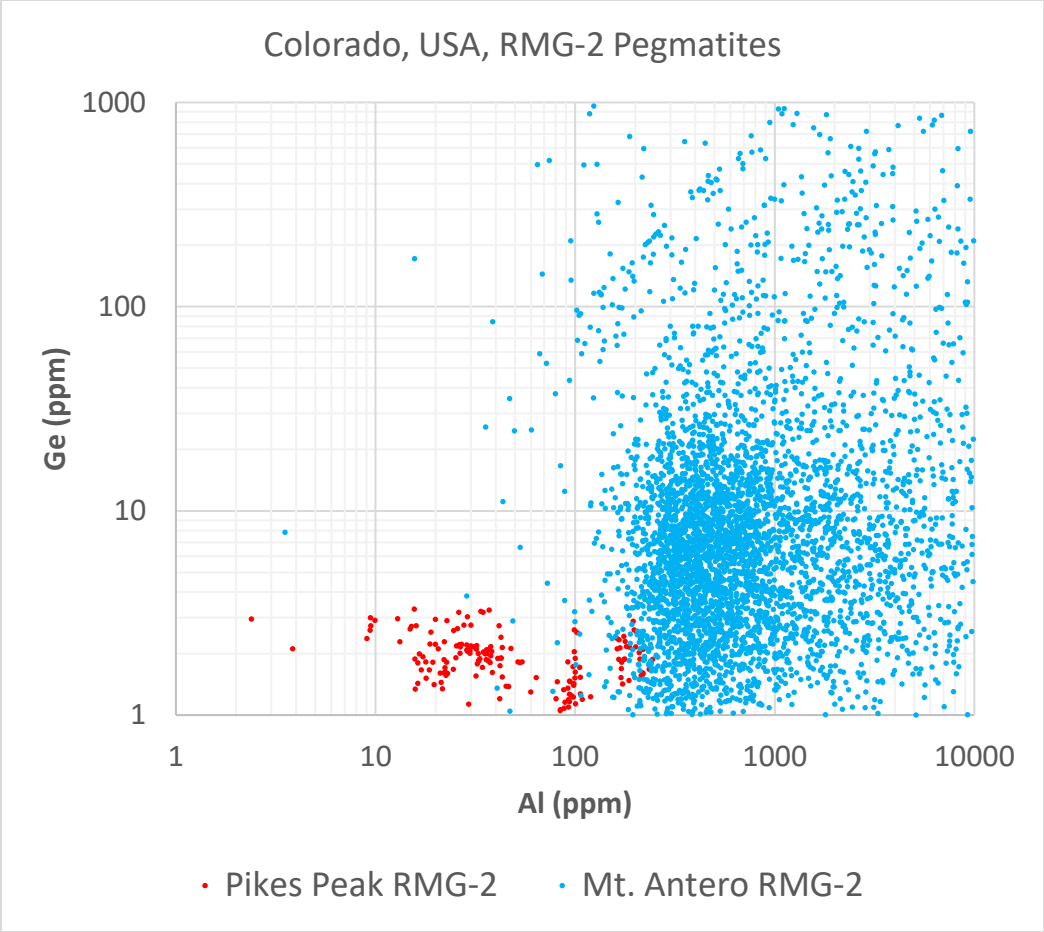


Figure 56: RMG-2 Ge versus Al trace element quartz data from Pikes Peak, Colorado and Mt. Antero, Colorado.

When comparing the Pikes Peak data from Figure 55 to that of different pegmatite classes on Figure 52, Pikes Peak RMG-2 data overlaps with DPA-2 pegmatites. RMG-2 pegmatites therefore seem to occupy a wide range of concentrations which are inherited from their parental granite.

Chapter 6 - Conclusions

The Mt. Antero pegmatites on the *Thank You Lord* mining claim are RMG-2 pegmatites, are geochemically similar, and were created by similar melts. Both beryl-poor and beryl-rich pegmatites exist on the claim and can exhibit USTs.

Euhedral beryl, including gem-quality beryl, started crystallizing first and anhedral beryl crystallized second while a singular melt evolved over time. Euhedral beryl shows evidence of the melt evolving and going from higher in concentrations of Li and Zn and lower in Mg, Sc, V, Mn, Fe, Ga, Rb, and Cs to the inverse. Anhedral beryl more closely resembles the rims of euhedral beryl and is more fractionated than the cores of the euhedral beryl.

The quartz of the Mt. Antero (RMG-2) pegmatites is chemically different than that of DPA-1, DPA-2, and RMG-1 pegmatites. The most notable differences are the higher Al, Be, B, Ga, and Rb relative to most DPA-1, DPA-2, and RMG-1 type pegmatites globally (Figs. 48, 49, 51, and 53). The higher boron content could be due to the absence of tourmaline as a crystallizing phase; hence, B concentration increases as differentiation progresses. The parental granite for these pegmatites, the California Granite, caused the higher Al, Ga, and Rb, as the pegmatites inherit the chemical characteristics of their parental granite at crystallization.

Future Work

Fluid inclusion work on the euhedral beryls and anhedral beryls should be conducted to better understand the relationship between the two. The signatures could reveal the nature of the melts and fluids and their differences (e.g., pegmatitic, magmatic, hydrothermal, metasomatic).

Concentrations of Na, K, and Ca in feldspar could be used to determine the evolution of feldspar through the UST zones. While the quartz and beryl chemistry are similar, the feldspar could help us better understand the crystallization sequence of the pegmatites through the zones.

Other trace element suites can be obtained from pegmatite beryl and granite beryl at other known locations in the Mt. Antero and Mt. White areas. This kind of trace element data could better characterize the chemical signature of the beryl and if it is similar across the entire area where beryl-rich pegmatites crop out.

References

Adams, J., 1953a, Beryllium deposits of the Mount Antero region, Chaffee County, Colorado: Geologic Survey Bulletin 982-D, p. 95–118, doi: 10.3133/b982d.

Balaram, V., Santosh, M., Satyanarayanan, M., Srinivas, N., and Gupta, H., 2024, Lithium: A review of applications, occurrence, exploration, extraction, recycling, analysis, and environmental impact: Geoscience Frontiers, v. 15, p. 101868, doi: 10.1016/j.gsf.2024.101868.

Černý, P., 2002, Mineralogy of Beryllium in Granitic Pegmatites: Reviews in Mineralogy and Geochemistry, v. 50, p. 405–444, doi: 10.2138/rmg.2002.50.10.

Černý, P., and Ercit, T.S., 2005, The Classification of Granitic Pegmatites Revisited: The Canadian Mineralogist, v. 43, p. 2005–2026, doi: 10.2113/gscanmin.43.6.2005.

Dharmapriya, P.L., Disanayaka, D.W.M., Pitawala, H.M.T.G.A., Malaviarachchi, S.P.K., and Subasinghe, N.D., 2025, Genesis, classification, tectonic setting and economic potential of global granitic pegmatites: A Review: Evolving Earth, v. 3, p. 100059, doi: 10.1016/j.eve.2025.100059.

Erichsen, L., Brueseke, M., and Busse, B., 2025, Reconnaissance textural observations of aquamarine and the beryllium-rich, gem-hosting pegmatite system of Mount Antero, Colorado (USA): Geological Society of America Abstracts with Programs, doi: 10.1130/abs/2025am-6899.

Fonseca Teixeira LM, Troch J, Allaz J and Bachmann O (2022) Magmatic to hydrothermal conditions in the transition from the A-type Pikes Peak granite (Colorado) to its related pegmatite. Front. Earth Sci. 10:976588. doi: 10.3389/feart.2022.976588

Jacobson, M.I., 1993, Antero aquamarines: Minerals from the Mount Antero - White Mountain region, Chaffee County, Colorado: Coeur d'Alene, ID, L.R. Ream Pub.

Jahns, R.H., and Burnham, C.W., 1969, Experimental Studies of Pegmatite Genesis; I. A Model for the Derivation and Crystallization of Granitic Pegmatites: Economic Geology, v. 64, p. 843–864, doi: 10.2113/gsecongeo.64.8.843.

Jochum, K.P., Wilson, S.A., Abouchami, W., Amini, M., Chmeleff, J., Eisenhauer, A., Hegner, E., Iaccheri, L.M., Kieffer, B., Krause, J., McDonough, W.F., 2011, GSD-1G and MPI-

79 DING reference glasses for in situ and bulk isotopic determination, Geostandards and Geoanalytical Research, v. 35, p. 193-226, doi: 10.1111/j.1751-908X.2010.00114.x

Kar, A., 1991, Fluid inclusion and trace element studies of the gem pegmatites of Mt. Antero, Colorado [thesis].

Kellogg, K.S., Shroba, R.R., Ruleman, C.A., Bohannon, R.G., McIntosh, W. C., Premo, W.R., Cosca, M.A., Moscati, R.J., and Brandt, T.R., 2017, Geologic map of the upper Arkansas River valley region, north-central Colorado: U.S. Geological Survey Scientific Investigations Map 3382, pamphlet 70 p., 2 sheets, scale 1:50,000, https://doi.org/10.3133/sim3382.

Lederer, G.W., Foley, N.K., Jaskula, B.W., and Ayuso, R.A., 2016a, Beryllium—a critical mineral commodity—resources, production, and Supply Chain: Fact Sheet, doi: 10.3133/fs20163081.

Lindgren, W., 1925, Metasomatism: Geological Society of America Bulletin, v. 36, p. 247–262, doi: 10.1130/gsab-36-247.

London, D., 2008, Pegmatites: Ottawa , Ontario, Mineralogical Association of Canada.

London, D., Morgan, G. B. (2012) The Pegmatite Puzzle. Elements, 8 (4) 263-268 doi:10.2113/gselements.8.4.263

McIntosh, W., and Chapin, C., 2004, Geochronology of the central Colorado volcanic field: New Mexico Bureau of Geology & Mineral Resources, v. 160, p. 205–238.

Mclemore, V.T., 2010, Beryllium resources in New Mexico and adjacent areas: New Mexico Bureau of Geology and Mineral Resources, doi: 10.58799/ofr-533.

Mills, R.D., and Coleman, D.S., 2013, Temporal and chemical connections between plutons and ignimbrites from the Mount Princeton Magmatic Center: Contributions to Mineralogy and Petrology, v. 165, p. 961–980, doi: 10.1007/s00410-012-0843-4.

Müller, A., Keyser, W., Simmons, W.B., Webber, K., Wise, M., Beurlen, H., Garate-Olave, I., Roda-Robles, E., and Galliski, M.Á., 2021, Quartz Chemistry of granitic pegmatites: Implications for classification, Genesis and exploration: Chemical Geology, v. 584, p. 120507, doi: 10.1016/j.chemgeo.2021.120507.

Müller, A., Simmons, W., Beurlen, H., Thomas, R., Ihlen, P.M., Wise, M., Roda-Robles, E., Neiva, A.M.R., and Zagorsky, V., 2022, A Proposed New Mineralogical Classification System for Granitic Pegmatites – Part I: History and the Need for a New Classification: The Canadian Mineralogist, v. 60, p. 203–227, doi: 10.3749/canmin.1700088.

Paton, C., Hellstrom, J., Paul, B., Woodhead, J., Hergt, J., 2011, Iolite: freeware for the visualisation and processing of mass spectrometric data, Journal of Analytical Atomic Spectrometry, v. 26, p. 2508-2518, doi: 10.1039/C1JA10172B

Pearce, J.A., Harris, N.B.W., and Tindle, A.G., 1984, Trace element discrimination diagrams for tectonic interpretation of granitic rocks: Journal of Petrology, v. 25, p. 956–983, doi: 10.1093/petrology/25.4.956 .

Pirajno, F. (1992). Greisen Systems. In: Hydrothermal Mineral Deposits. Springer, Berlin, Heidelberg. https://doi.org/10.1007/978-3-642-75671-9_10

Reid, R., 1963, Reconnaissance Geology of the Sawtooth Range: Moscow, ID, Idaho Bureau of Mines and Geology, v. Pamphlet 129.

U.S. Geological Survey, 2025, About the 2025 list of critical minerals: https://www.usgs.gov/programs/mineral-resources-program/science/about-2025-list-critical-minerals

Shannon, J.R., 1988, Geology of the Mount Aetna Cauldron Complex, Sawatch Range, Colorado, Colorado School of Mines, Ph.D. dissertation, 434 p.

Schulz, K.J., Piatak, N.M., and Papp, J.F., 2017, Niobium and tantalum, chap. M *of* Schulz, K.J., DeYoung, J.H., Jr., Seal, R.R., II, and Bradley, D.C., eds., Critical mineral resources of the United States—Economic and environmental geology and prospects for future supply: U.S. Geological Survey Professional Paper 1802, p. M1–M34, https://doi.org/10.3133/pp1802M.

Sharp, W., 1976, Geologic Map and Details of the Beryllium and Molybdenum Occurrences Mount Antero, Chaffee County, Colorado: USGS map.

Shigley, J.E., and Kampf, A.R., 1982, Gem-bearing pegmatites: A Review: Gems & Gemology, v. 20, p. 64–77, doi: 10.5741/gems.20.2.64.

Simmons, W.B., Pezzotta, F., Shigley, J.E., and Beurlen, H., 2012, Granitic pegmatites as sources of colored gemstones: Elements, v. 8, p. 281–287, doi: 10.2113/gselements.8.4.281.

Simmons, W.B., Webber, K.L., Falster, A.U., Roda-Robles, E., and Dallaire, D.A., 2022, Pegmatology: Pegmatite Mineralogy, Petrology and Petrogenesis: Cana, VA, Rubellite Press.

Switzer, G., 1929, Granite Pegmatites of the Mt Antero Region, Colorado: American Mineralogist, v. 24, p. 791–809, http://www.minsocam.org/msa/collectors_corner/arc/comtantero.htm.

Troch, J., Huber, C., and Bachmann, O., 2022, The physical and chemical evolution of magmatic fluids in near-solidus silicic magma reservoirs: Implications for the formation of Pegmatites: American Mineralogist, v. 107, p. 190–205, doi: 10.2138/am-2021-7915.

Wark, D.A., and Watson, E.B., 2006, TitaniQ: A titanium-in-quartz geothermometer: Contributions to Mineralogy and Petrology, v. 152, p. 743–754, doi: 10.1007/s00410-006-0132-1.

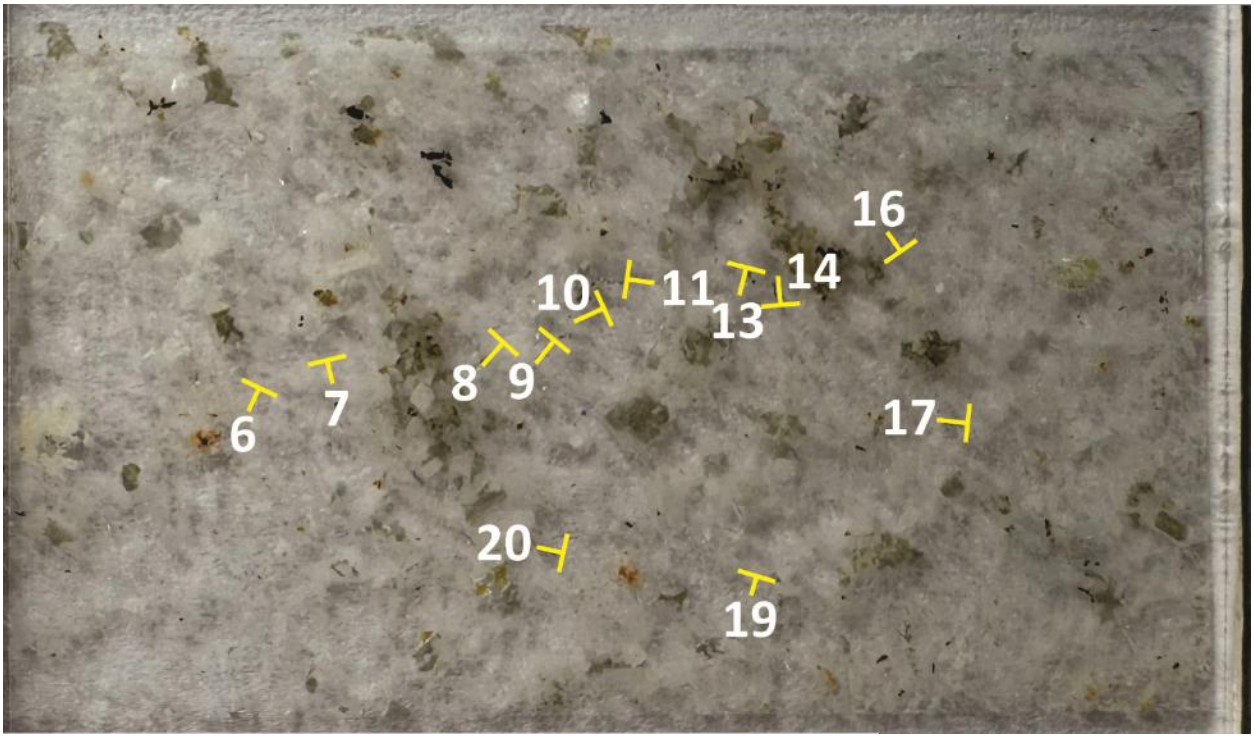
Wegert, D., Parker, D., and Ren, M., 2013, The Nathrop Domes, Colorado: Geochemistry and Petrogenesis of a topaz rhyolite: Rocky Mountain Geology, v. 48, p. 1–14, doi: 10.2113/gsrocky.48.1.1.

Whalen, J.B., Currie, K.L., and Chappell, B.W., 1987, A-type granites: Geochemical characteristics, discrimination and petrogenesis: Contributions to Mineralogy and Petrology, v. 95, p. 407–419, doi: 10.1007/BF00402202

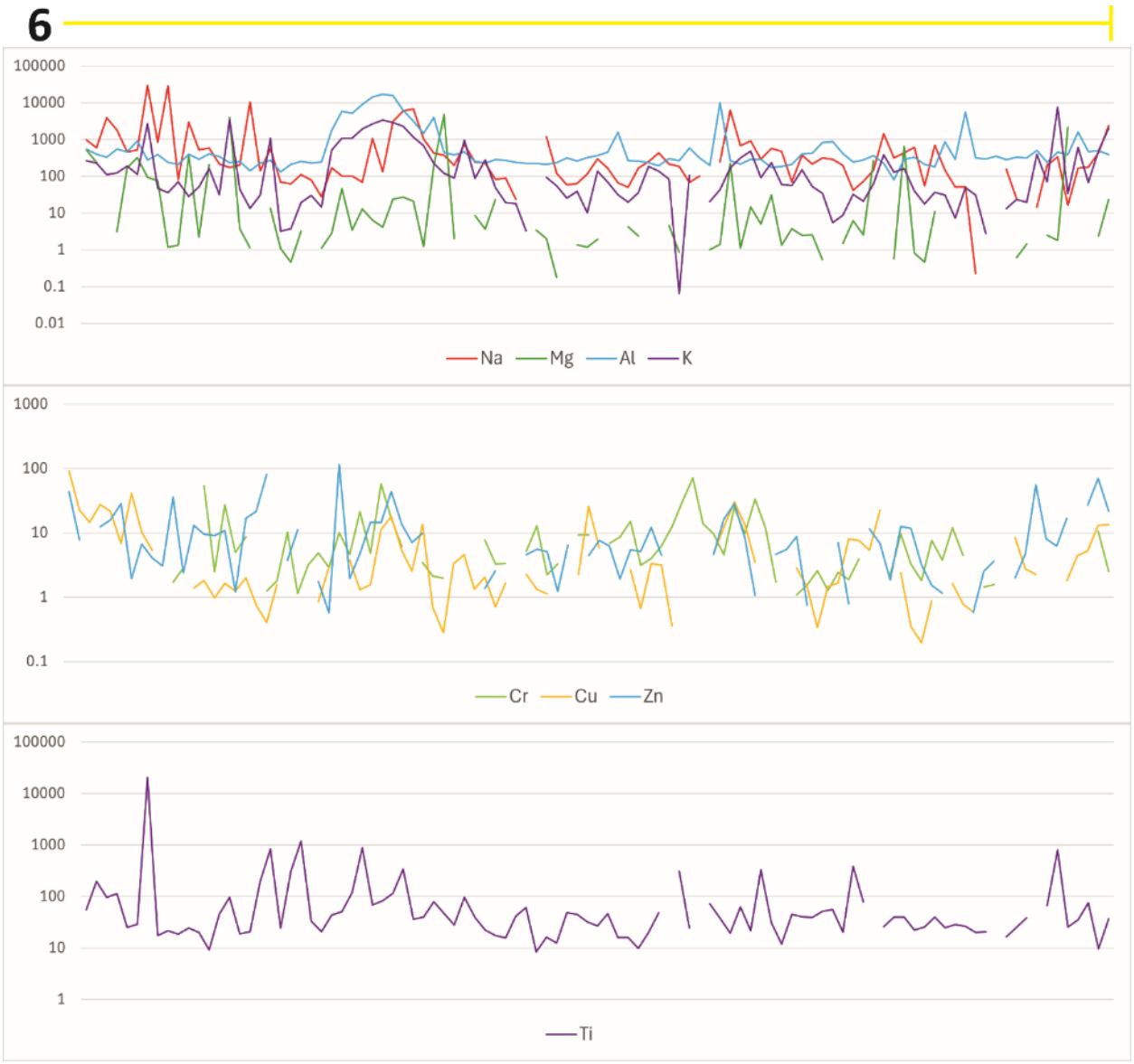
Wise, M.A., Müller, A., and Simmons, W.B., 2022, A proposed new mineralogical classification system for granitic pegmatites: The Canadian Mineralogist, v. 60, p. 229–248, doi: 10.3749/canmin.1800006.

Wood D.L., Nassau K. 1968. The characterization of beryl and emerald by visible and infrared absorption spectroscopy. *The American Mineralogist*, 53(5-6):777-800.

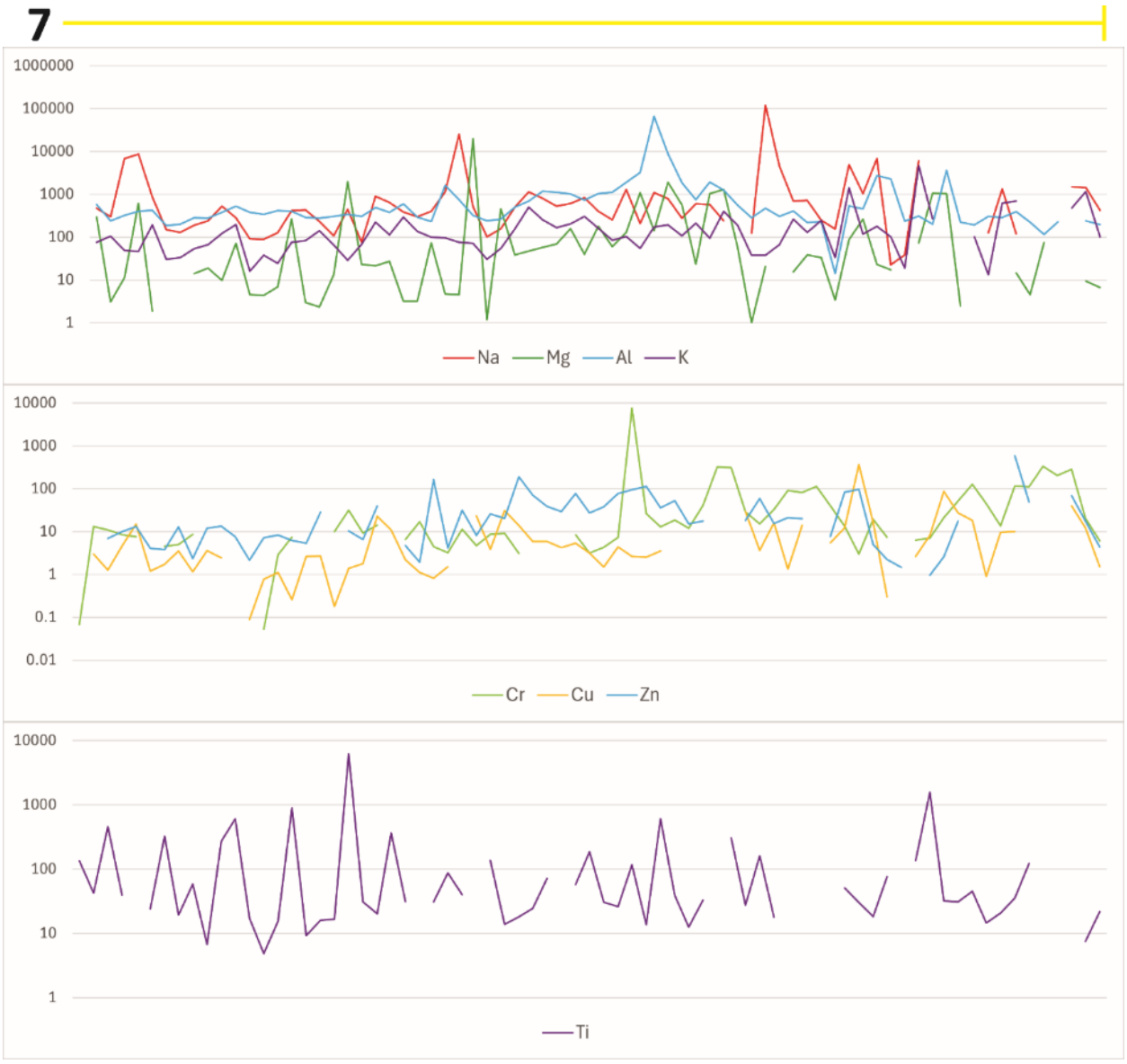
Appendix A - Thick Sections and Concentration (ppm) Versus Transect Length LA-ICP-MS Graphs



Appendix Figure 1: Sample LE25-3A1, 100 micron double polished thick section of California Granite transition zone proximal to pegmatite LE25-3A3. The yellow (quartz transect) line labelled 6 corresponds to LA-ICP-MS transect line LE25-3A1.6.



Appendix Figure 2: Concentrations (ppm) versus transect length. Sample LE25-3A1.6 is a quartz transect from the California Granite transition zone proximal to pegmatite LE25-3A3.



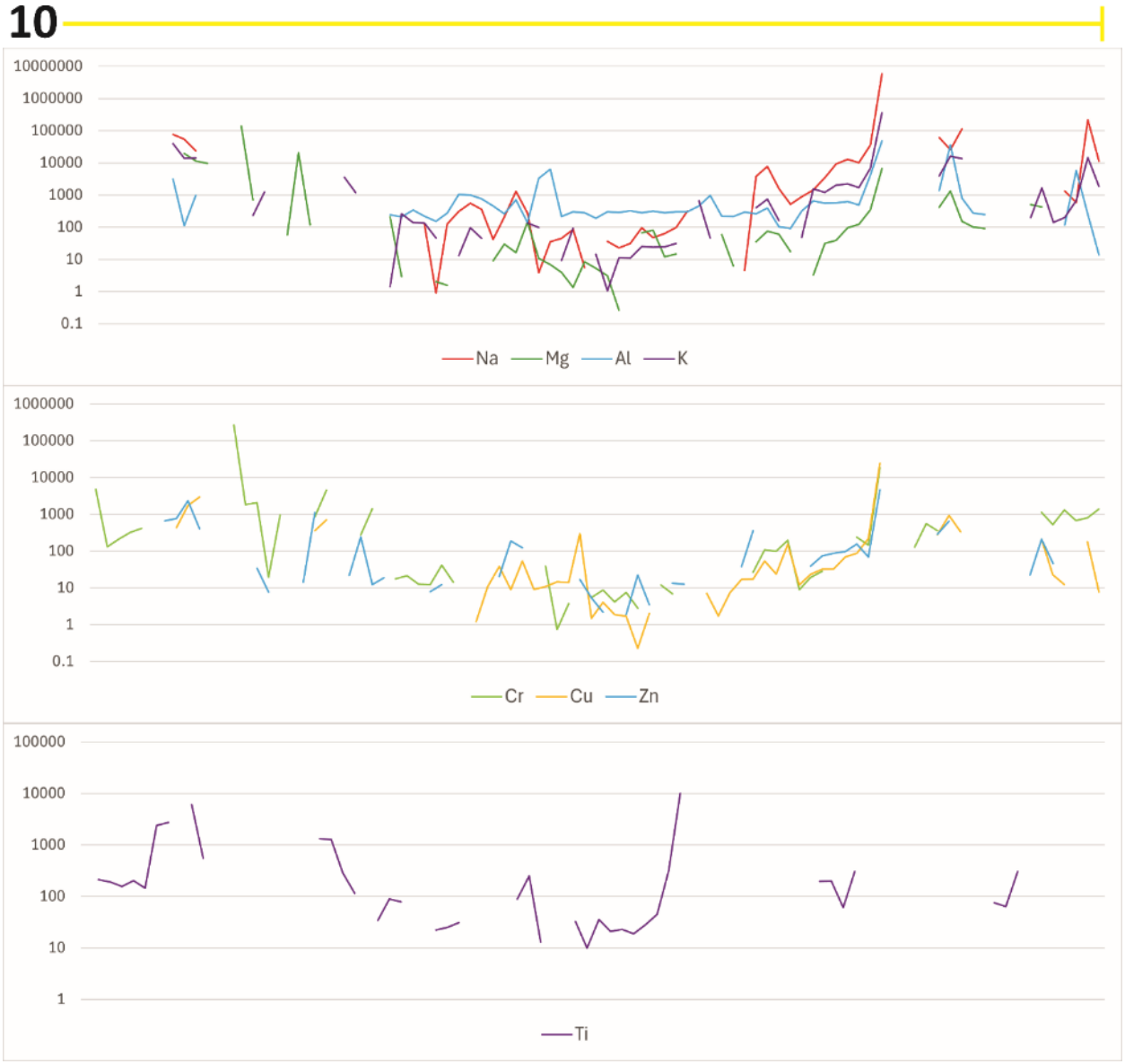
Appendix Figure 3: Concentrations (ppm) versus transect length. Sample LE25-3A1.7 is a quartz transect from the California Granite transition zone proximal to pegmatite LE25-3A3.



Appendix Figure 4: Concentrations (ppm) versus transect length. Sample LE25-3A1.8 is a quartz transect from the California Granite transition zone proximal to pegmatite LE25-3A3.



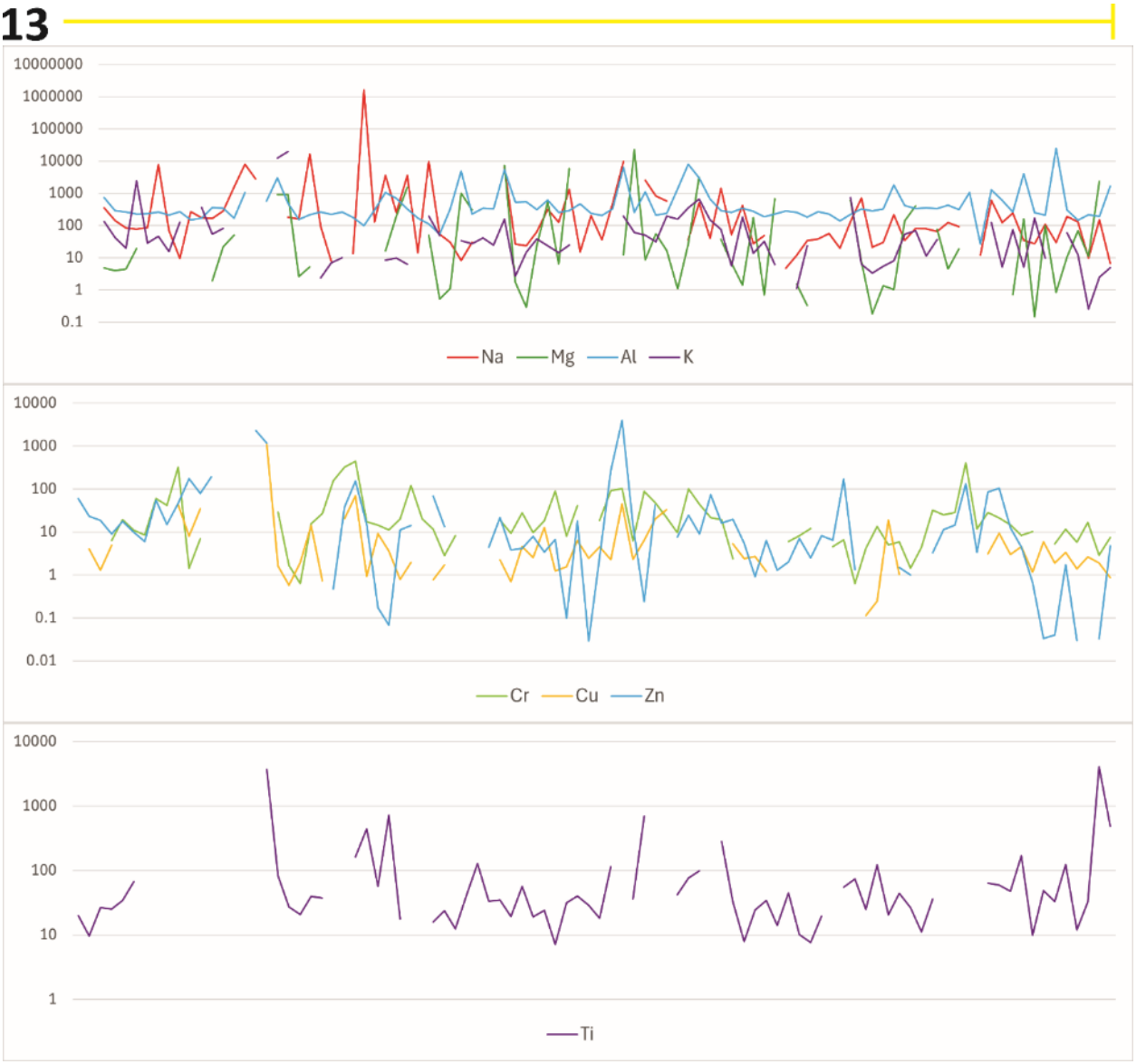
Appendix Figure 5: Concentrations (ppm) versus transect length. Sample LE25-3A1.9 is a quartz transect from the California Granite transition zone proximal to pegmatite LE25-3A3.



Appendix Figure 6: Concentrations (ppm) versus transect length. Sample LE25-3A1.10 is a quartz transect from the California Granite transition zone proximal to pegmatite LE25-3A3.



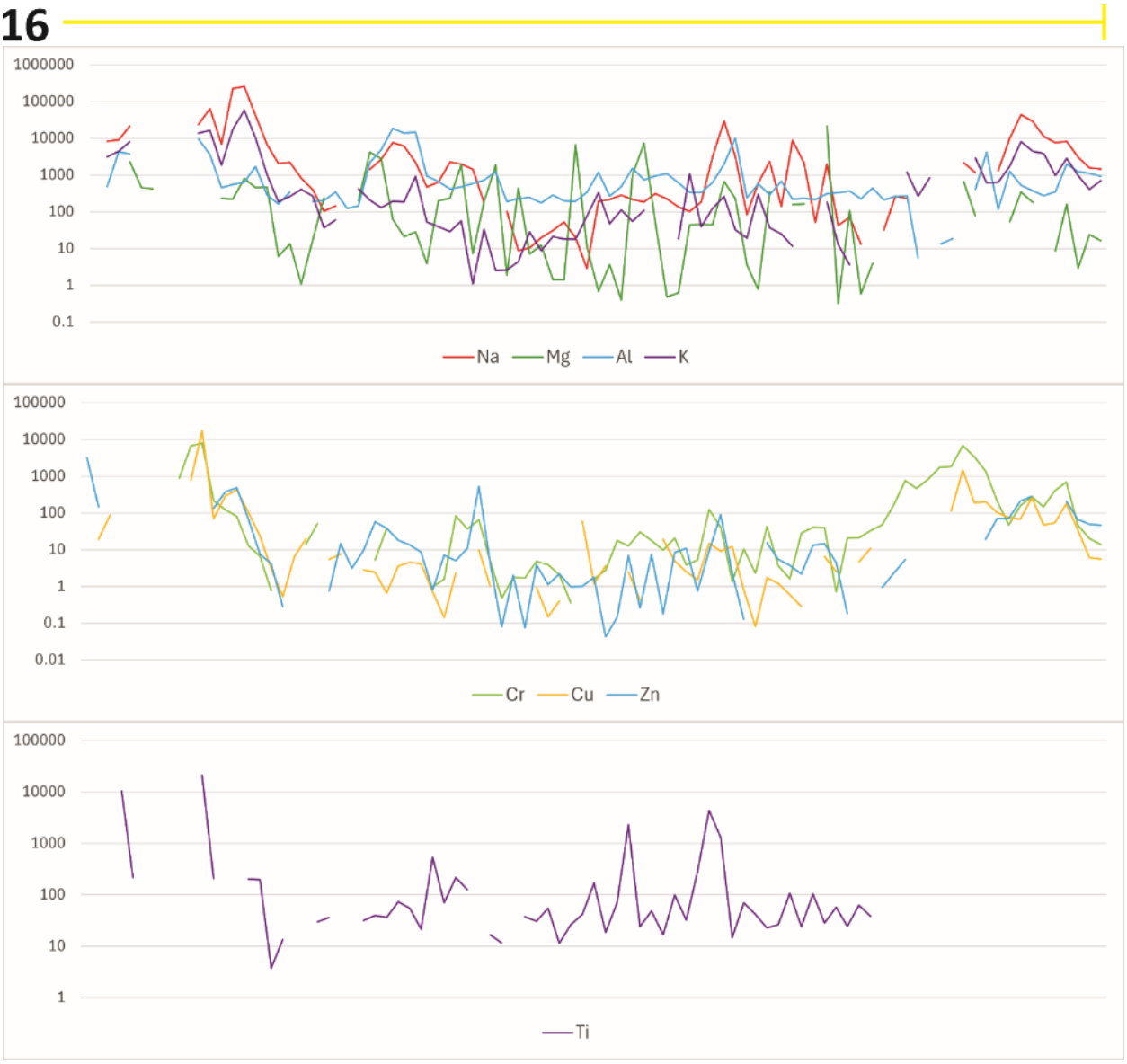
Appendix Figure 7: Concentrations (ppm) versus transect length. Sample LE25-3A1.11 is a quartz transect from the California Granite transition zone proximal to pegmatite LE25-3A3.



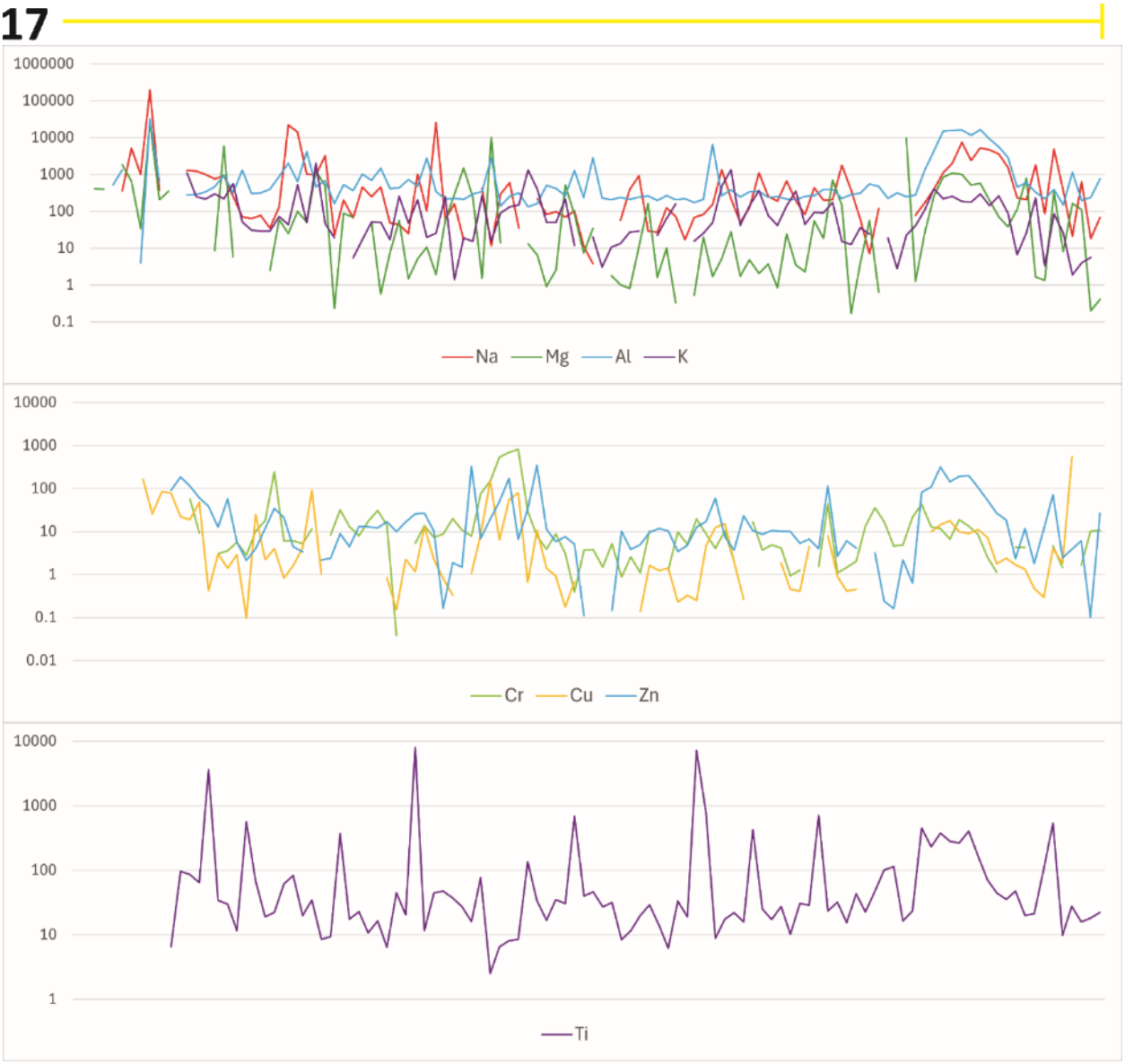
Appendix Figure 8: Concentrations (ppm) versus transect length. Sample LE25-3A1.13 is a quartz transect from the California Granite transition zone proximal to pegmatite LE25-3A3.



Appendix Figure 9: Concentrations (ppm) versus transect length. Sample LE25-3A1.14 is a quartz transect from the California Granite transition zone proximal to pegmatite LE25-3A3.



Appendix Figure 10: Concentrations (ppm) versus transect length. Sample LE25-3A1.16 is a quartz transect from the California Granite transition zone proximal to pegmatite LE25-3A3.



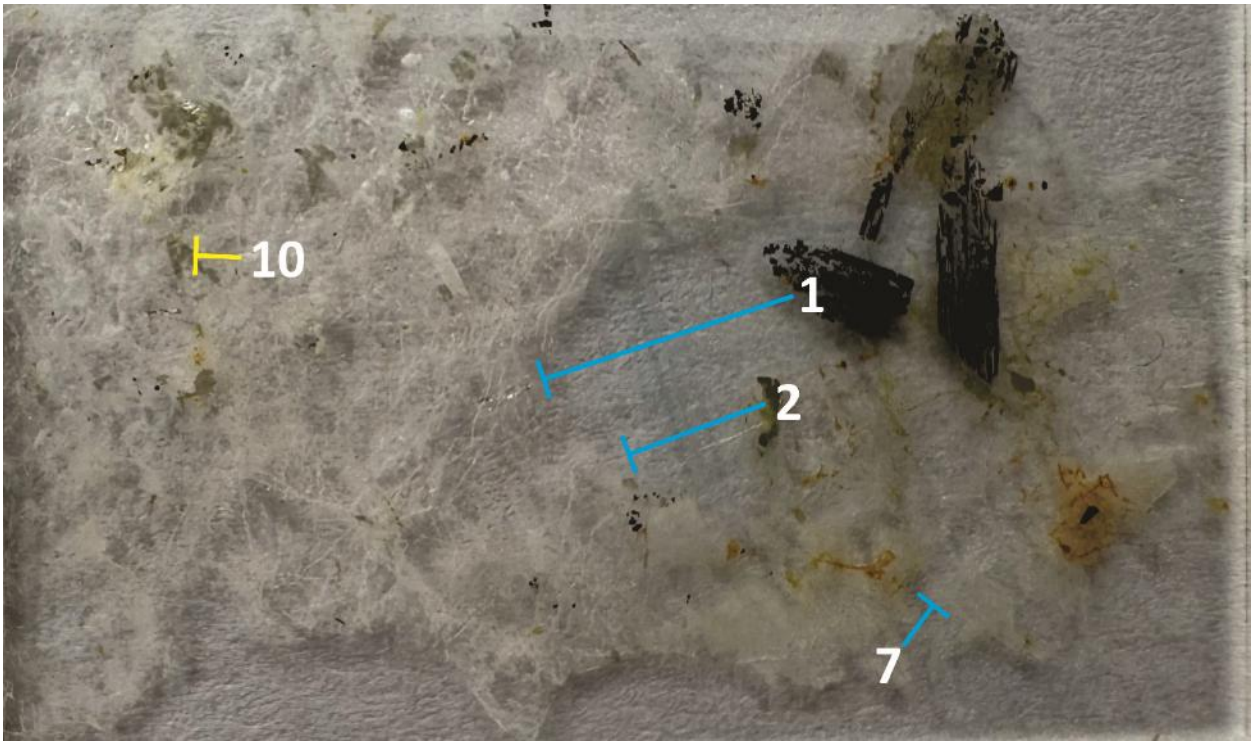
Appendix Figure 11: Concentrations (ppm) versus transect length. Sample LE25-3A1.17 is a quartz transect from the California Granite transition zone proximal to pegmatite LE25-3A3.



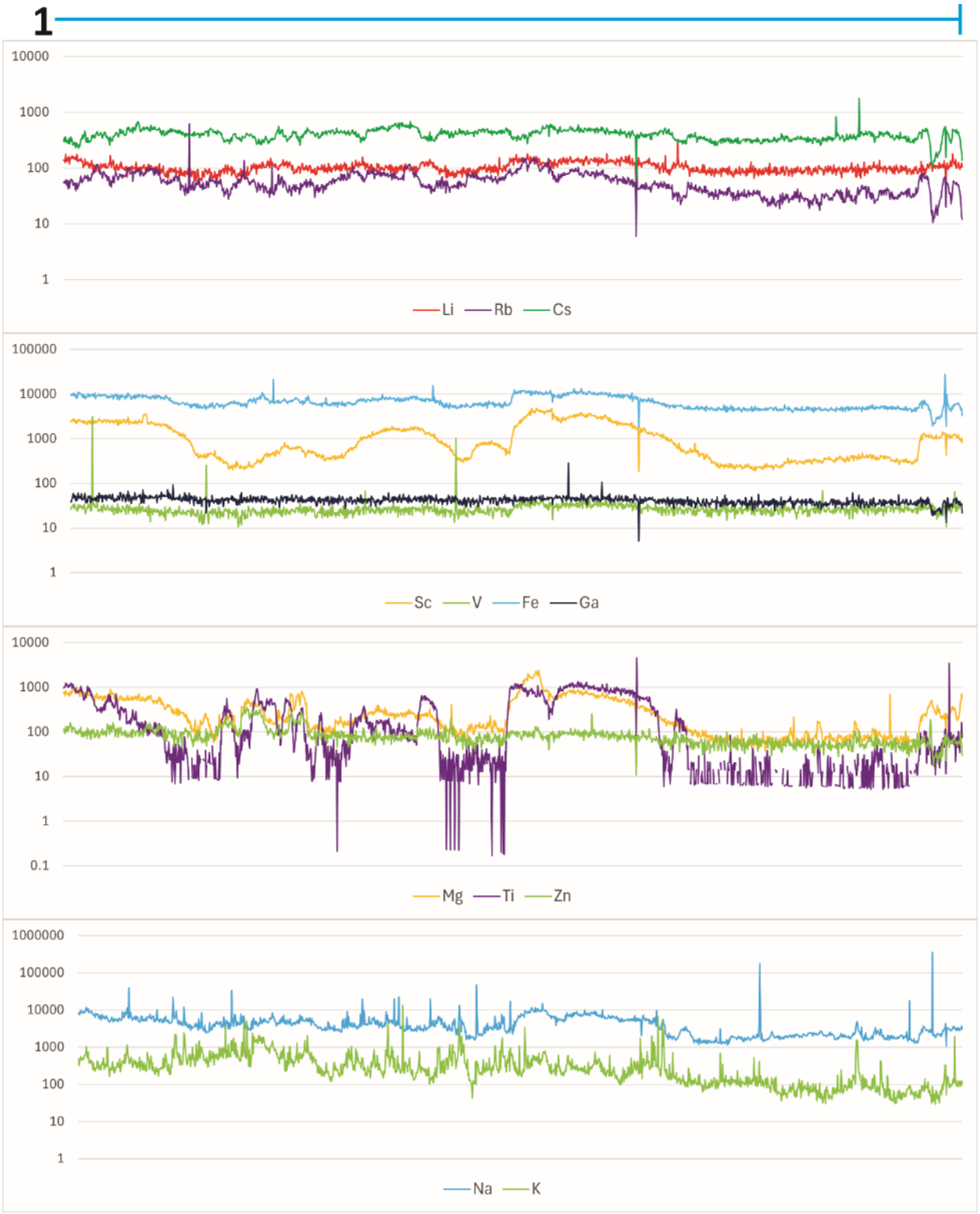
Appendix Figure 12: Concentrations (ppm) versus transect length. Sample LE25-3A1.19 is a quartz transect from the California Granite transition zone proximal to pegmatite LE25-3A3.



Appendix Figure 13: Concentrations (ppm) versus transect length. Sample LE25-3A1.20 is a quartz transect from the California Granite transition zone proximal to pegmatite LE25-3A3.



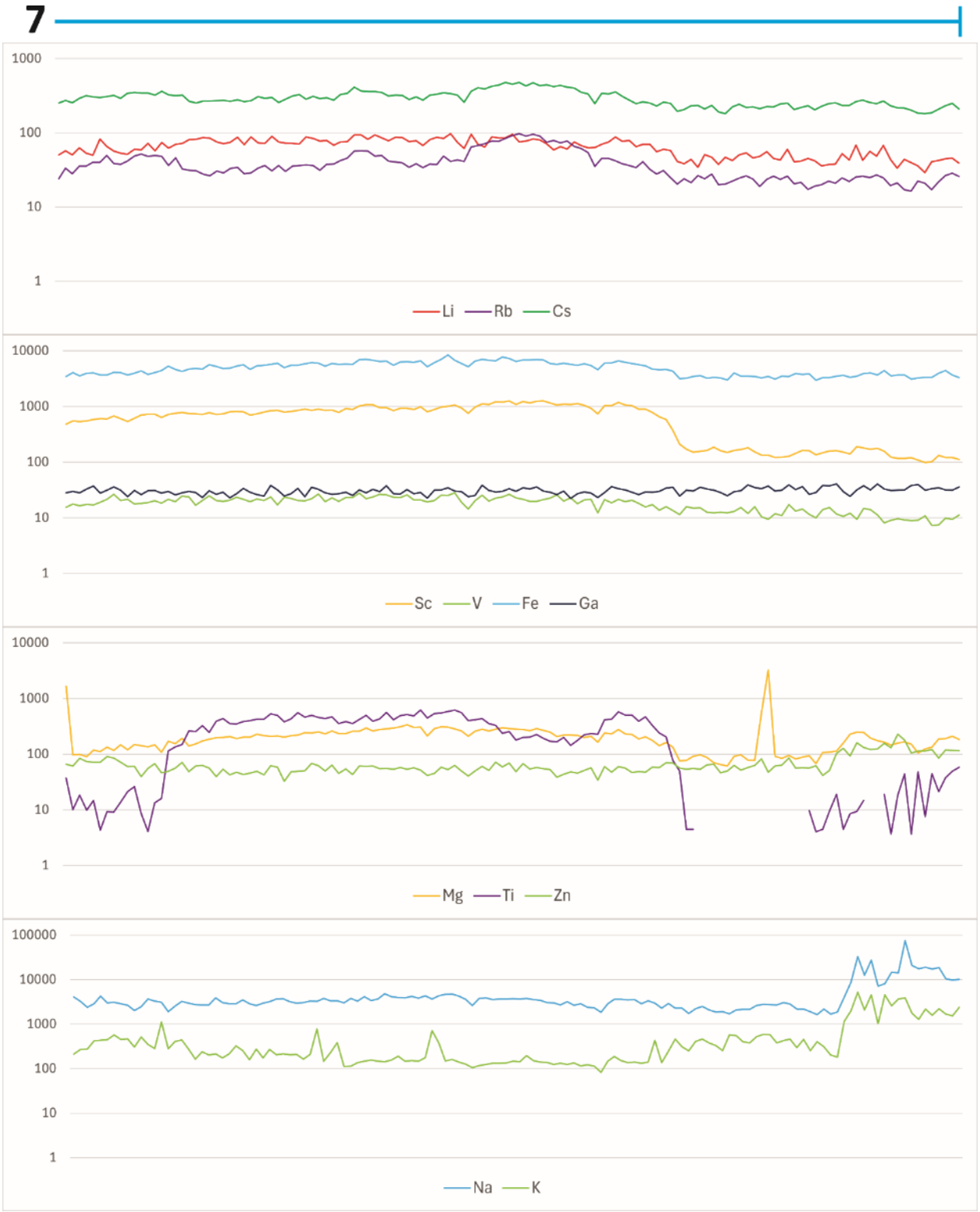
Appendix Figure 14: Sample LE25-3A5, 100 micron double polished thick section of a pegmatite core zone. Blue (beryl transect) and yellow (quartz transect) lines and numbers correspond to LA-ICP-MS transect lines (e.g., LE25-3A5.1 is the blue line labelled 1).



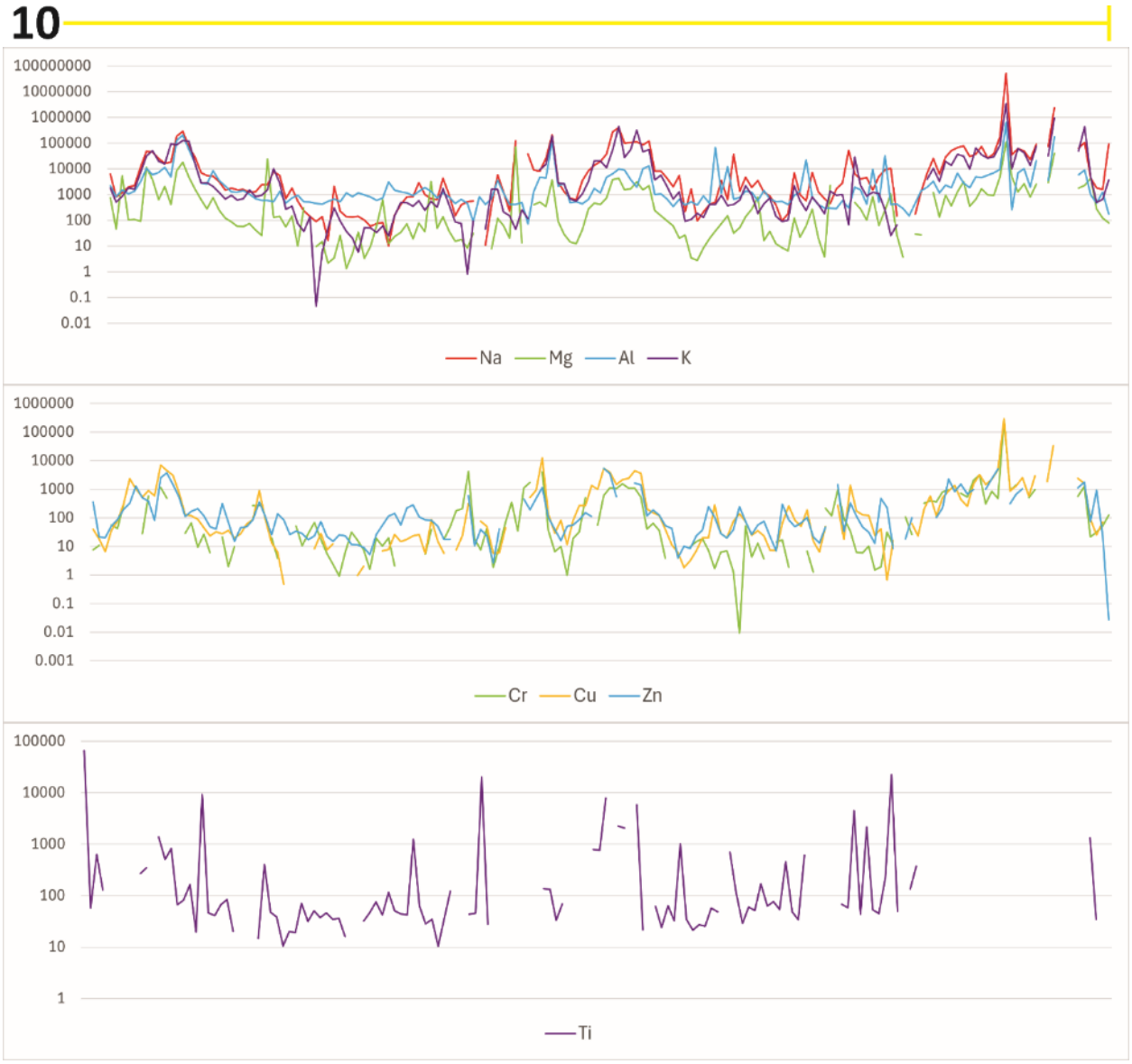
Appendix Figure 15: Concentrations (ppm) versus transect length. Sample LE25-3A5.1 is a beryl transect from pegmatite LE25-3A5.



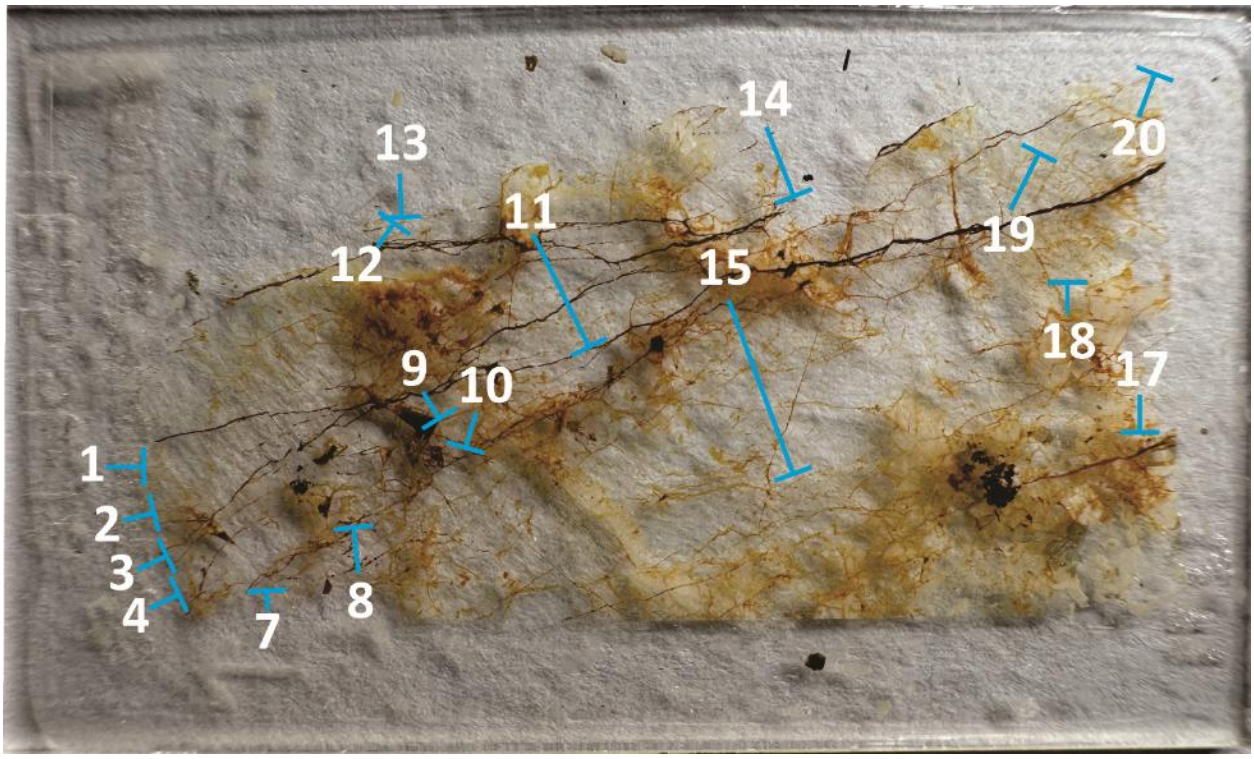
Appendix Figure 16: Concentrations (ppm) versus transect length. Sample LE25-3A5.2 is a beryl transect from pegmatite LE25-3A5.



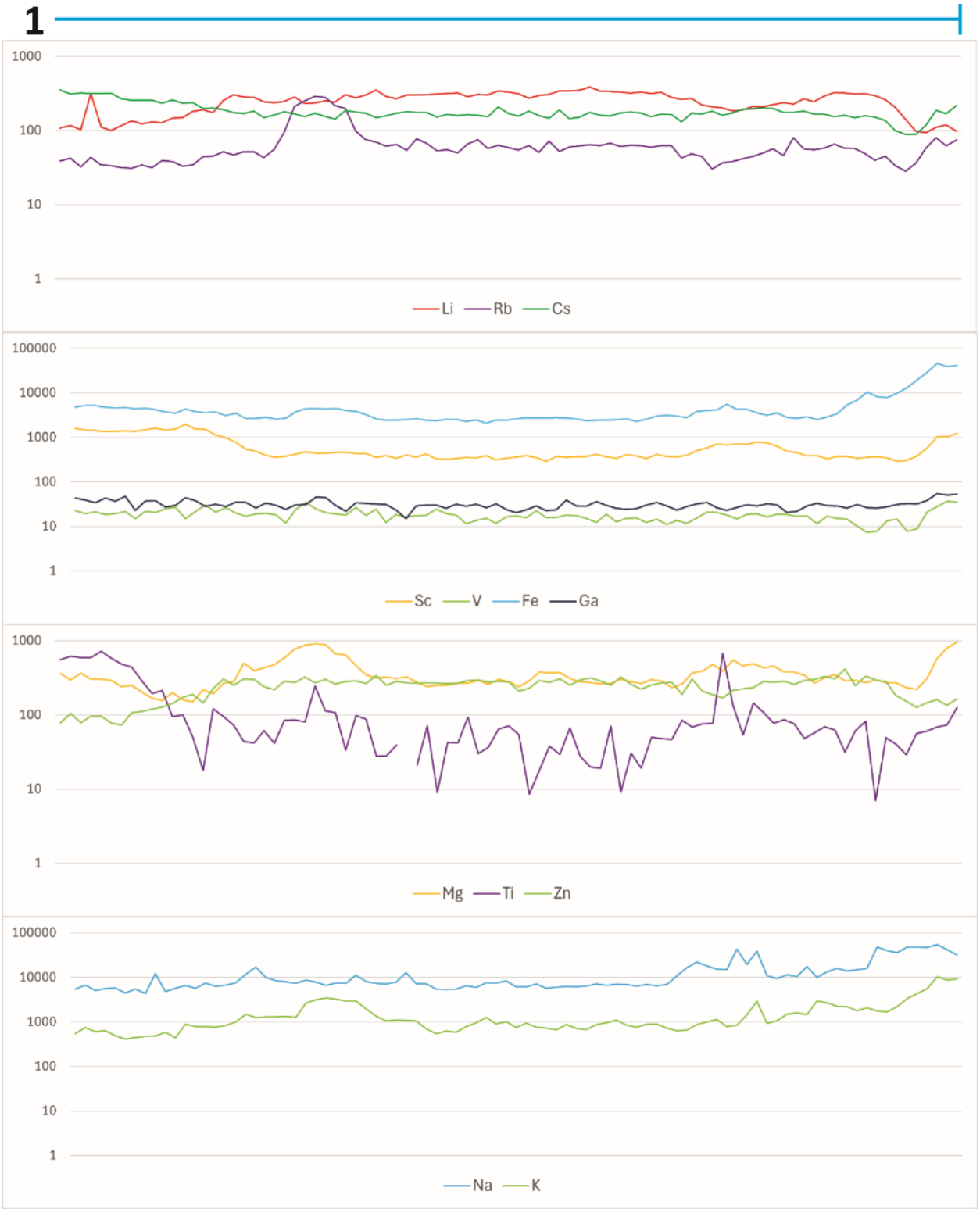
Appendix Figure 17: Concentrations (ppm) versus transect length. Sample LE25-3A5.7 is a beryl transect from pegmatite LE25-3A5.



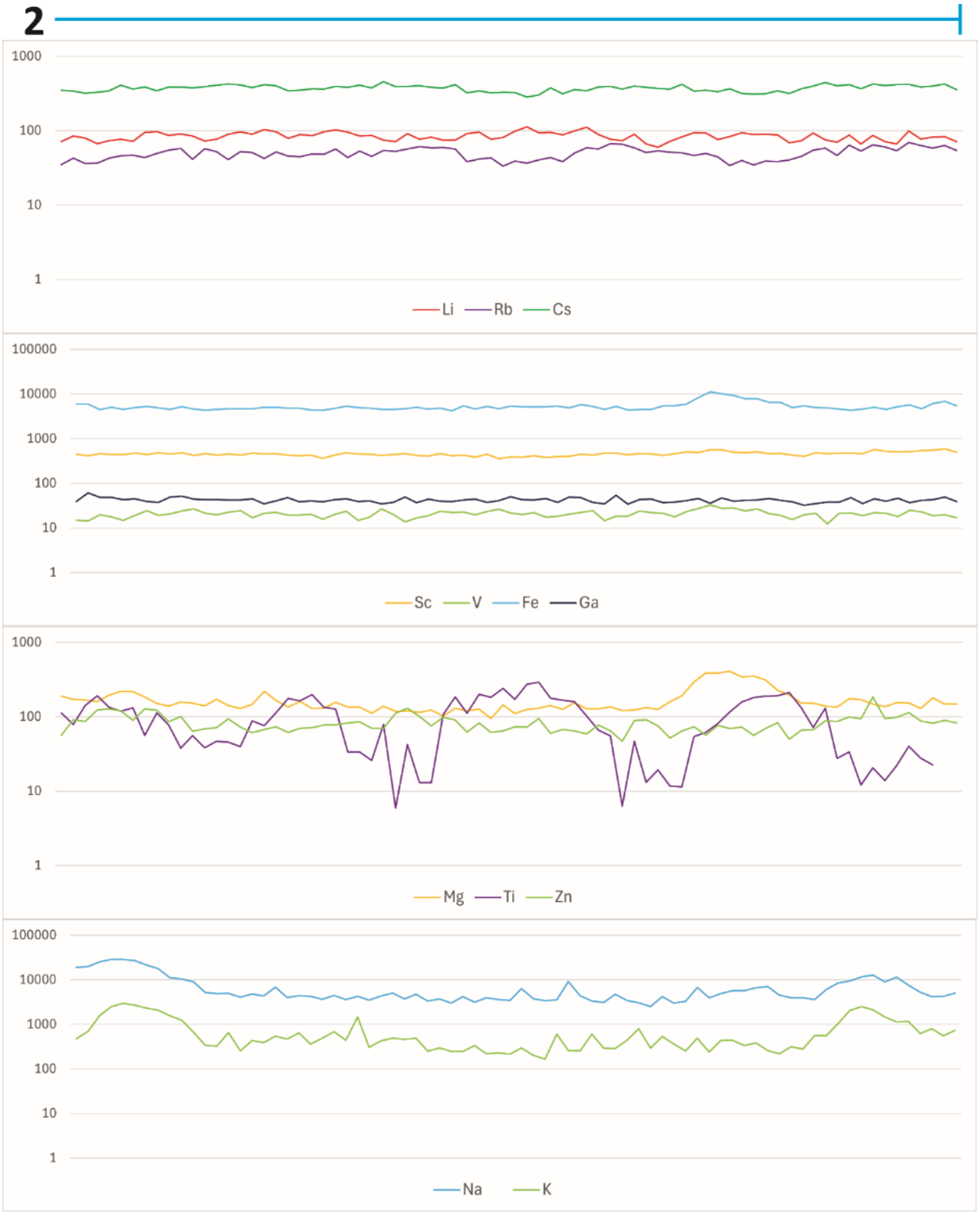
Appendix Figure 18: Concentrations (ppm) versus transect length. Sample LE25-3A5.10 is a quartz transect from pegmatite LE25-3A5.



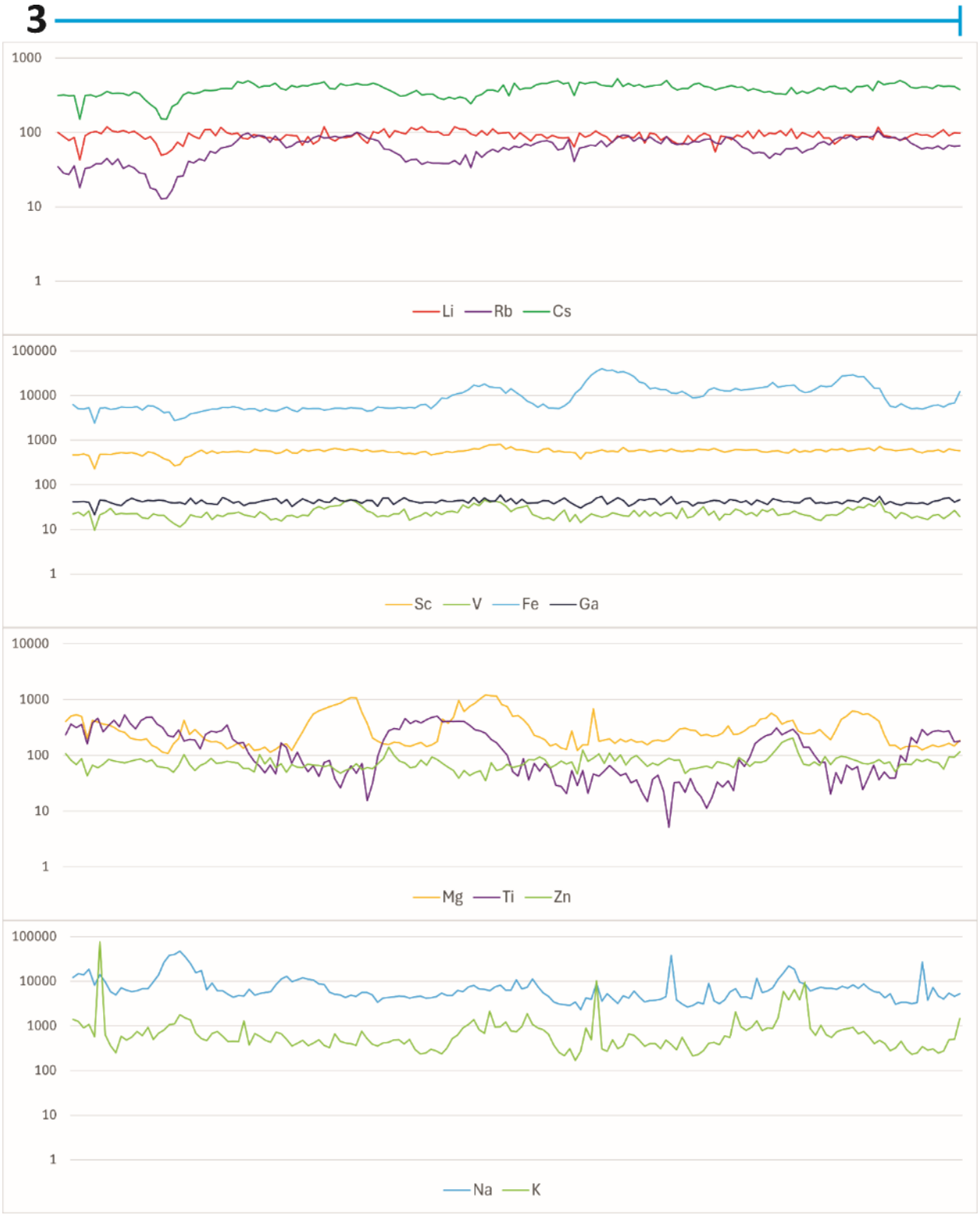
Appendix Figure 19: Sample LE25-5L-1A, 100 micron double polished thick section of a pegmatite core zone. Blue (beryl transect) lines and numbers correspond to LA-ICP-MS transect lines (e.g., LE25-5L-1A.1 is the blue line labelled 1).



Appendix Figure 20: Concentrations (ppm) versus transect length. Sample LE25-5L-1A.1 is a beryl transect from pegmatite LE25-5L.



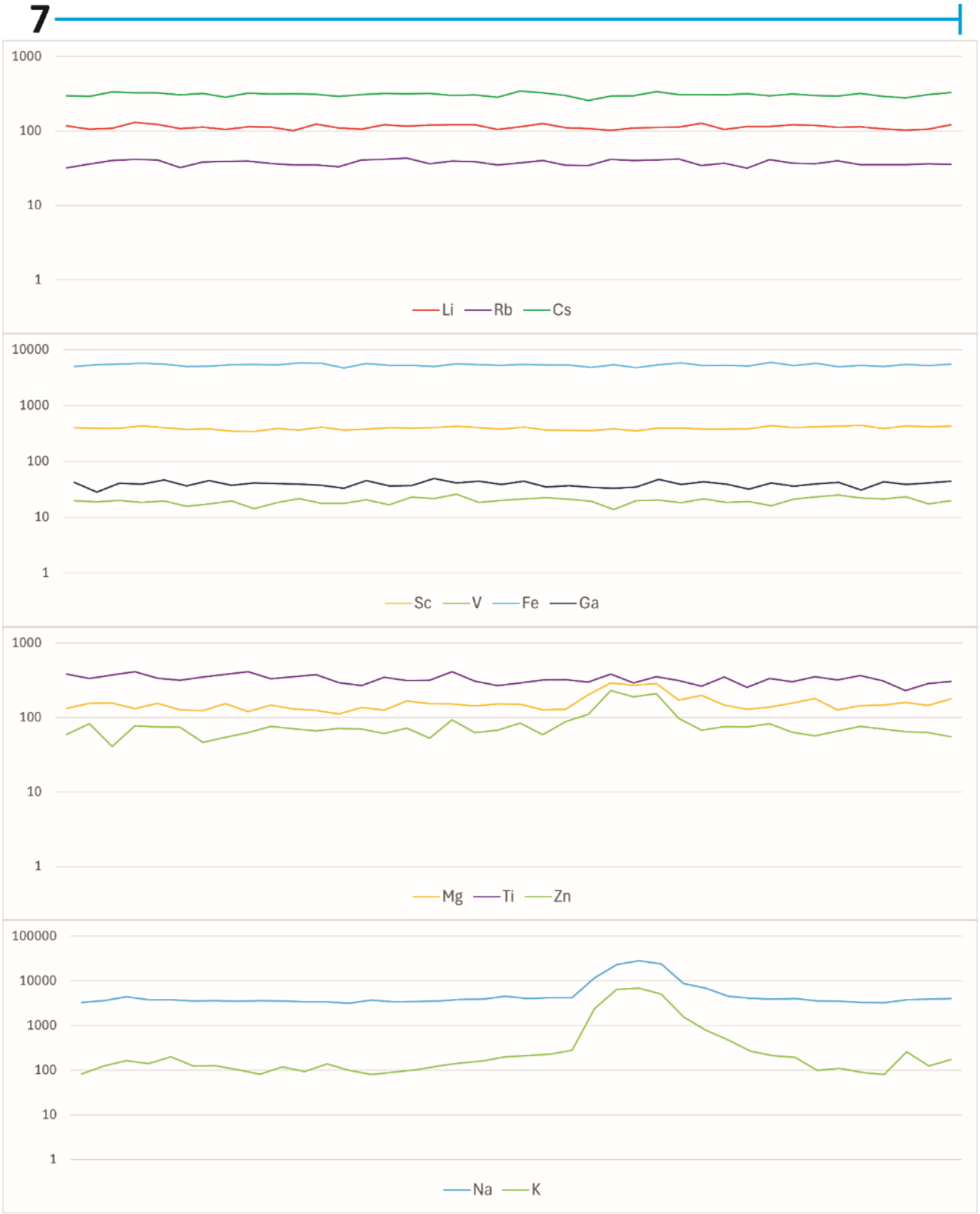
Appendix Figure 21: Concentrations (ppm) versus transect length. Sample LE25-5L-1A.2 is a beryl transect from pegmatite LE25-5L.



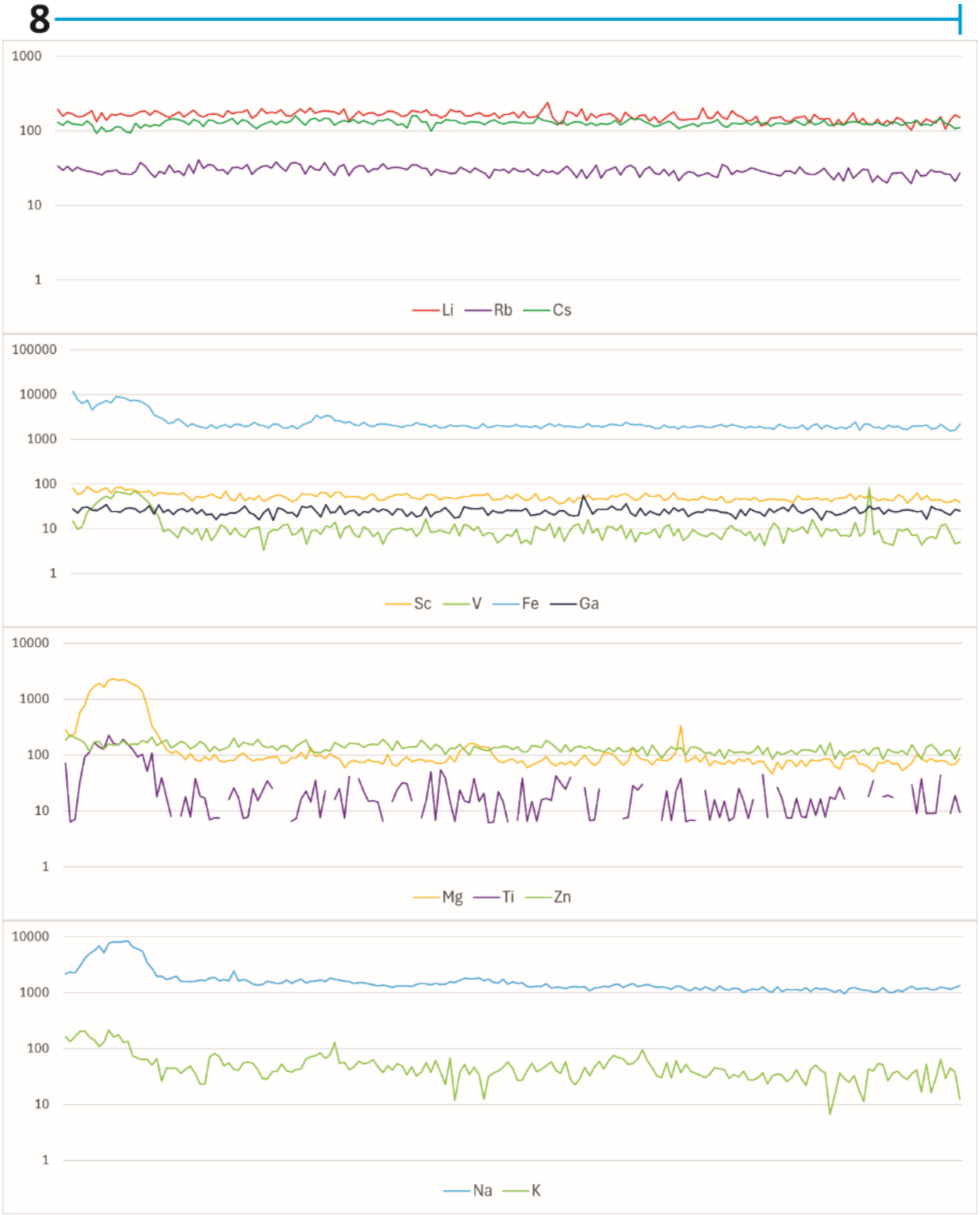
Appendix Figure 22: Concentrations (ppm) versus transect length. Sample LE25-5L-1A.3 is a beryl transect from pegmatite LE25-5L.



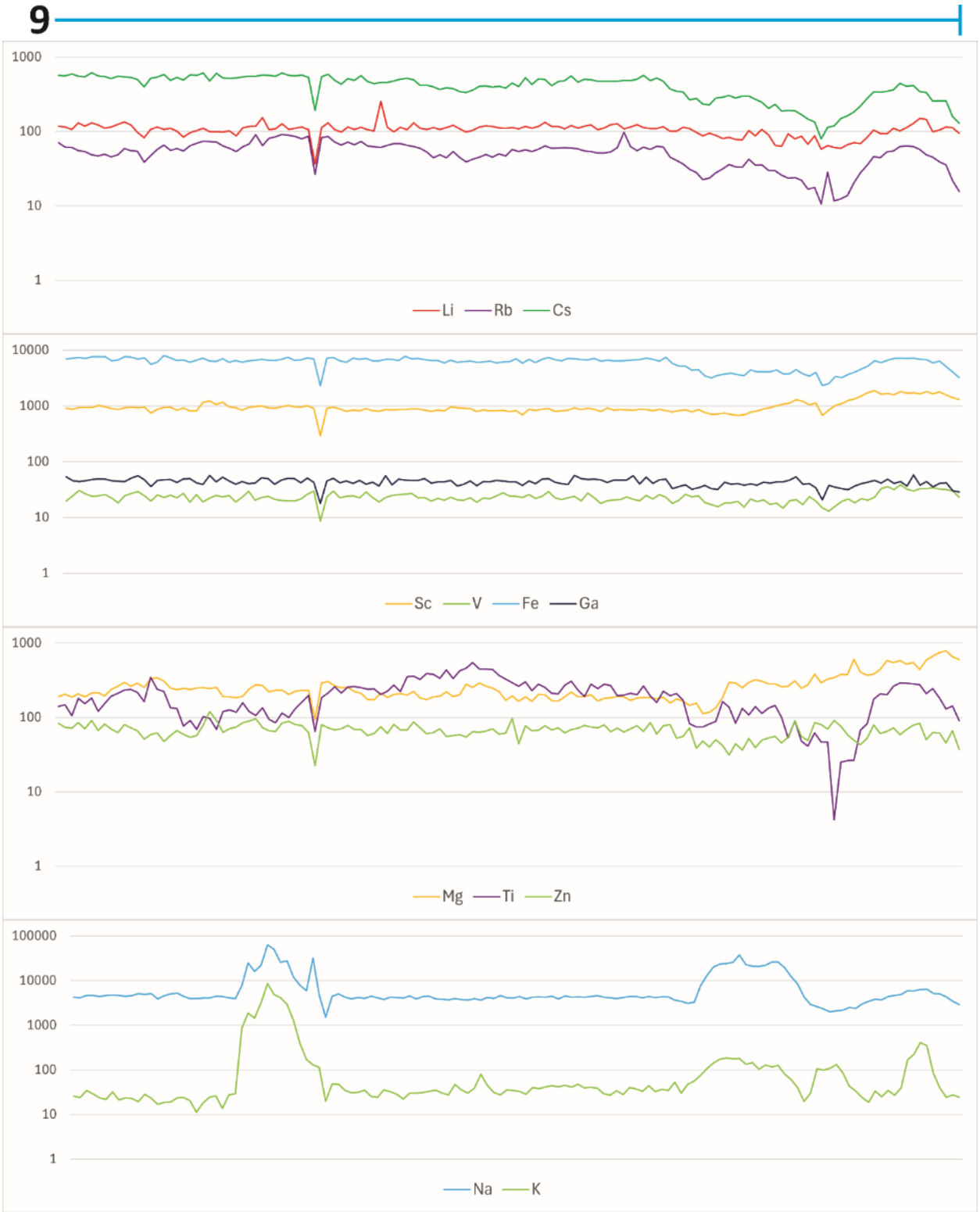
Appendix Figure 23: Concentrations (ppm) versus transect length. Sample LE25-5L-1A.4 is a beryl transect from pegmatite LE25-5L.



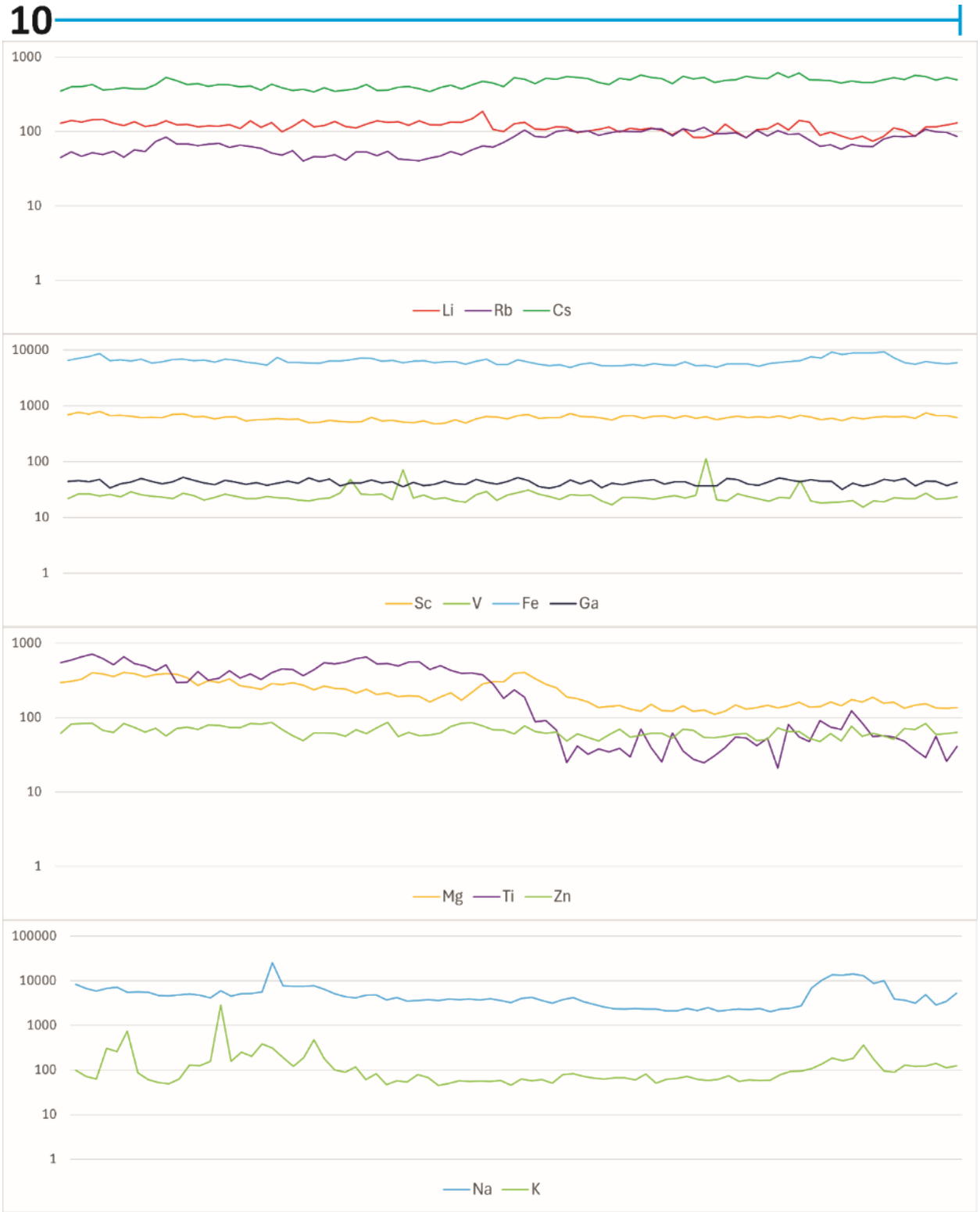
Appendix Figure 24: Concentrations (ppm) versus transect length. Sample LE25-5L-1A.7 is a beryl transect from pegmatite LE25-5L.



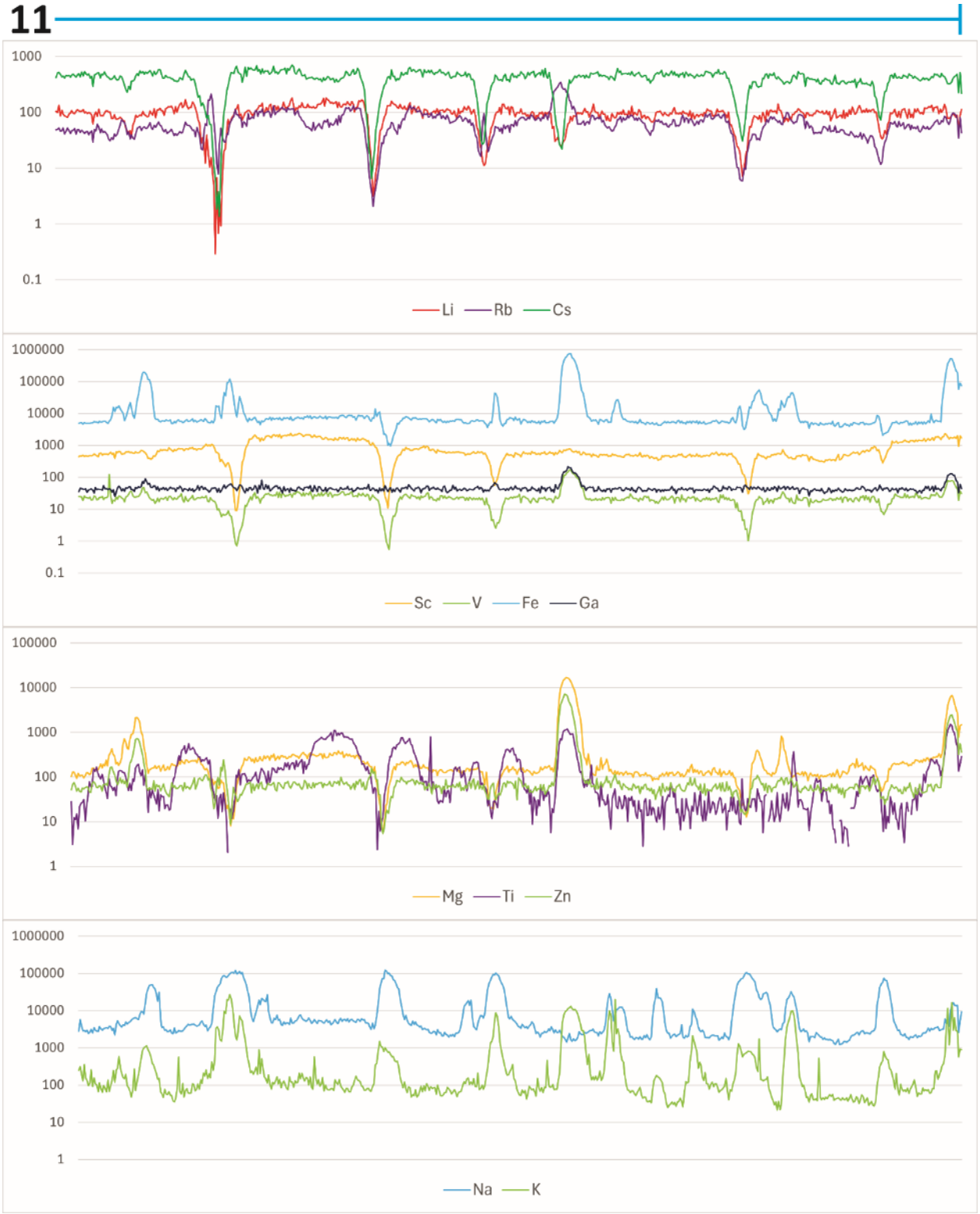
Appendix Figure 25: Concentrations (ppm) versus transect length. Sample LE25-5L-1A.8 is a beryl transect from pegmatite LE25-5L.



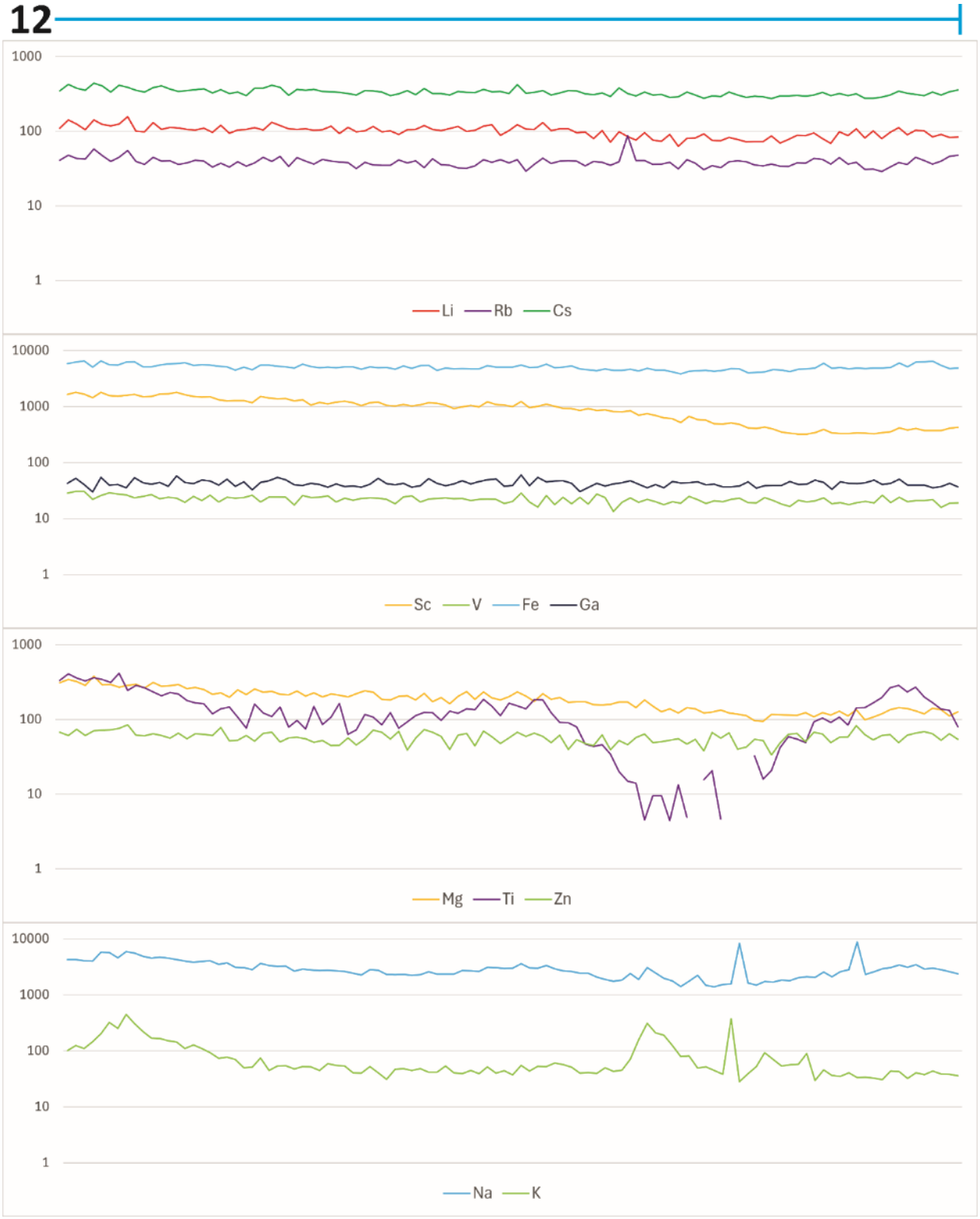
Appendix Figure 26: Concentrations (ppm) versus transect length. Sample LE25-5L-1A.9 is a beryl transect from pegmatite LE25-5L.



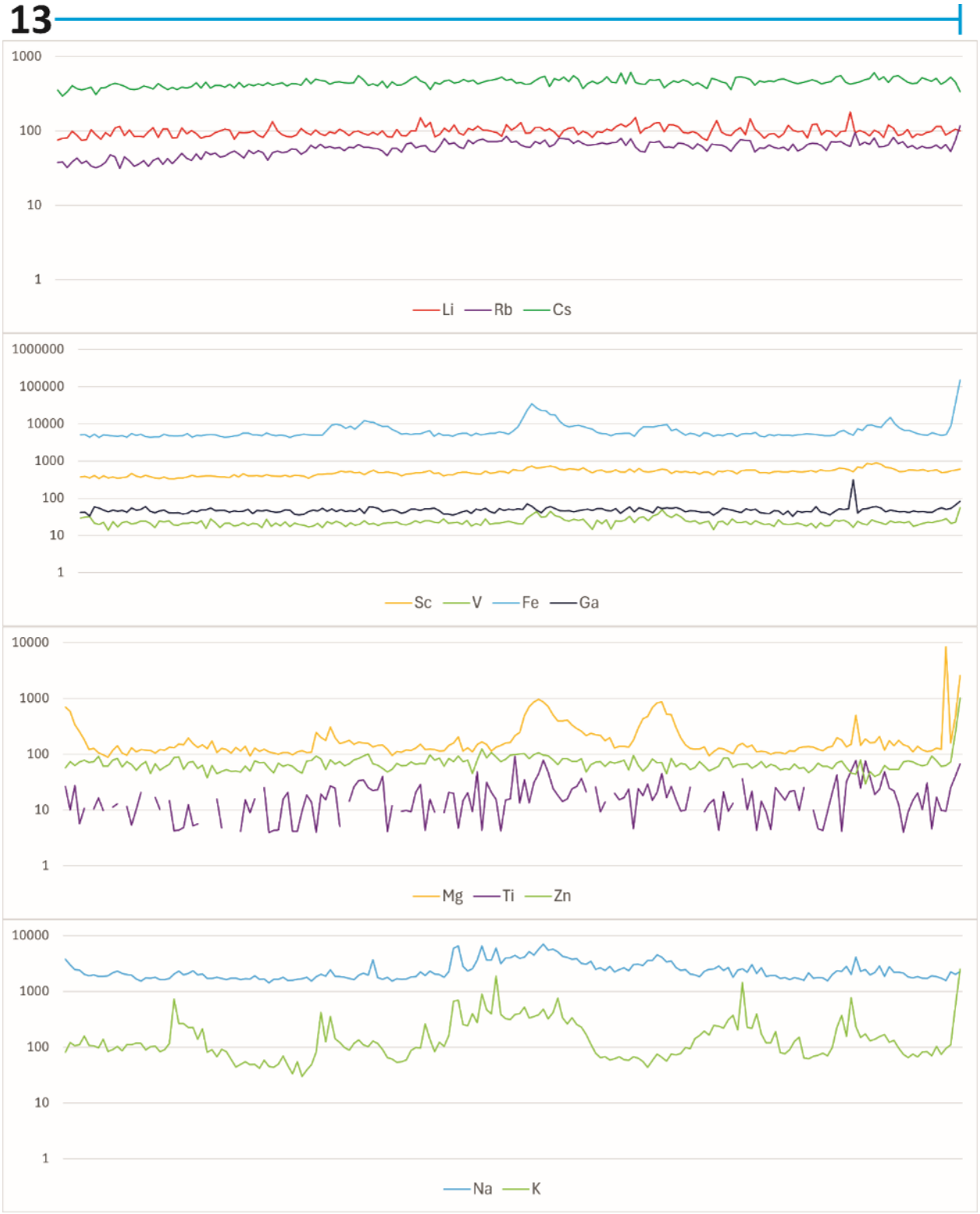
Appendix Figure 27: Concentrations (ppm) versus transect length. Sample LE25-5L-1A.10 is a beryl transect from pegmatite LE25-5L.



Appendix Figure 28: Concentrations (ppm) versus transect length. Sample LE25-5L-1A.11 is a beryl transect from pegmatite LE25-5L.



Appendix Figure 29: Concentrations (ppm) versus transect length. Sample LE25-5L-1A.12 is a beryl transect from pegmatite LE25-5L.



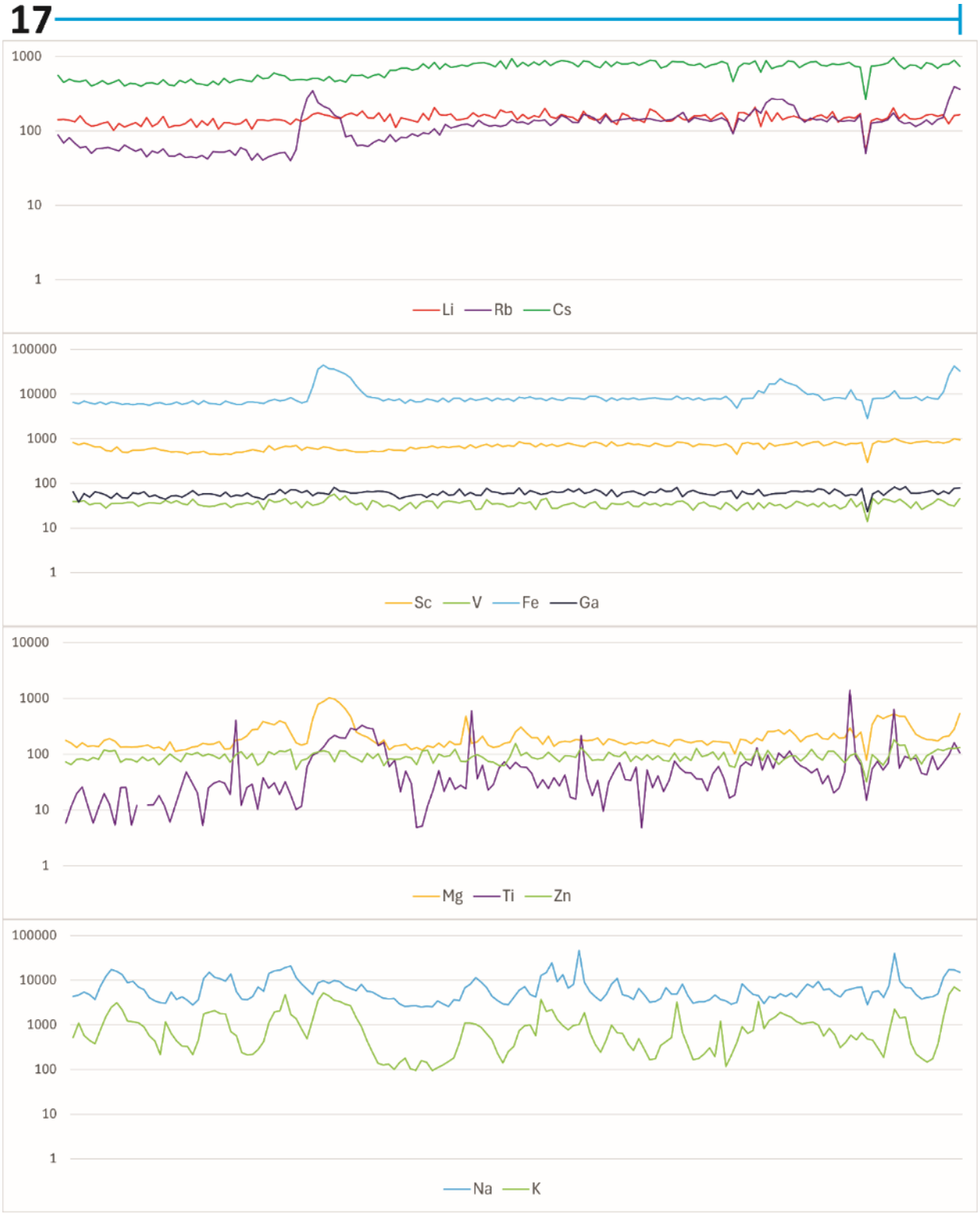
Appendix Figure 30: Concentrations (ppm) versus transect length. Sample LE25-5L-1A.13 is a beryl transect from pegmatite LE25-5L.



Appendix Figure 31: Concentrations (ppm) versus transect length. Sample LE25-5L-1A.14 is a beryl transect from pegmatite LE25-5L.



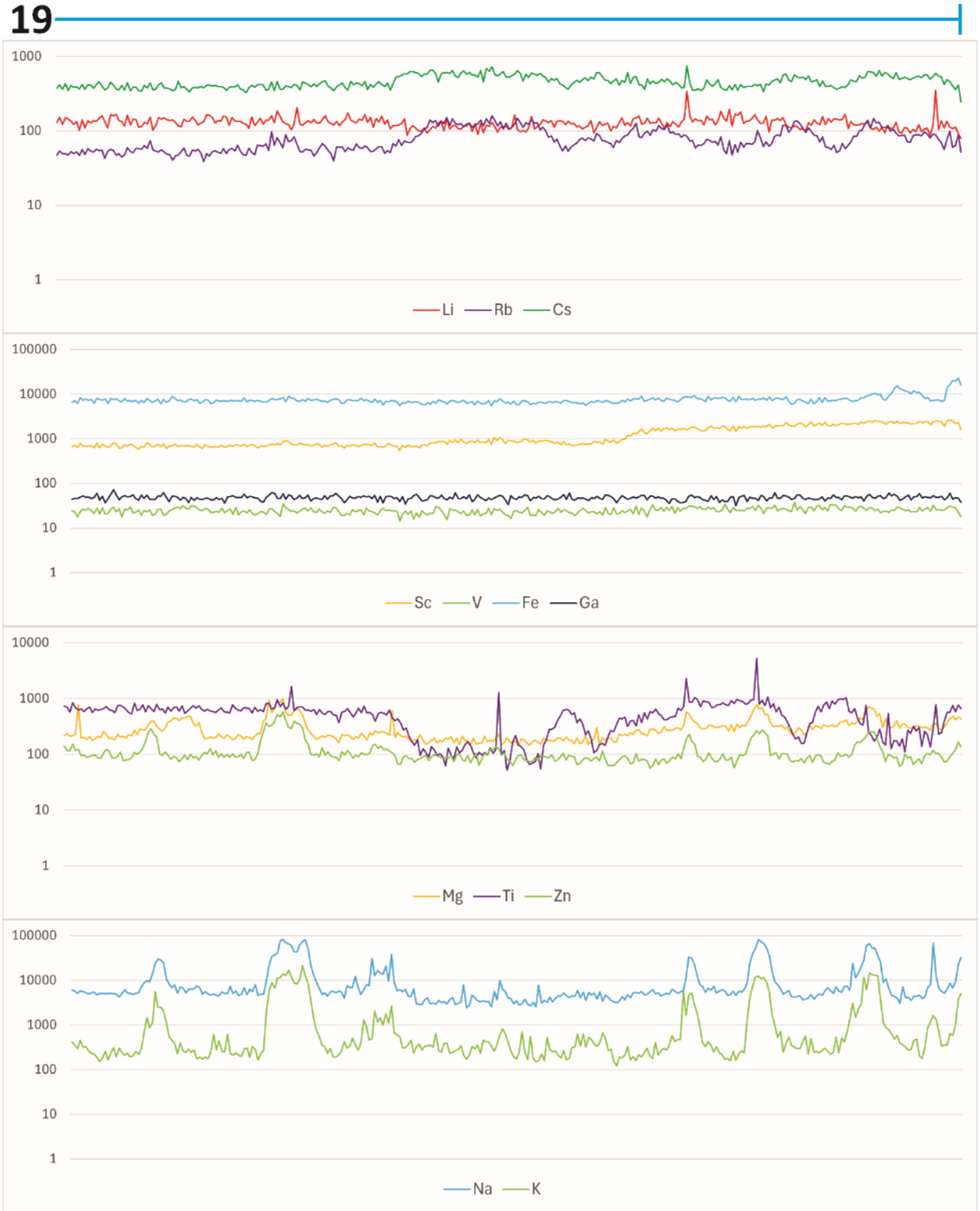
Appendix Figure 32: Concentrations (ppm) versus transect length. Sample LE25-5L-1A.15 is a beryl transect from pegmatite LE25-5L.



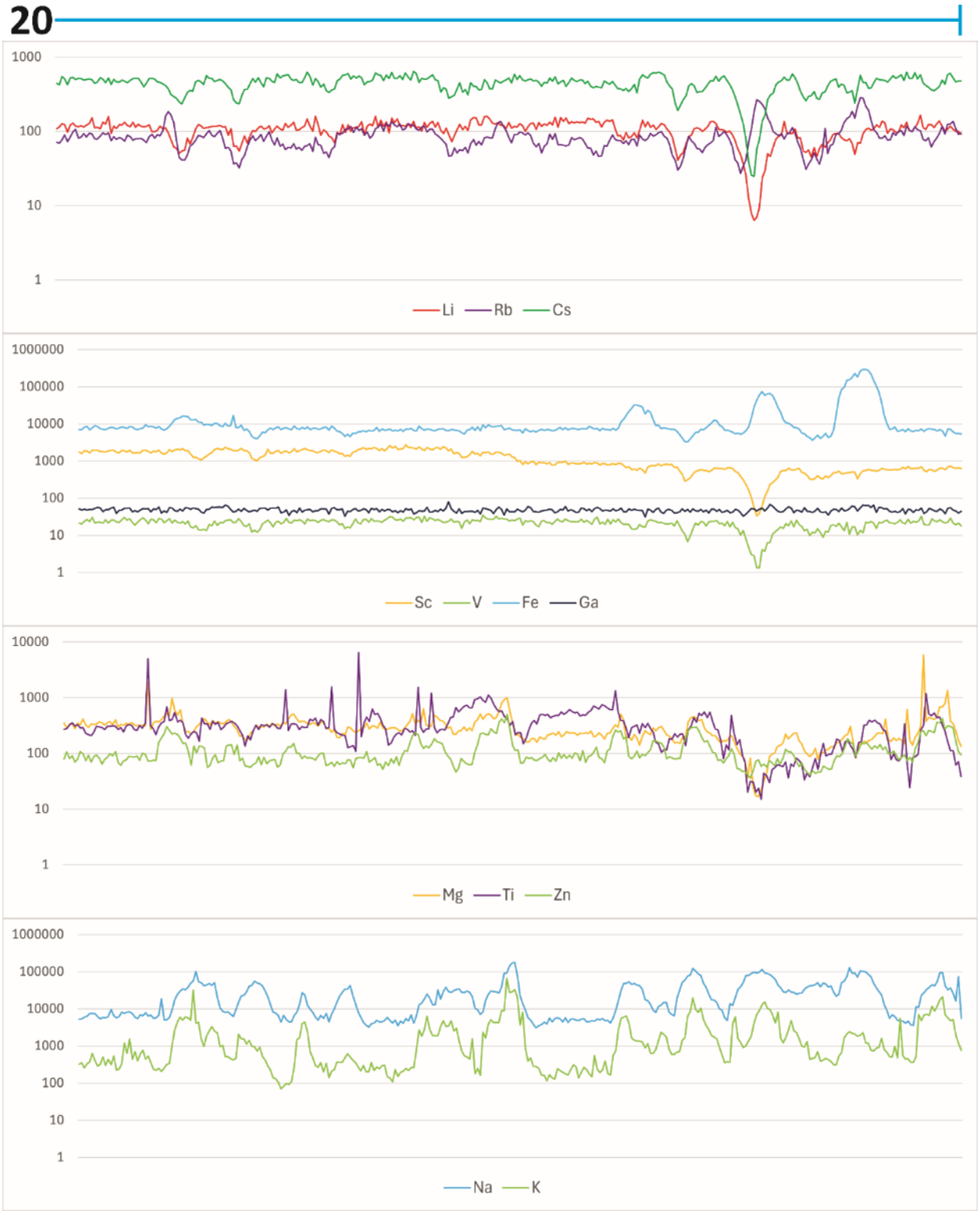
Appendix Figure 33: Concentrations (ppm) versus transect length. Sample LE25-5L-1A.17 is a beryl transect from pegmatite LE25-5L.



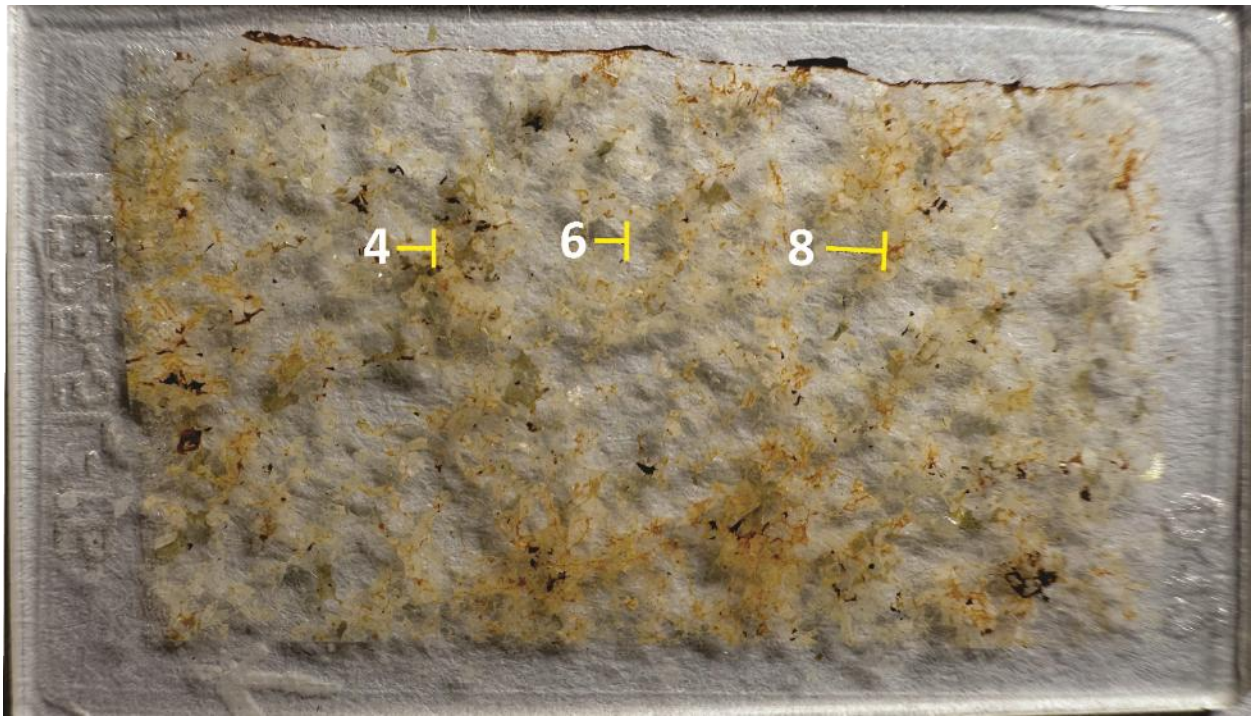
Appendix Figure 34: Concentrations (ppm) versus transect length. Sample LE25-5L-1A.18 is a beryl transect from pegmatite LE25-5L.



Appendix Figure 35: Concentrations (ppm) versus transect length. Sample LE25-5L-1A.19 is a beryl transect from pegmatite LE25-5L.



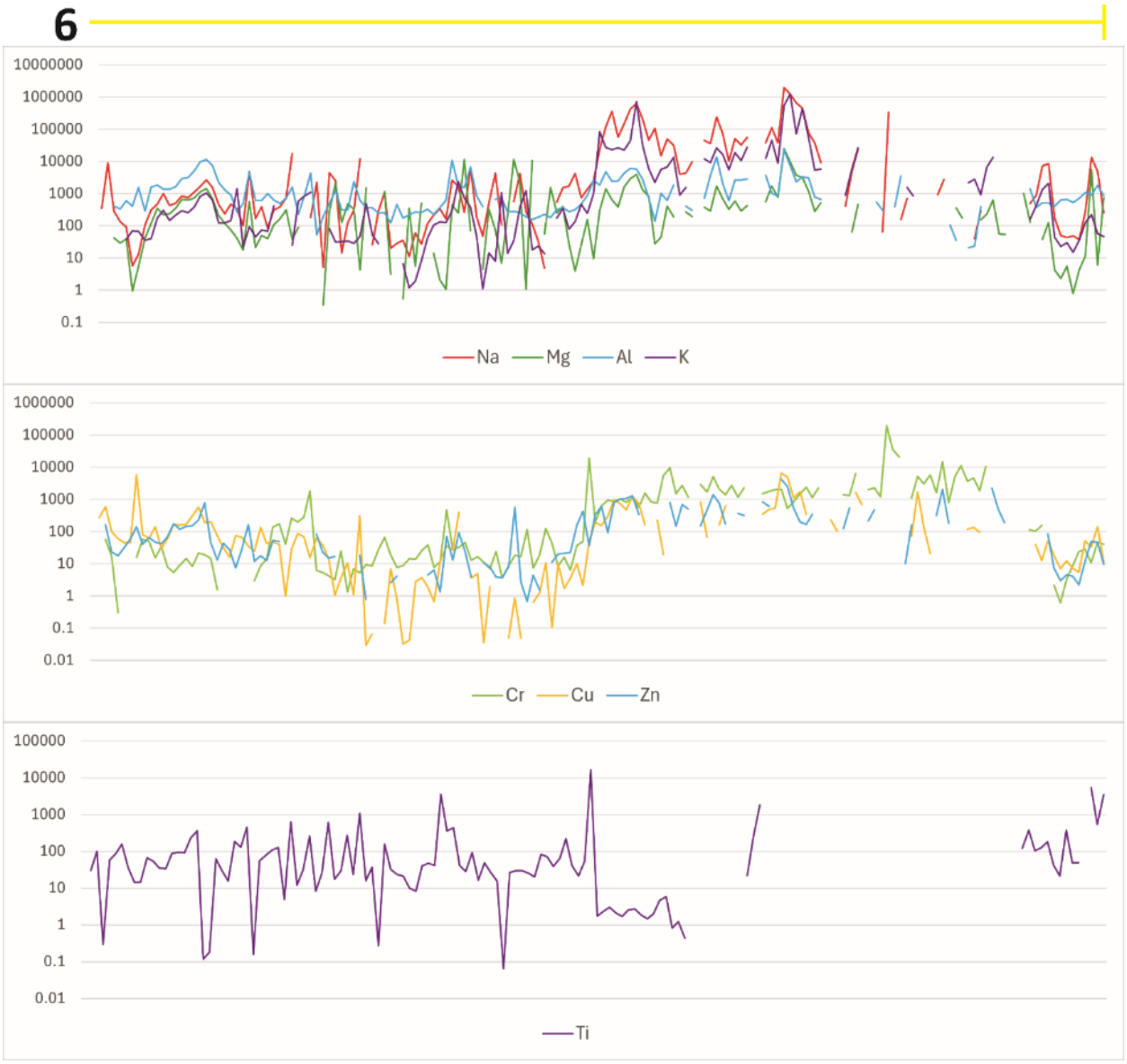
Appendix Figure 36: Concentrations (ppm) versus transect length. Sample LE25-5L-1A.20 is a beryl transect from pegmatite LE25-5L.



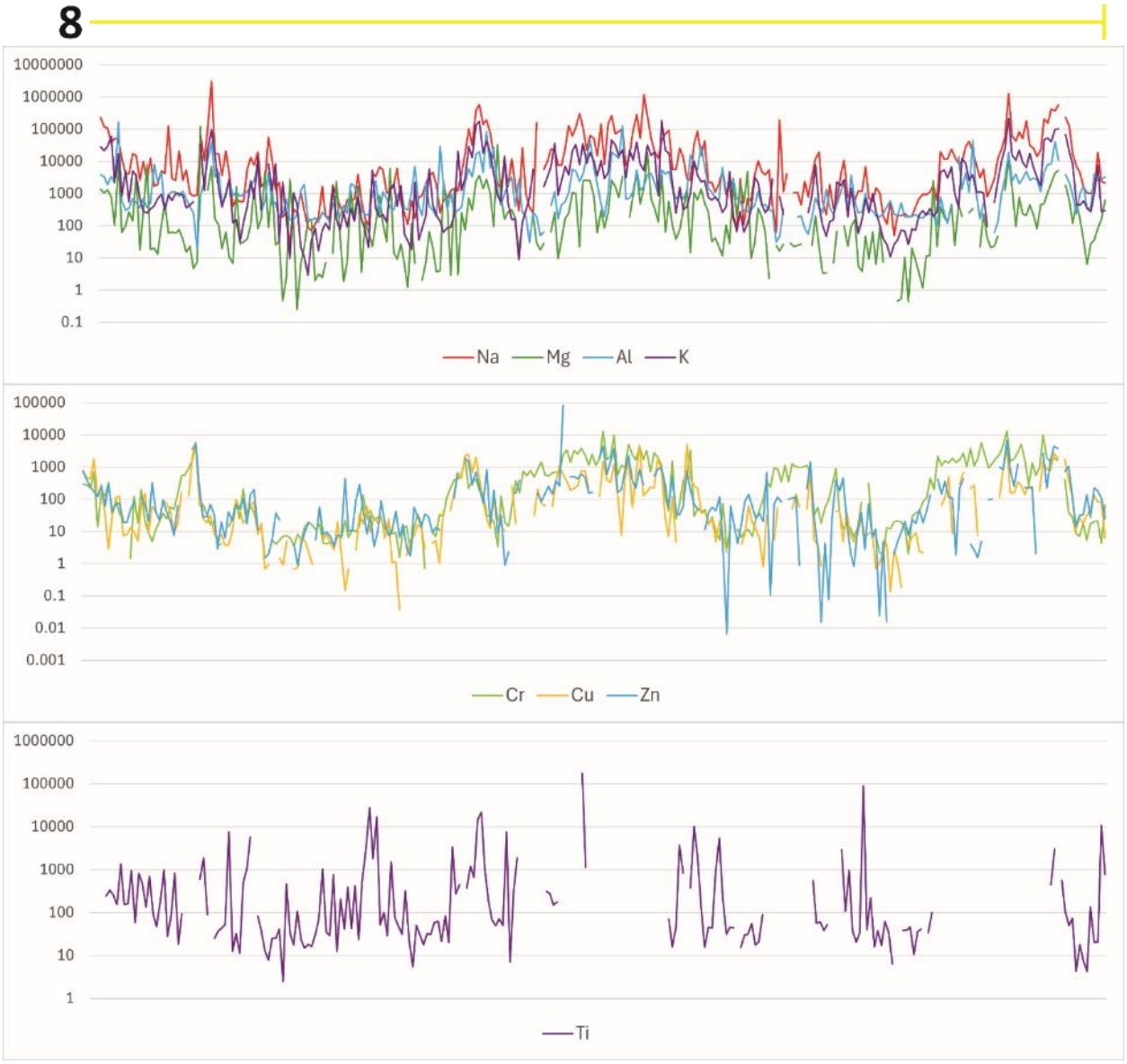
Appendix Figure 37: Sample LE25-5L-1B, 100 micron double polished thick section of pegmatite transition zone proximal to pegmatite LE25-5L. The yellow (quartz transect) line labelled 6 corresponds to LA-ICP-MS transect line LE25-5L-1B.6.



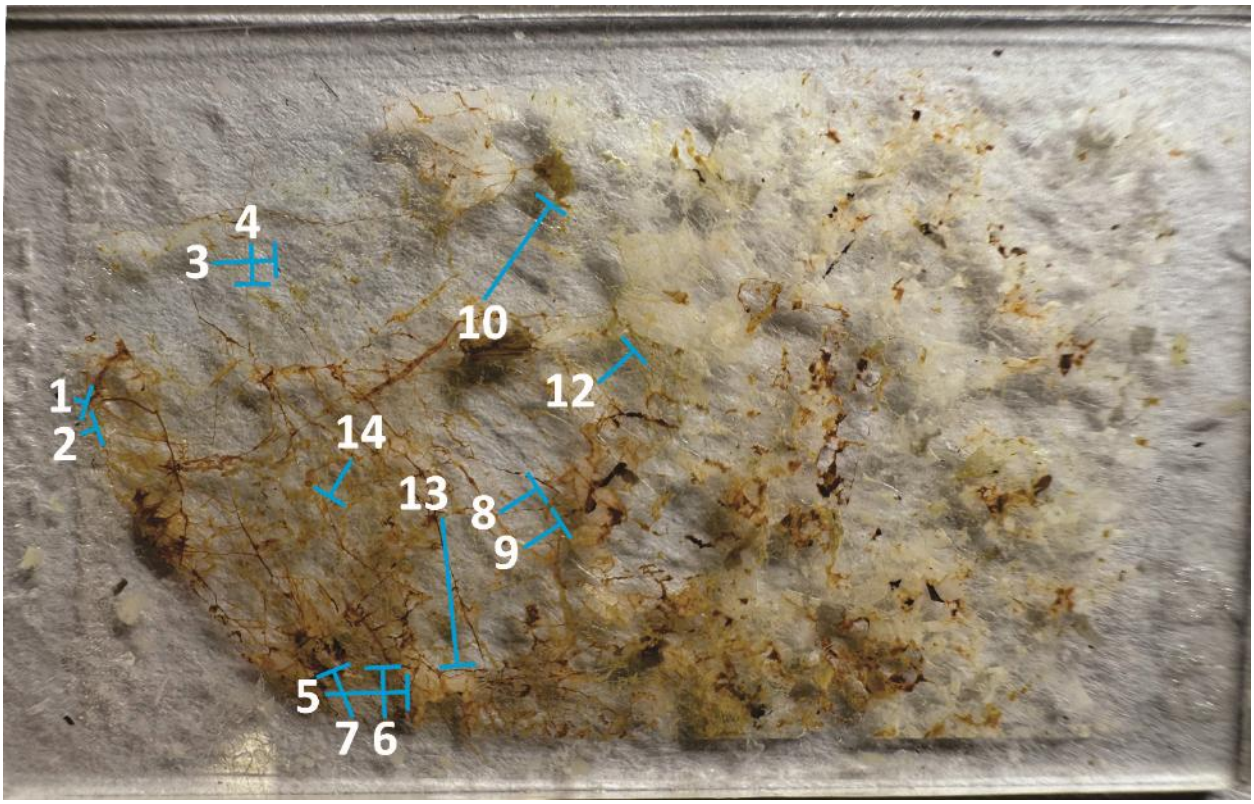
Appendix Figure 38: Concentrations (ppm) versus transect length. Sample LE25-5L-1B.4 is a quartz transect from pegmatite LE25-5L.



Appendix Figure 39: Concentrations (ppm) versus transect length. Sample LE25-5L-1B.6 is a quartz transect from pegmatite LE25-5L.



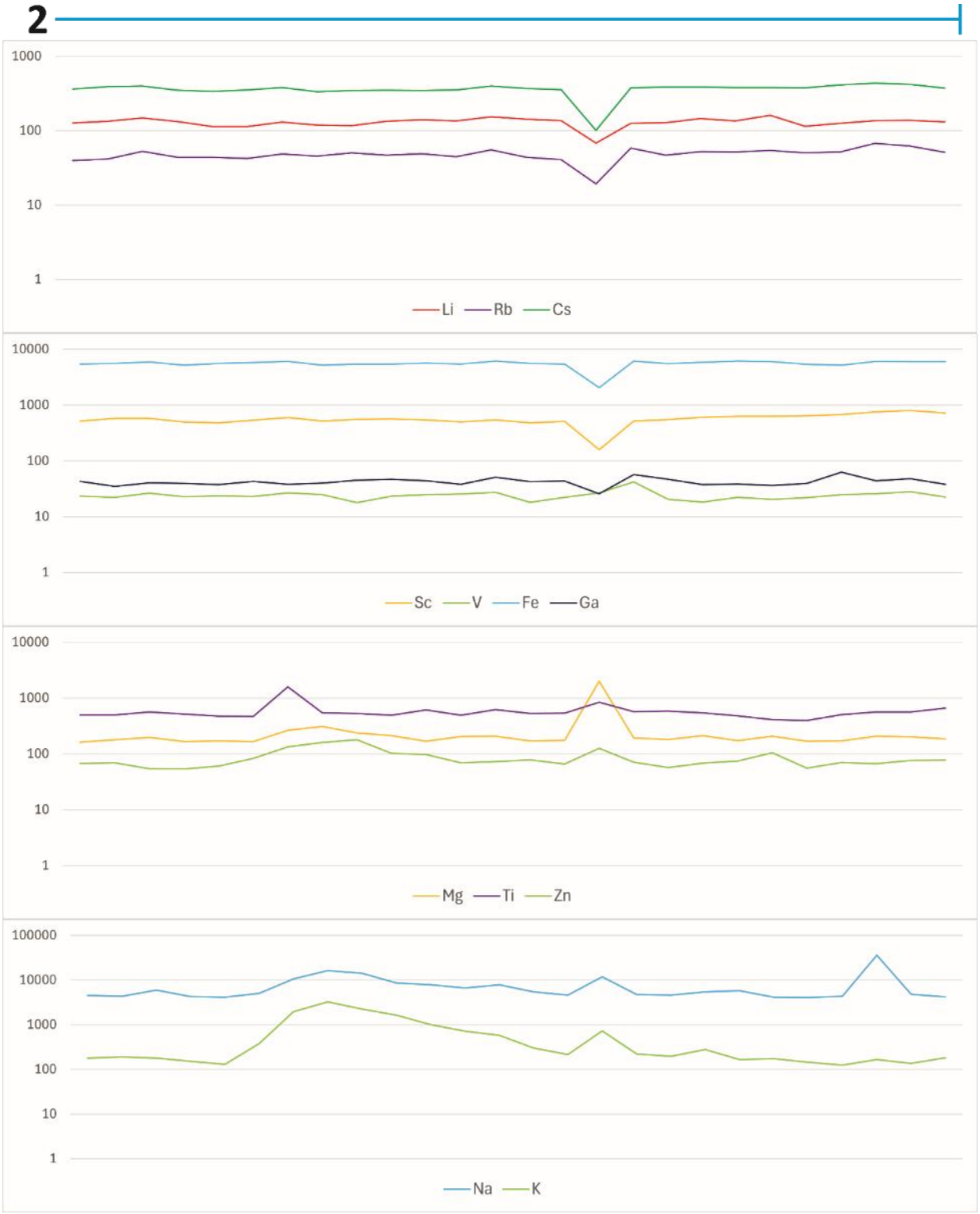
Appendix Figure 40: Concentrations (ppm) versus transect length. Sample LE25-5L-1B.8 is a quartz transect from pegmatite LE25-5L.



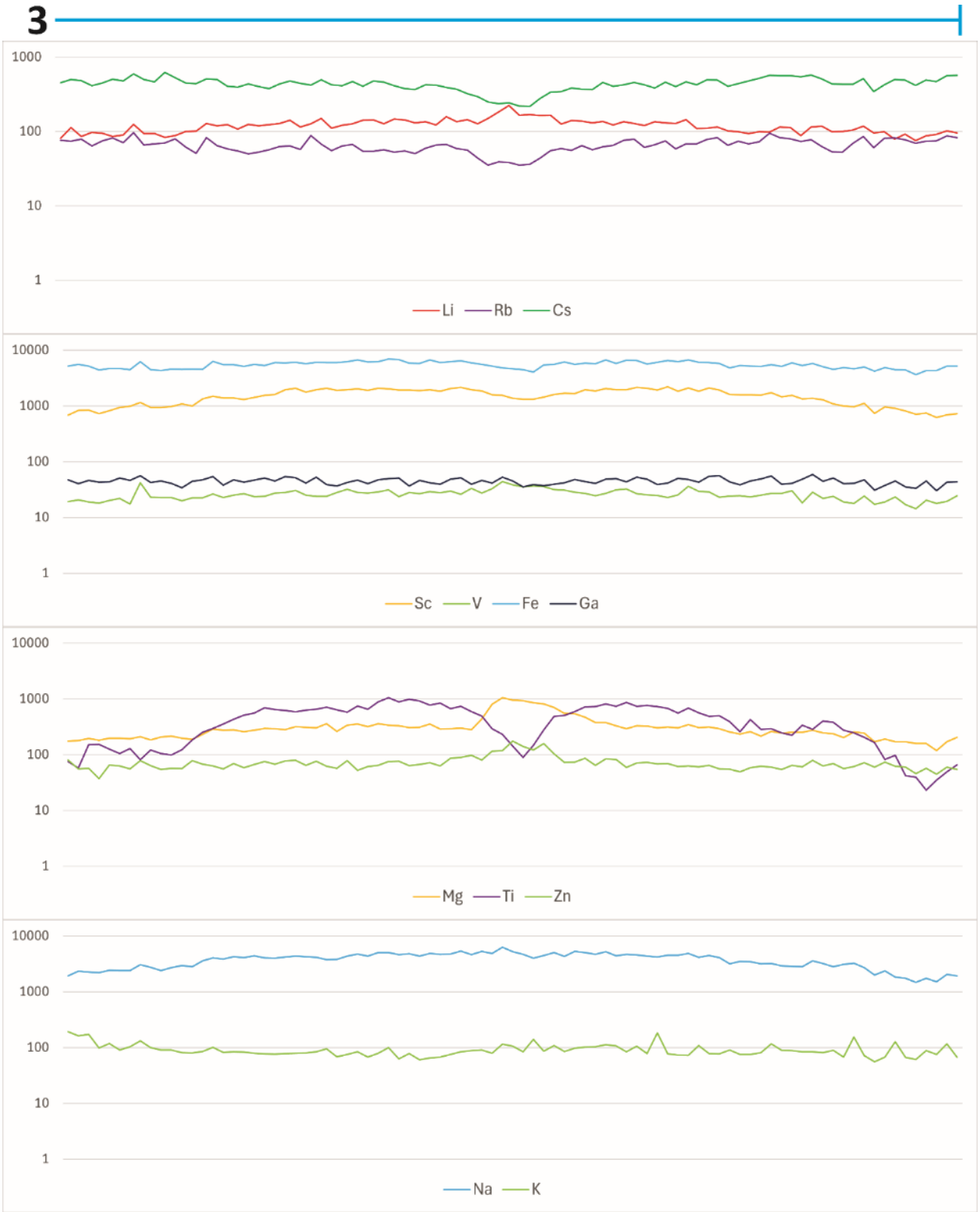
Appendix Figure 41: Sample LE25-5L-1B, 100 micron double polished thick section of pegmatite core zone LE25-5L. The blue (beryl transect) line labelled 1 corresponds to LA-ICP-MS transect line LE25-5L-2A.1.



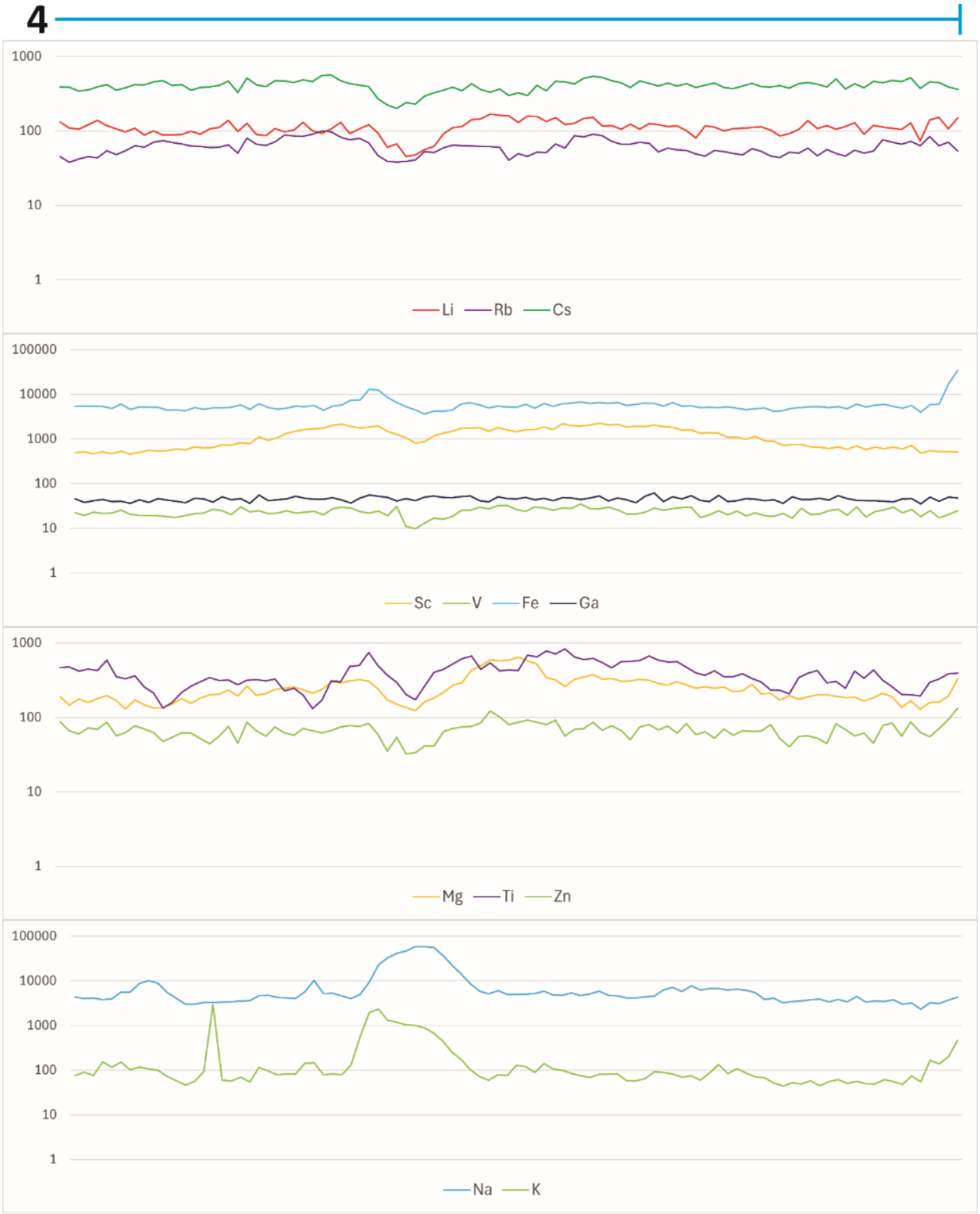
Appendix Figure 42: Concentrations (ppm) versus transect length. Sample LE25-5L-2A.1 is a beryl transect from pegmatite LE25-5L.



Appendix Figure 43: Concentrations (ppm) versus transect length. Sample LE25-5L-2A.2 is a beryl transect from pegmatite LE25-5L.



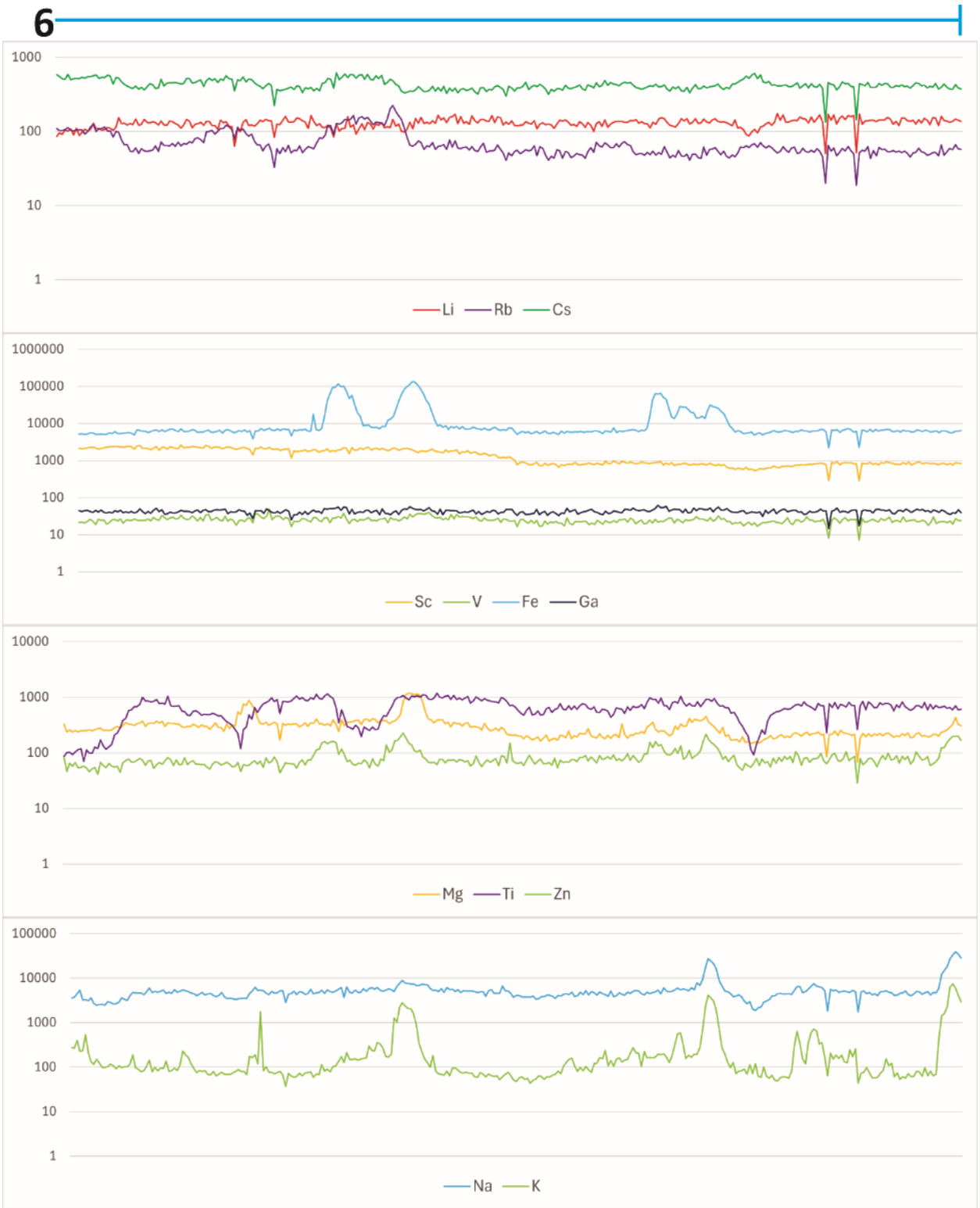
Appendix Figure 44: Concentrations (ppm) versus transect length. Sample LE25-5L-2A.3 is a beryl transect from pegmatite LE25-5L.



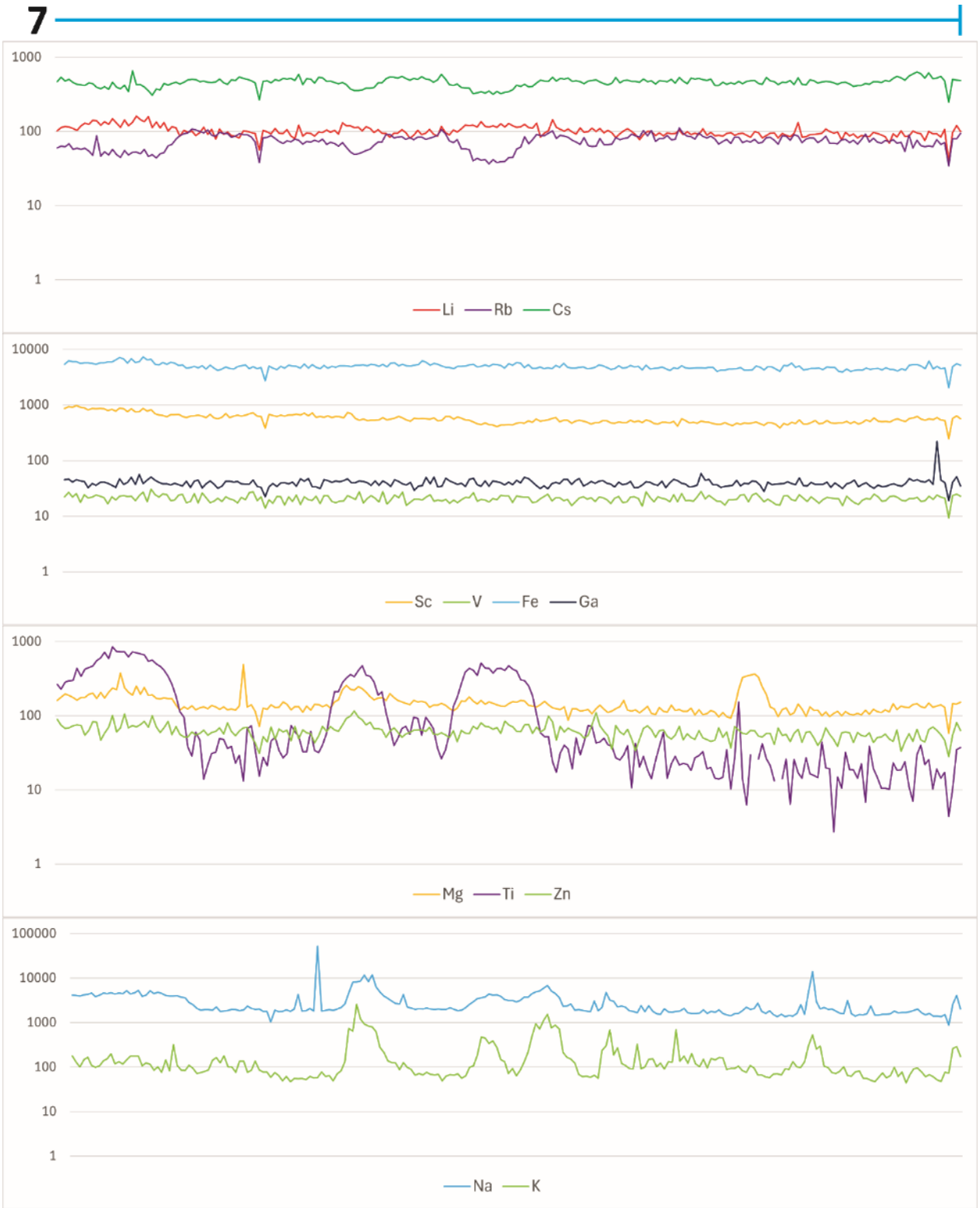
Appendix Figure 45: Concentrations (ppm) versus transect length. Sample LE25-5L-2A.4 is a beryl transect from pegmatite LE25-5L.



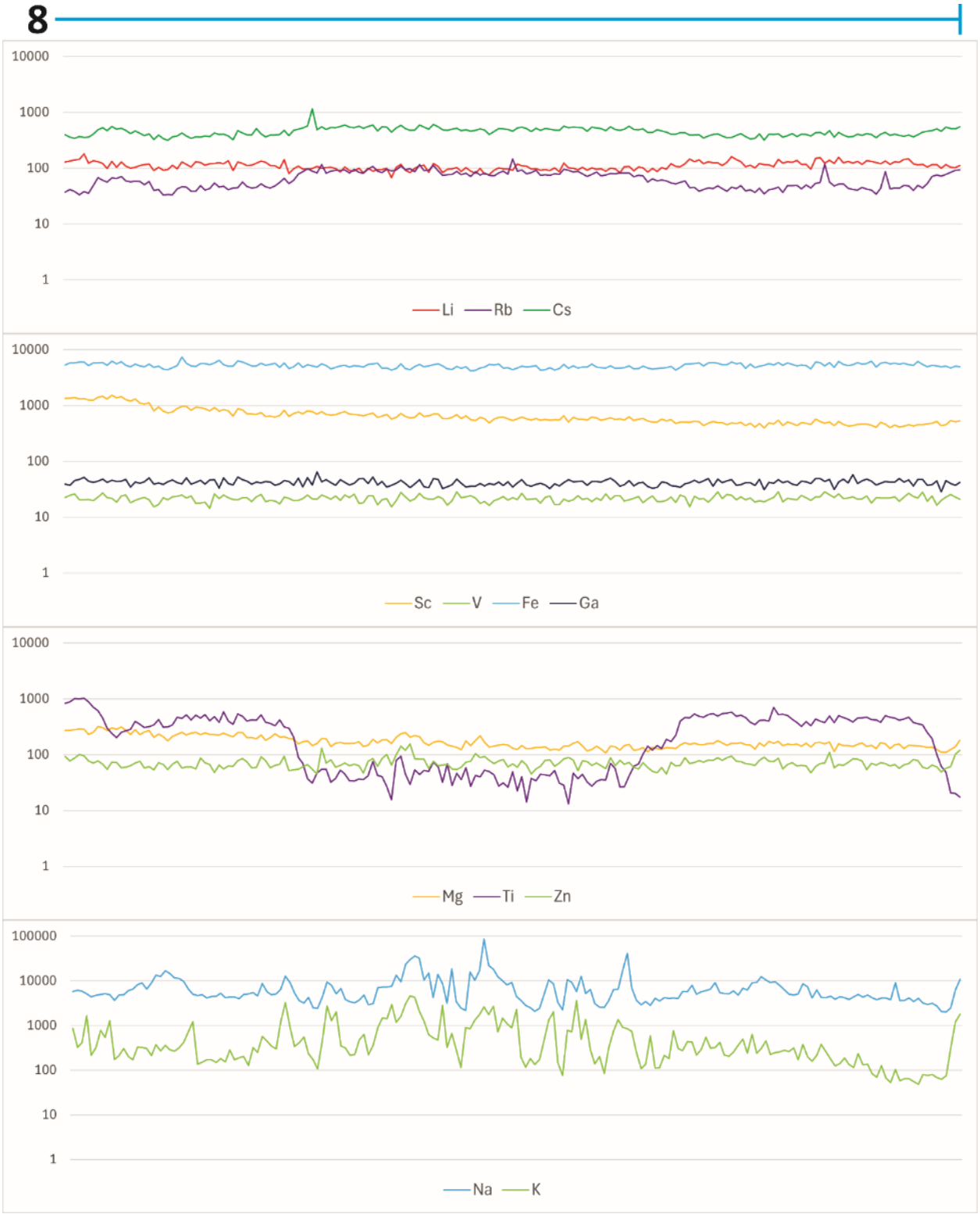
Appendix Figure 46: Concentrations (ppm) versus transect length. Sample LE25-5L-2A.5 is a beryl transect from pegmatite LE25-5L.



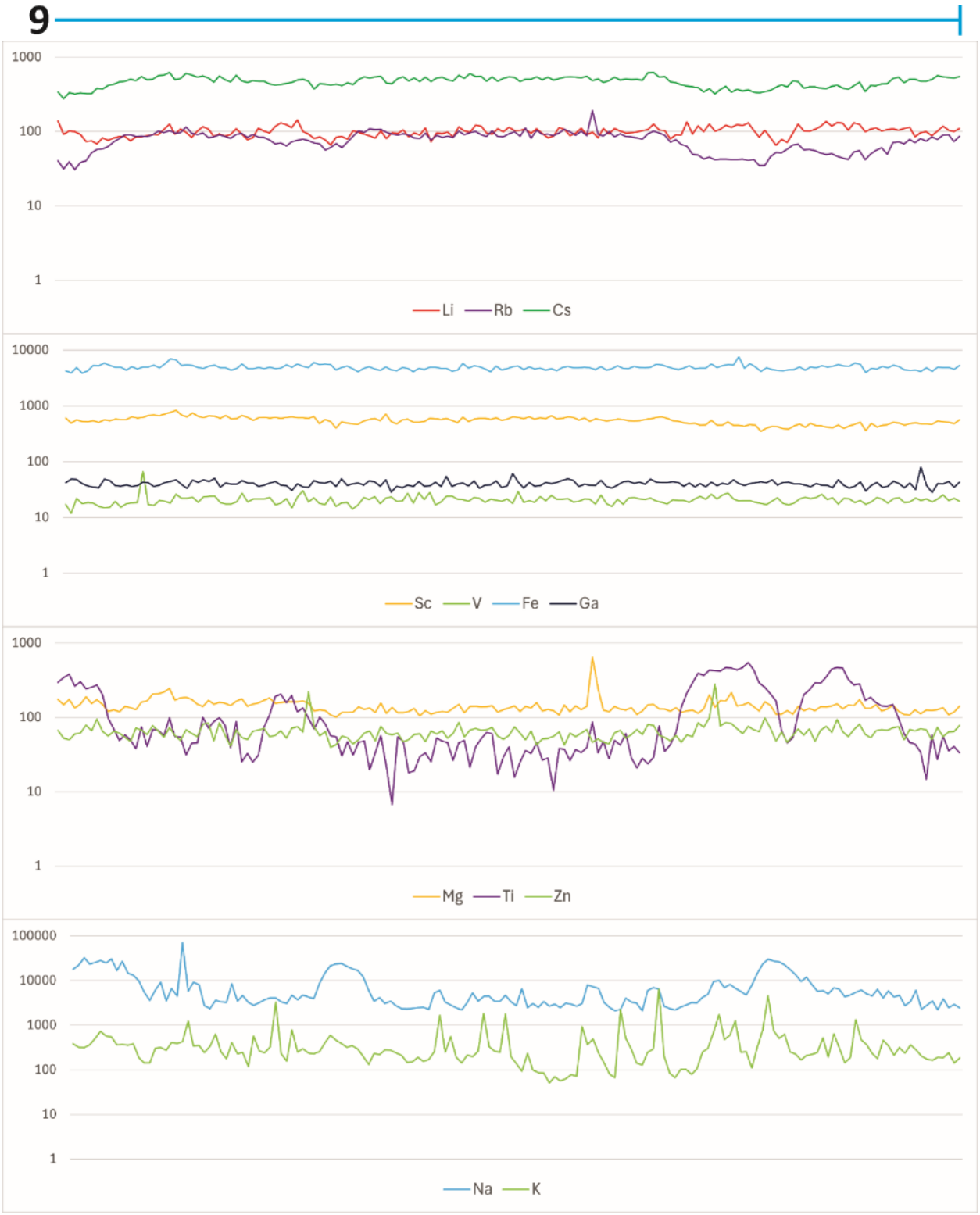
Appendix Figure 47: Concentrations (ppm) versus transect length. Sample LE25-5L-2A.6 is a beryl transect from pegmatite LE25-5L.



Appendix Figure 48: Concentrations (ppm) versus transect length. Sample LE25-5L-2A.7 is a beryl transect from pegmatite LE25-5L.



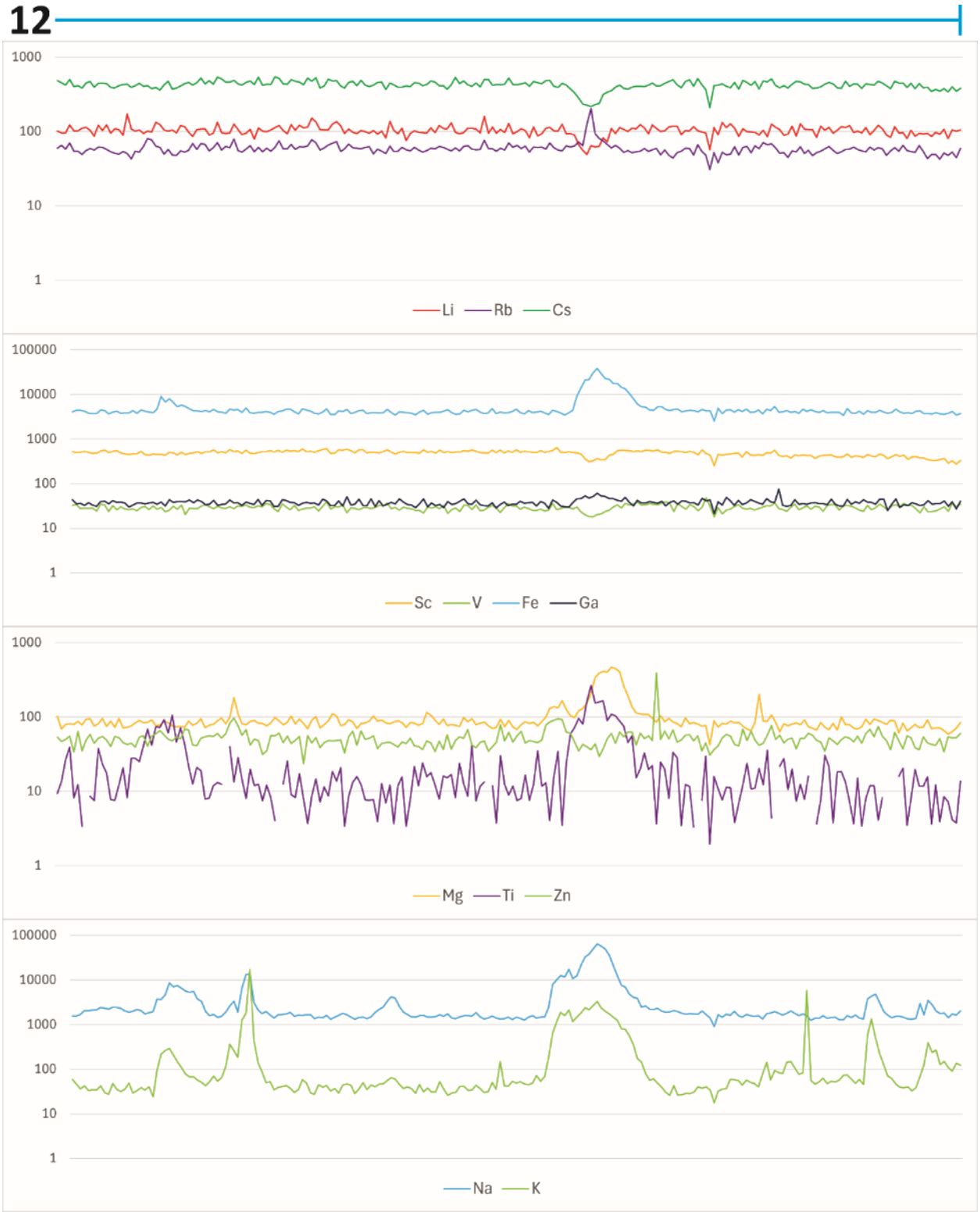
Appendix Figure 49: Concentrations (ppm) versus transect length. Sample LE25-5L-2A.8 is a beryl transect from pegmatite LE25-5L.



Appendix Figure 50: Concentrations (ppm) versus transect length. Sample LE25-5L-2A.9 is a beryl transect from pegmatite LE25-5L.



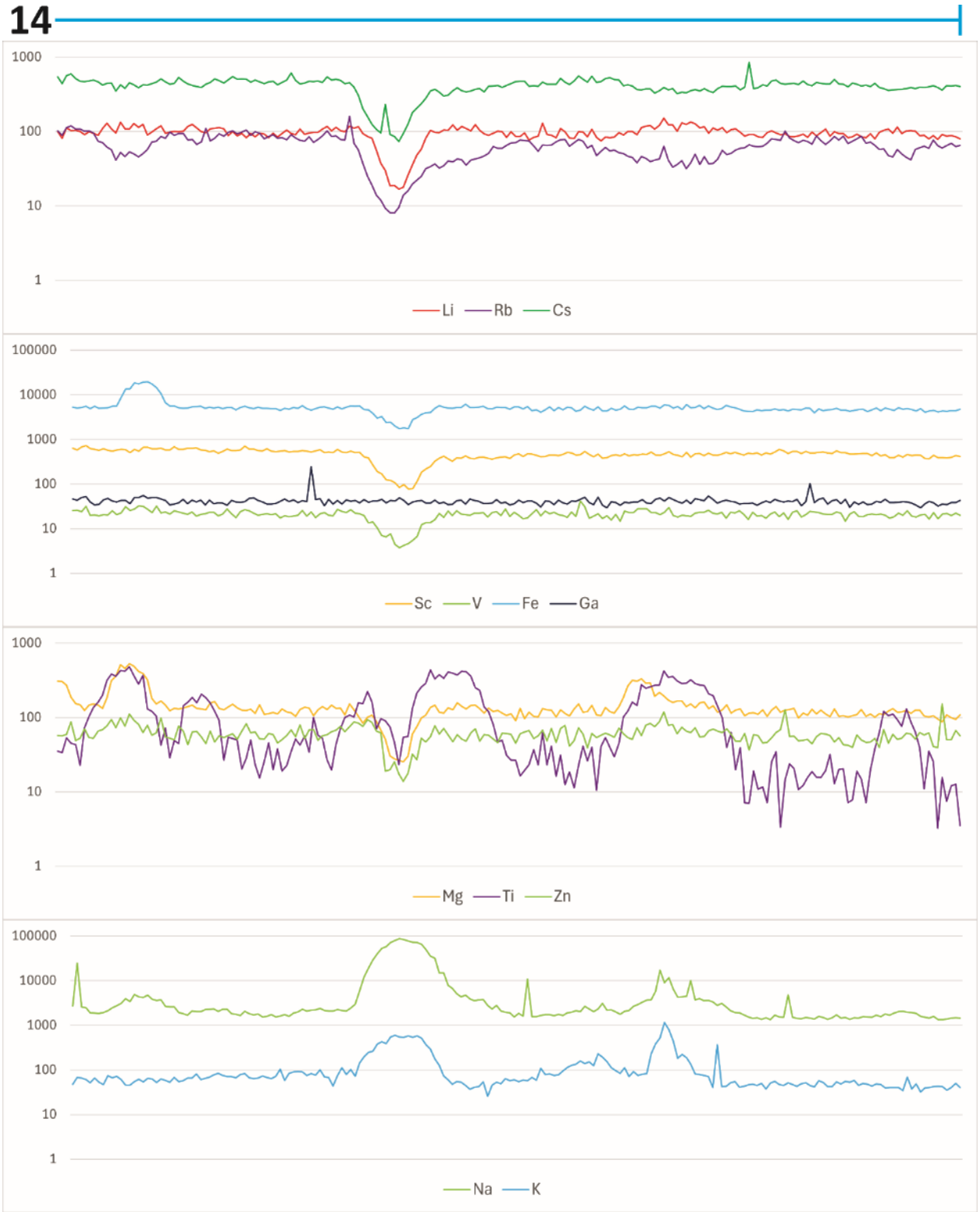
Appendix Figure 51: Concentrations (ppm) versus transect length. Sample LE25-5L-2A.10 is a beryl transect from pegmatite LE25-5L.



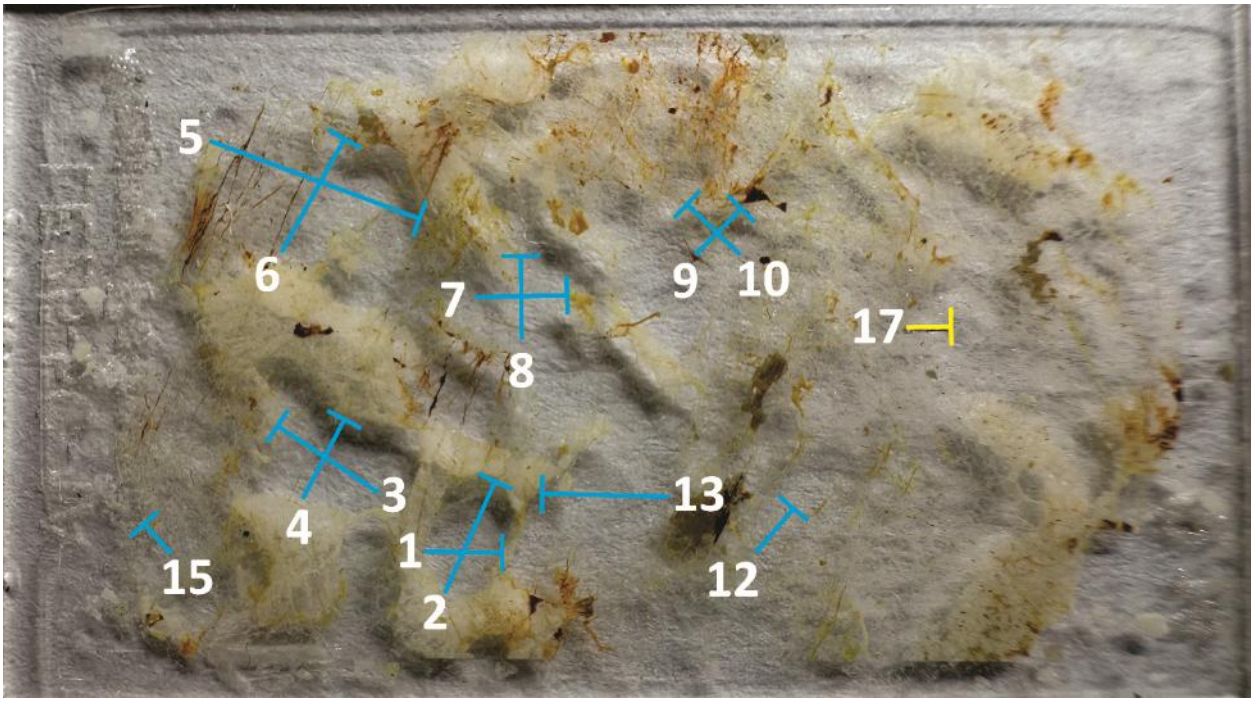
Appendix Figure 52: Concentrations (ppm) versus transect length. Sample LE25-5L-2A.12 is a beryl transect from pegmatite LE25-5L.



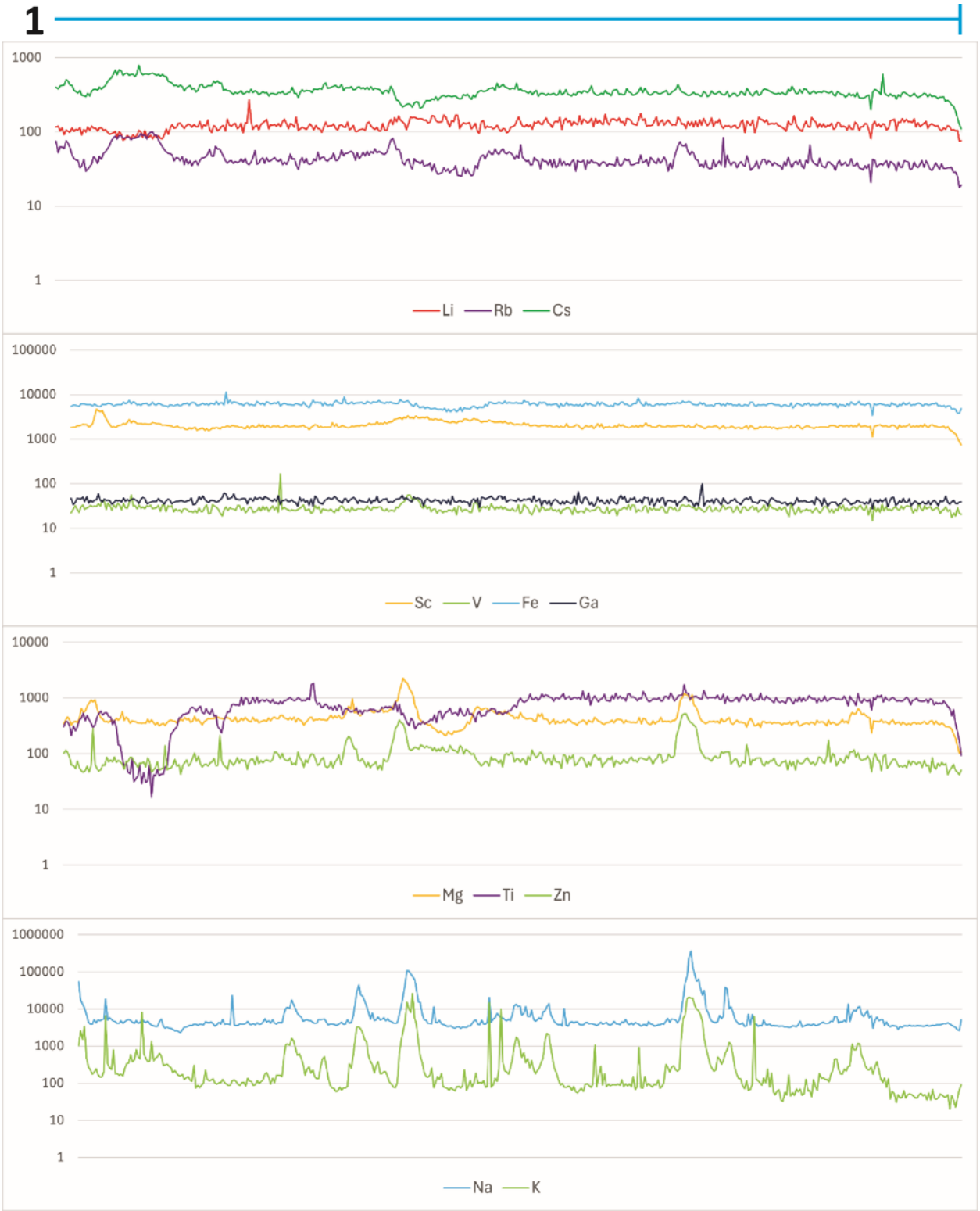
Appendix Figure 53: Concentrations (ppm) versus transect length. Sample LE25-5L-2A.13 is a beryl transect from pegmatite LE25-5L.



Appendix Figure 54: Concentrations (ppm) versus transect length. Sample LE25-5L-2A.14 is a beryl transect from pegmatite LE25-5L.



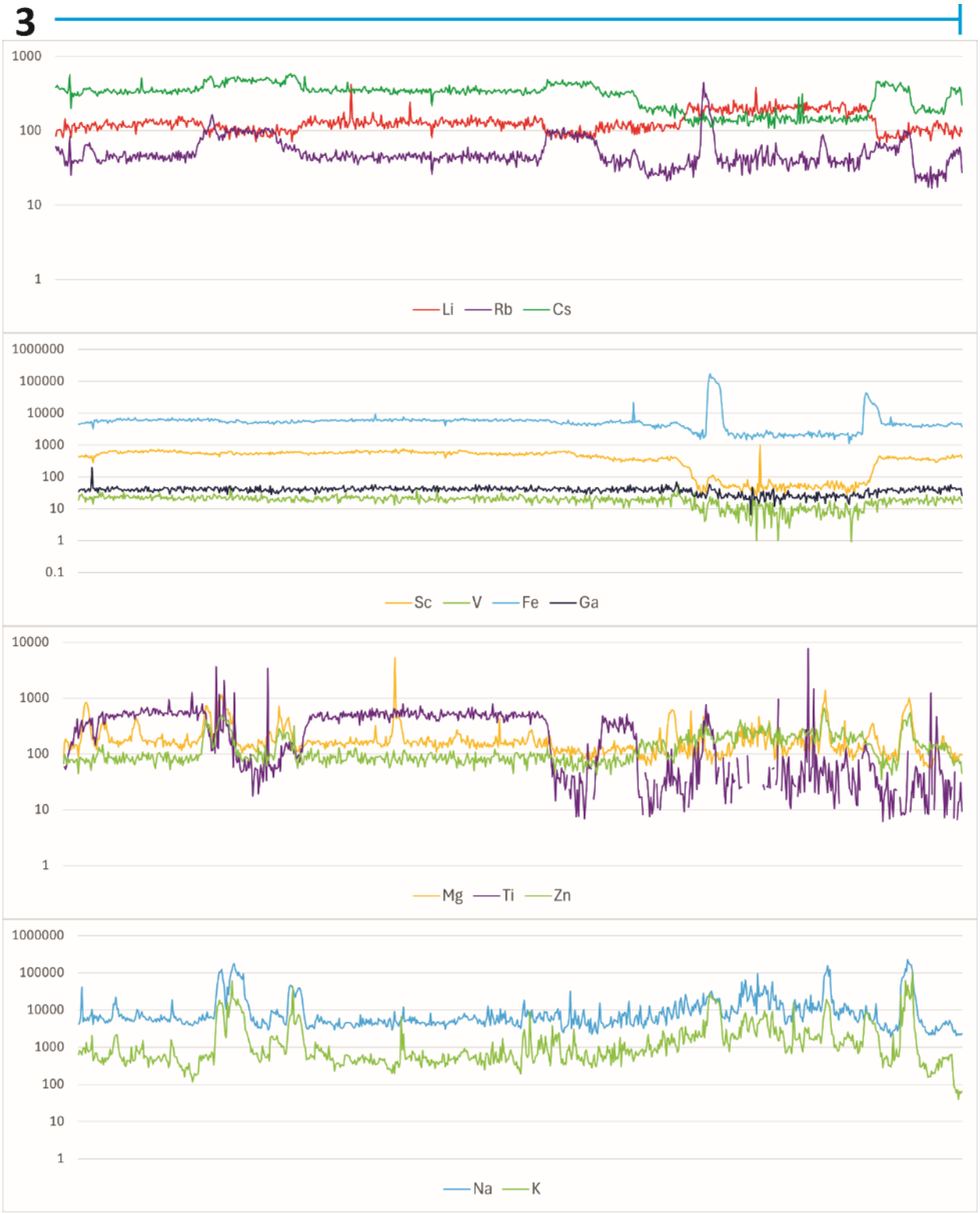
Appendix Figure 55: Sample LE25-5C-1A, 100 micron double polished thick section of a pegmatite core zone. Blue (beryl transect) and yellow (quartz transect) lines and numbers correspond to LA-ICP-MS transect lines (e.g., LE25-5C-1A.5 is the blue line labelled 5).



Appendix Figure 56: Concentrations (ppm) versus transect length. Sample LE25-5C-1A.1 is a beryl transect from pegmatite LE25-5C.



Appendix Figure 57: Concentrations (ppm) versus transect length. Sample LE25-5C-1A.2 is a beryl transect from pegmatite LE25-5C.



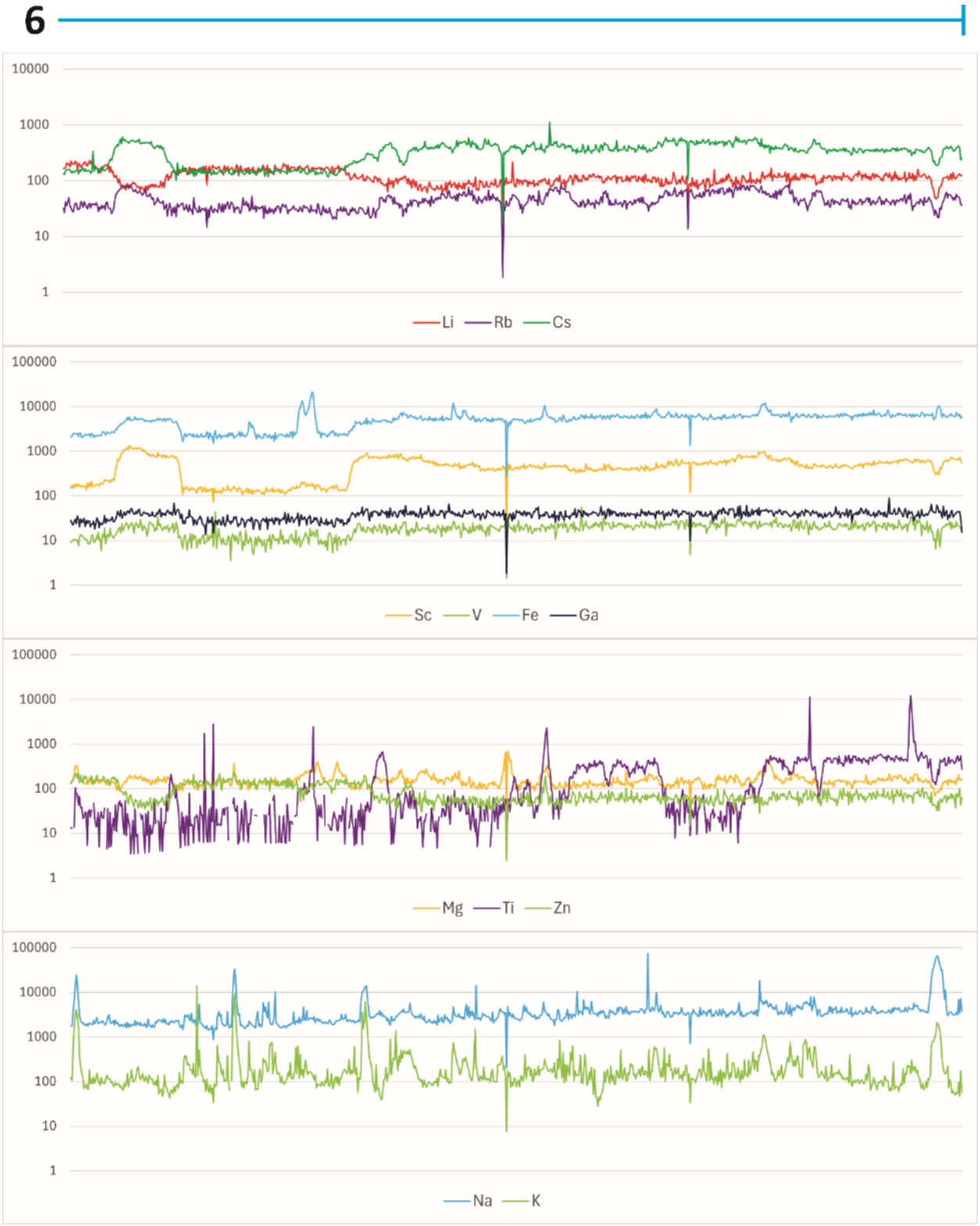
Appendix Figure 58: Concentrations (ppm) versus transect length. Sample LE25-5C-1A.3 is a beryl transect from pegmatite LE25-5C.



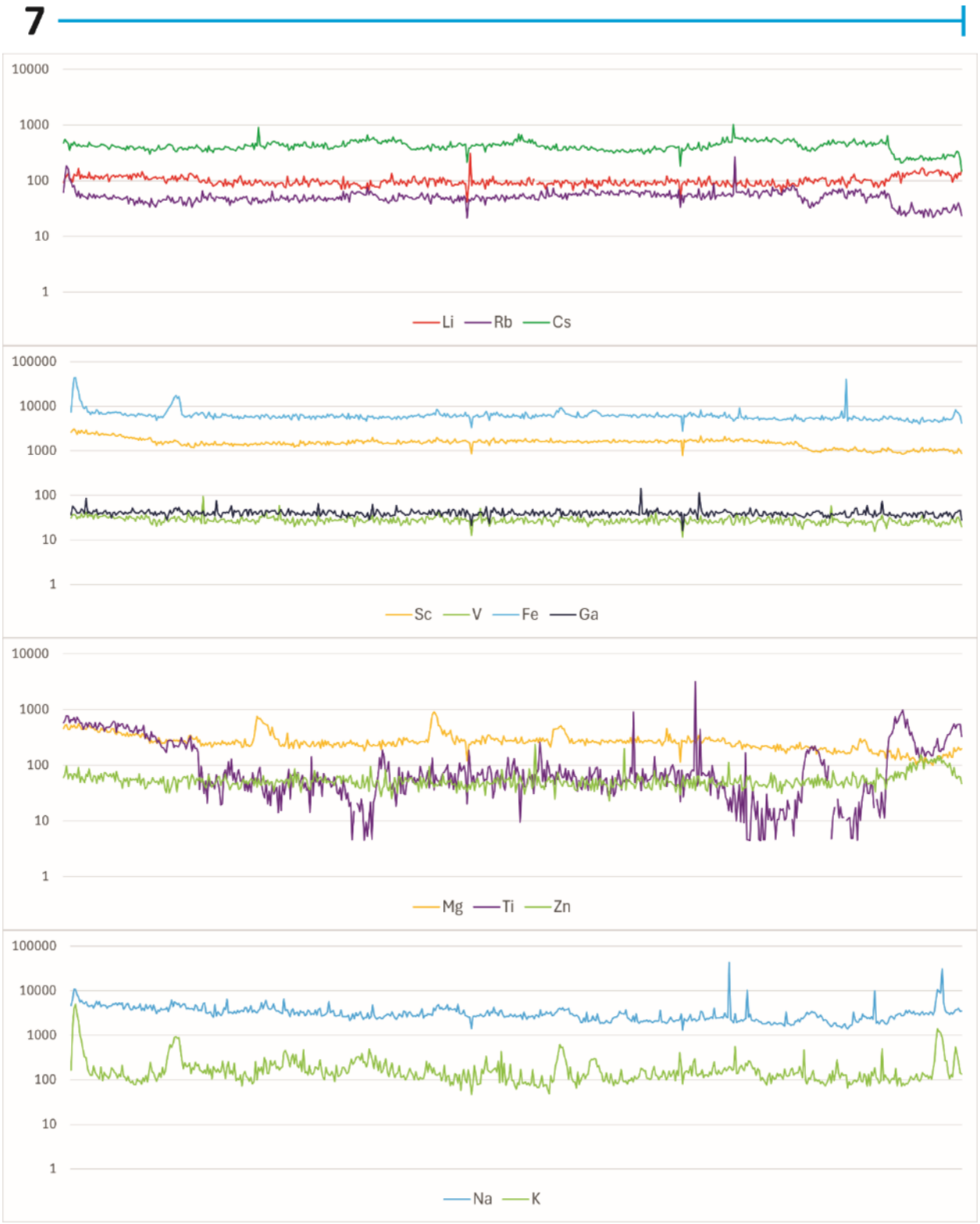
Appendix Figure 59: Concentrations (ppm) versus transect length. Sample LE25-5C-1A.4 is a beryl transect from pegmatite LE25-5C.



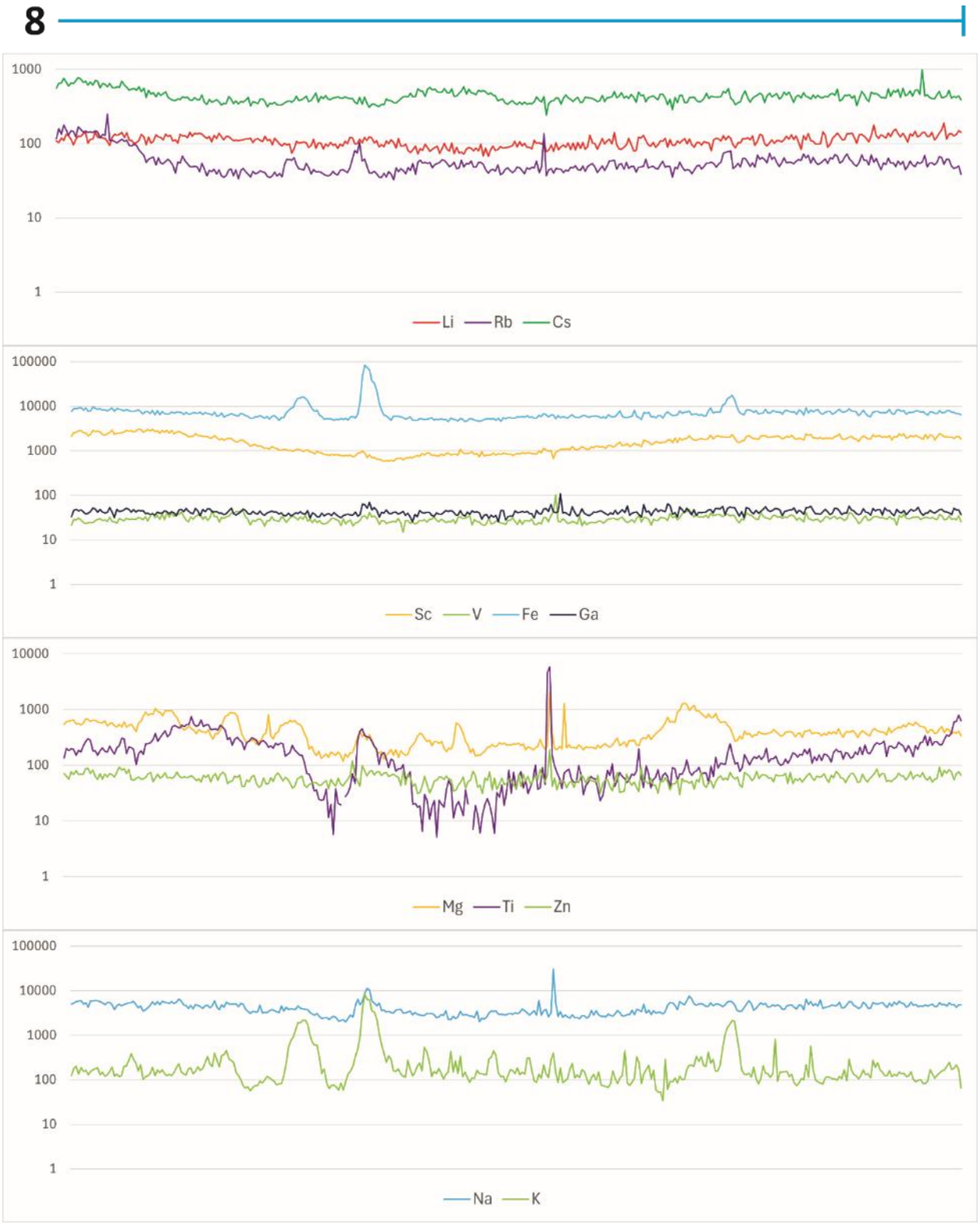
Appendix Figure 60: Concentrations (ppm) versus transect length. Sample LE25-5C-1A.5 is a beryl transect from pegmatite LE25-5C.



Appendix Figure 61: Concentrations (ppm) versus transect length. Sample LE25-5C-1A.6 is a beryl transect from pegmatite LE25-5C.



Appendix Figure 62: Concentrations (ppm) versus transect length. Sample LE25-5C-1A.7 is a beryl transect from pegmatite LE25-5C.



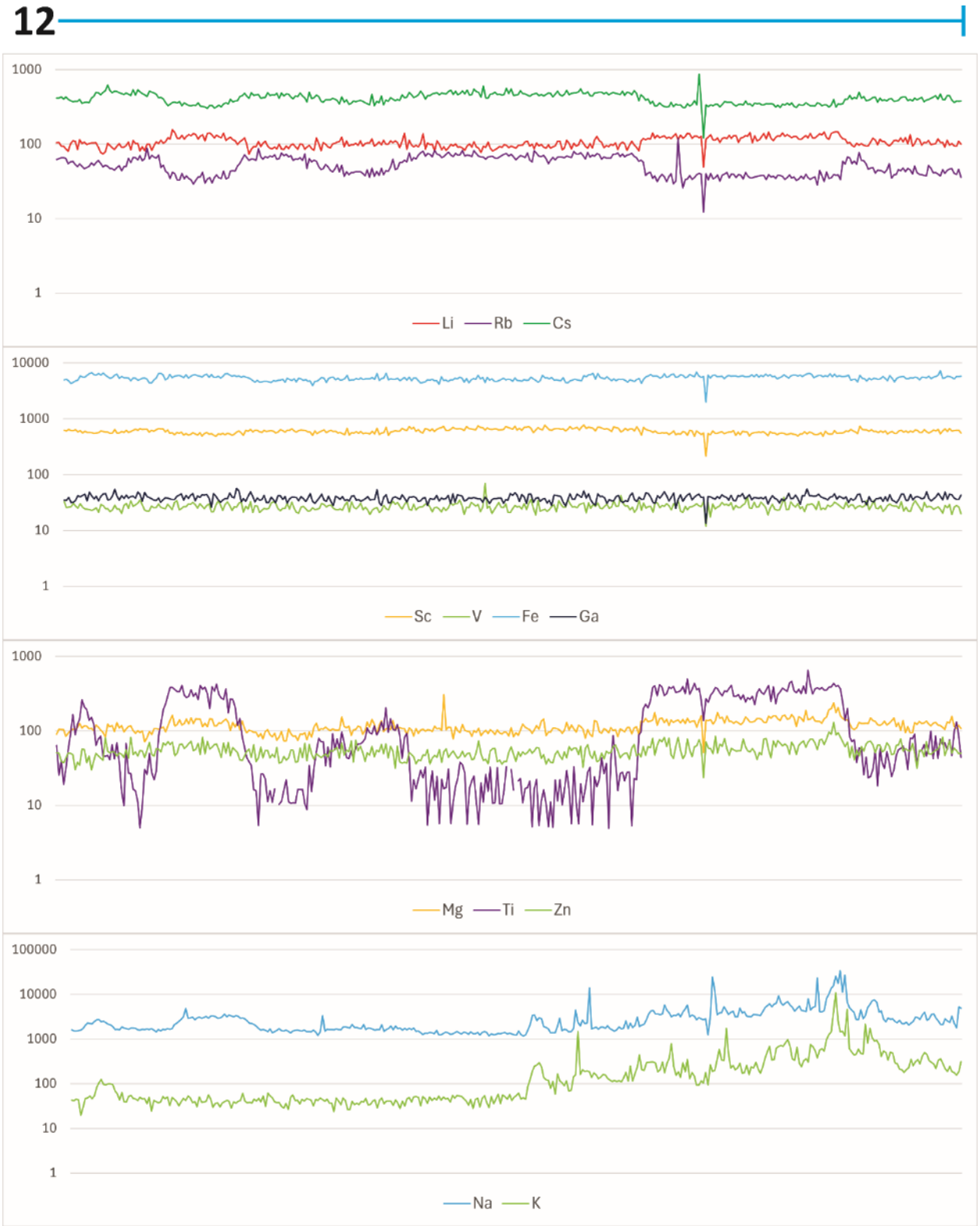
Appendix Figure 63: Concentrations (ppm) versus transect length. Sample LE25-5C-1A.8 is a beryl transect from pegmatite LE25-5C.



Appendix Figure 64: Concentrations (ppm) versus transect length. Sample LE25-5C-1A.9 is a beryl transect from pegmatite LE25-5C.



Appendix Figure 65: Concentrations (ppm) versus transect length. Sample LE25-5C-1A.10 is a beryl transect from pegmatite LE25-5C.



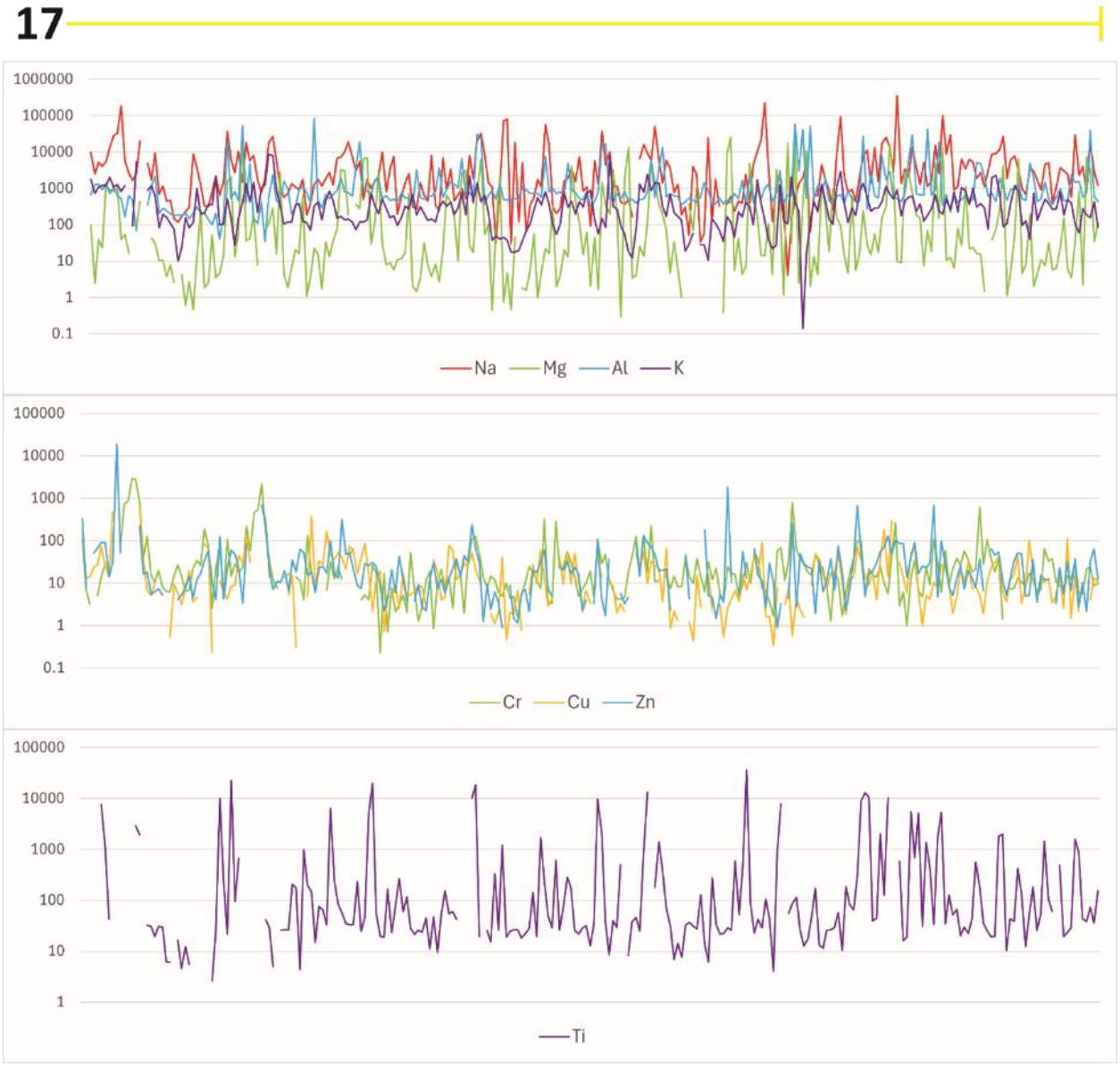
Appendix Figure 66: Concentrations (ppm) versus transect length. Sample LE25-5C-1A.12 is a beryl transect from pegmatite LE25-5C.



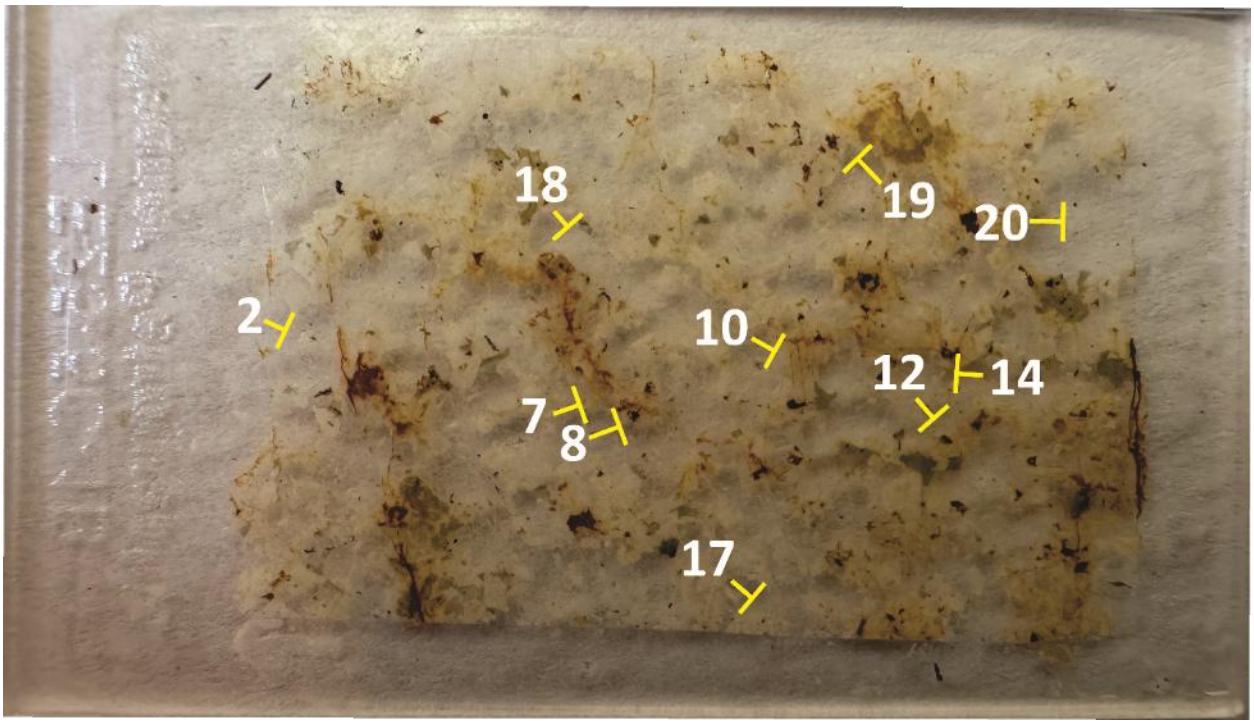
Appendix Figure 67: Concentrations (ppm) versus transect length. Sample LE25-5C-1A.13 is a beryl transect from pegmatite LE25-5C.



Appendix Figure 68: Concentrations (ppm) versus transect length. Sample LE25-5C-1A.15 is a beryl transect from pegmatite LE25-5C.



Appendix Figure 69: Concentrations (ppm) versus transect length. Sample LE25-5C-1A.17 is a quartz transect from pegmatite LE25-5C.



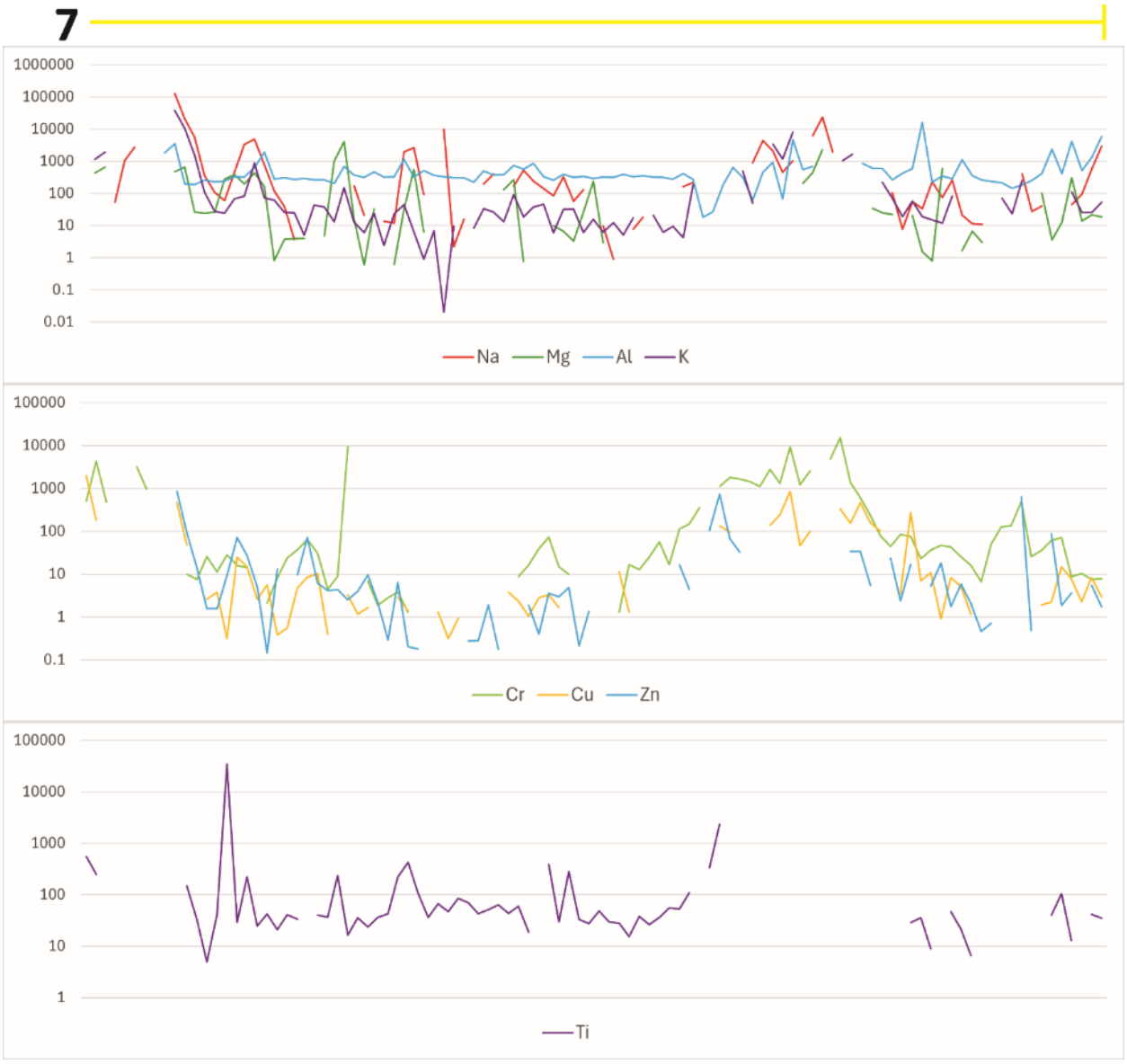
Appendix Figure 70: Sample LE25-5C-1B, 100 micron double polished thick section of pegmatite transition zone proximal to pegmatite LE25-5L. The yellow (quartz transect) line labelled 2 corresponds to LA-ICP-MS transect line LE25-5C-1B.2.



Appendix Figure 71: Concentrations (ppm) versus transect length. Sample LE25-5C-1B.2 is a quartz transect from pegmatite LE25-5C.



Appendix Figure 72: Concentrations (ppm) versus transect length. Sample LE25-5C-1B.6 is a quartz transect from pegmatite LE25-5C.



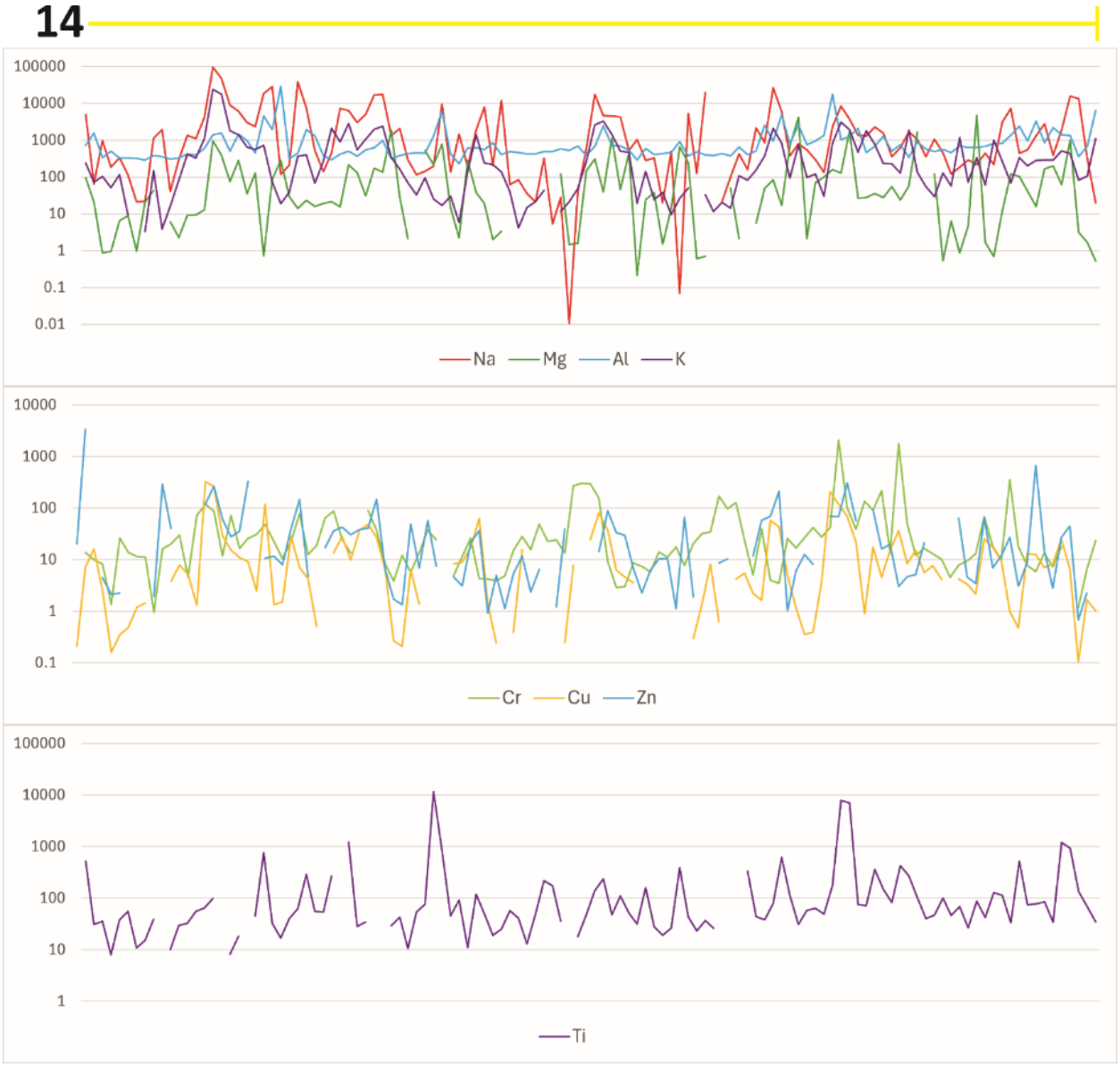
Appendix Figure 73: Concentrations (ppm) versus transect length. Sample LE25-5C-1B.7 is a quartz transect from pegmatite LE25-5C.



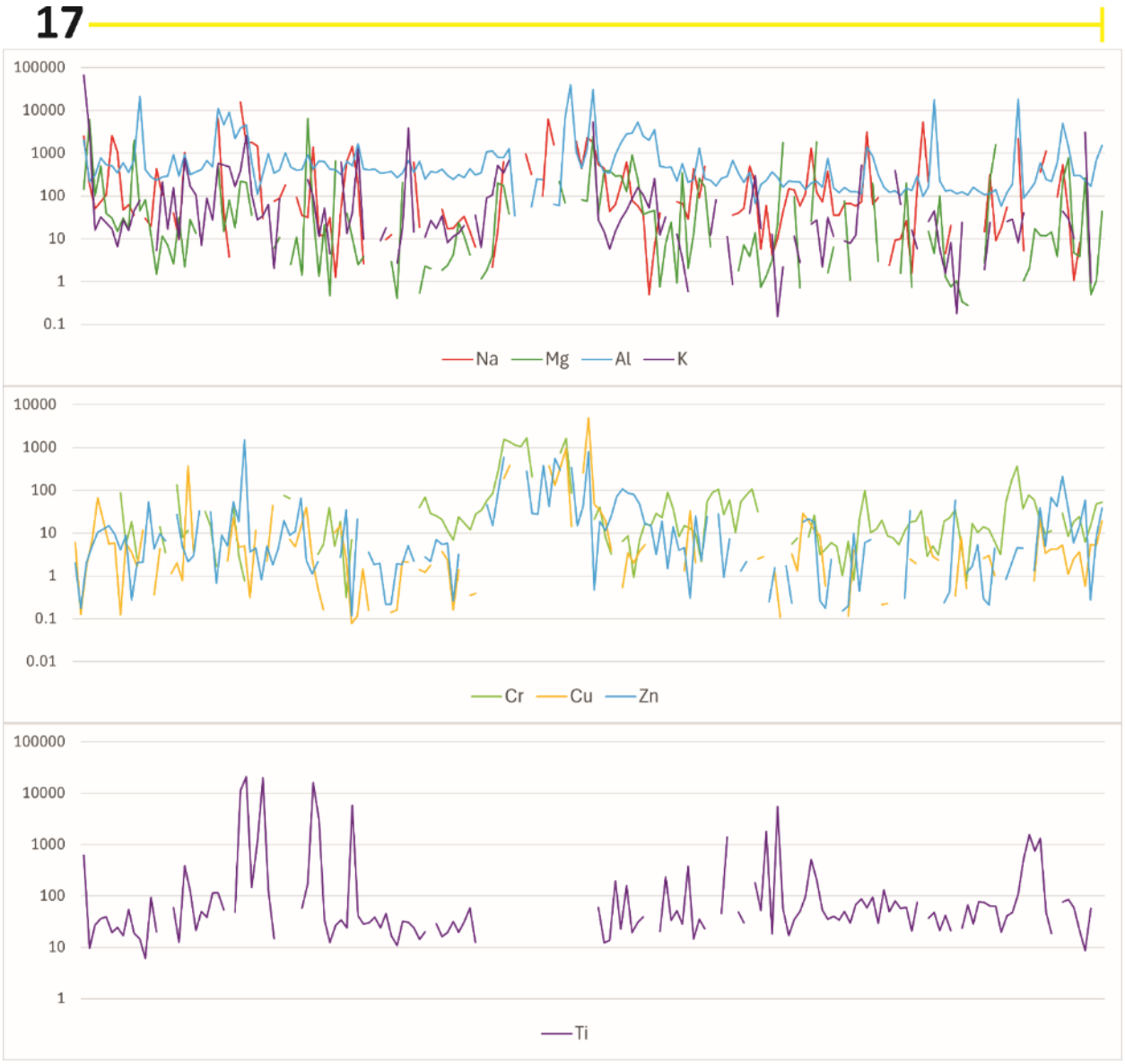
Appendix Figure 74: Concentrations (ppm) versus transect length. Sample LE25-5C-1B.8 is a quartz transect from pegmatite LE25-5C.



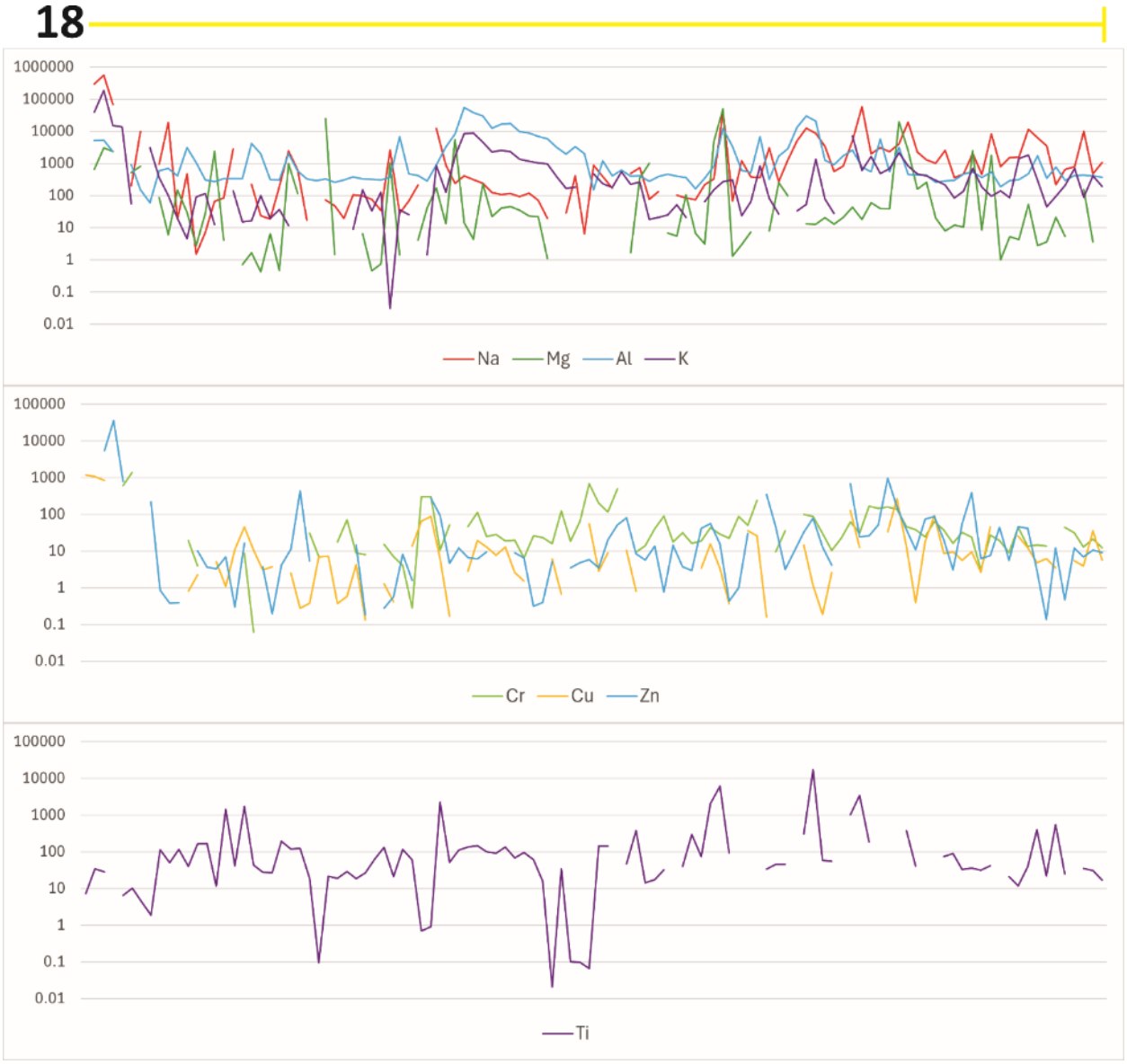
Appendix Figure 75: Concentrations (ppm) versus transect length. Sample LE25-5C-1B.12 is a quartz transect from pegmatite LE25-5C.



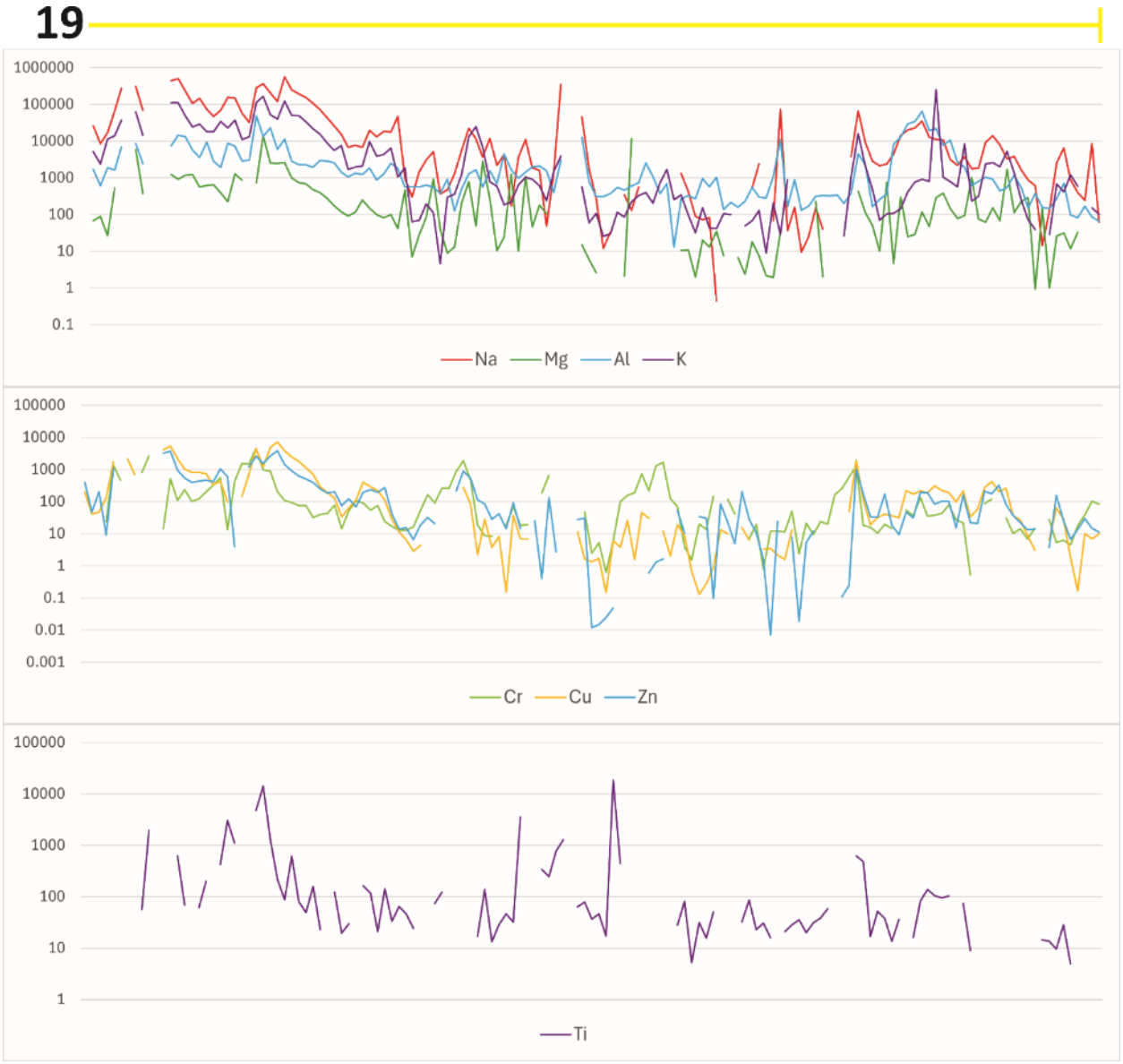
Appendix Figure 76: Concentrations (ppm) versus transect length. Sample LE25-5C-1B.14 is a quartz transect from pegmatite LE25-5C.



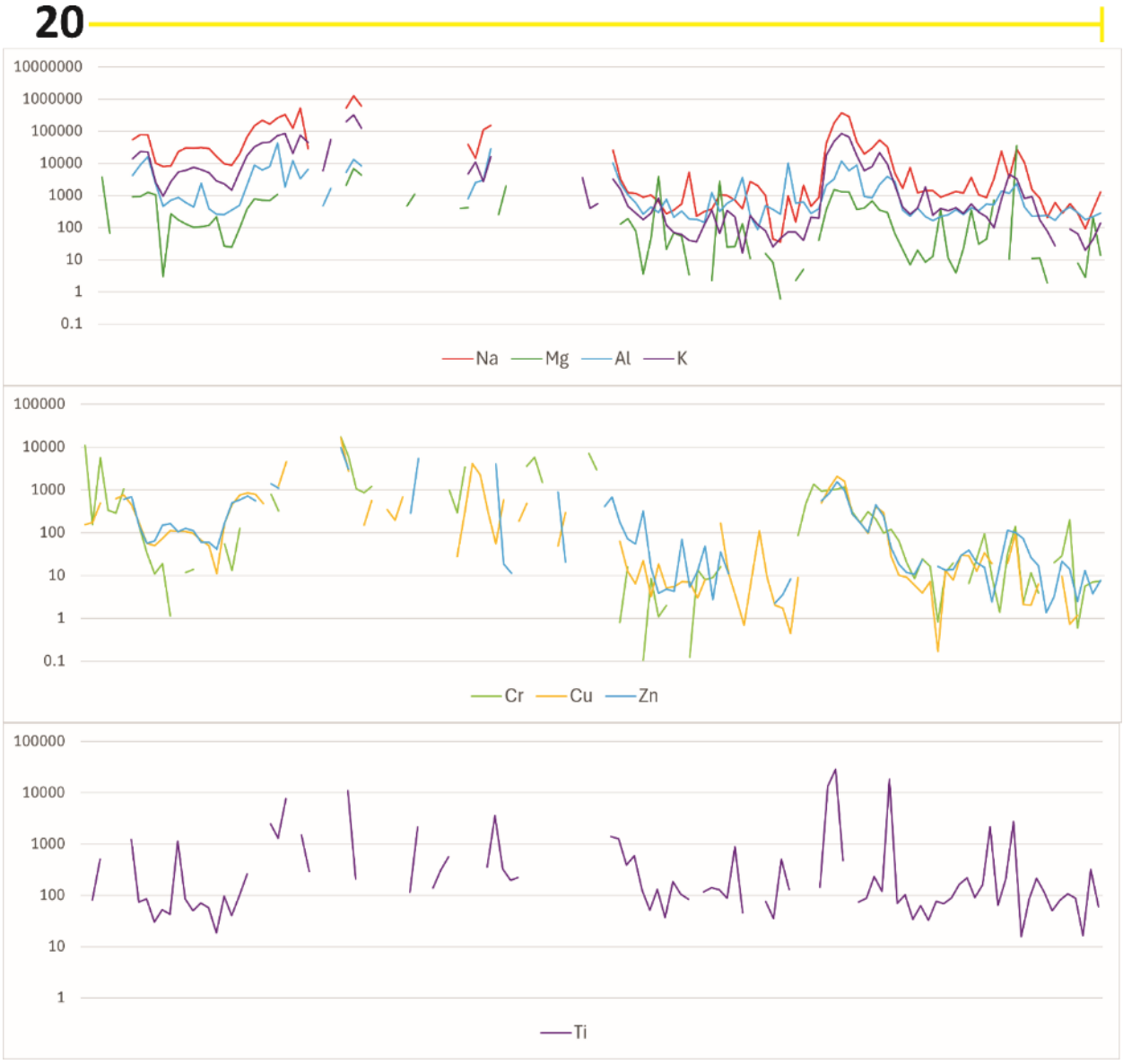
Appendix Figure 77: Concentrations (ppm) versus transect length. Sample LE25-5C-1B.17 is a quartz transect from pegmatite LE25-5C.



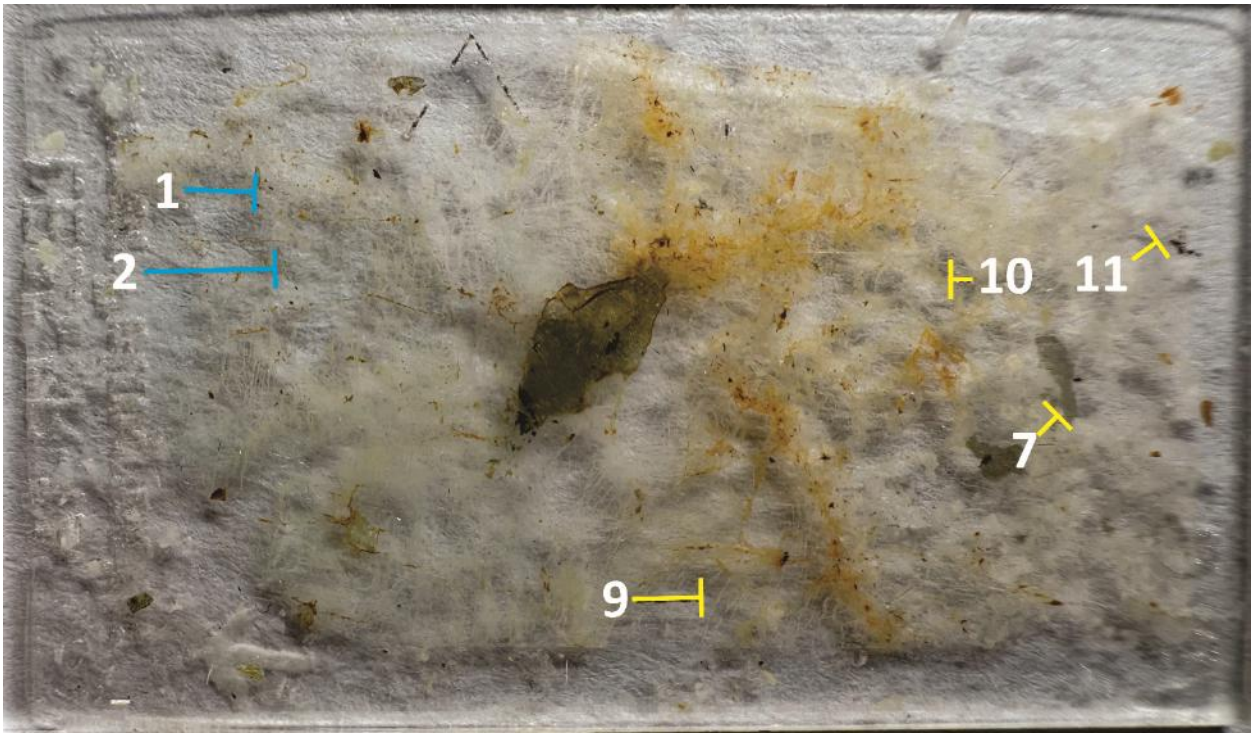
Appendix Figure 78: Concentrations (ppm) versus transect length. Sample LE25-5C-1B.18 is a quartz transect from pegmatite LE25-5C.



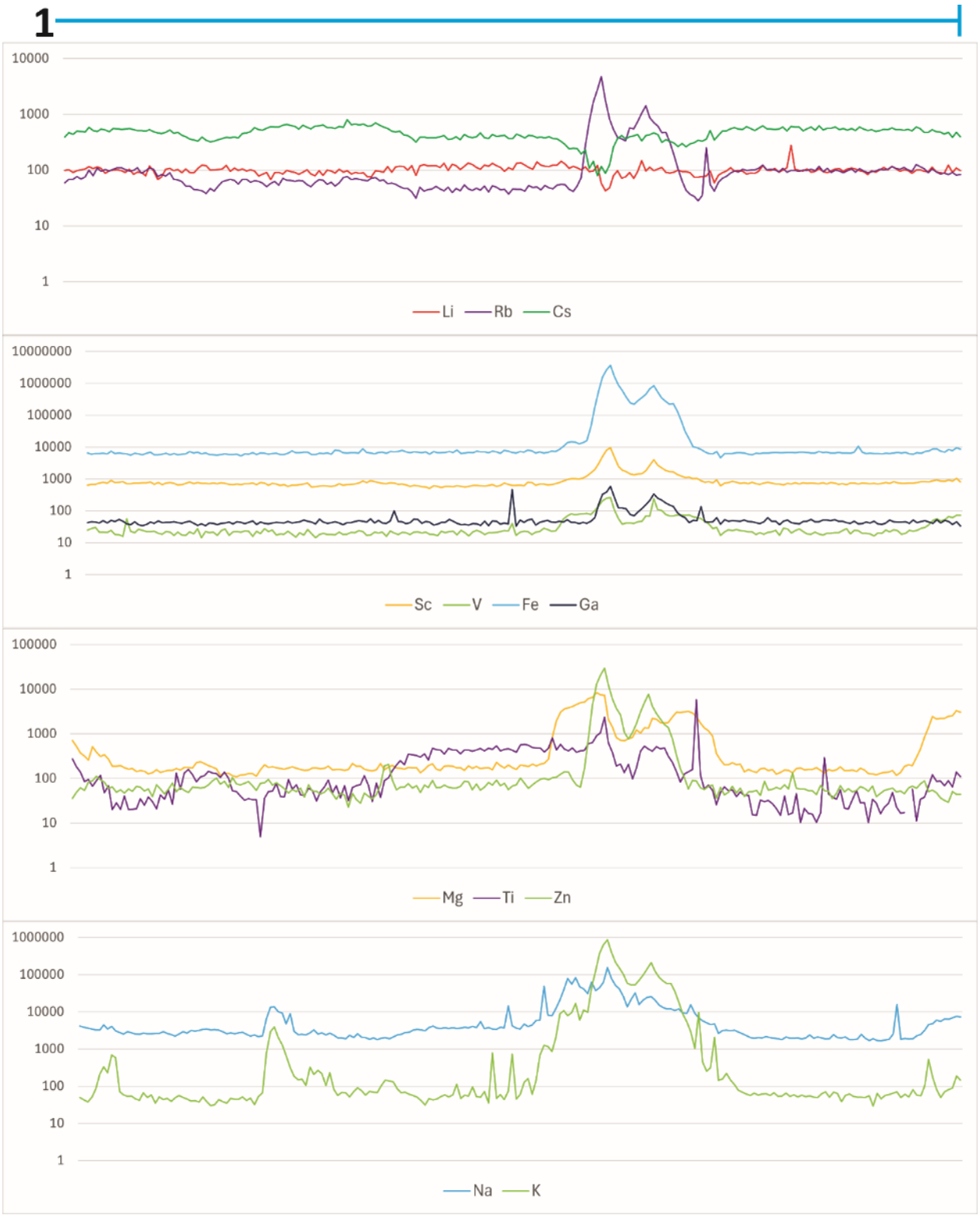
Appendix Figure 79: Concentrations (ppm) versus transect length. Sample LE25-5C-1B.19 is a quartz transect from pegmatite LE25-5C.



Appendix Figure 80: Concentrations (ppm) versus transect length. Sample LE25-5C-1B.20 is a quartz transect from pegmatite LE25-5C.



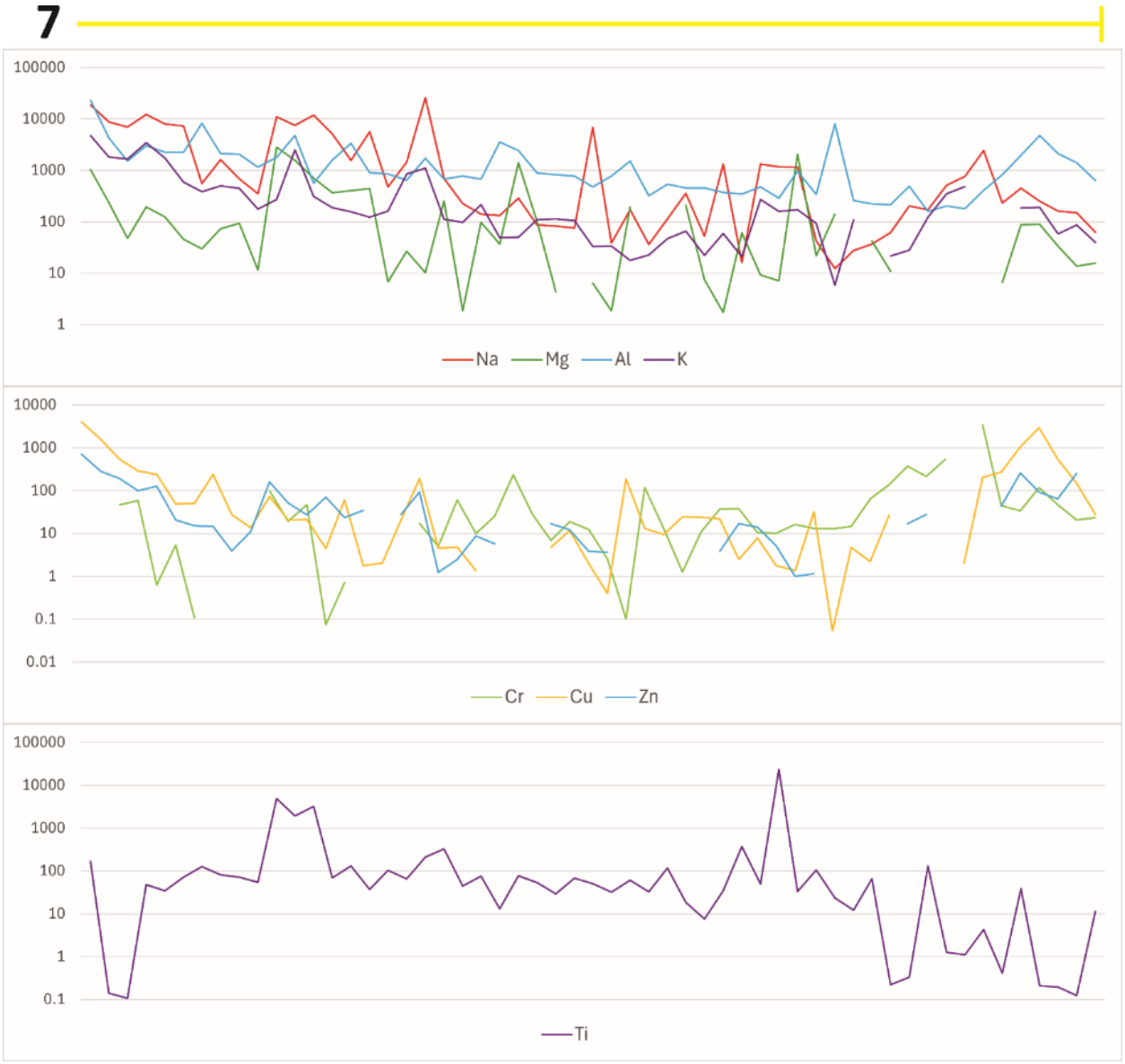
Appendix Figure 81: Sample LE25-5R-1A, 100 micron double polished thick section of a pegmatite core zone. Blue (beryl transect) and yellow (quartz transect) lines and numbers correspond to LA-ICP-MS transect lines (e.g., LE25-5R-1A.1 is the blue line labelled 1).



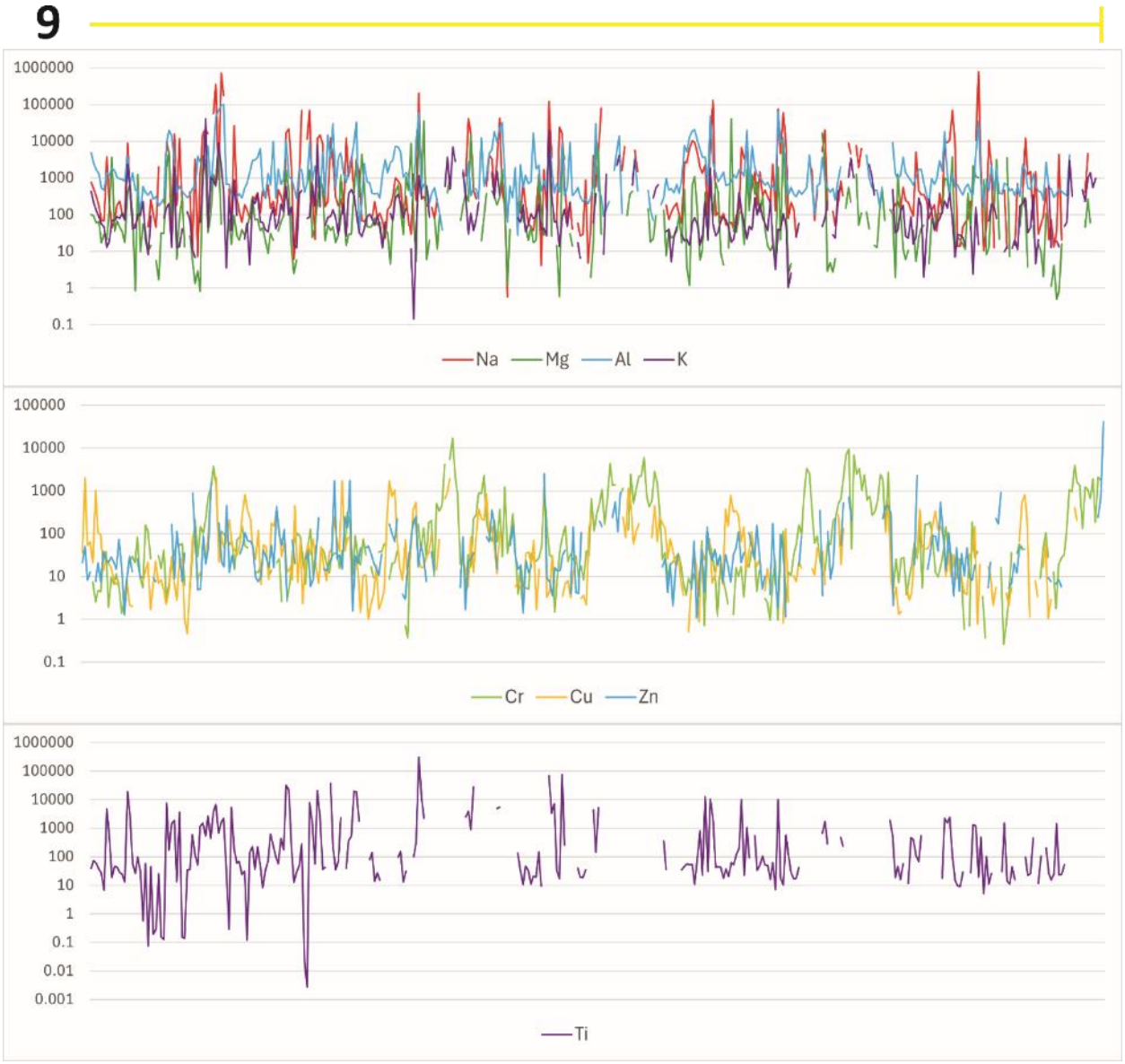
Appendix Figure 82: Concentrations (ppm) versus transect length. Sample LE25-5R-1A.1 is a beryl transect from pegmatite LE25-5R.



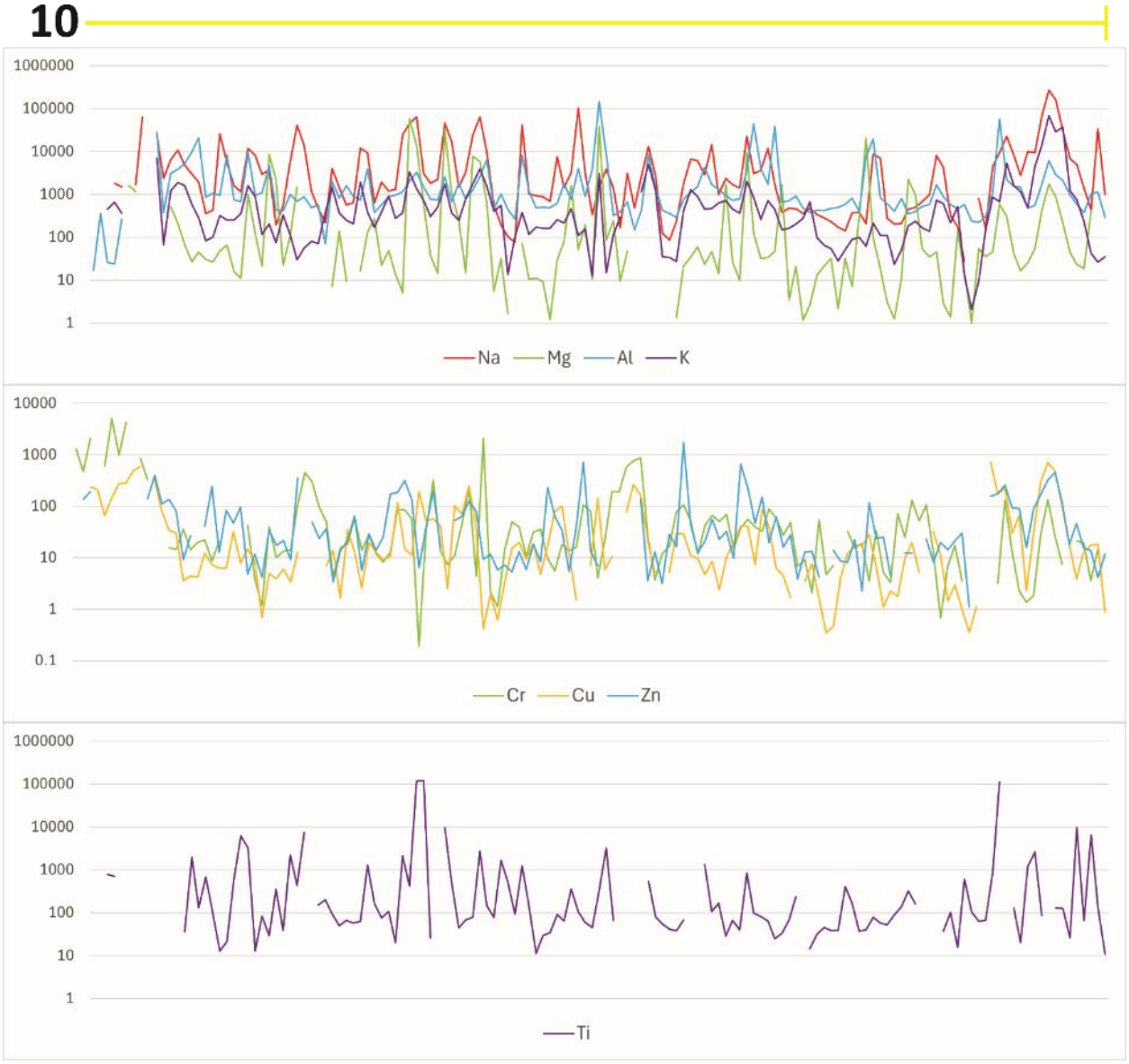
Appendix Figure 83: Concentrations (ppm) versus transect length. Sample LE25-5R-1A.2 is a beryl transect from pegmatite LE25-5R.



Appendix Figure 84: Concentrations (ppm) versus transect length. Sample LE25-5R-1A.7 is a quartz transect from pegmatite LE25-5R.



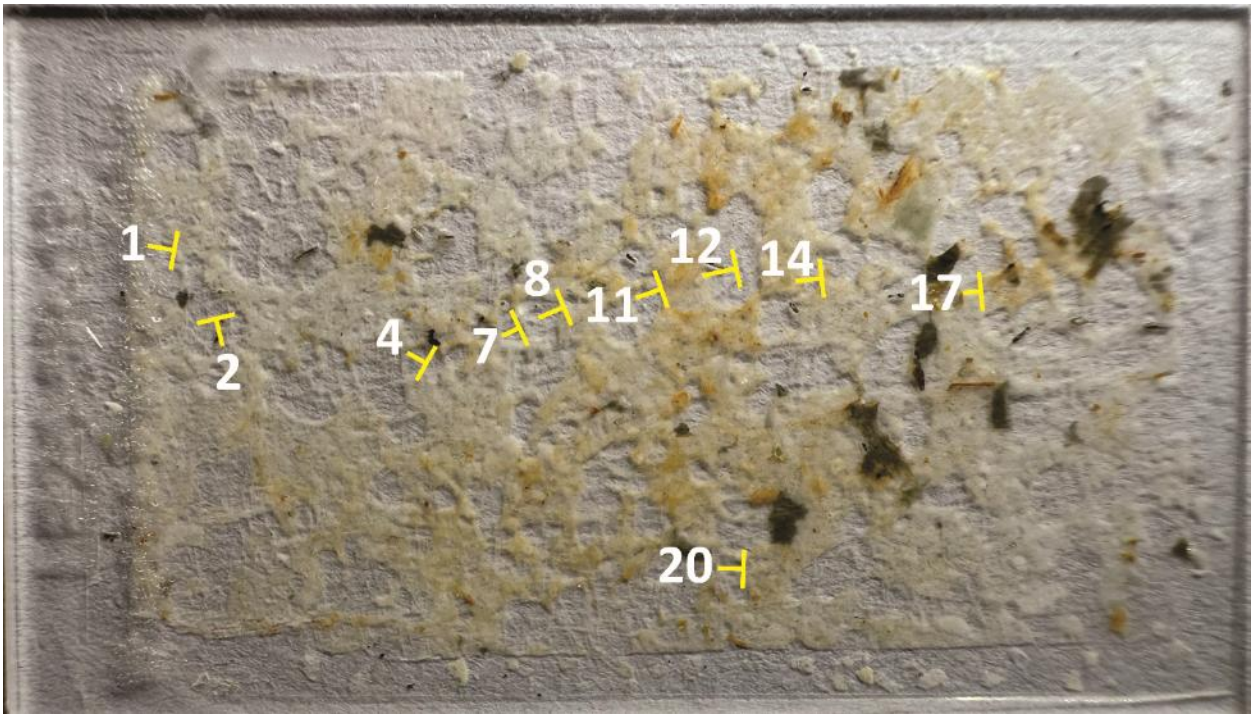
Appendix Figure 85: Concentrations (ppm) versus transect length. Sample LE25-5R-1A.9 is a quartz transect from pegmatite LE25-5R.



Appendix Figure 86: Concentrations (ppm) versus transect length. Sample LE25-5R-1A.10 is a quartz transect from pegmatite LE25-5R.



Appendix Figure 87: Concentrations (ppm) versus transect length. Sample LE25-5R-1A.11 is a quartz transect from pegmatite LE25-5R.



Appendix Figure 88: Sample LE25-5R-1B, 100 micron double polished thick section of pegmatite transition zone proximal to pegmatite LE25-5L. The yellow (quartz transect) line labelled 2 corresponds to LA-ICP-MS transect line LE25-5R-1B.2.



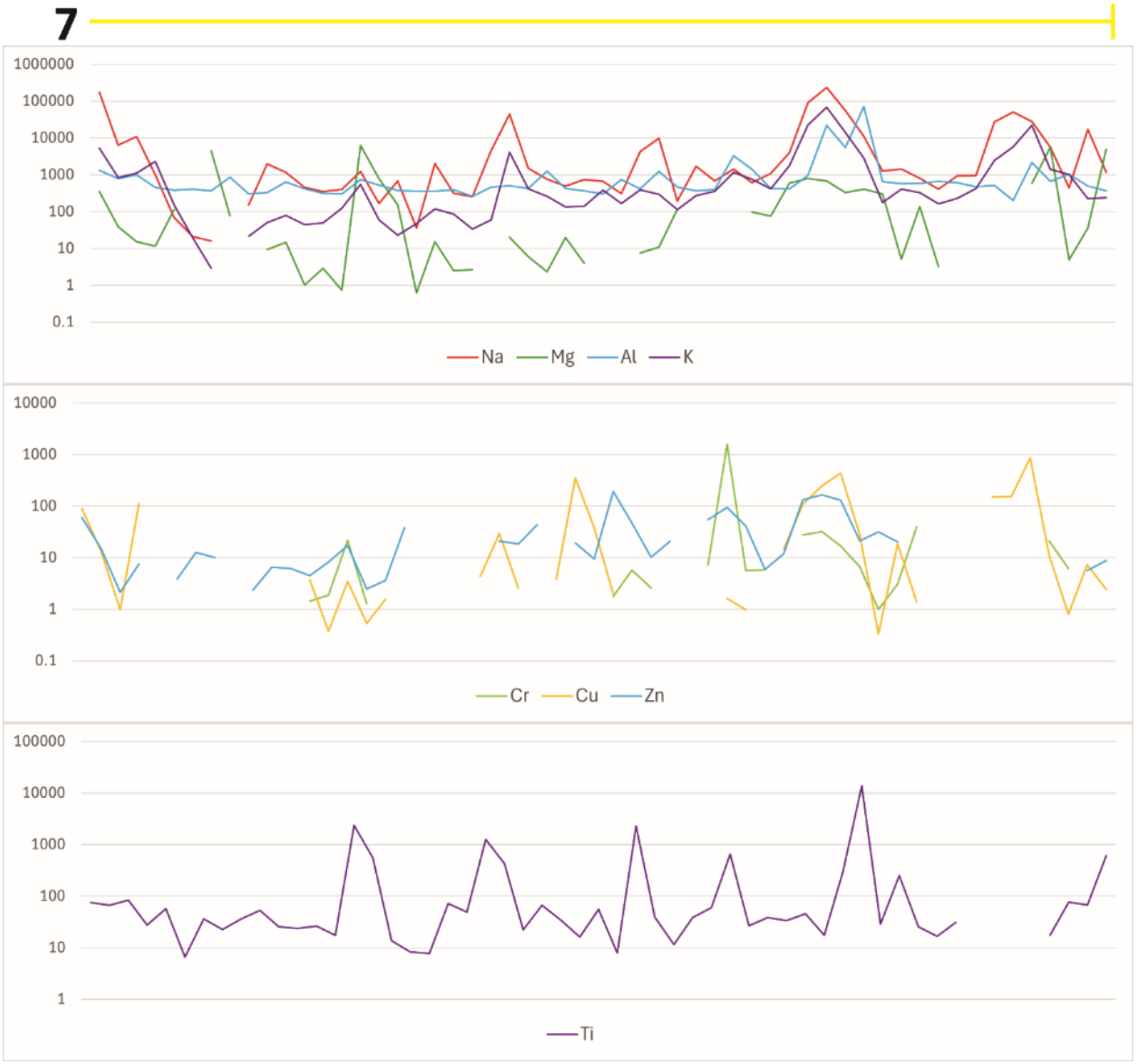
Appendix Figure 89: Concentrations (ppm) versus transect length. Sample LE25-5R-1B.1 is a quartz transect from pegmatite LE25-5R.



Appendix Figure 90: Concentrations (ppm) versus transect length. Sample LE25-5R-1B.2 is a quartz transect from pegmatite LE25-5R.



Appendix Figure 91: Concentrations (ppm) versus transect length. Sample LE25-5R-1B.4 is a quartz transect from pegmatite LE25-5R.



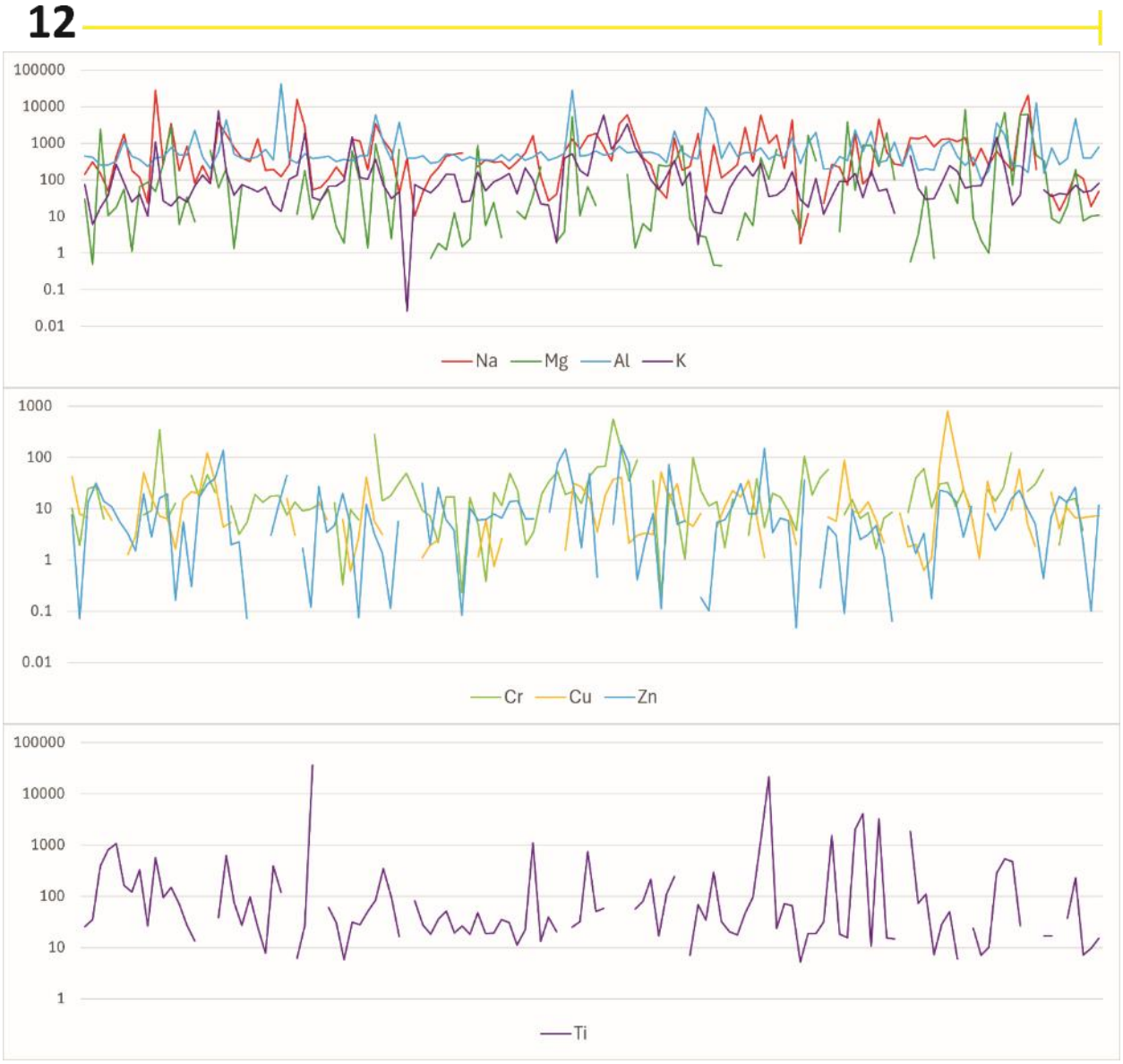
Appendix Figure 92: Concentrations (ppm) versus transect length. Sample LE25-5R-1B.4 is a quartz transect from pegmatite LE25-5R.



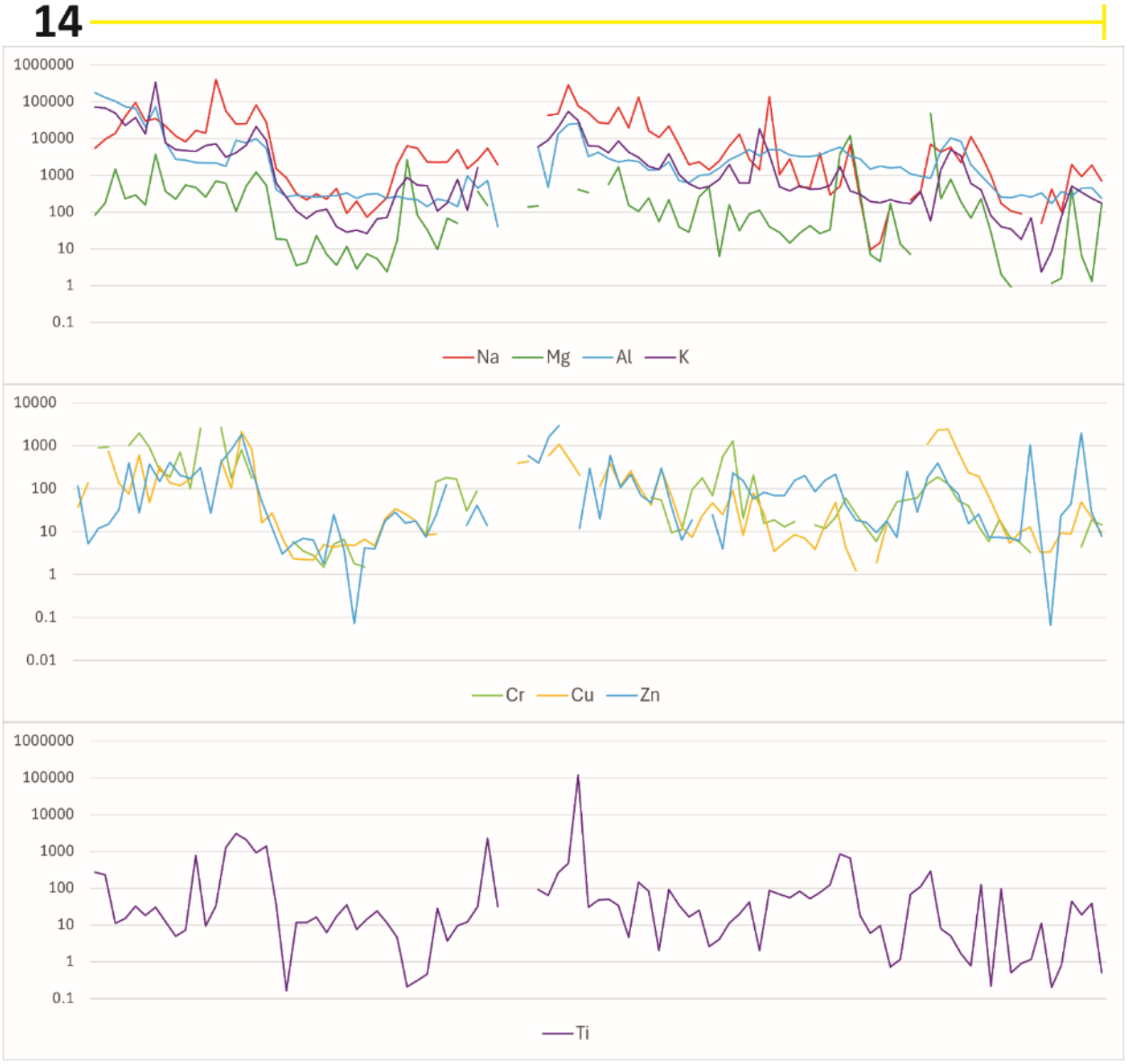
Appendix Figure 93: Concentrations (ppm) versus transect length. Sample LE25-5R-1B.8 is a quartz transect from pegmatite LE25-5R.



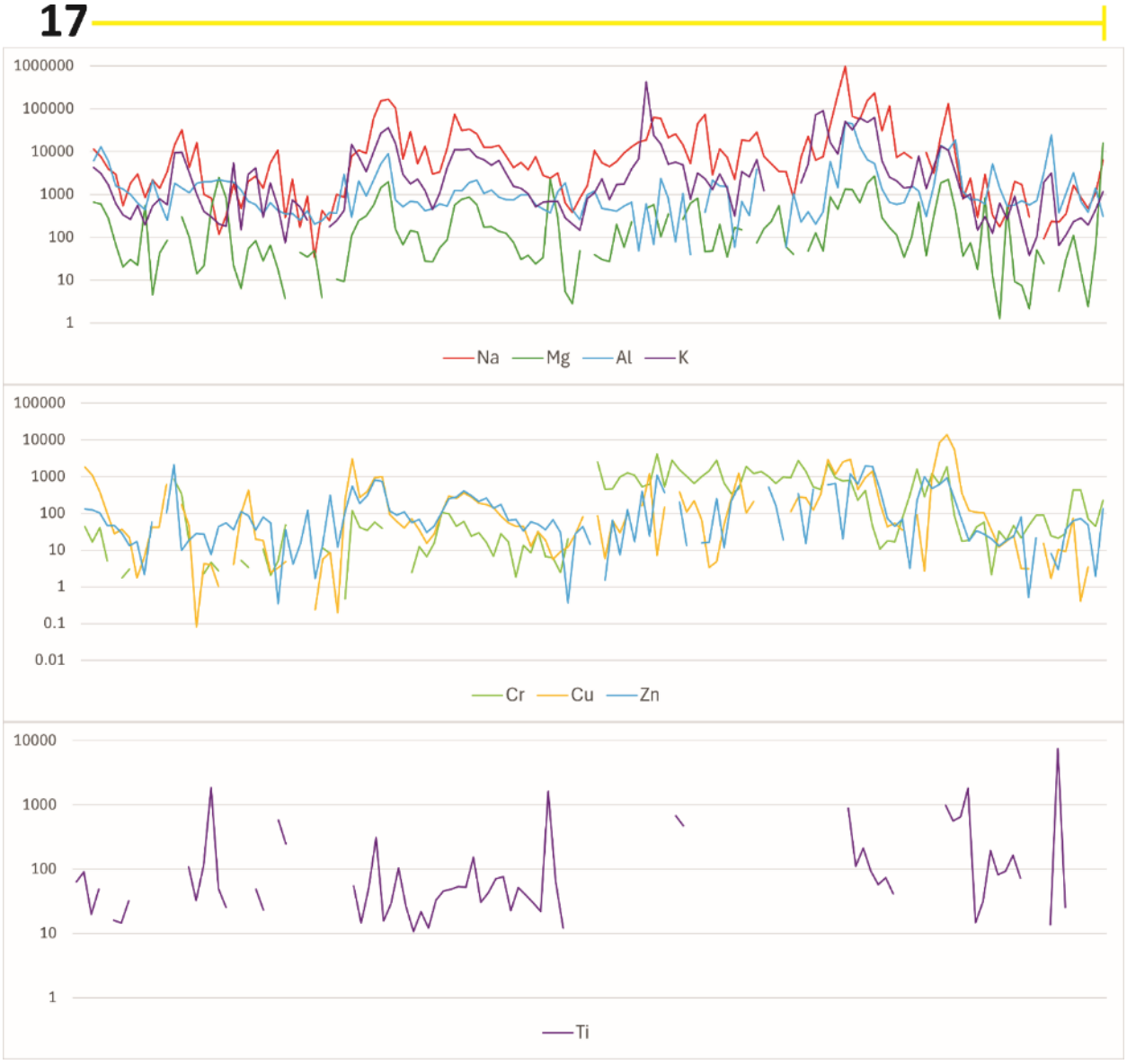
Appendix Figure 94: Concentrations (ppm) versus transect length. Sample LE25-5R-1B.11 is a quartz transect from pegmatite LE25-5R.



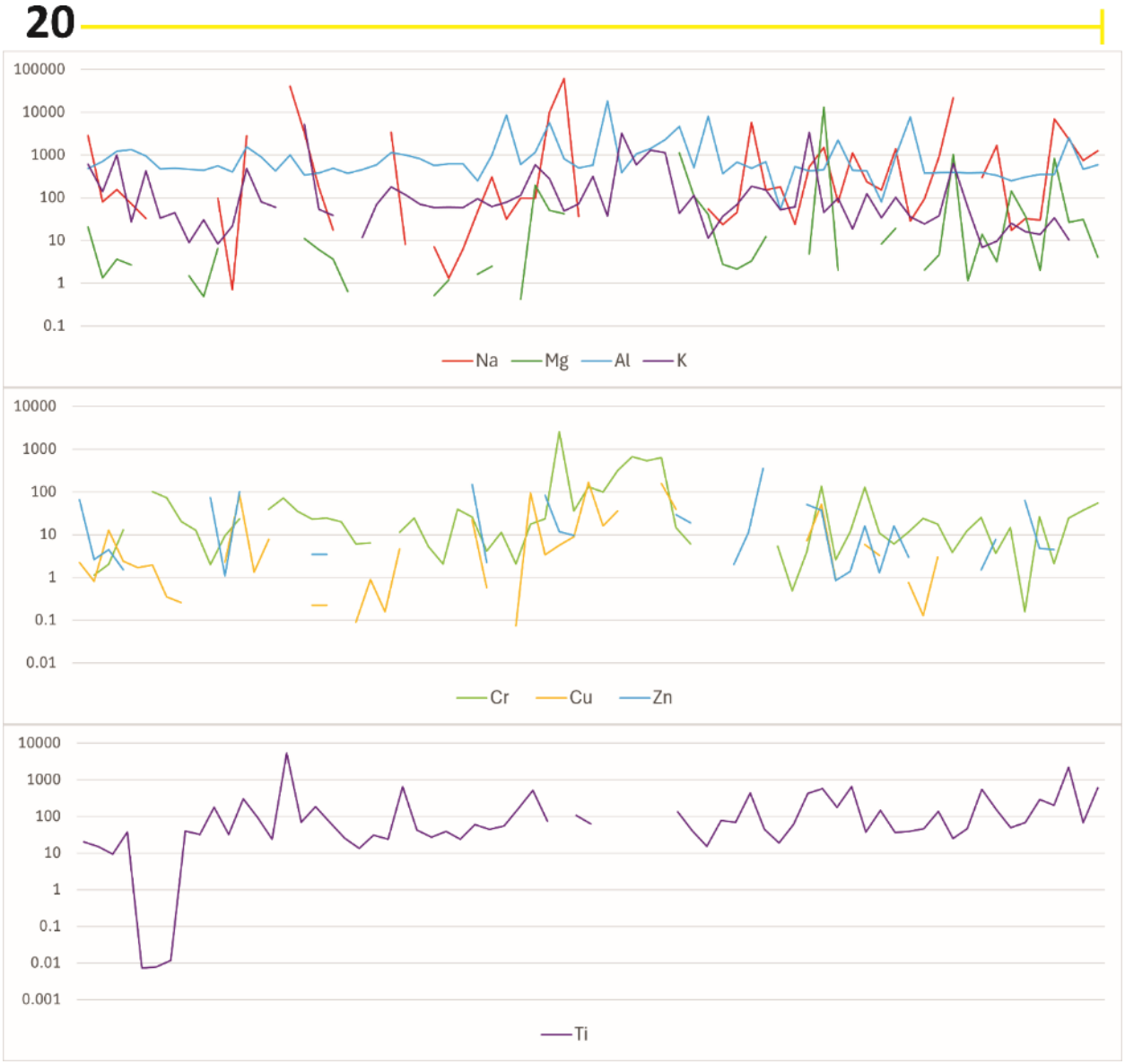
Appendix Figure 95: Concentrations (ppm) versus transect length. Sample LE25-5R-1B.12 is a quartz transect from pegmatite LE25-5R.



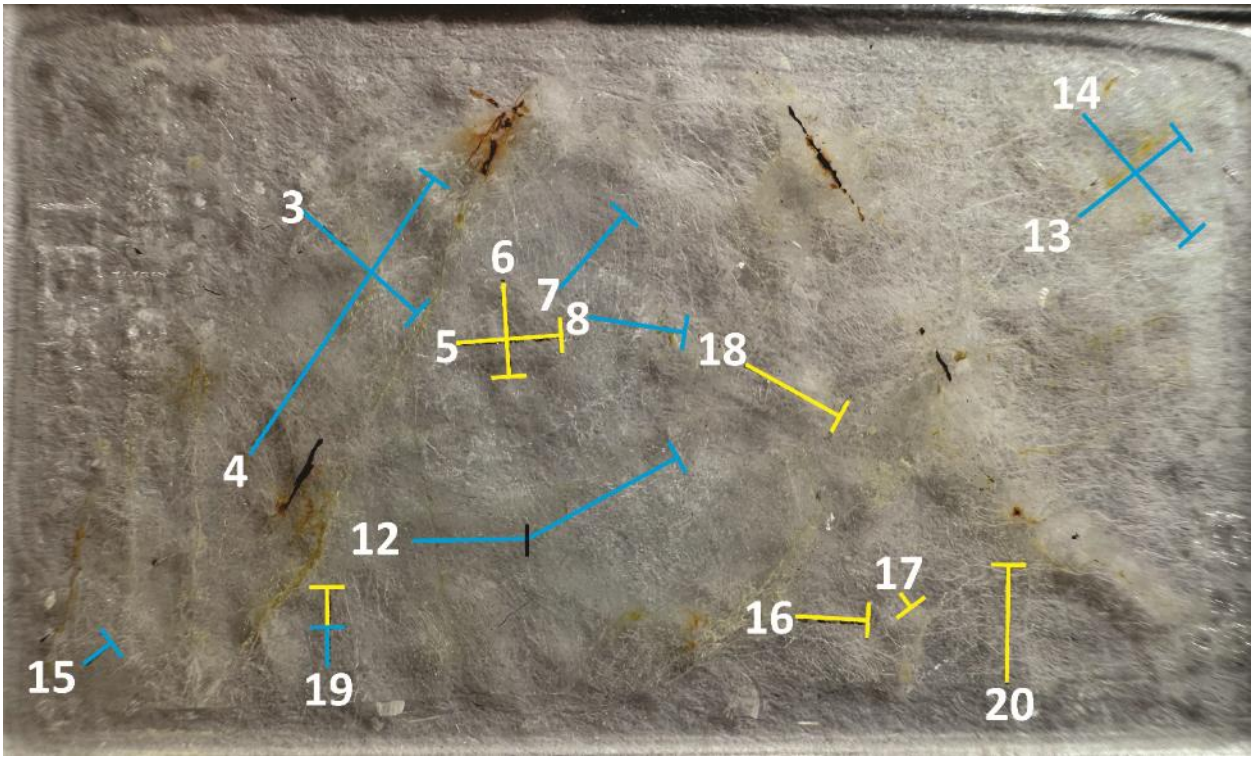
Appendix Figure 96: Concentrations (ppm) versus transect length. Sample LE25-5R-1B.14 is a quartz transect from pegmatite LE25-5R.



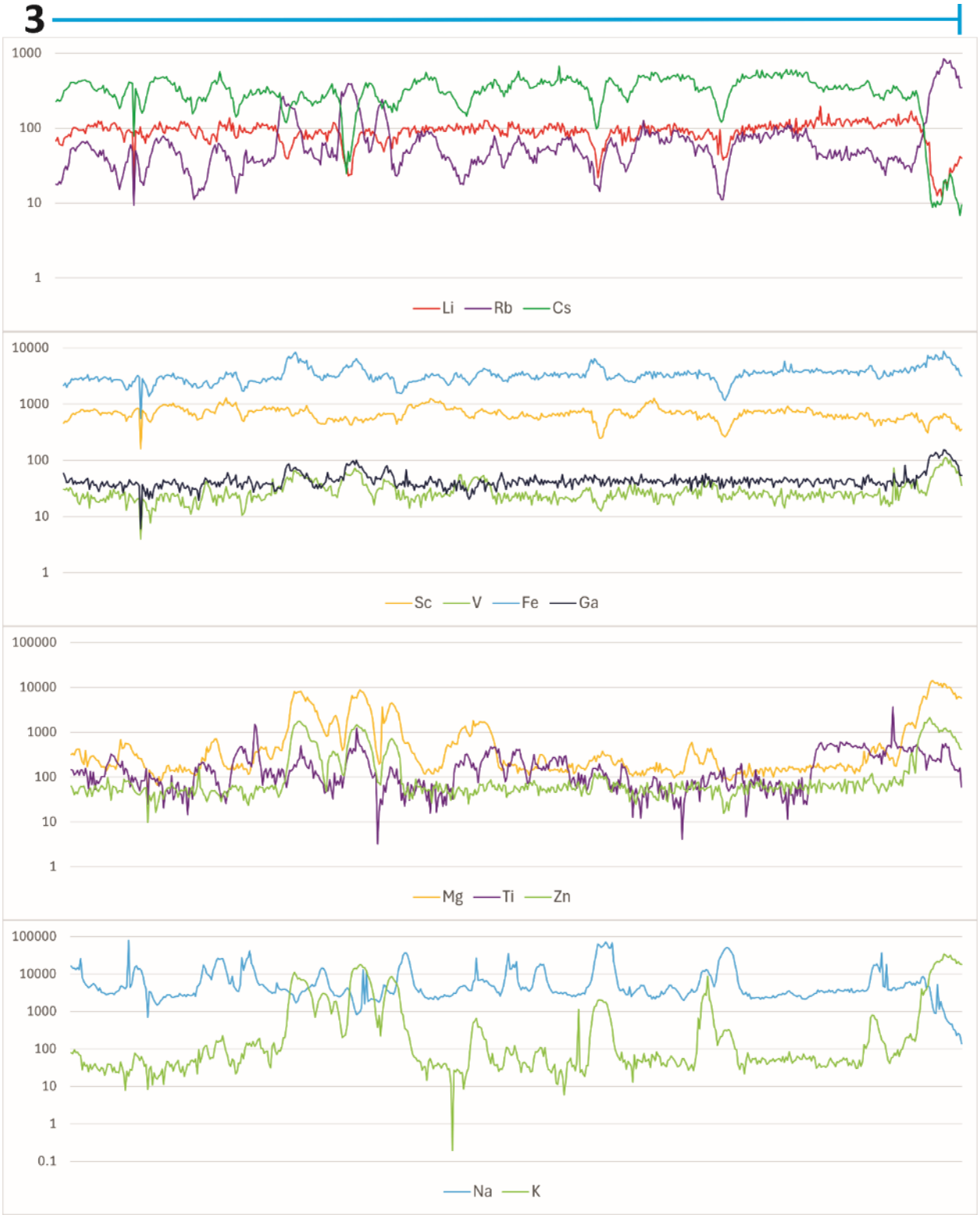
Appendix Figure 97: Concentrations (ppm) versus transect length. Sample LE25-5R-1B.17 is a quartz transect from pegmatite LE25-5R.



Appendix Figure 98: Concentrations (ppm) versus transect length. Sample LE25-5R-1B.20 is a quartz transect from pegmatite LE25-5R.



Appendix Figure 99: Sample LE25-6-1, 100 micron double polished thick section of a pegmatite core zone. Blue (beryl transect) and yellow (quartz transect) lines and numbers correspond to LA-ICP-MS transect lines (e.g., LE25-6-1.3 is the blue line labelled 3).



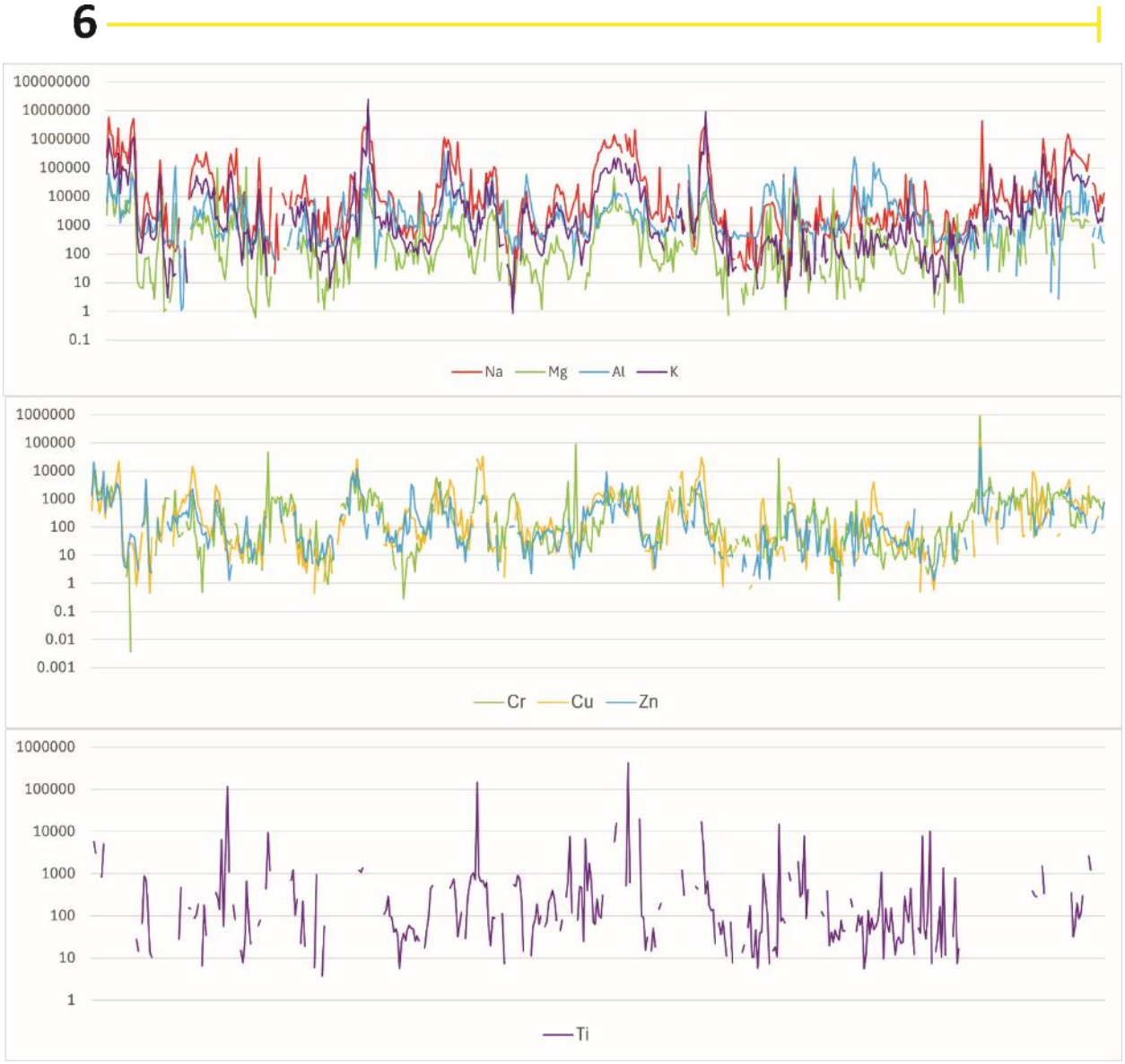
Appendix Figure 100: Concentrations (ppm) versus transect length. Sample LE25-6-1.3 is a beryl transect from pegmatite LE25-6.



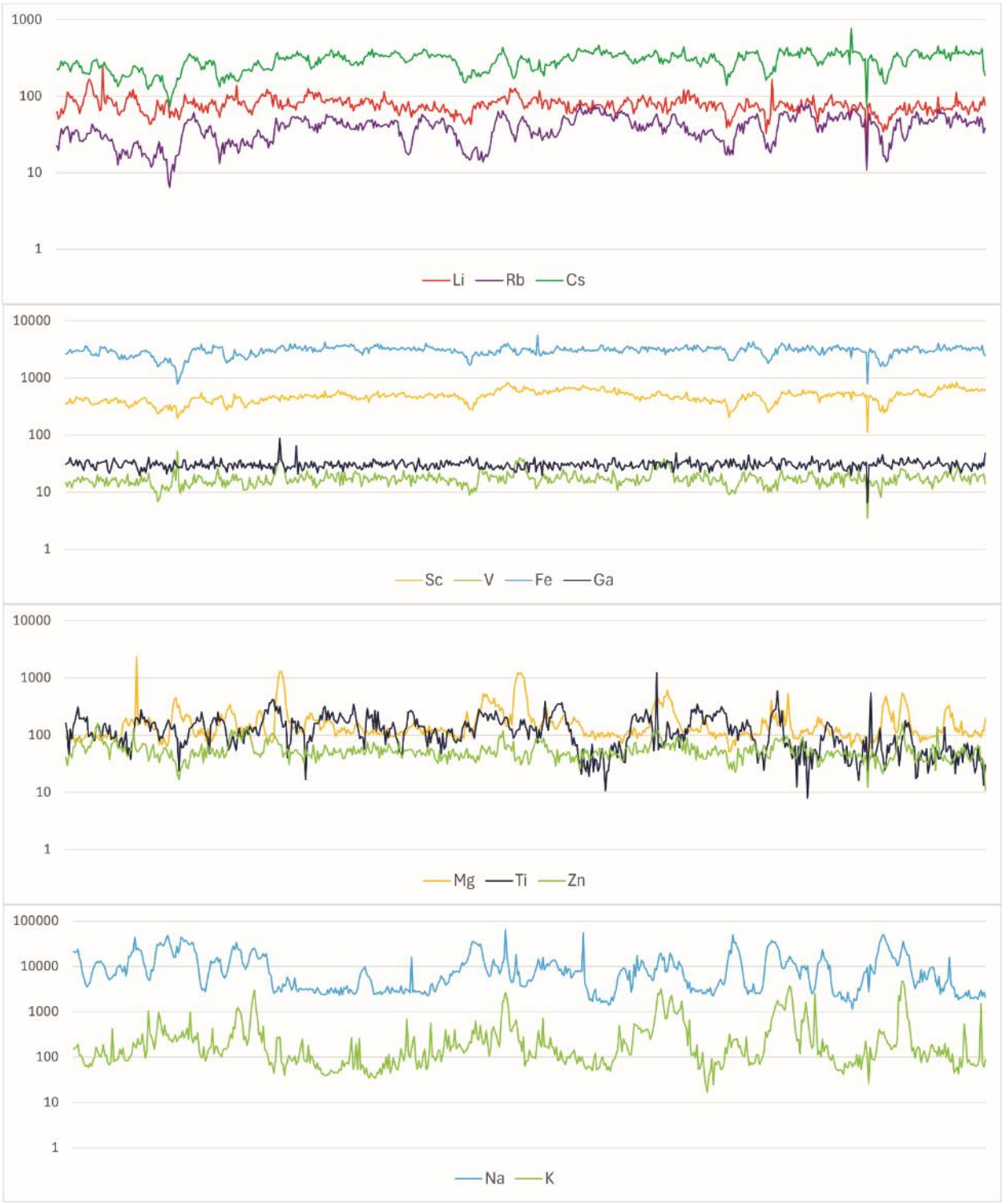
Appendix Figure 101: Concentrations (ppm) versus transect length. Sample LE25-6-1.4 is a beryl transect from pegmatite LE25-6.



Appendix Figure 102: Concentrations (ppm) versus transect length. Sample LE25-6-1.5 is a quartz transect from pegmatite LE25-6.



Appendix Figure 103: Concentrations (ppm) versus transect length. Sample LE25-6-1.6 is a quartz transect from pegmatite LE25-6.



Appendix Figure 104: Concentrations (ppm) versus transect length. Sample LE25-6-1.7 is a beryl transect from pegmatite LE25-6.



Appendix Figure 105: Concentrations (ppm) versus transect length. Sample LE25-6-1.8 is a beryl transect from pegmatite LE25-6.



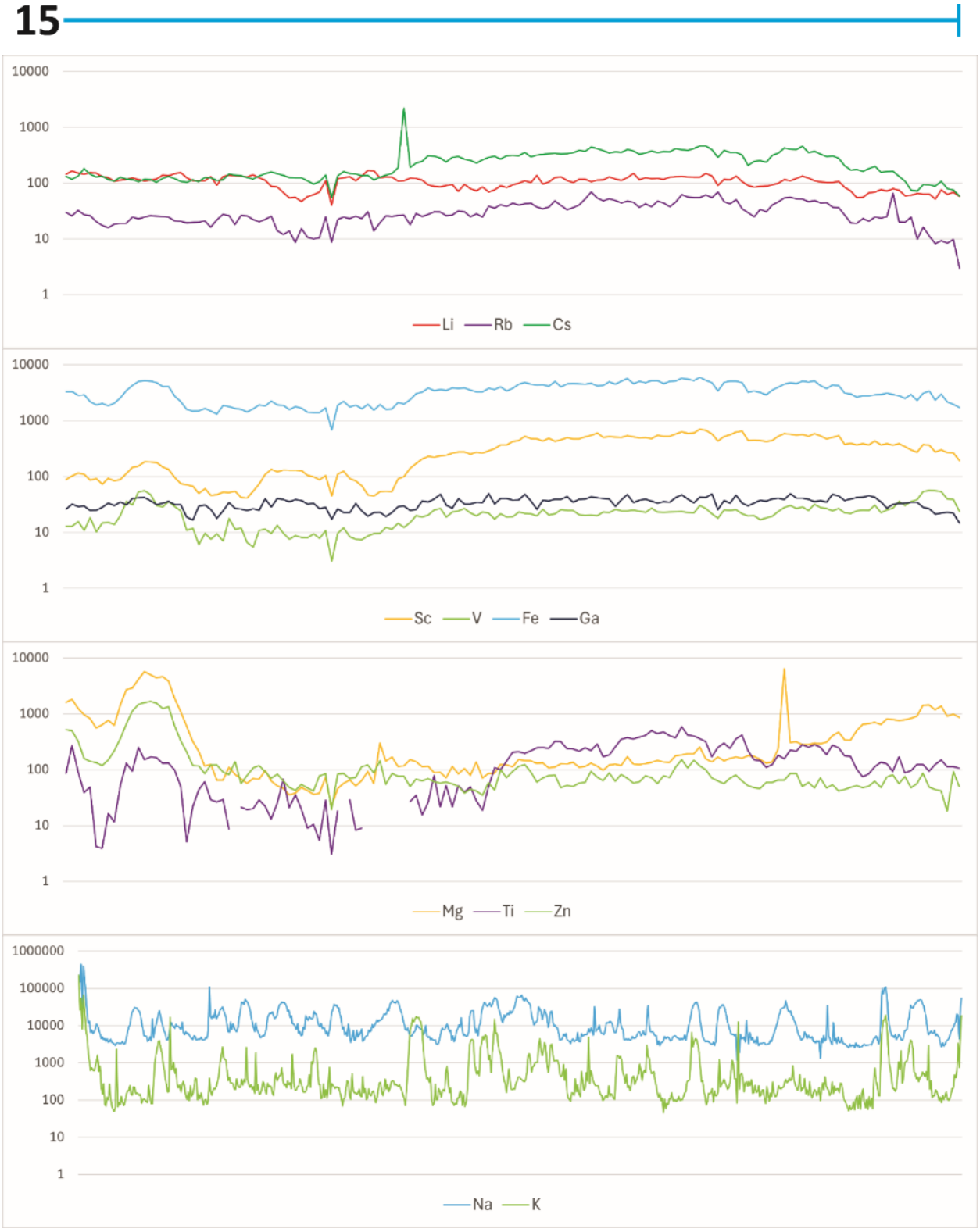
Appendix Figure 106: Concentrations (ppm) versus transect length. Sample LE25-6-1.12 is a beryl transect from pegmatite LE25-6.



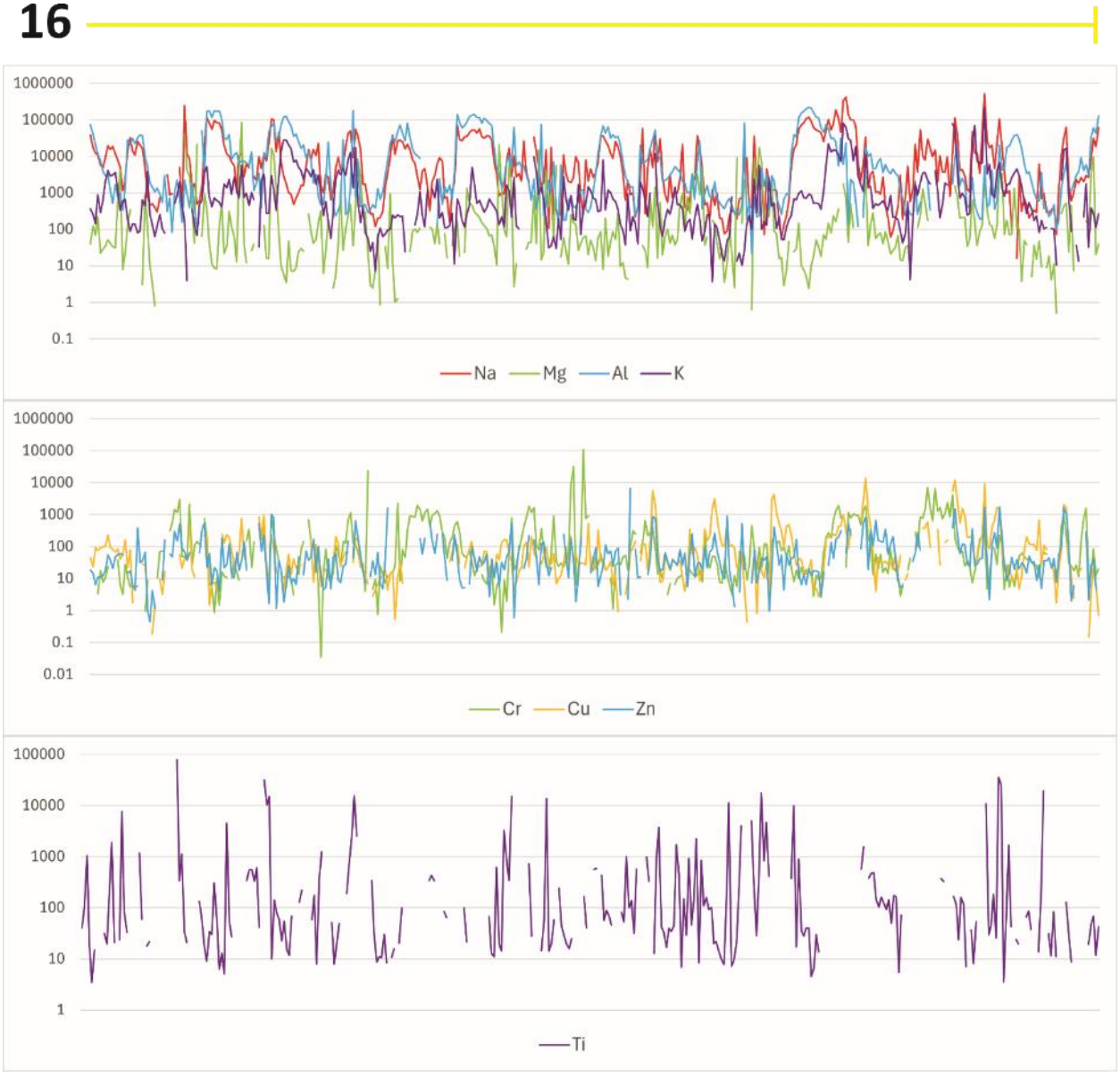
Appendix Figure 107: Concentrations (ppm) versus transect length. Sample LE25-6-1.13 is a beryl transect from pegmatite LE25-6.



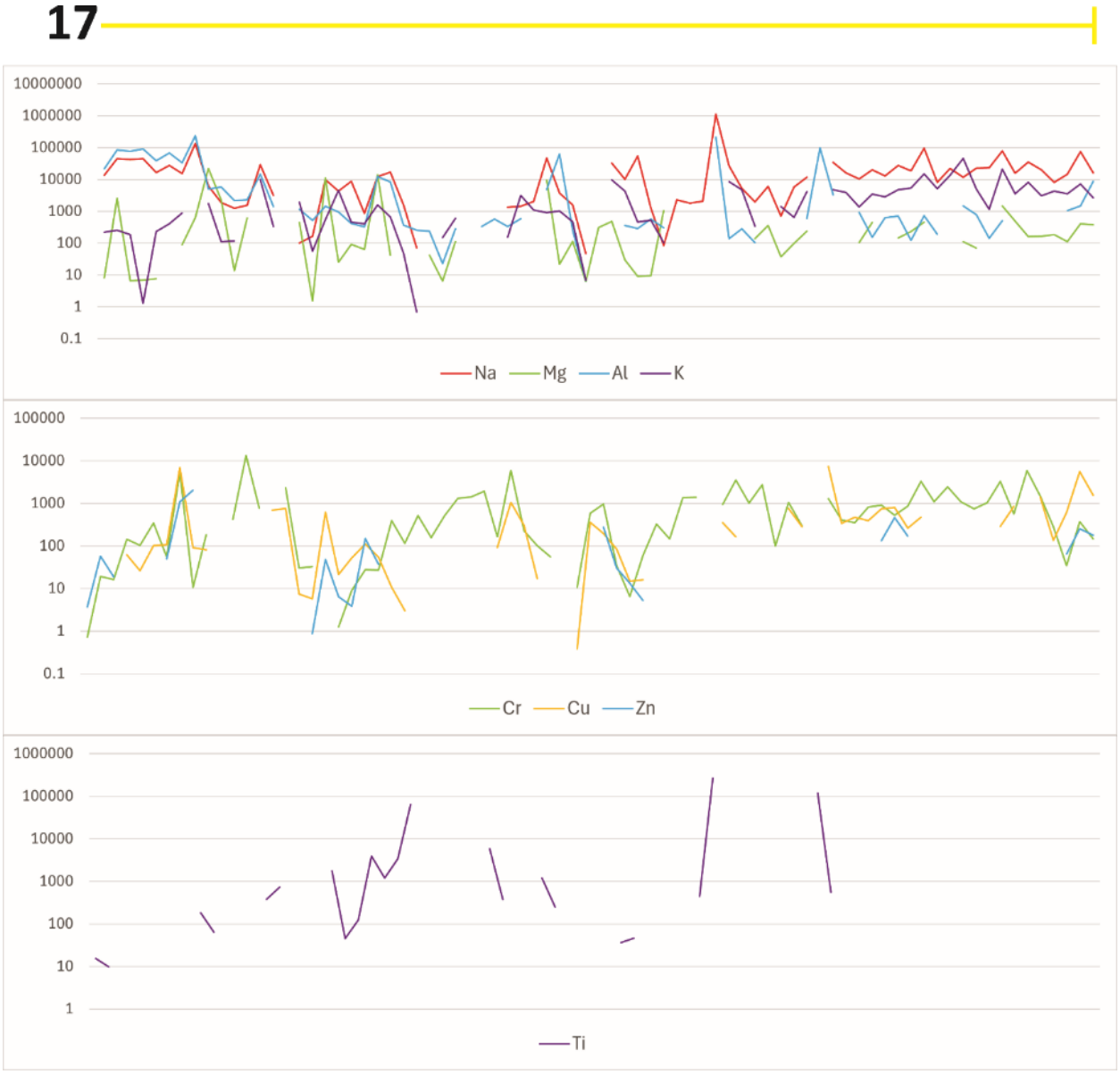
Appendix Figure 108: Concentrations (ppm) versus transect length. Sample LE25-6-1.14 is a beryl transect from pegmatite LE25-6.



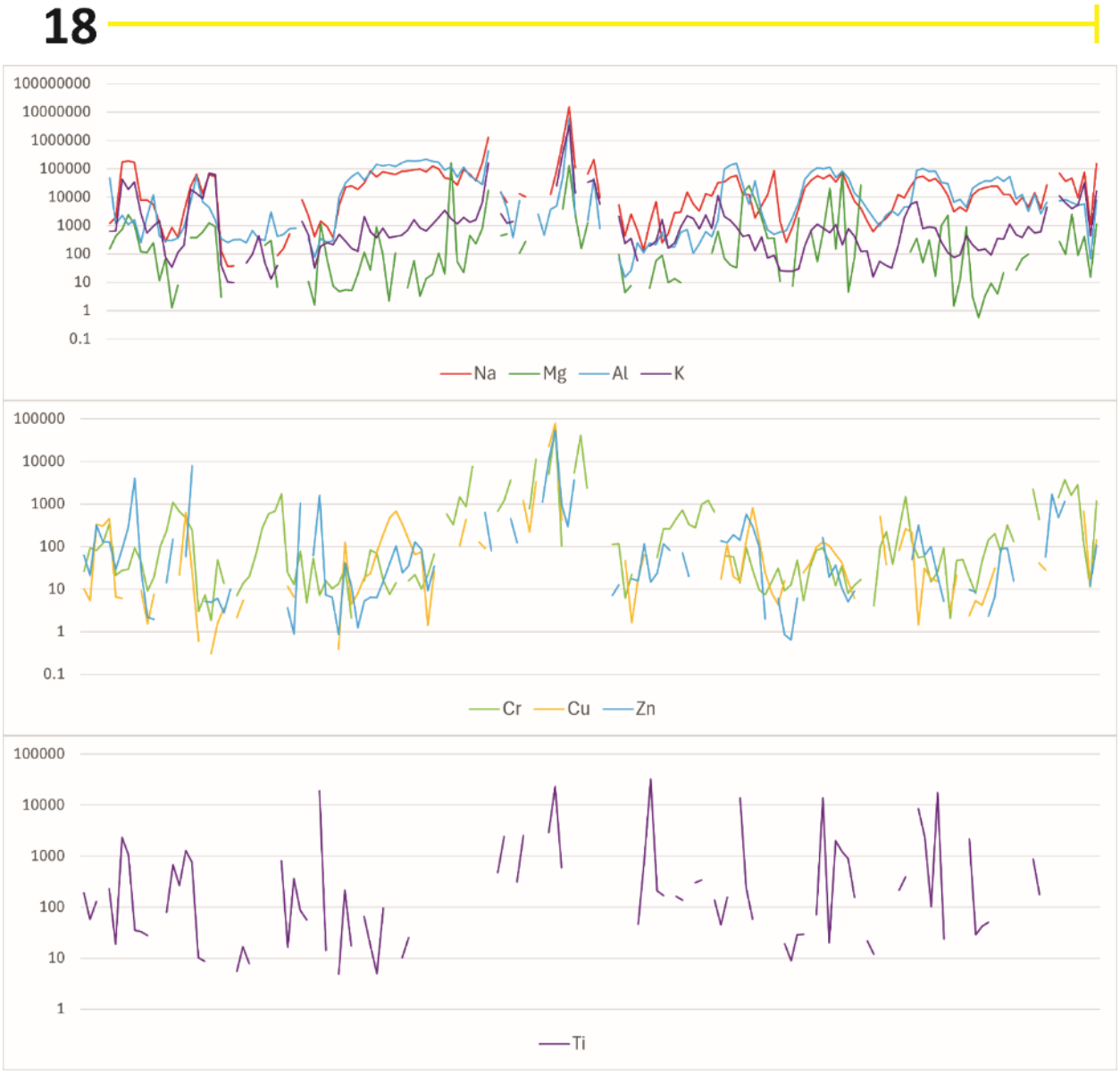
Appendix Figure 109: Concentrations (ppm) versus transect length. Sample LE25-6-1.15 is a beryl transect from pegmatite LE25-6.



Appendix Figure 110: Concentrations (ppm) versus transect length. Sample LE25-6-1.16 is a quartz transect from pegmatite LE25-6.



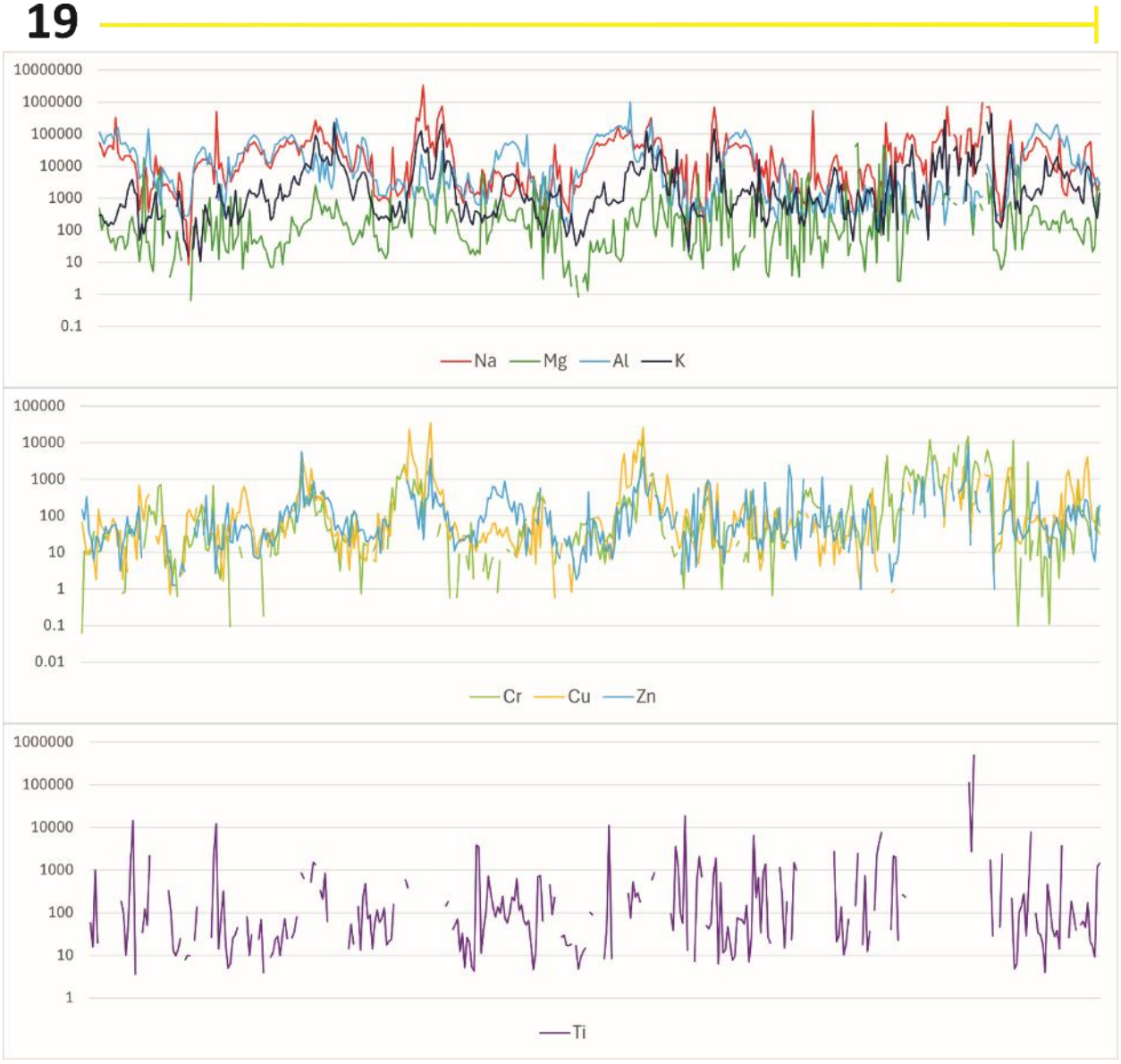
Appendix Figure 111: Concentrations (ppm) versus transect length. Sample LE25-6-1.17 is a quartz transect from pegmatite LE25-6.



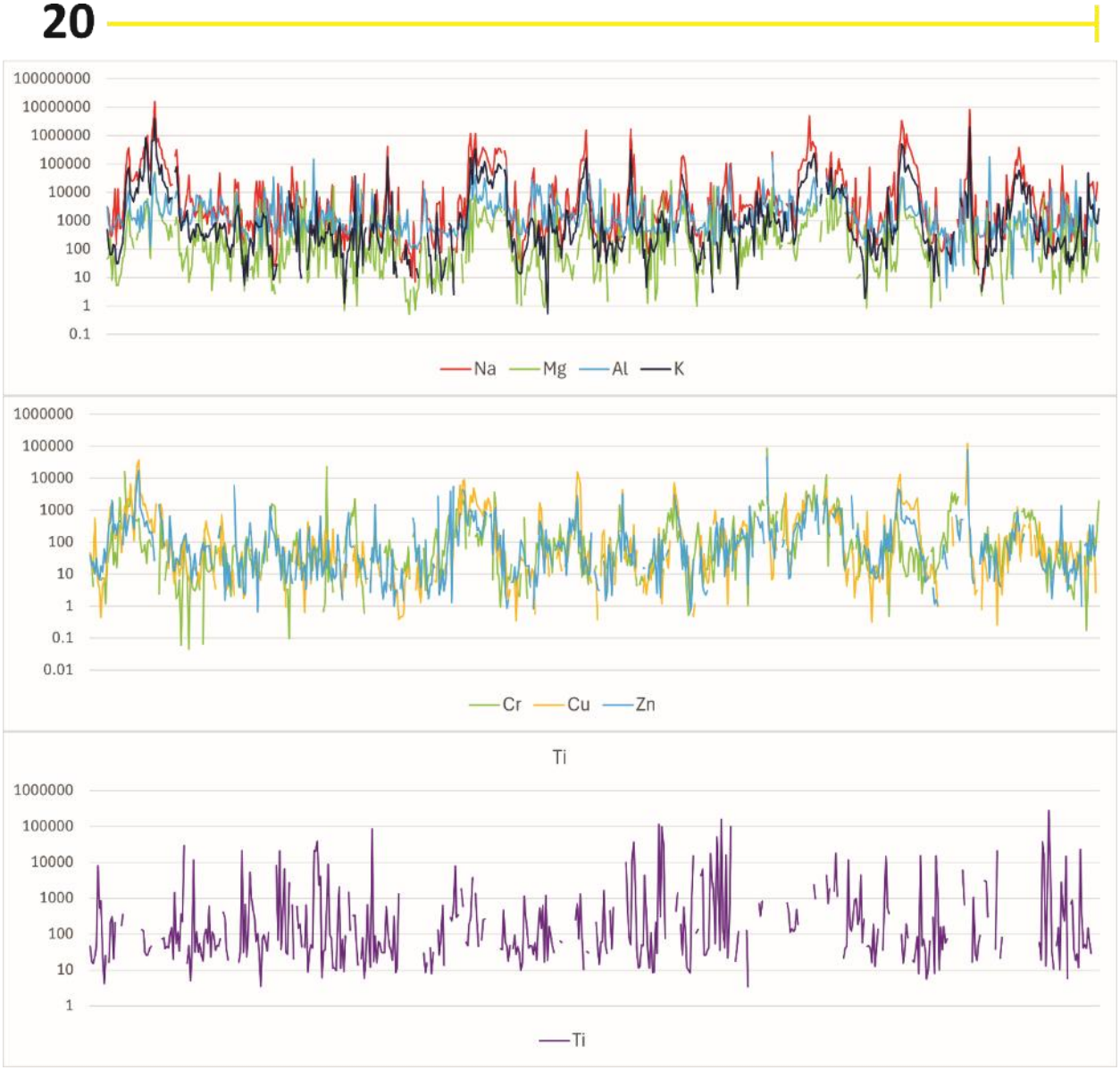
Appendix Figure 112: Concentrations (ppm) versus transect length. Sample LE25-6-1.18 is a quartz transect from pegmatite LE25-6.



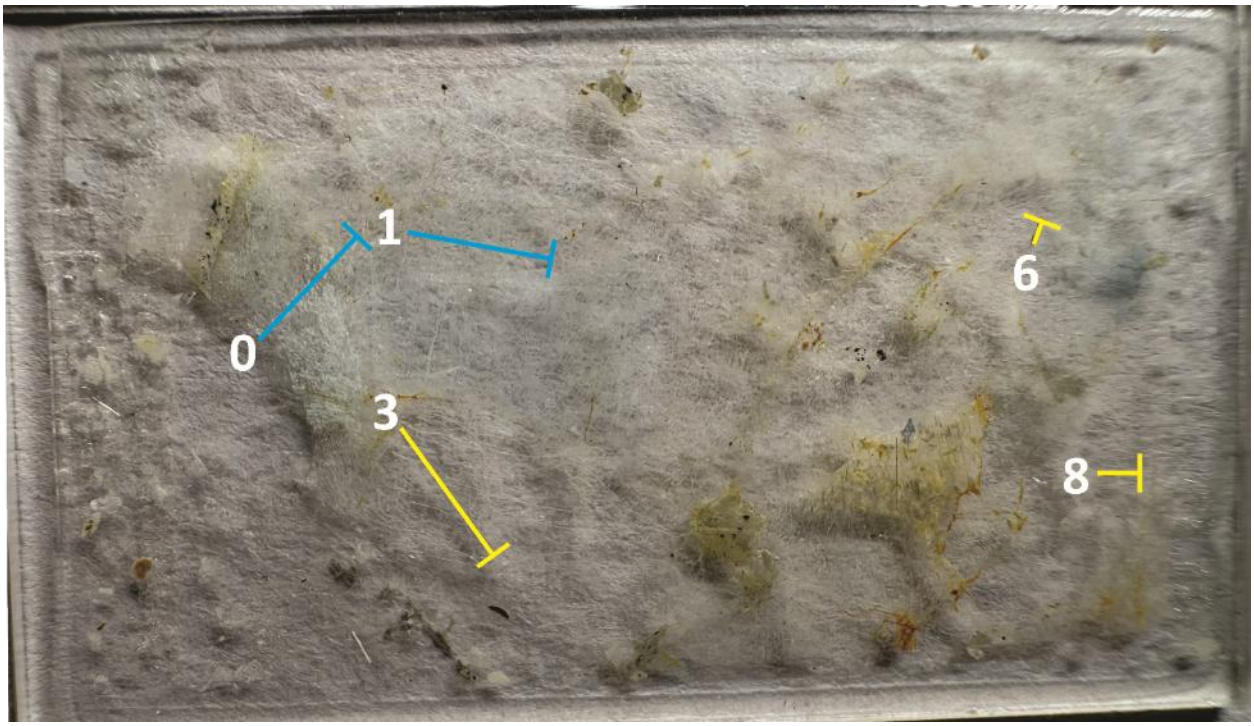
Appendix Figure 113: Concentrations (ppm) versus transect length. Sample LE25-6-1.19 is a beryl transect from pegmatite LE25-6.



Appendix Figure 114: Concentrations (ppm) versus transect length. Sample LE25-6-1.19 is a quartz transect from pegmatite LE25-6.



Appendix Figure 115: Concentrations (ppm) versus transect length. Sample LE25-6-1.20 is a quartz transect from pegmatite LE25-6.



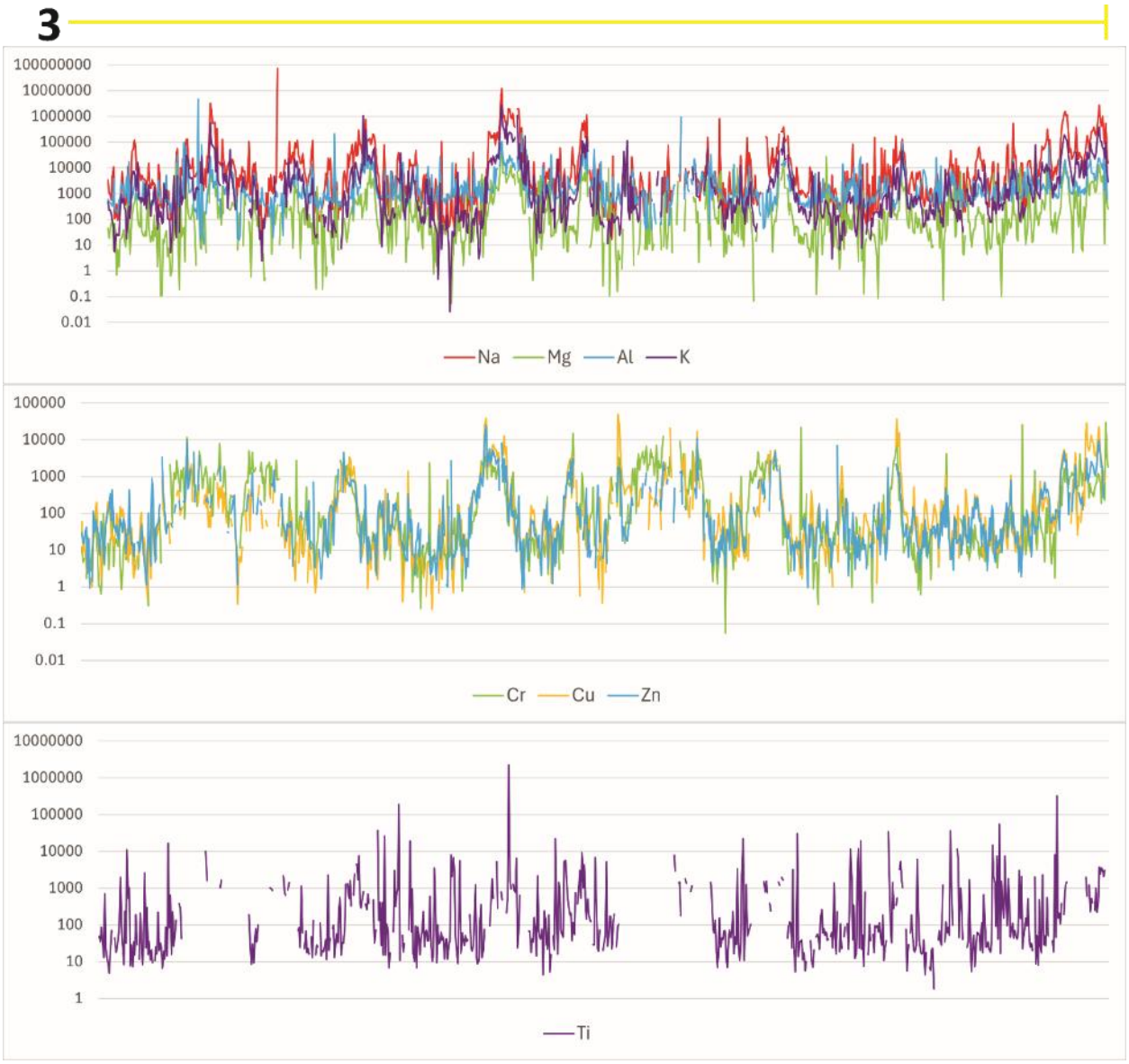
Appendix Figure 116: Sample LE25-6-2, 100 micron double polished thick section of a pegmatite core zone. Blue (beryl transect) and yellow (quartz transect) lines and numbers correspond to LA-ICP-MS transect lines (e.g., LE25-6-2.1 is the blue line labelled 1).



Appendix Figure 117: Concentrations (ppm) versus transect length. Sample LE25-6-2.0 is a beryl transect from pegmatite LE25-6.



Appendix Figure 118: Concentrations (ppm) versus transect length. Sample LE25-6-2.1 is a beryl transect from pegmatite LE25-6.



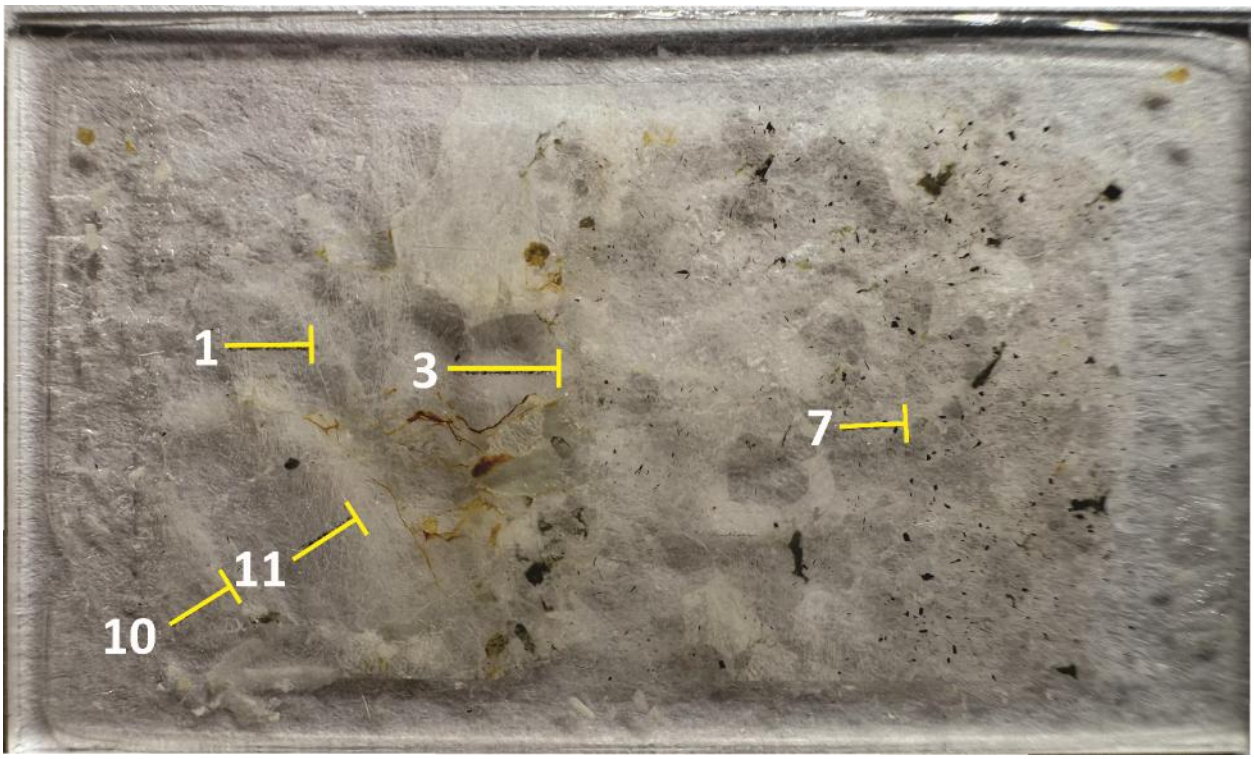
Appendix Figure 119: Concentrations (ppm) versus transect length. Sample LE25-6-2.3 is a quartz transect from pegmatite LE25-6.



Appendix Figure 120: Concentrations (ppm) versus transect length. Sample LE25-6-2.6 is a quartz transect from pegmatite LE25-6.



Appendix Figure 121: Concentrations (ppm) versus transect length. Sample LE25-6-2.8 is a quartz transect from pegmatite LE25-6.



Appendix Figure 122: Sample LE25-7-1A, 100 micron double polished thick section of pegmatite LE25-7 core zone. The yellow (quartz transect) line labelled 1 corresponds to LA-ICP-MS transect line LE25-7-1A.1.



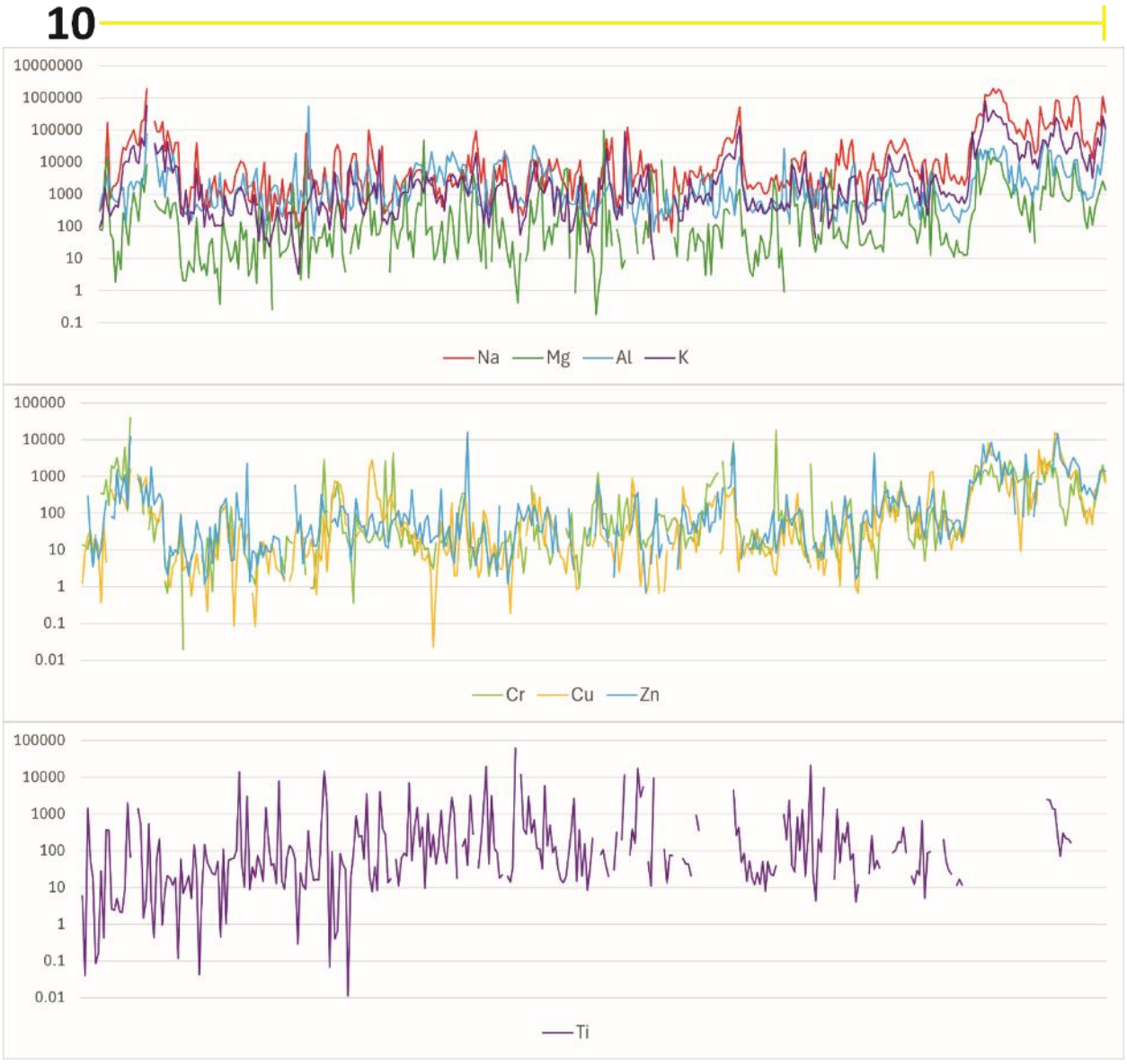
Appendix Figure 123: Concentrations (ppm) versus transect length. Sample LE25-7-1A.1 is a quartz transect from pegmatite LE25-7.



Appendix Figure 124: Concentrations (ppm) versus transect length. Sample LE25-7-1A.3 is a quartz transect from pegmatite LE25-7.



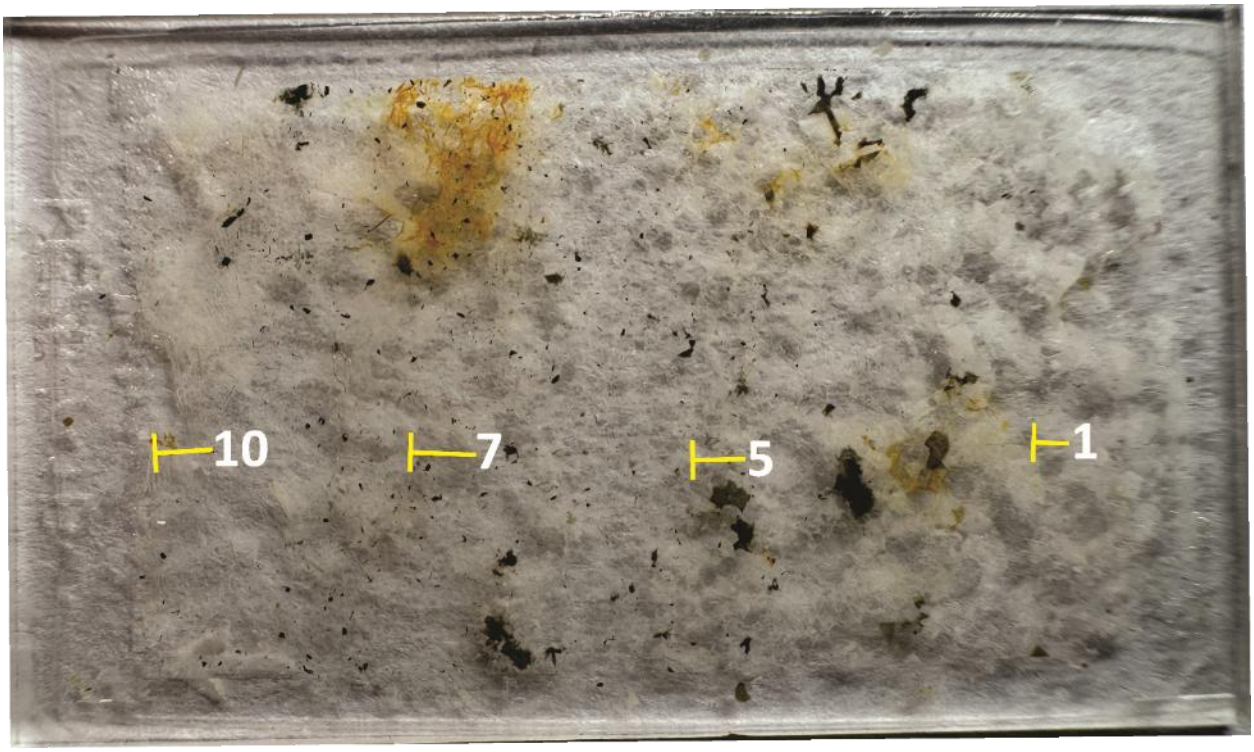
Appendix Figure 125: Concentrations (ppm) versus transect length. Sample LE25-7-1A.7 is a quartz transect from pegmatite LE25-7.



Appendix Figure 126: Concentrations (ppm) versus transect length. Sample LE25-7-1A.10 is a quartz transect from pegmatite LE25-7.



Appendix Figure 127: Concentrations (ppm) versus transect length. Sample LE25-7-1A.11 is a quartz transect from pegmatite LE25-7.



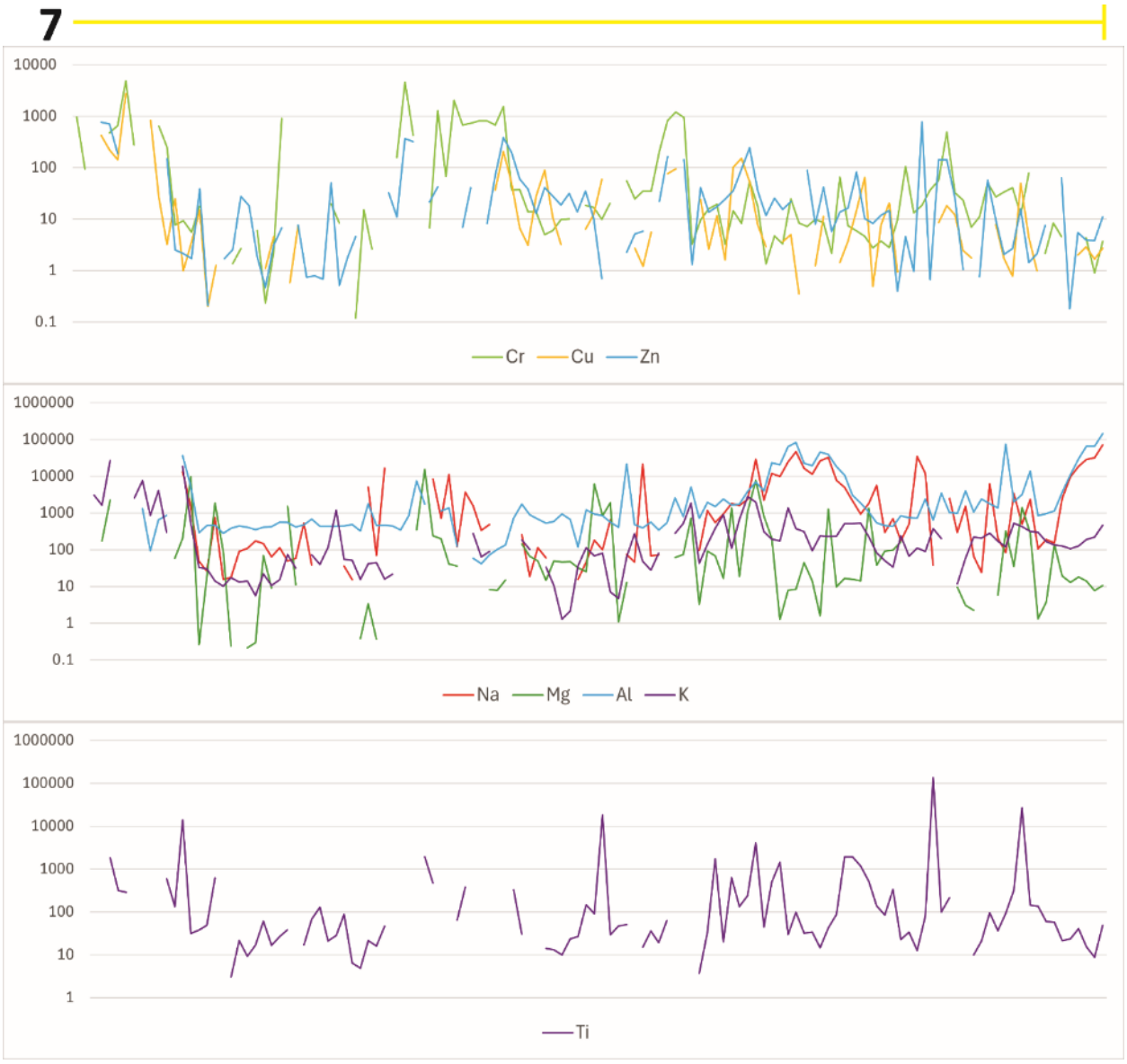
Appendix Figure 128: Sample LE25-7-1B, 100 micron double polished thick section of pegmatite transition zone proximal to pegmatite LE25-7. The yellow (quartz transect) line labelled 2 corresponds to LA-ICP-MS transect line LE25-7-1B.



Appendix Figure 129: Concentrations (ppm) versus transect length. Sample LE25-7-1B.1 is a quartz transect from pegmatite LE25-7.



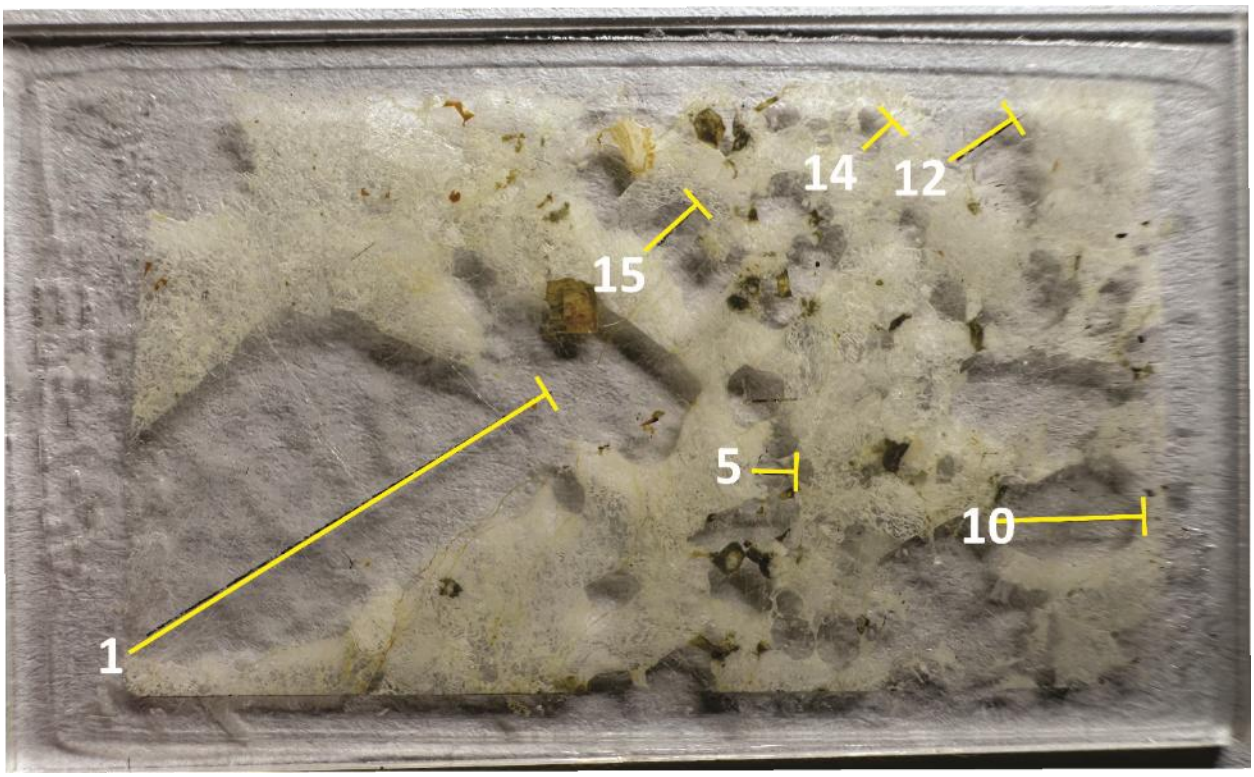
Appendix Figure 130: Concentrations (ppm) versus transect length. Sample LE25-7-1B.5 is a quartz transect from pegmatite LE25-7.



Appendix Figure 131: Concentrations (ppm) versus transect length. Sample LE25-7-1B.7 is a quartz transect from pegmatite LE25-7.



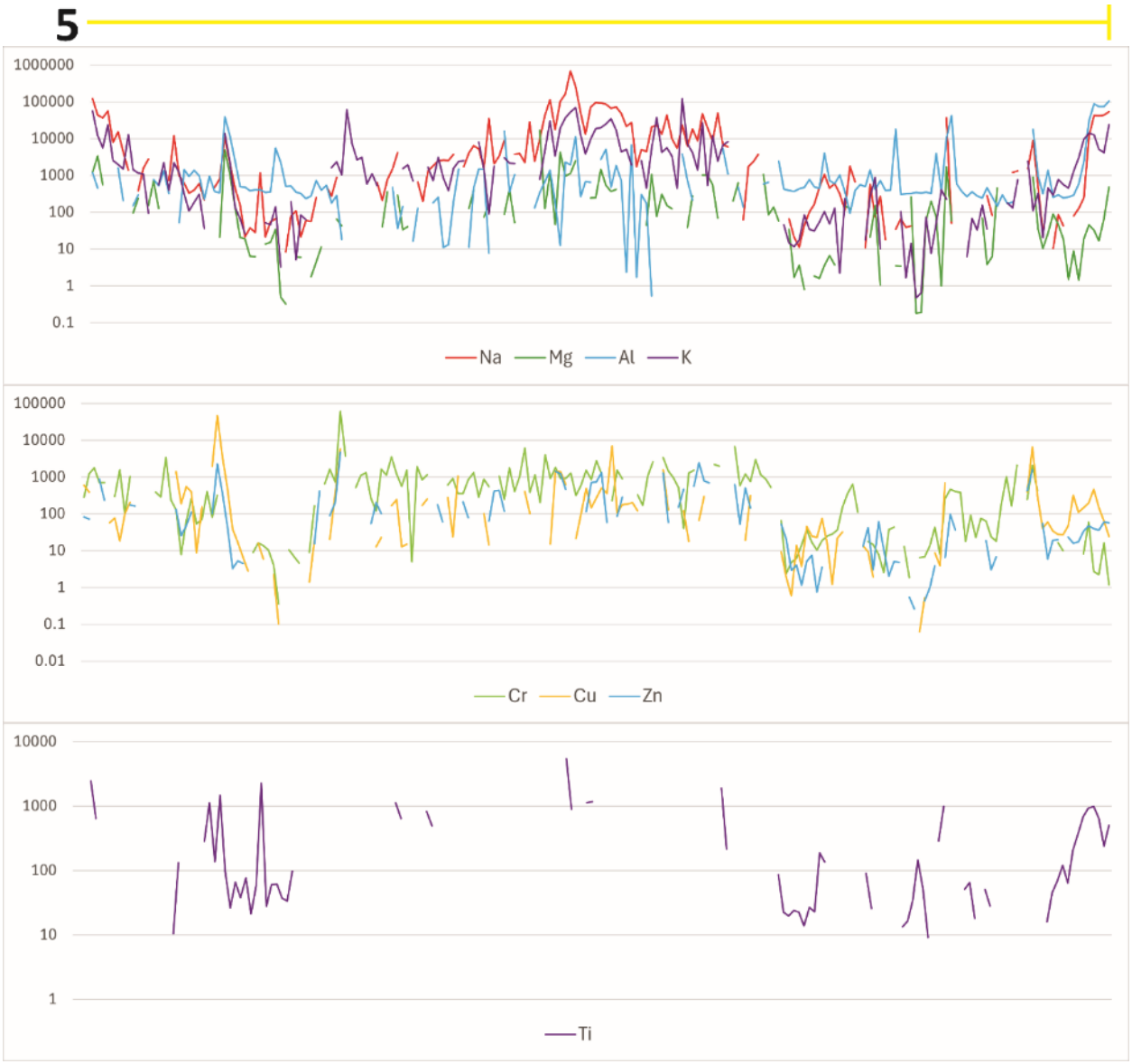
Appendix Figure 132: Concentrations (ppm) versus transect length. Sample LE25-7-1B.10 is a quartz transect from pegmatite LE25-7.



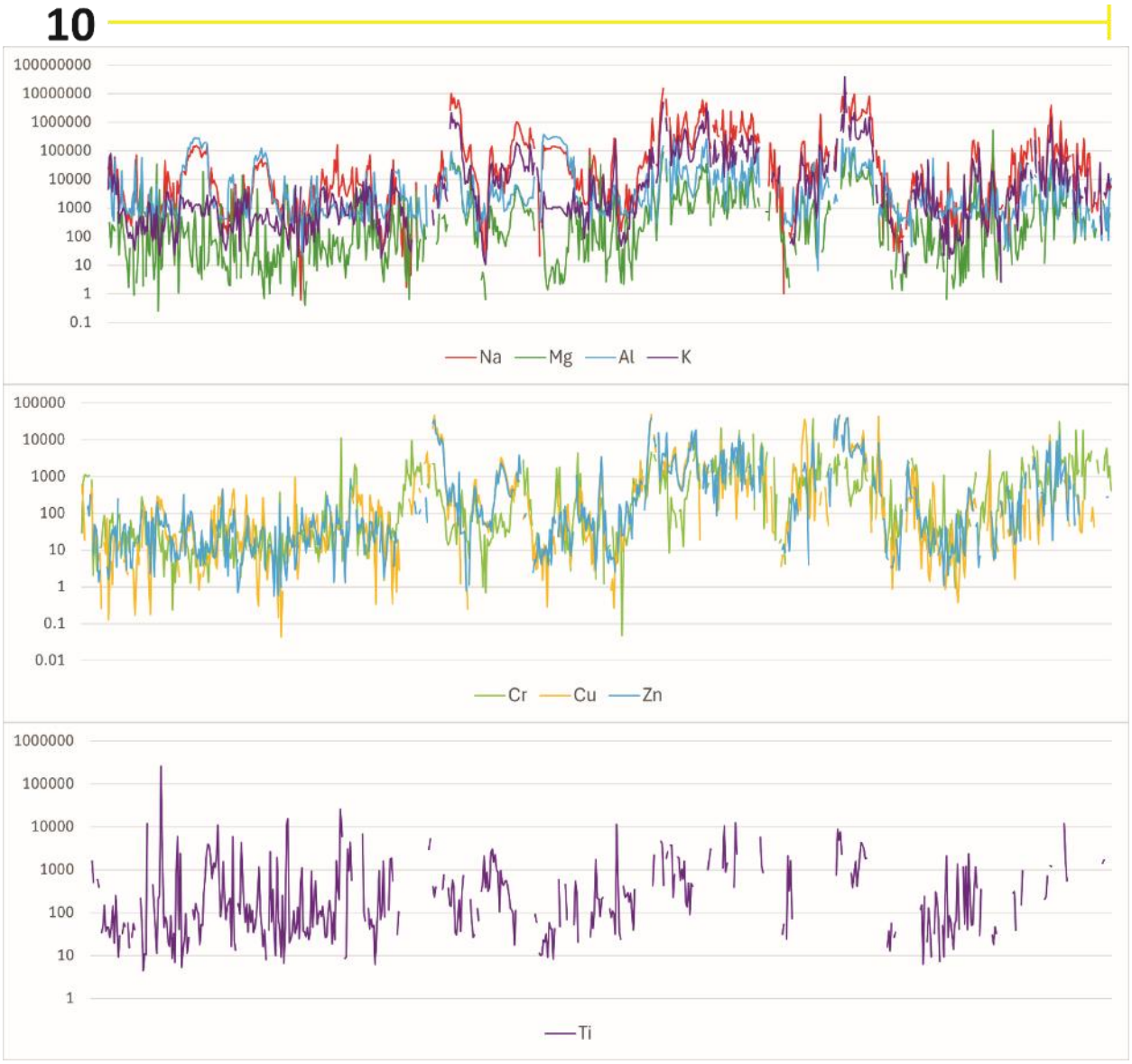
Appendix Figure 133: Sample LE25-7-2A, 100 micron double polished thick section of pegmatite LE25-7 core zone. The yellow (quartz transect) line labelled 1 corresponds to LA-ICP-MS transect line LE25-7-2A.1.



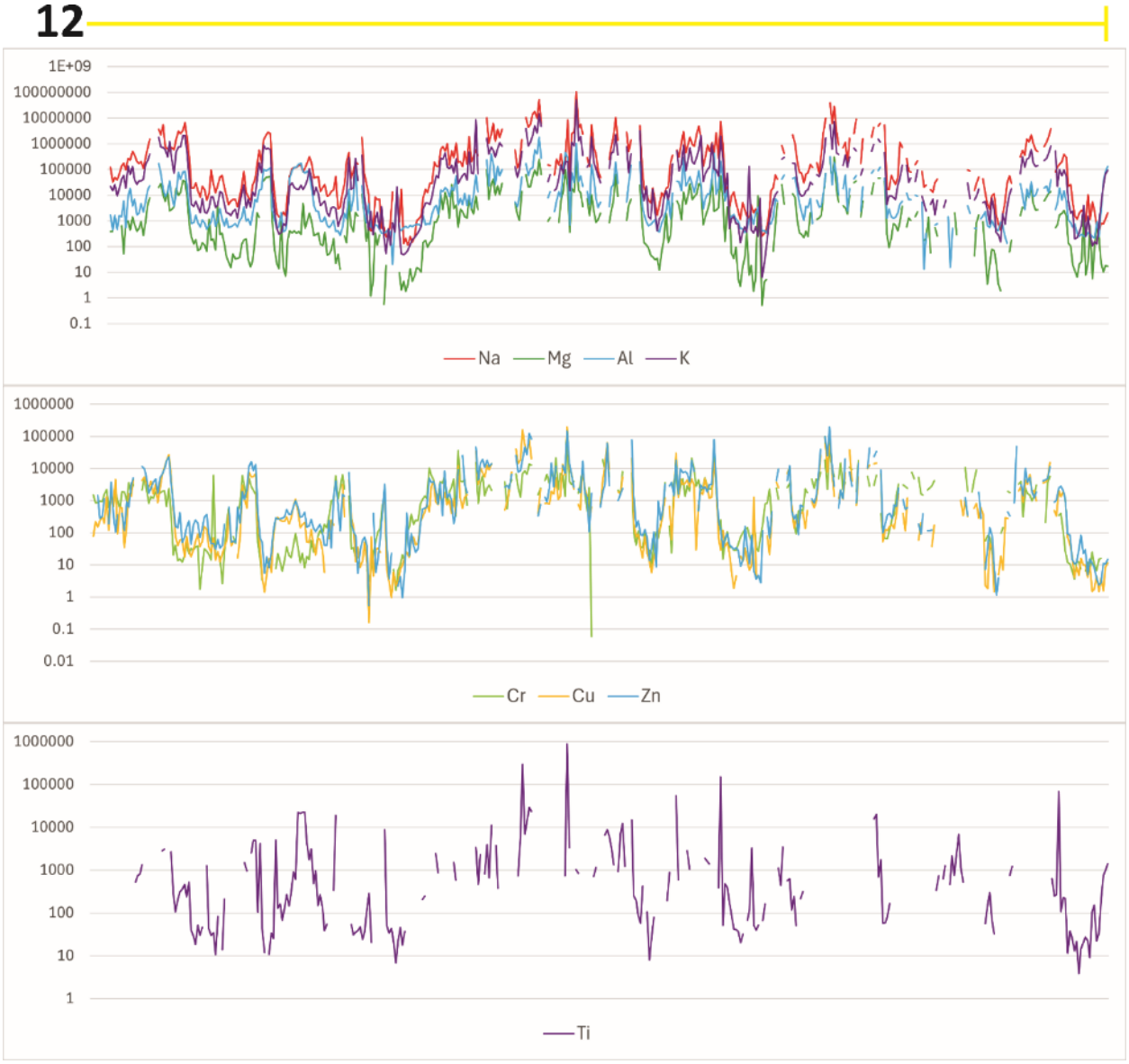
Appendix Figure 134: Concentrations (ppm) versus transect length. Sample LE25-7-2A.1 is a quartz transect from pegmatite LE25-7.



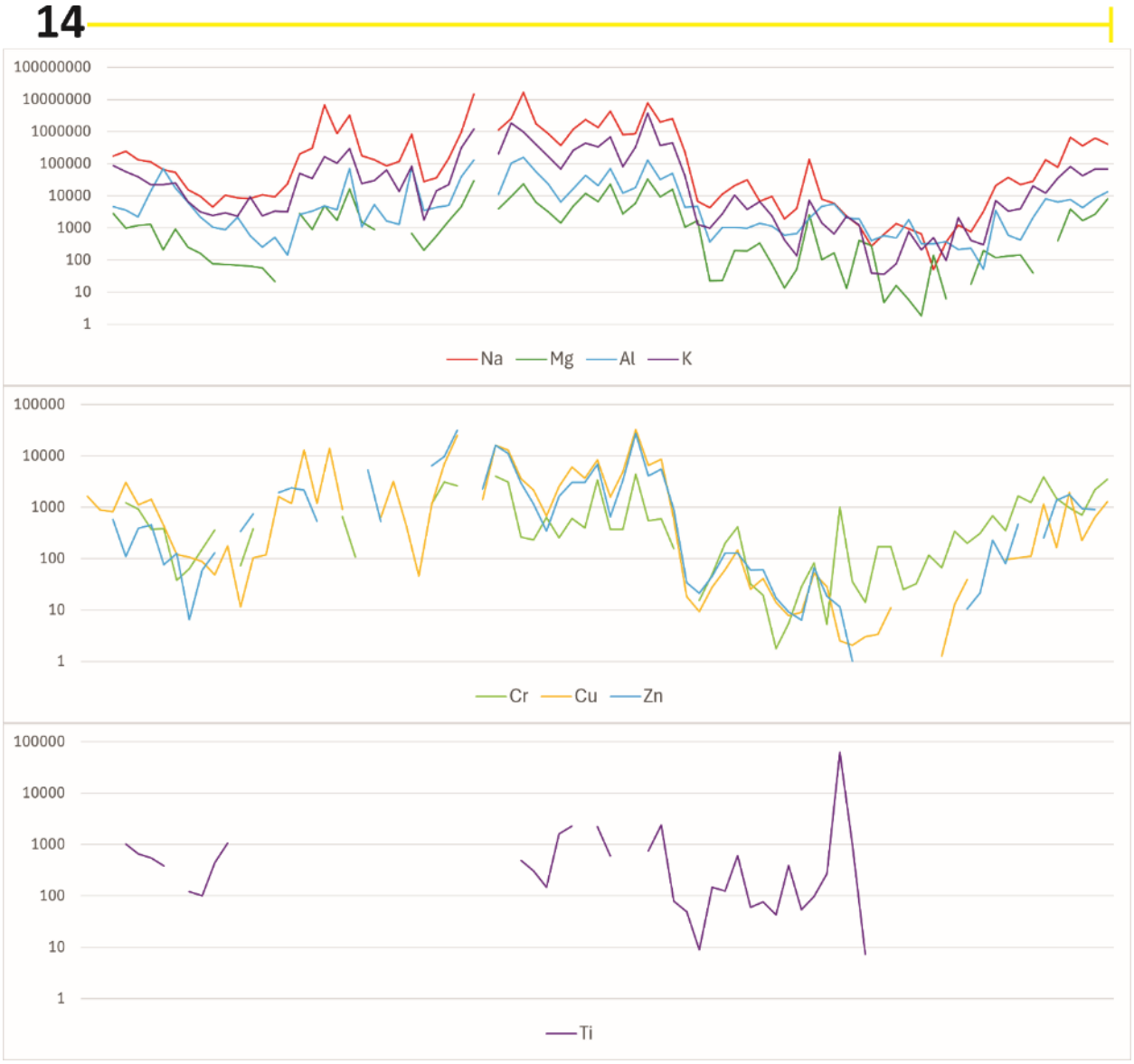
Appendix Figure 135: Concentrations (ppm) versus transect length. Sample LE25-7-2A.5 is a quartz transect from pegmatite LE25-7.



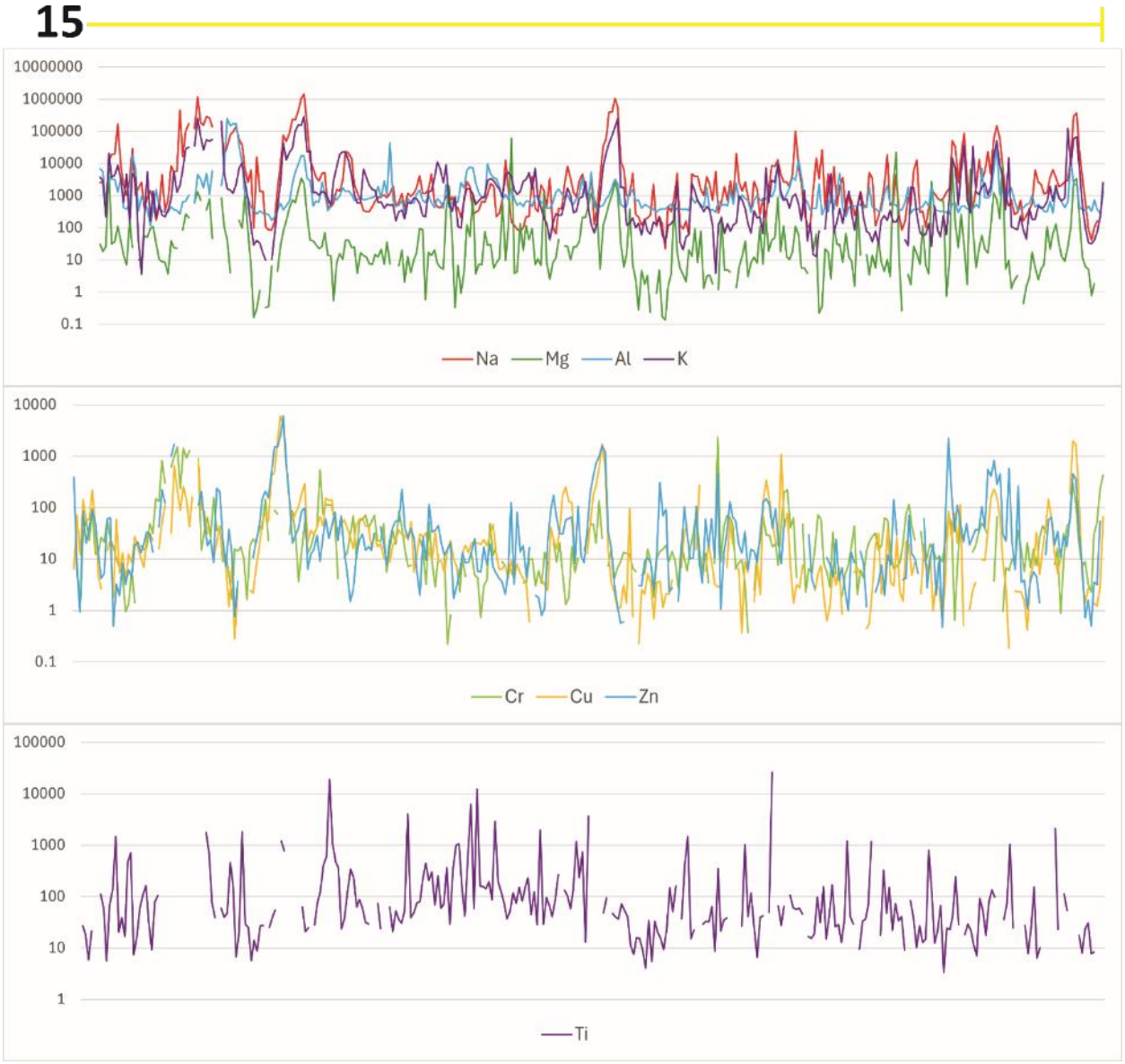
Appendix Figure 136: Concentrations (ppm) versus transect length. Sample LE25-7-2A.10 is a quartz transect from pegmatite LE25-7.



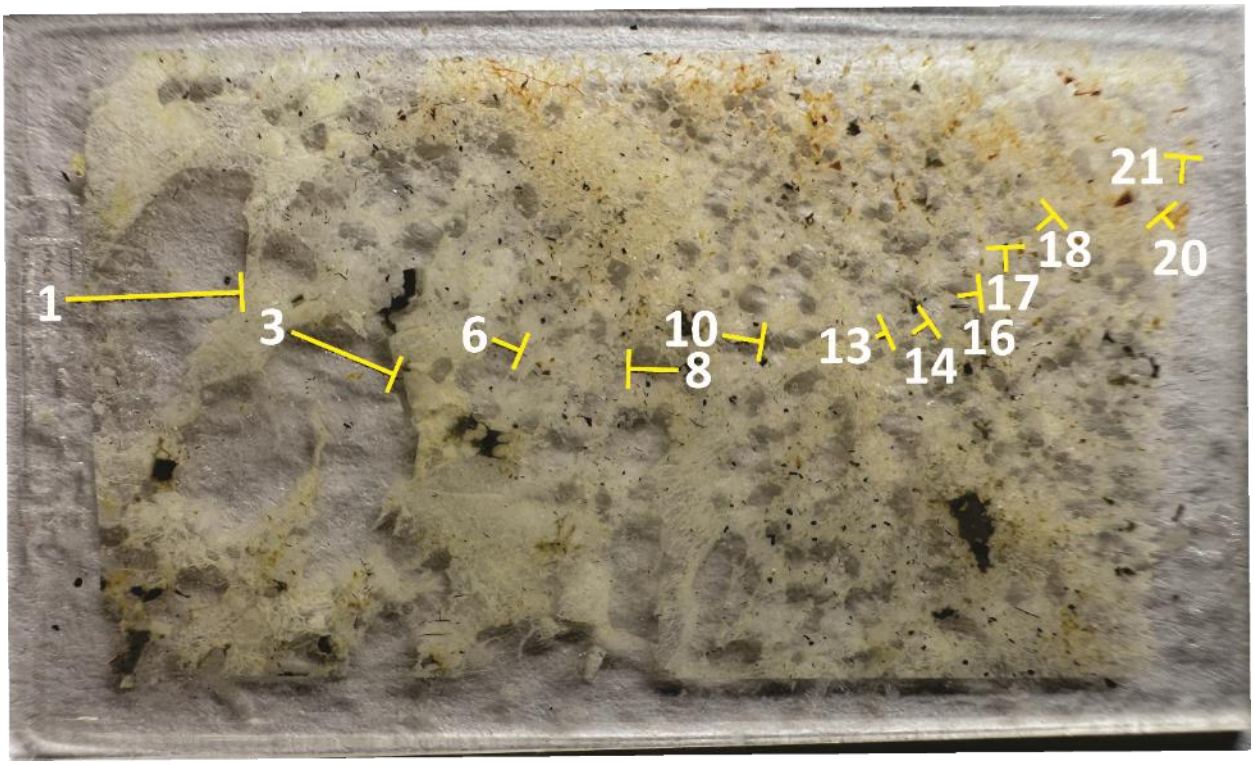
Appendix Figure 137: Concentrations (ppm) versus transect length. Sample LE25-7-2A.12 is a quartz transect from pegmatite LE25-7.



Appendix Figure 138: Concentrations (ppm) versus transect length. Sample LE25-7-2A.14 is a quartz transect from pegmatite LE25-7.



Appendix Figure 139: Concentrations (ppm) versus transect length. Sample LE25-7-2A.15 is a quartz transect from pegmatite LE25-7.



Appendix Figure 140: Sample LE25-7-2B, 100 micron double polished thick section of pegmatite transition zone proximal to pegmatite LE25-7. The yellow (quartz transect) line labelled 3 corresponds to LA-ICP-MS transect line LE25-7-2B.3.



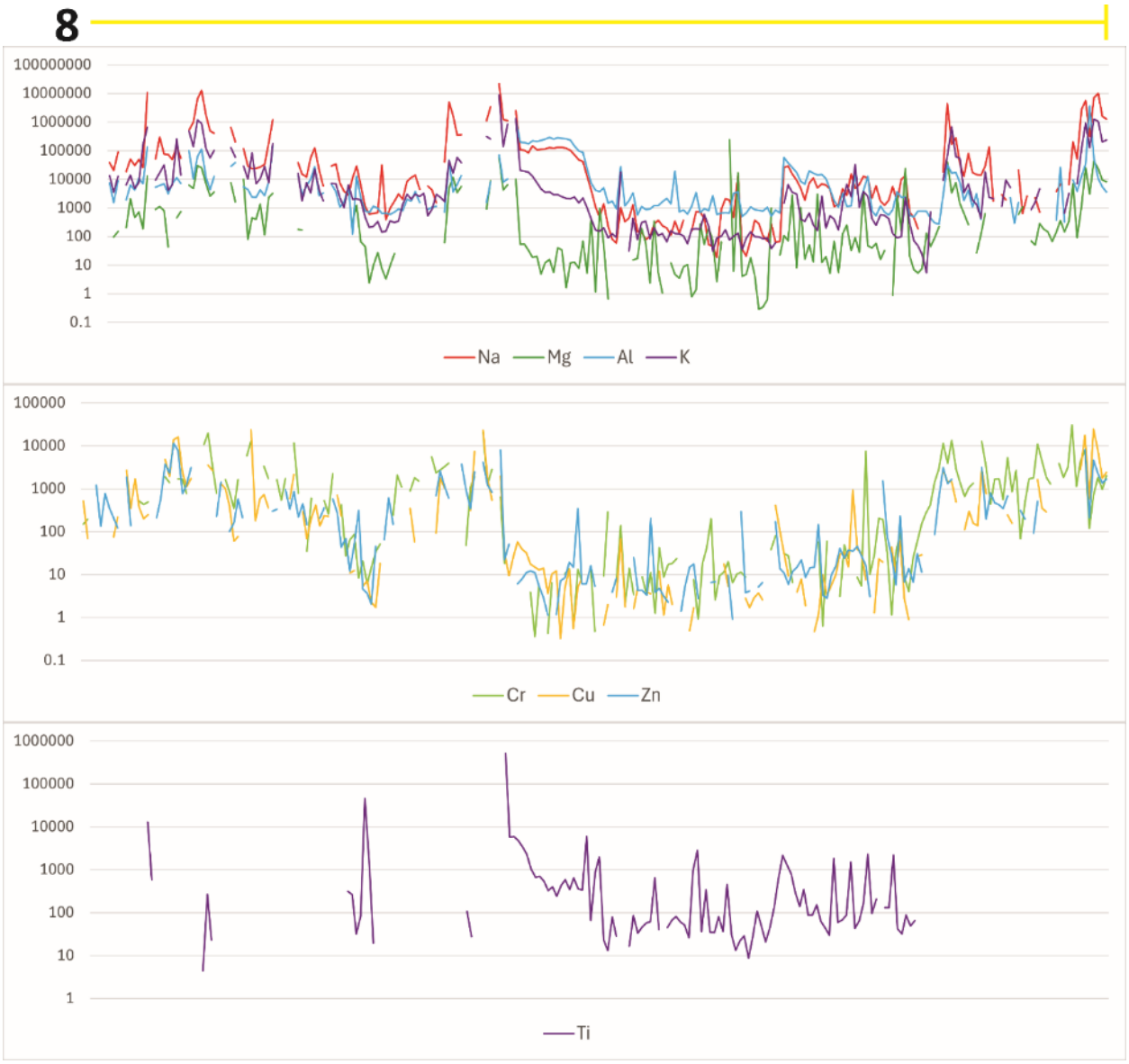
Appendix Figure 141: Concentrations (ppm) versus transect length. Sample LE25-7-2B.1 is a quartz transect from pegmatite LE25-7.



Appendix Figure 142: Concentrations (ppm) versus transect length. Sample LE25-7-2B.3 is a quartz transect from pegmatite LE25-7.



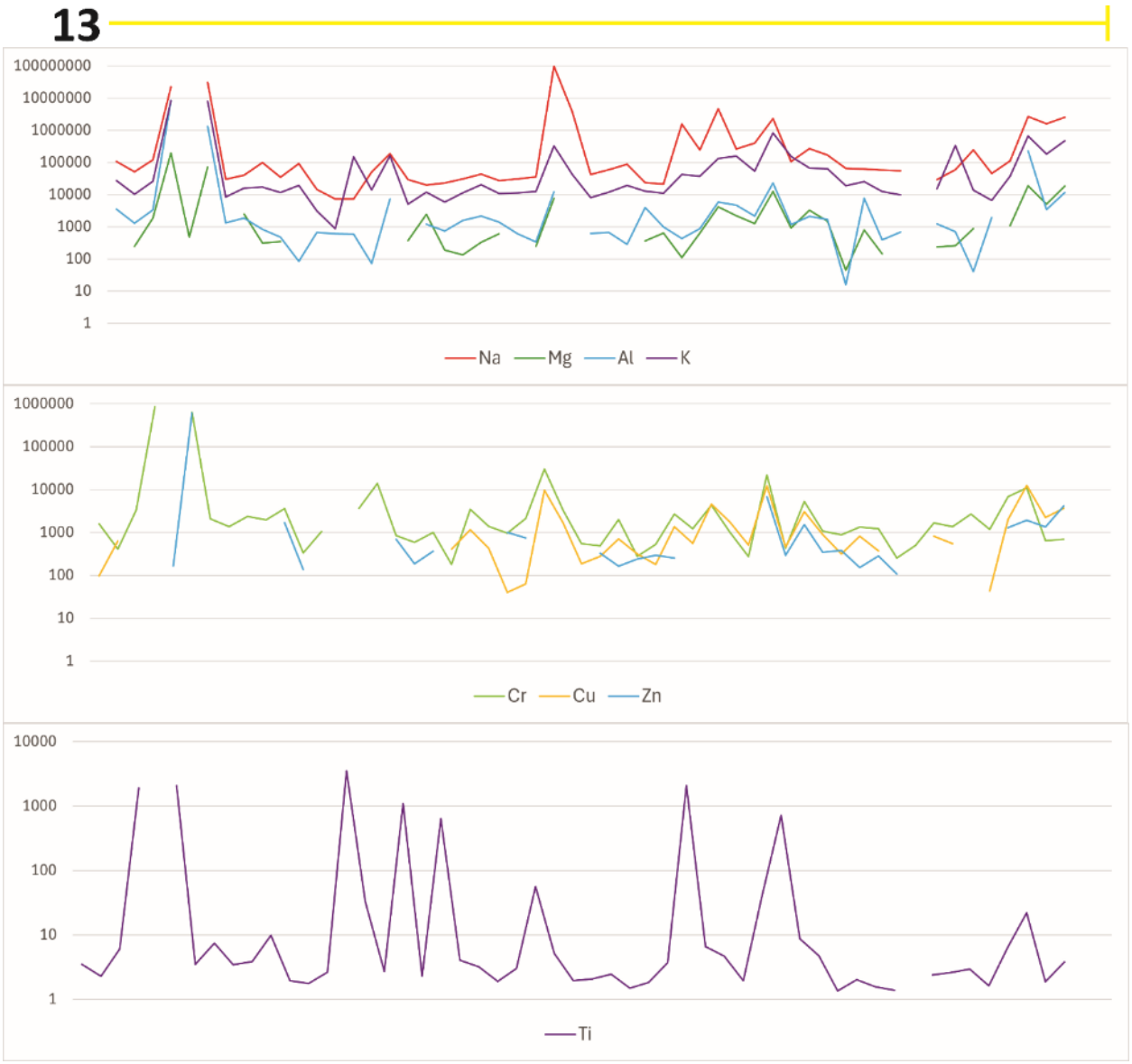
Appendix Figure 143: Concentrations (ppm) versus transect length. Sample LE25-7-2B.6 is a quartz transect from pegmatite LE25-7.



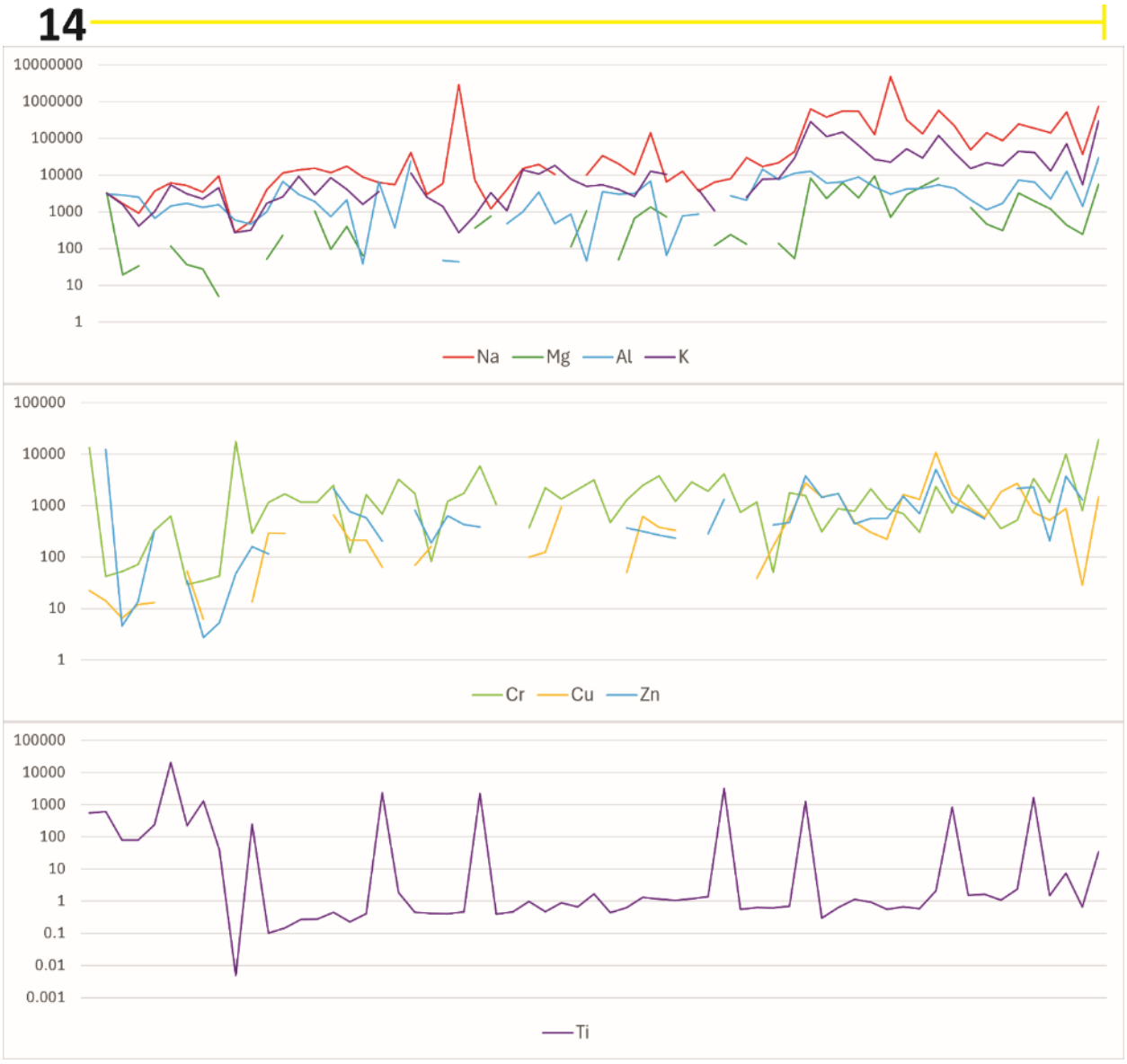
Appendix Figure 144: Concentrations (ppm) versus transect length. Sample LE25-7-2B.8 is a quartz transect from pegmatite LE25-7.



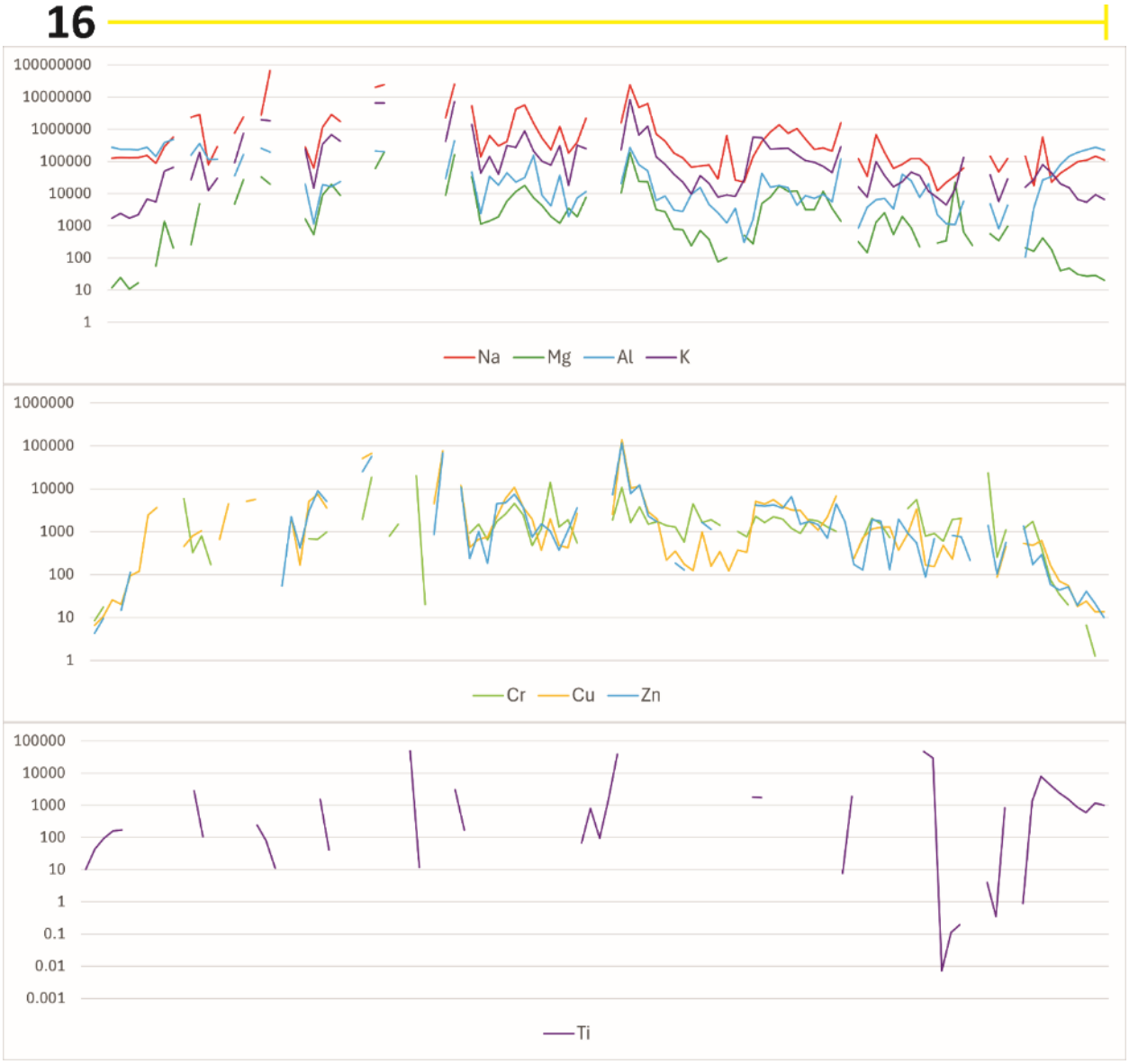
Appendix Figure 145: Concentrations (ppm) versus transect length. Sample LE25-7-2B.10 is a quartz transect from pegmatite LE25-7.



Appendix Figure 146: Concentrations (ppm) versus transect length. Sample LE25-7-2B.13 is a quartz transect from pegmatite LE25-7.



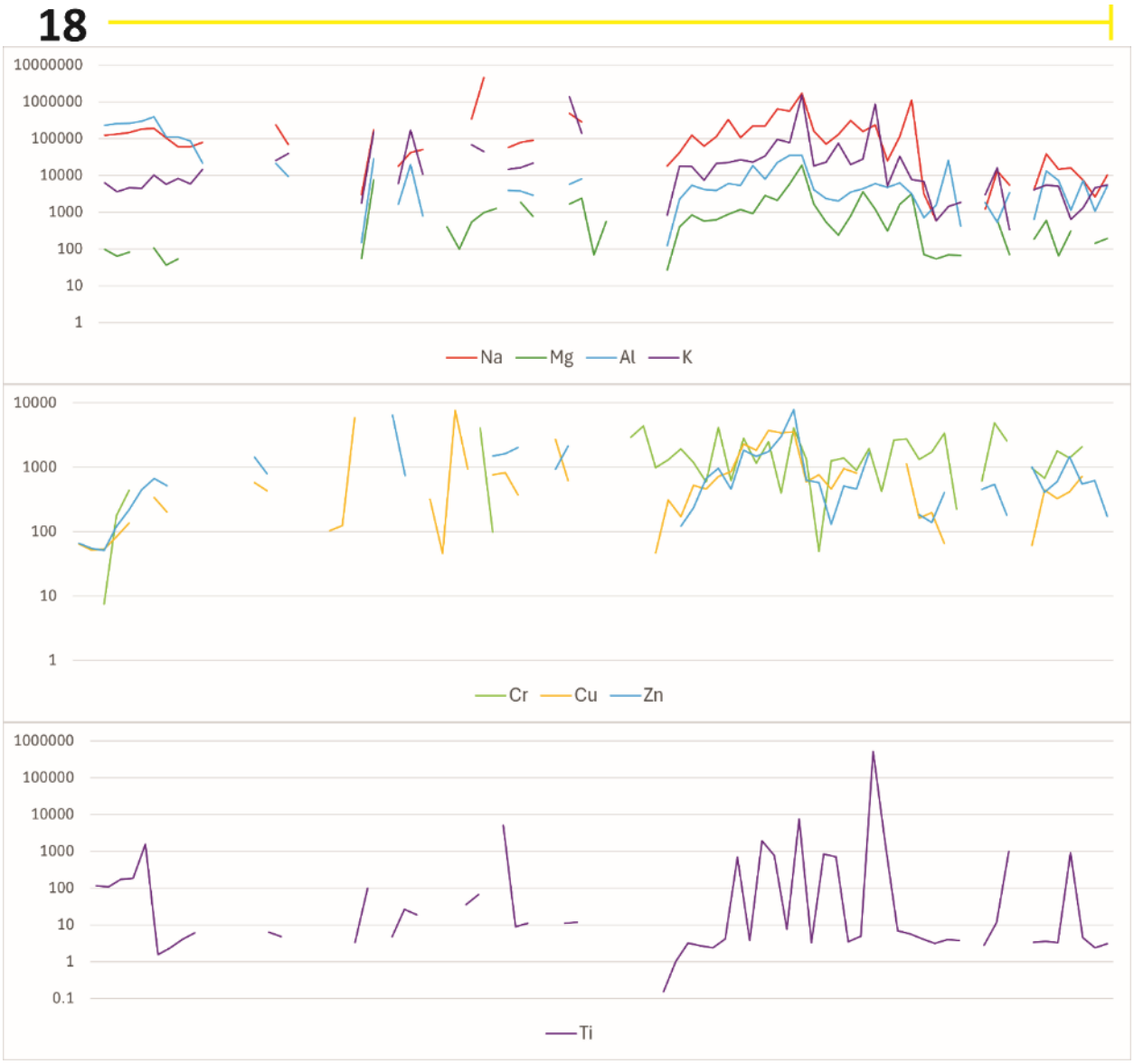
Appendix Figure 147: Concentrations (ppm) versus transect length. Sample LE25-7-2B.14 is a quartz transect from pegmatite LE25-7.



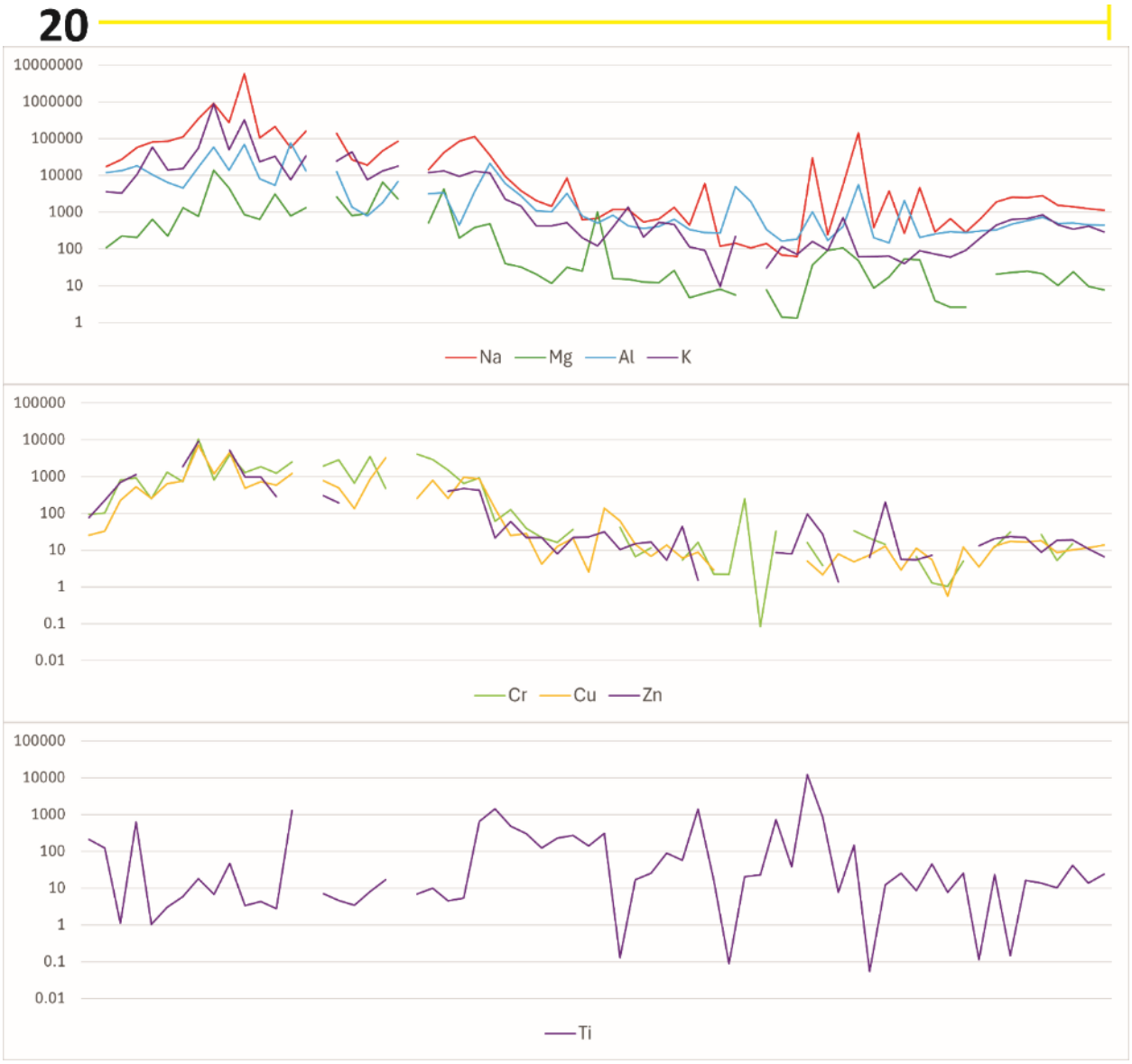
Appendix Figure 148: Concentrations (ppm) versus transect length. Sample LE25-7-2B.16 is a quartz transect from pegmatite LE25-7.



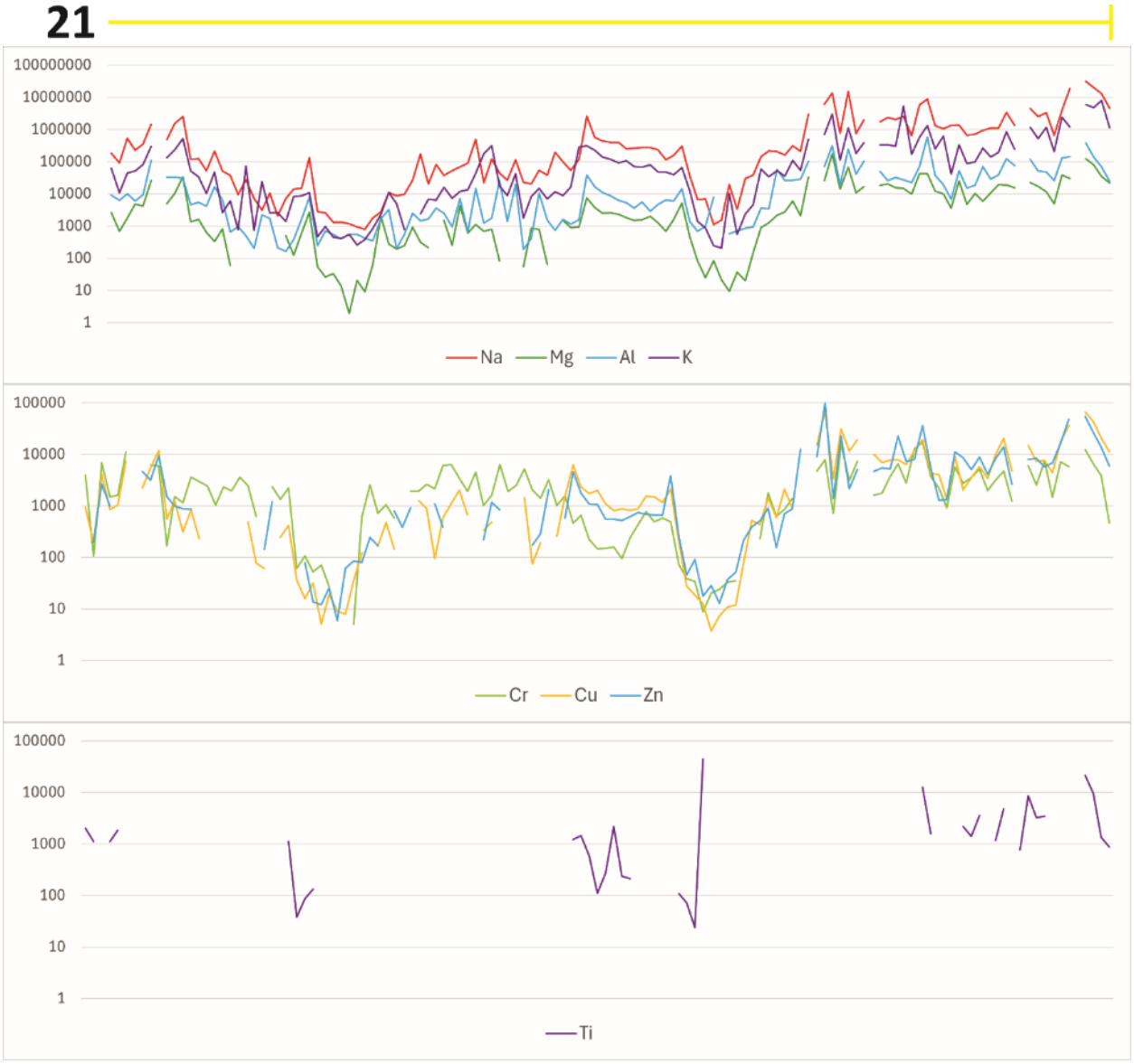
Appendix Figure 149: Concentrations (ppm) versus transect length. Sample LE25-7-2B.17 is a quartz transect from pegmatite LE25-7.



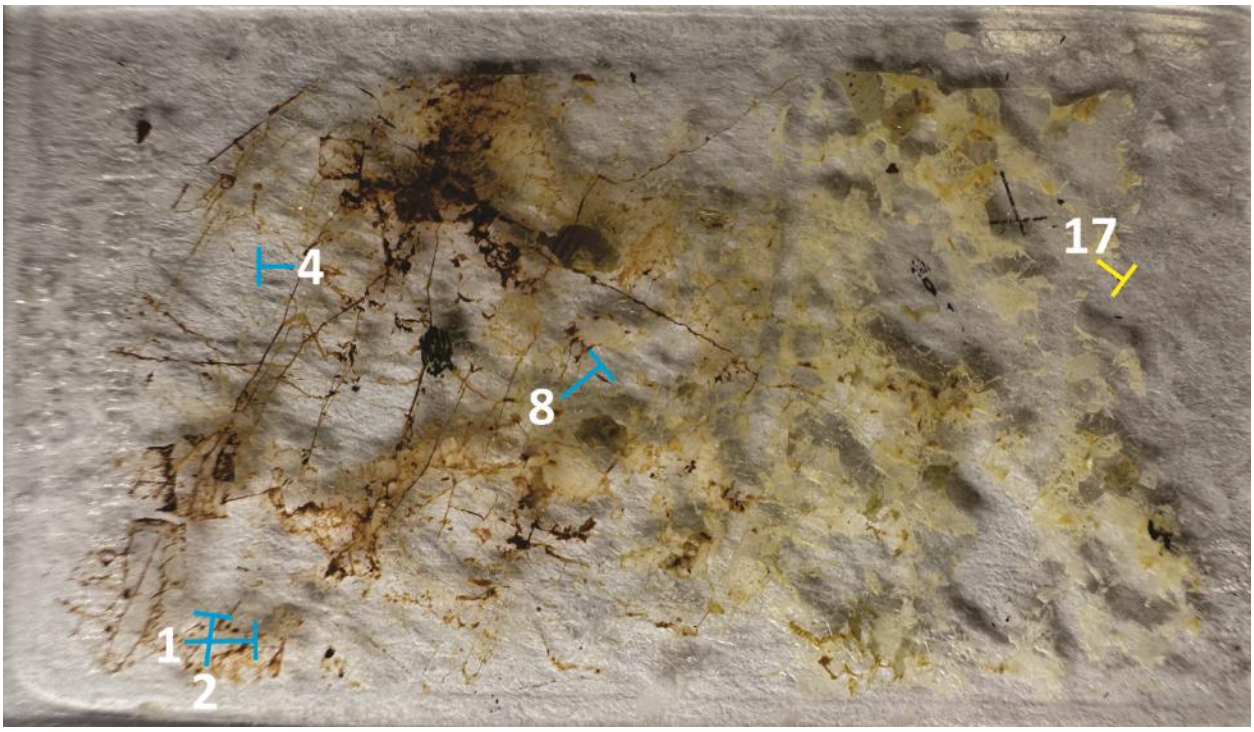
Appendix Figure 150: Concentrations (ppm) versus transect length. Sample LE25-7-2B.18 is a quartz transect from pegmatite LE25-7.



Appendix Figure 151: Concentrations (ppm) versus transect length. Sample LE25-7-2B.20 is a quartz transect from pegmatite LE25-7.



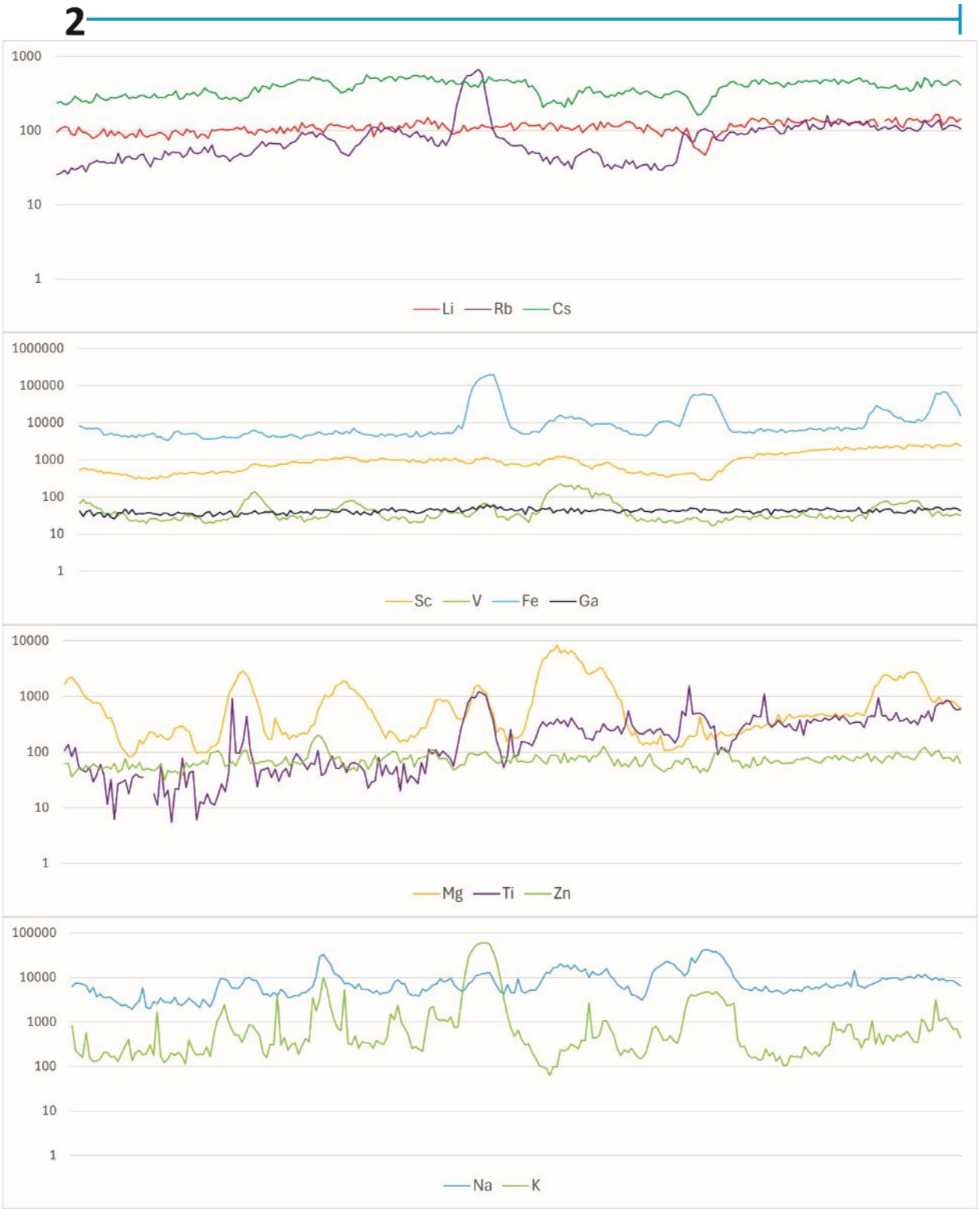
Appendix Figure 152: Concentrations (ppm) versus transect length. Sample LE25-7-2B.21 is a quartz transect from pegmatite LE25-7.



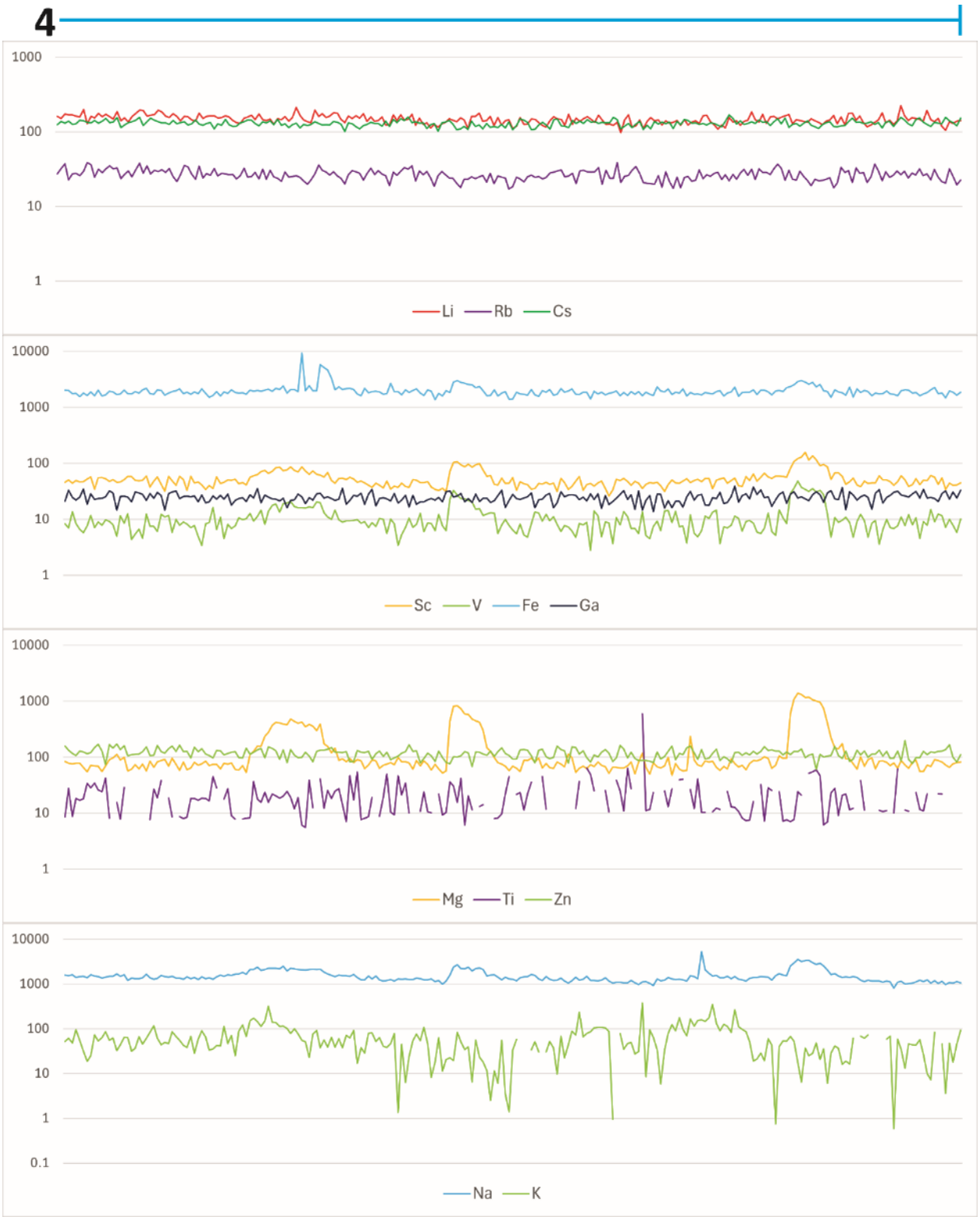
Appendix Figure 153: Sample LE25-8-1, 100 micron double polished thick section of a pegmatite core zone LE25-8. Blue (beryl transect) and yellow (quartz transect) lines and numbers correspond to LA-ICP-MS transect lines (e.g., LE25-8-1.1 is the blue line labelled 1).



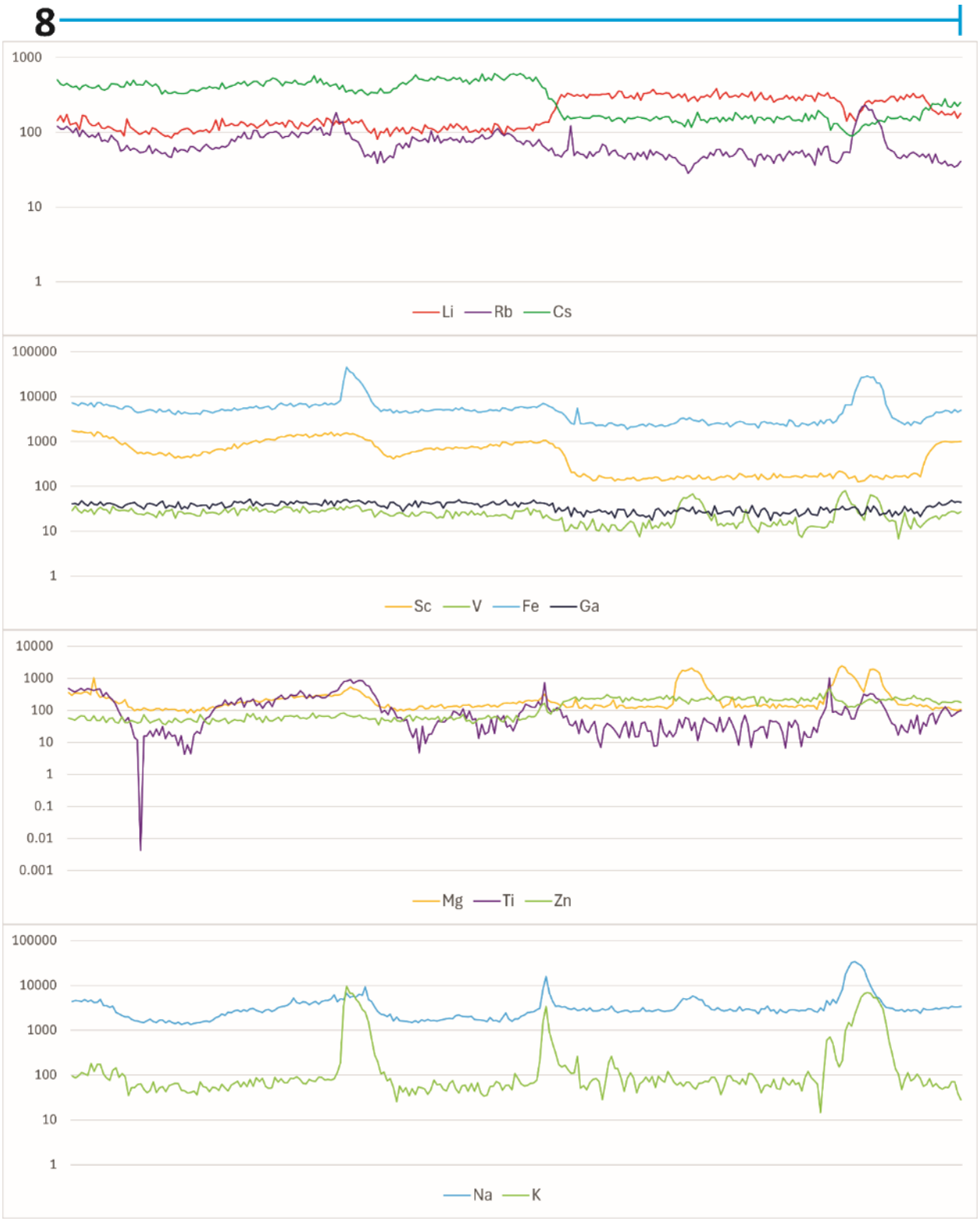
Appendix Figure 154: Concentrations (ppm) versus transect length. Sample LE25-8-1.1 is a beryl transect from pegmatite LE25-8.



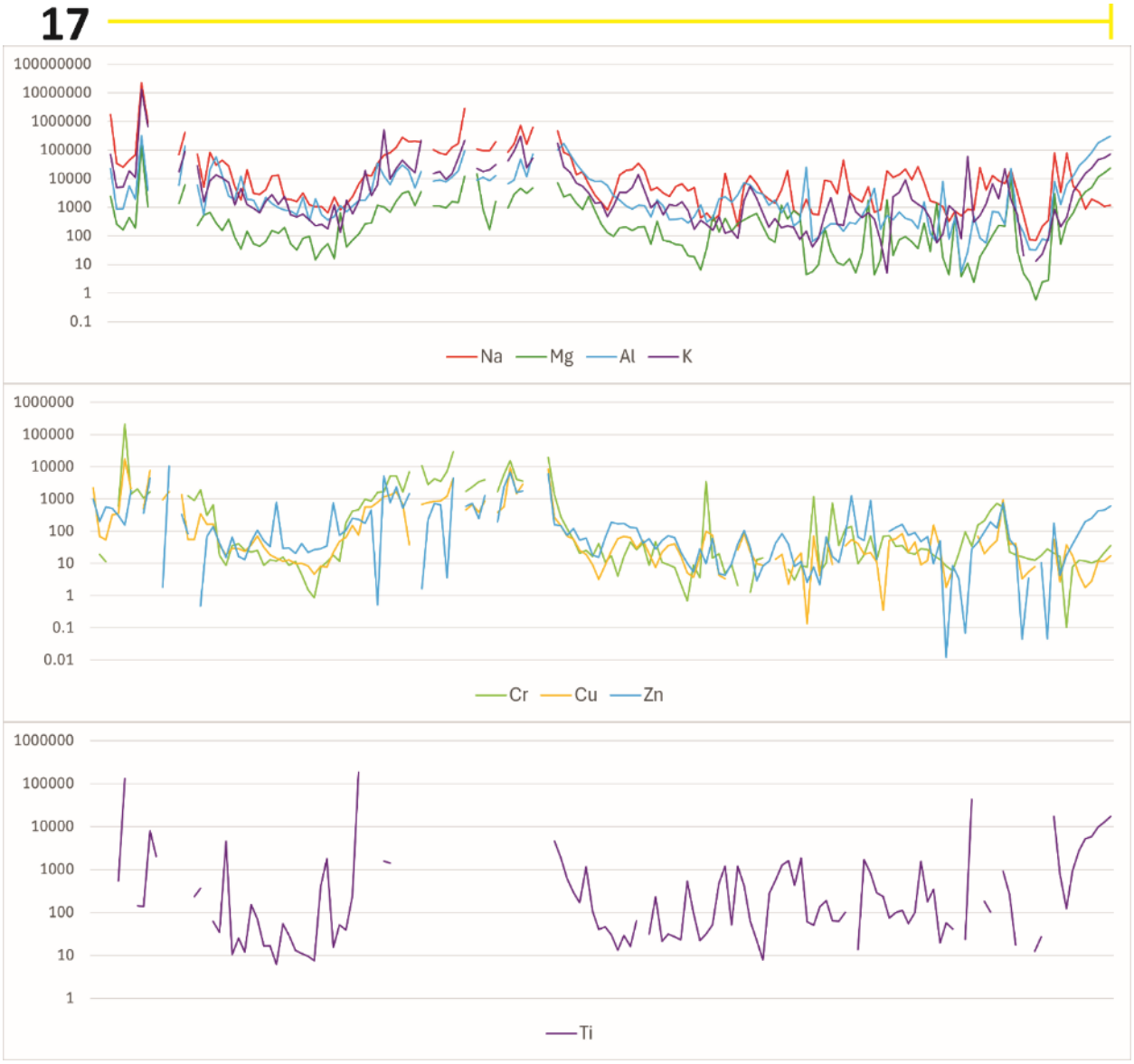
Appendix Figure 155: Concentrations (ppm) versus transect length. Sample LE25-8-1.2 is a beryl transect from pegmatite LE25-8.



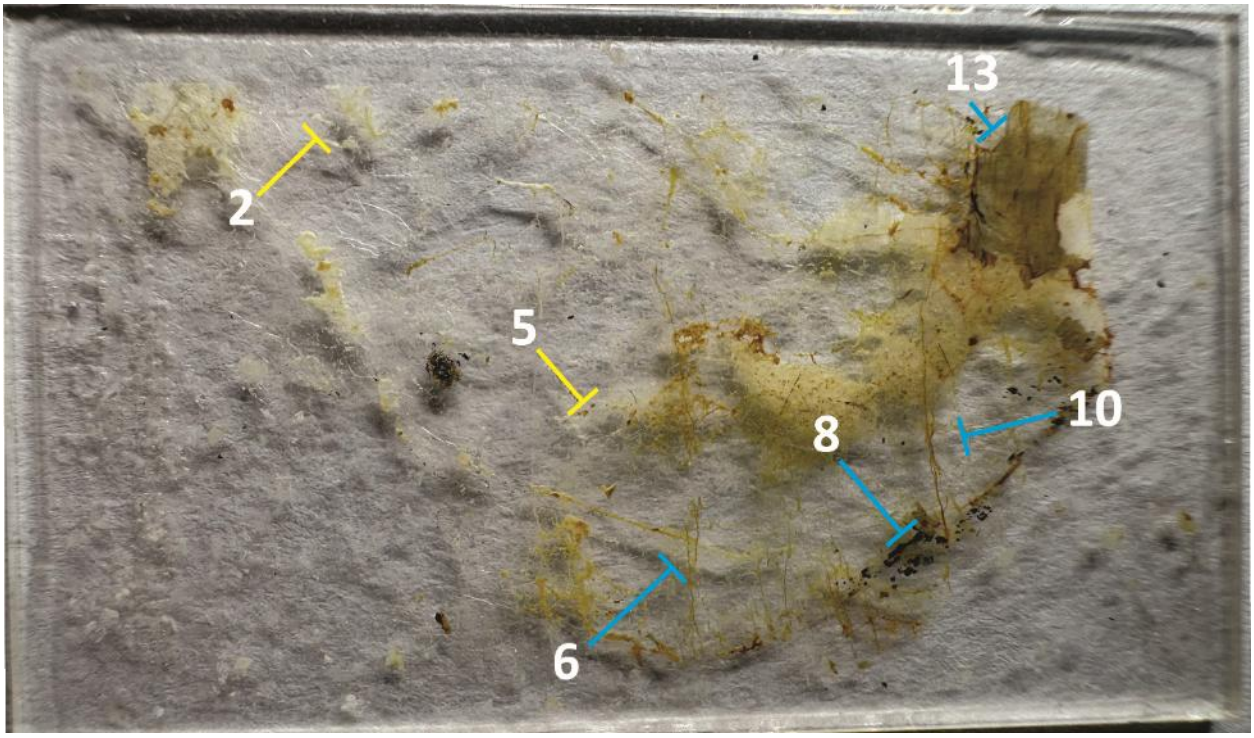
Appendix Figure 156: Concentrations (ppm) versus transect length. Sample LE25-8-1.4 is a beryl transect from pegmatite LE25-8.



Appendix Figure 157: Concentrations (ppm) versus transect length. Sample LE25-8-1.8 is a beryl transect from pegmatite LE25-8.



Appendix Figure 158: Concentrations (ppm) versus transect length. Sample LE25-8-1.17 is a quartz transect from pegmatite LE25-8.



Appendix Figure 159: Sample LE25-8-2, 100 micron double polished thick section of a pegmatite core zone. Blue (beryl transect) and yellow (quartz transect) lines and numbers correspond to LA-ICP-MS transect lines (e.g., LE25-8-2.6 is the blue line labelled 6).



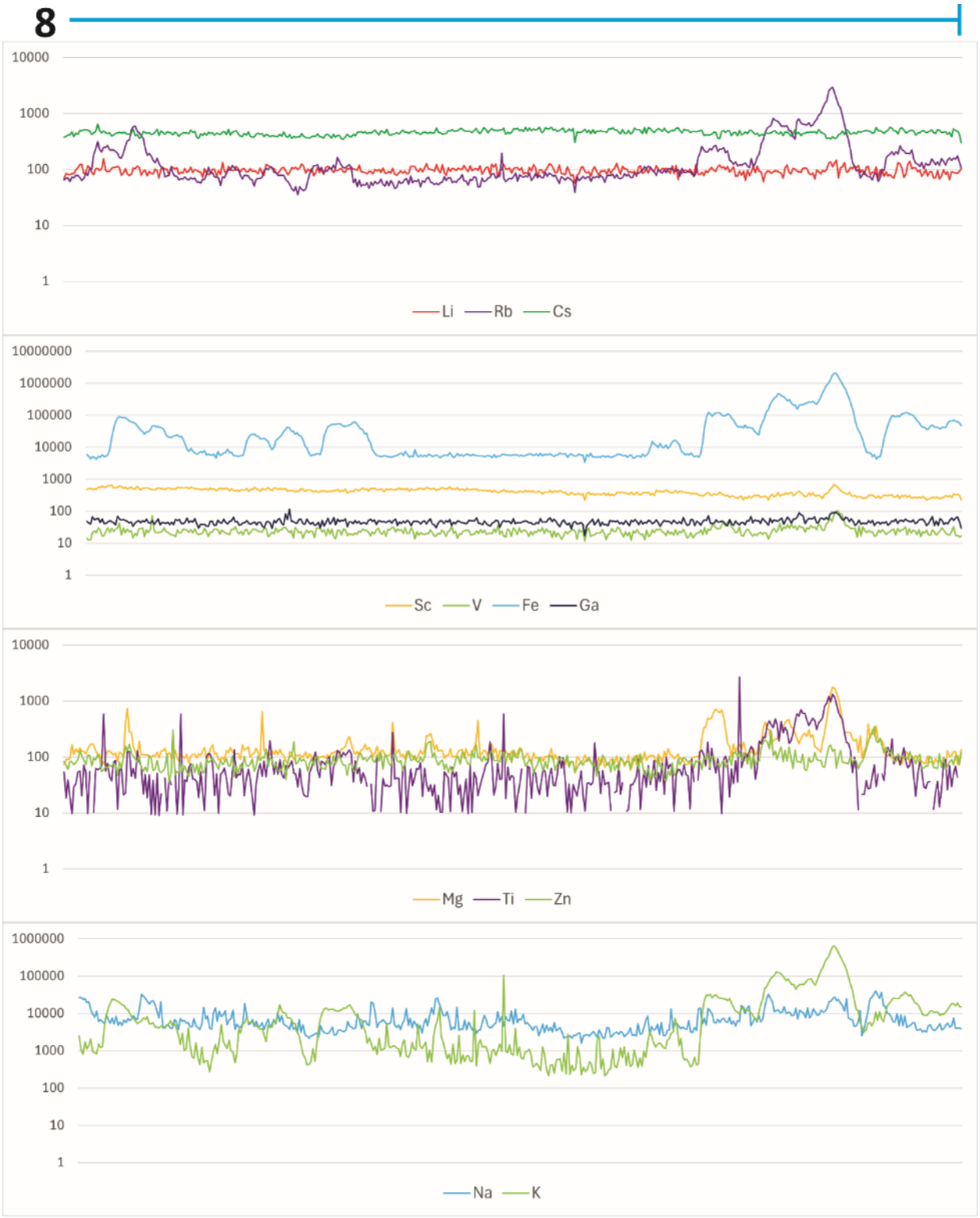
Appendix Figure 160: Concentrations (ppm) versus transect length. Sample LE25-8-2.2 is a quartz transect from pegmatite LE25-8.



Appendix Figure 161: Concentrations (ppm) versus transect length. Sample LE25-8-2.5 is a quartz transect from pegmatite LE25-8.



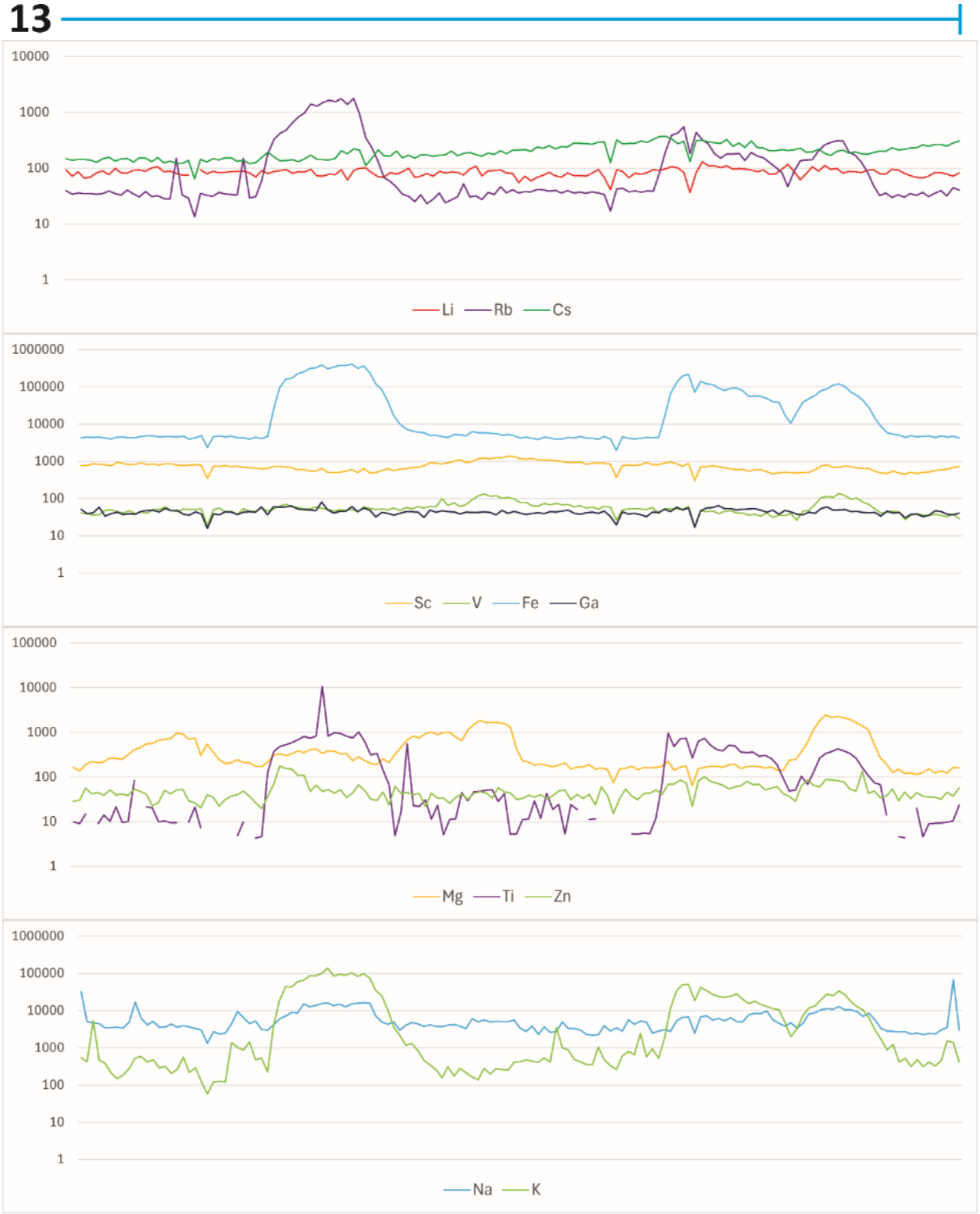
Appendix Figure 162: Concentrations (ppm) versus transect length. Sample LE25-8-2.6 is a beryl transect from pegmatite LE25-8.



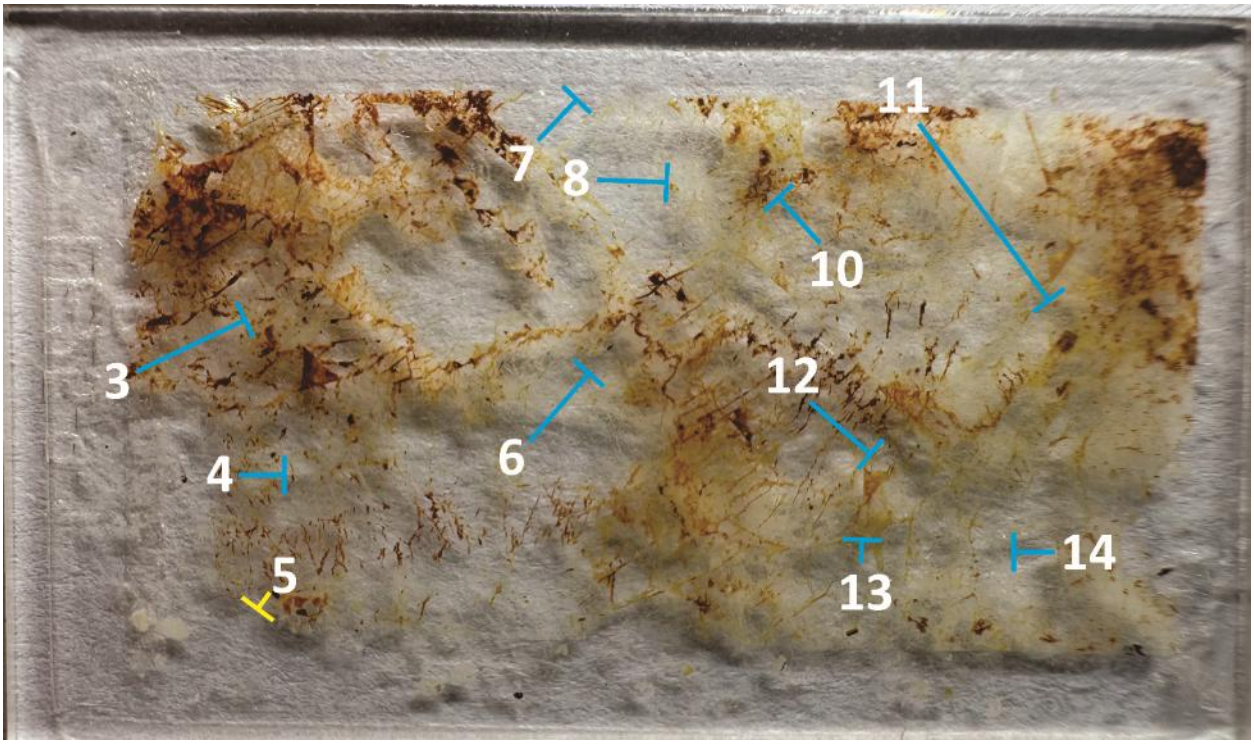
Appendix Figure 163: Concentrations (ppm) versus transect length. Sample LE25-8-2.8 is a beryl transect from pegmatite LE25-8.



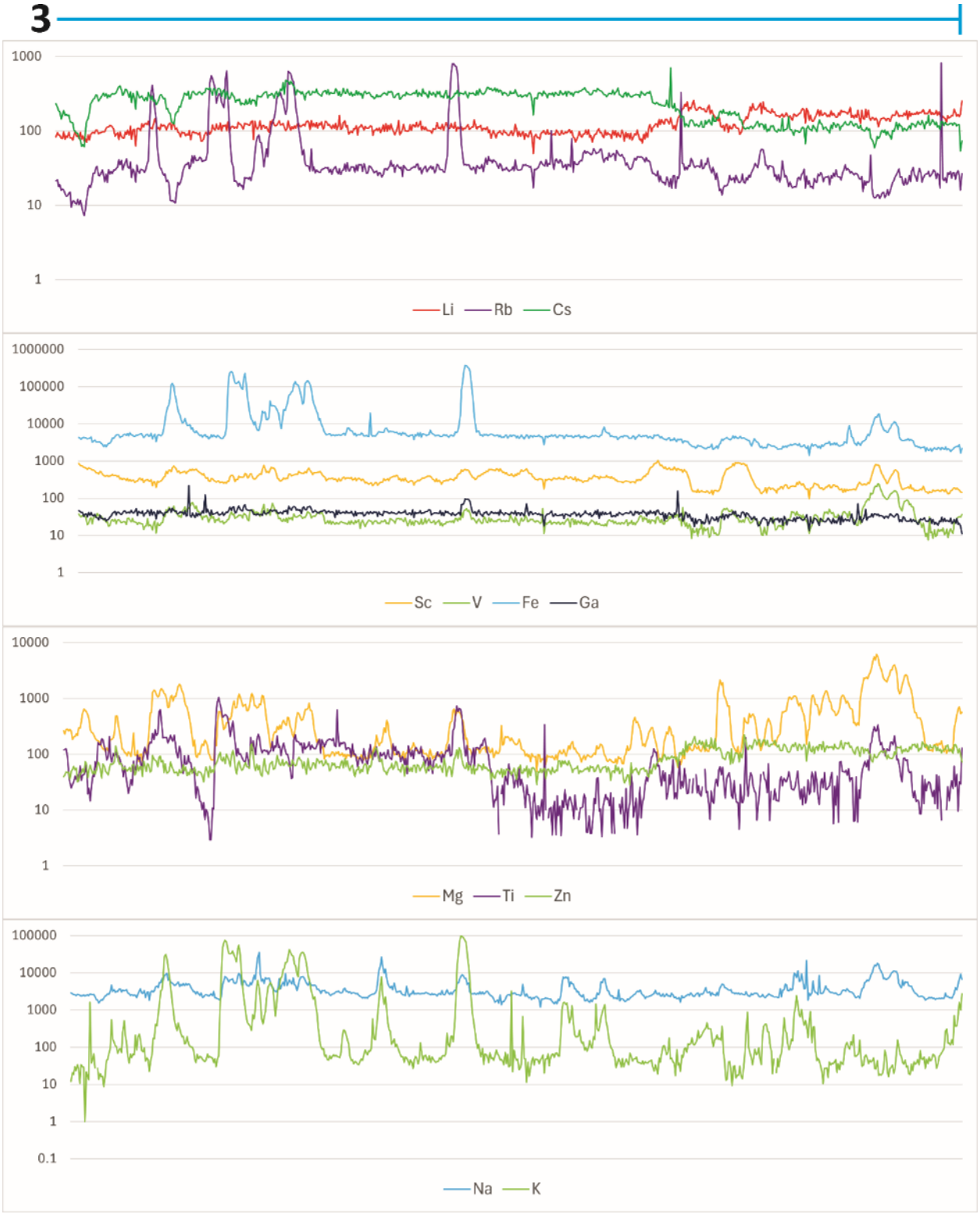
Appendix Figure 164: Concentrations (ppm) versus transect length. Sample LE25-8-2.10 is a beryl transect from pegmatite LE25-8.



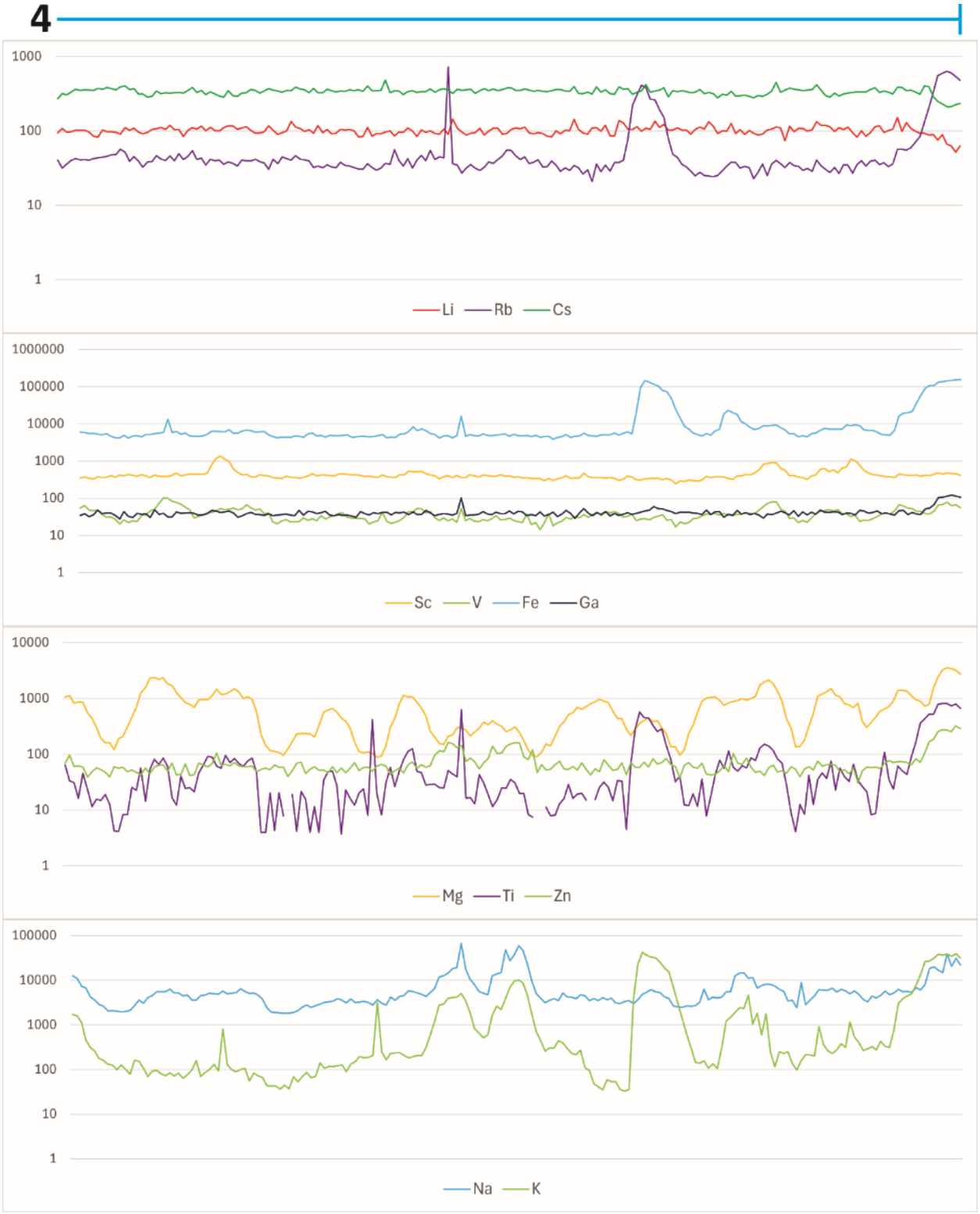
Appendix Figure 165: Concentrations (ppm) versus transect length. Sample LE25-8-2.13 is a beryl transect from pegmatite LE25-8.



Appendix Figure 166: Sample LE25-9-1, 100 micron double polished thick section of pegmatite LE25-9 core zone. Blue (beryl transect) and yellow (quartz transect) lines and numbers correspond to LA-ICP-MS transect lines (e.g., LE25-9-1.3 is the blue line labelled 3).



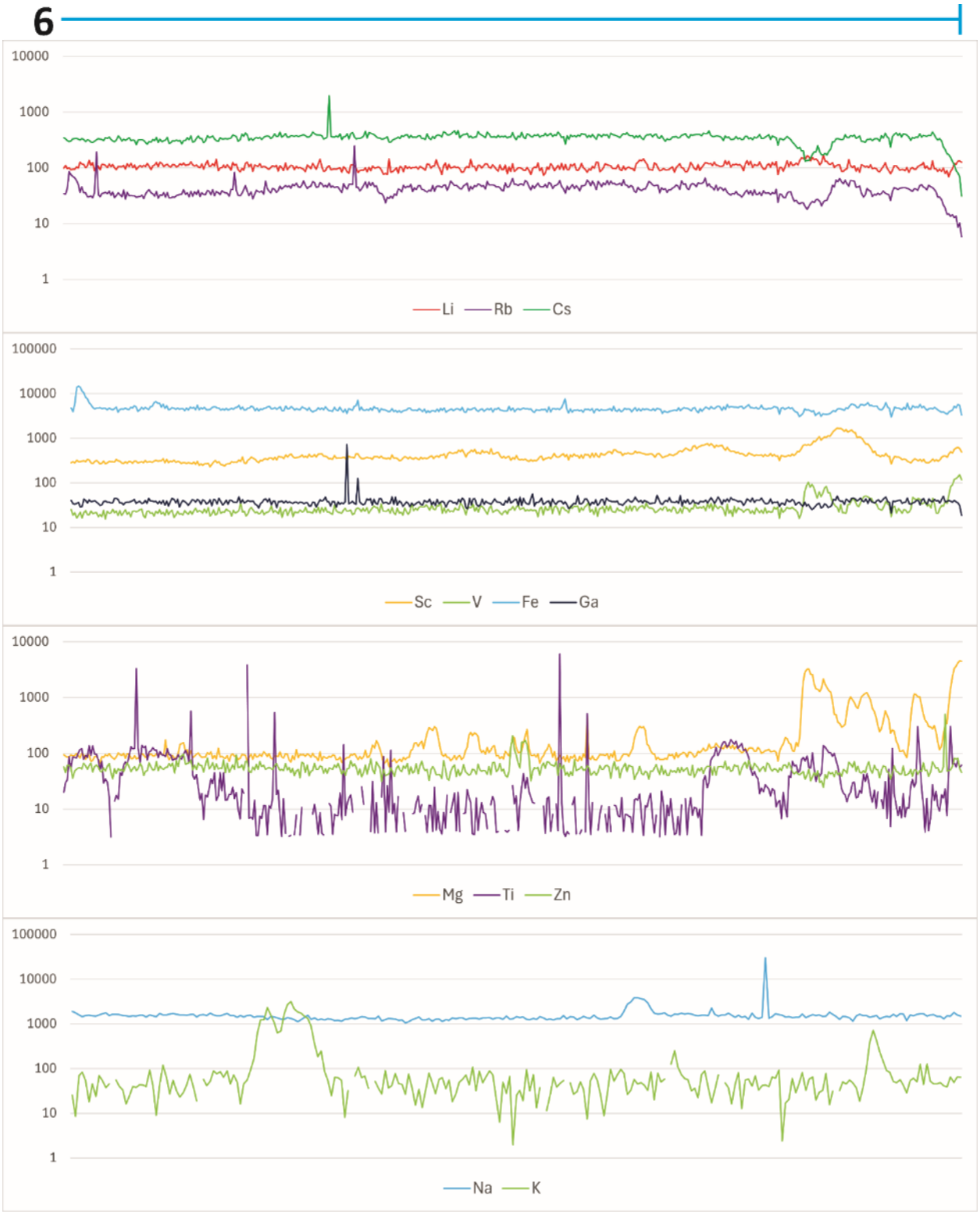
Appendix Figure 167: Concentrations (ppm) versus transect length. Sample LE25-9-1.3 is a beryl transect from pegmatite LE25-9.



Appendix Figure 168: Concentrations (ppm) versus transect length. Sample LE25-9-1.4 is a beryl transect from pegmatite LE25-9.



Appendix Figure 169: Concentrations (ppm) versus transect length. Sample LE25-9-1.5 is a quartz transect from pegmatite LE25-9.



Appendix Figure 170: Concentrations (ppm) versus transect length. Sample LE25-9-1.6 is a beryl transect from pegmatite LE25-9.



Appendix Figure 171: Concentrations (ppm) versus transect length. Sample LE25-9-1.7 is a beryl transect from pegmatite LE25-9.



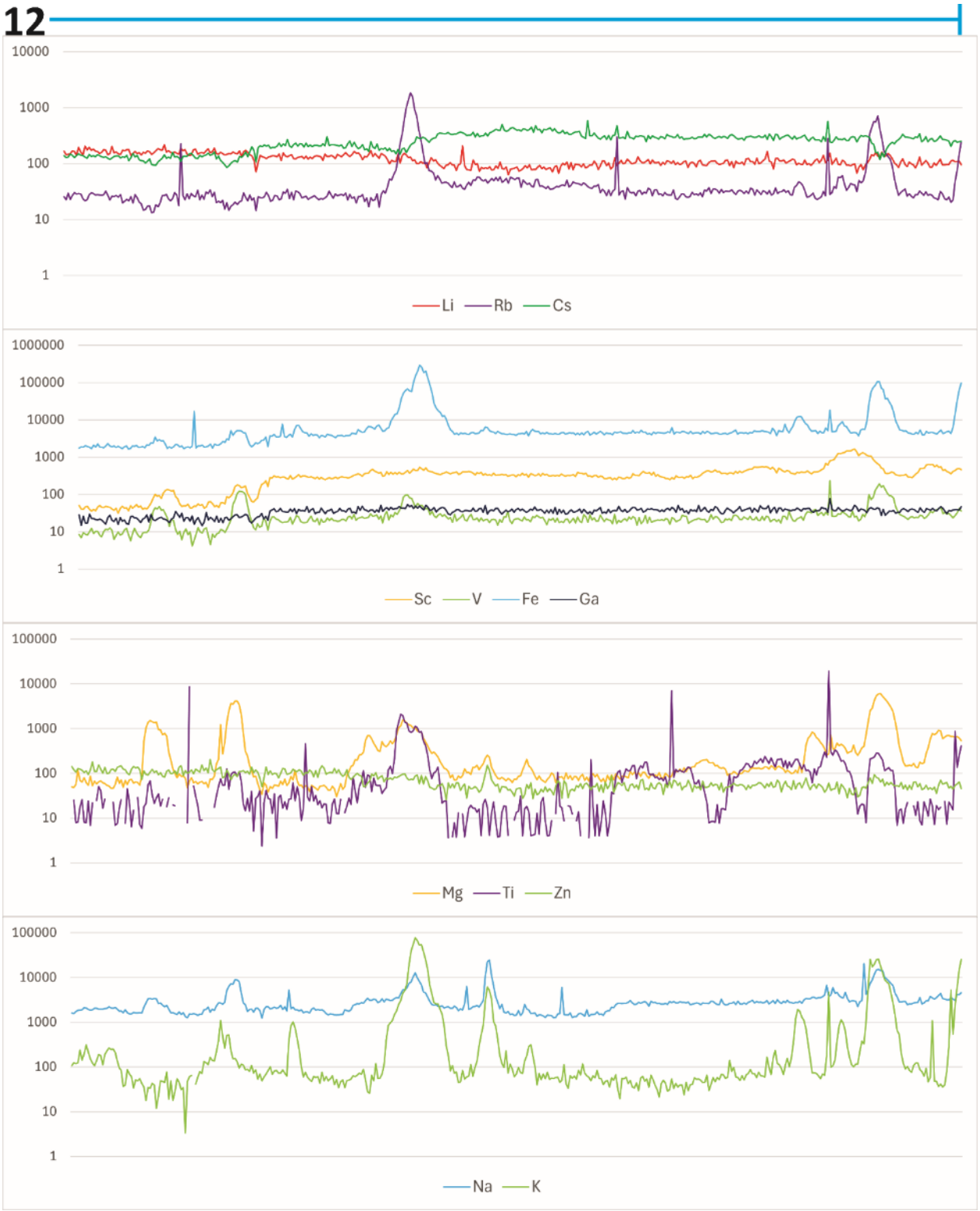
Appendix Figure 172: Concentrations (ppm) versus transect length. Sample LE25-9-1.8 is a beryl transect from pegmatite LE25-9.



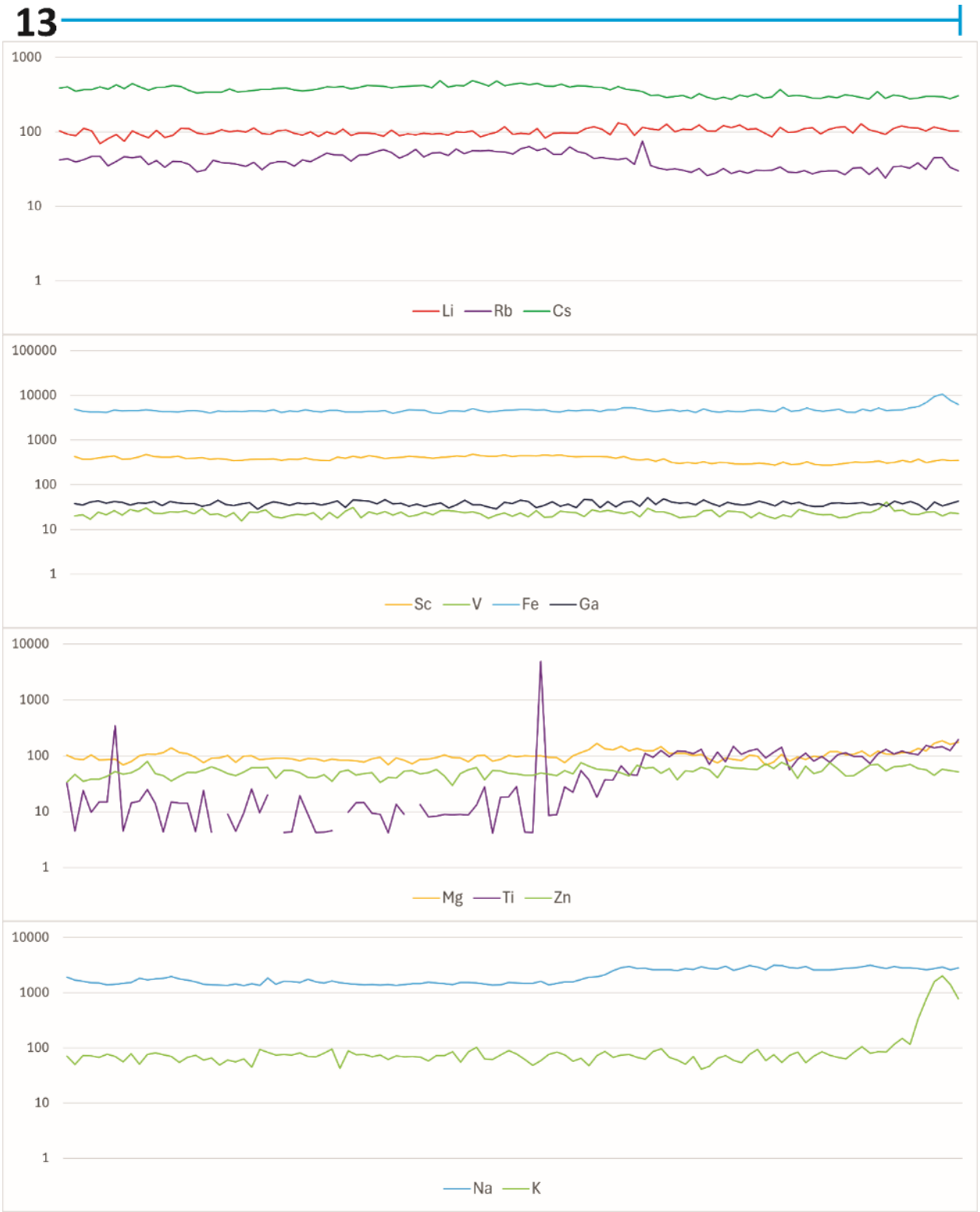
Appendix Figure 173: Concentrations (ppm) versus transect length. Sample LE25-9-1.10 is a beryl transect from pegmatite LE25-9.



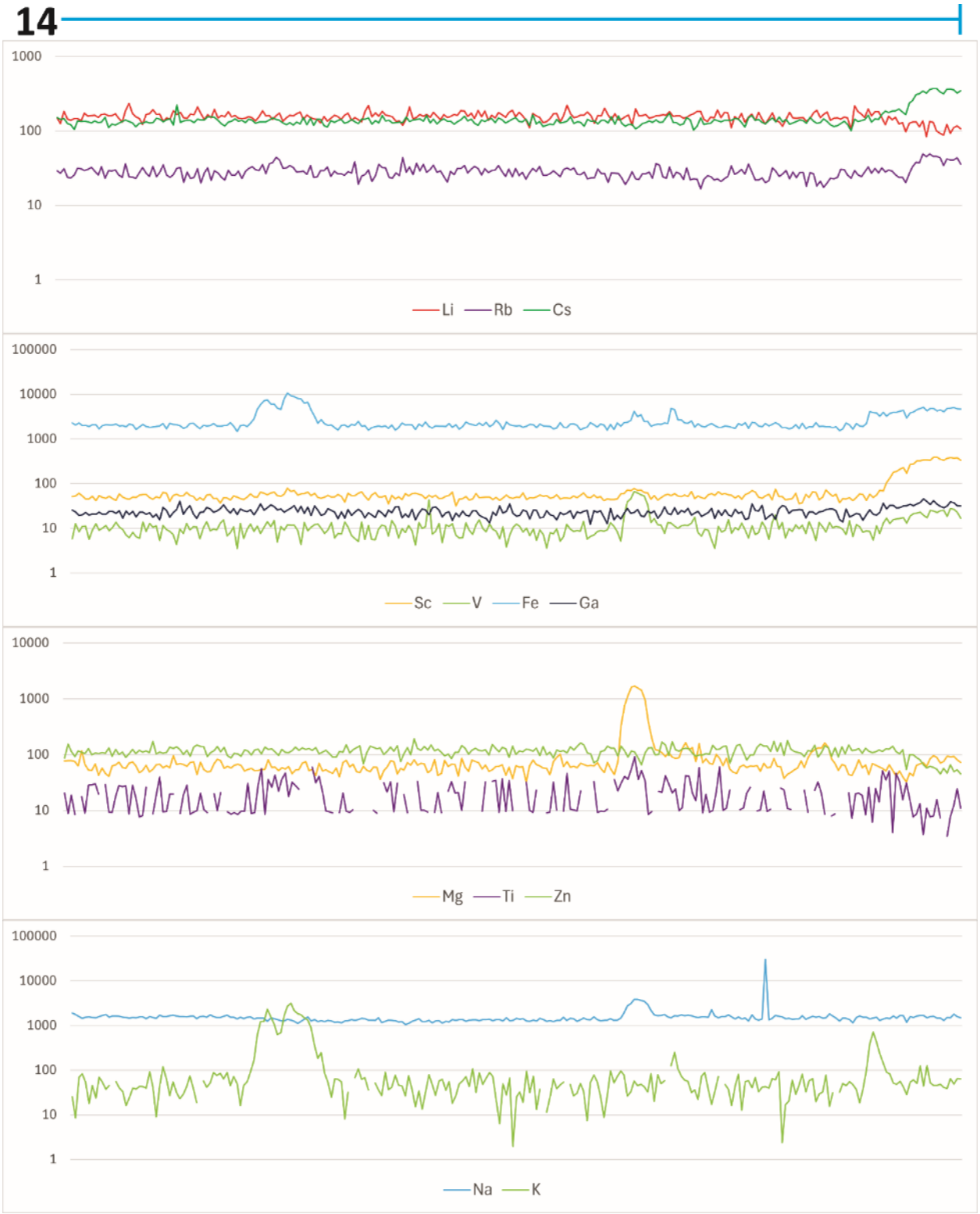
Appendix Figure 174: Concentrations (ppm) versus transect length. Sample LE25-9-1.11 is a beryl transect from pegmatite LE25-9.



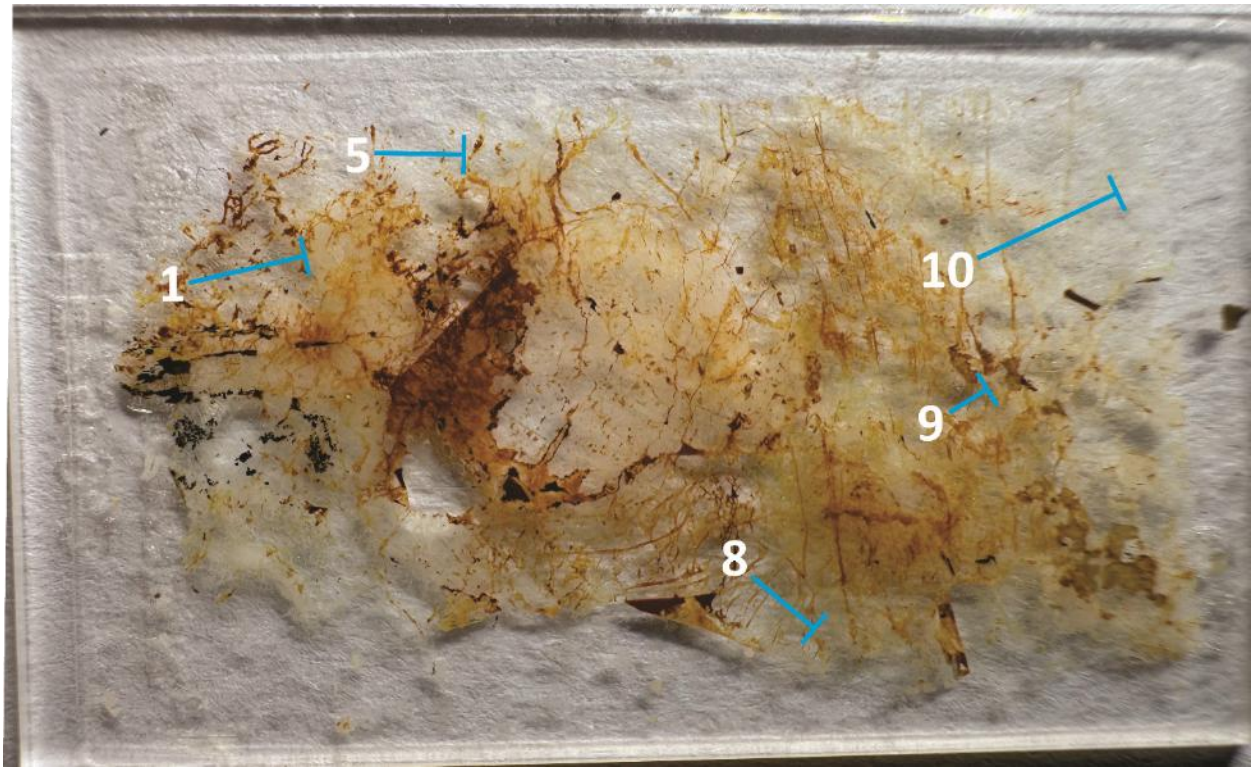
Appendix Figure 175: Concentrations (ppm) versus transect length. Sample LE25-9-1.12 is a beryl transect from pegmatite LE25-9.



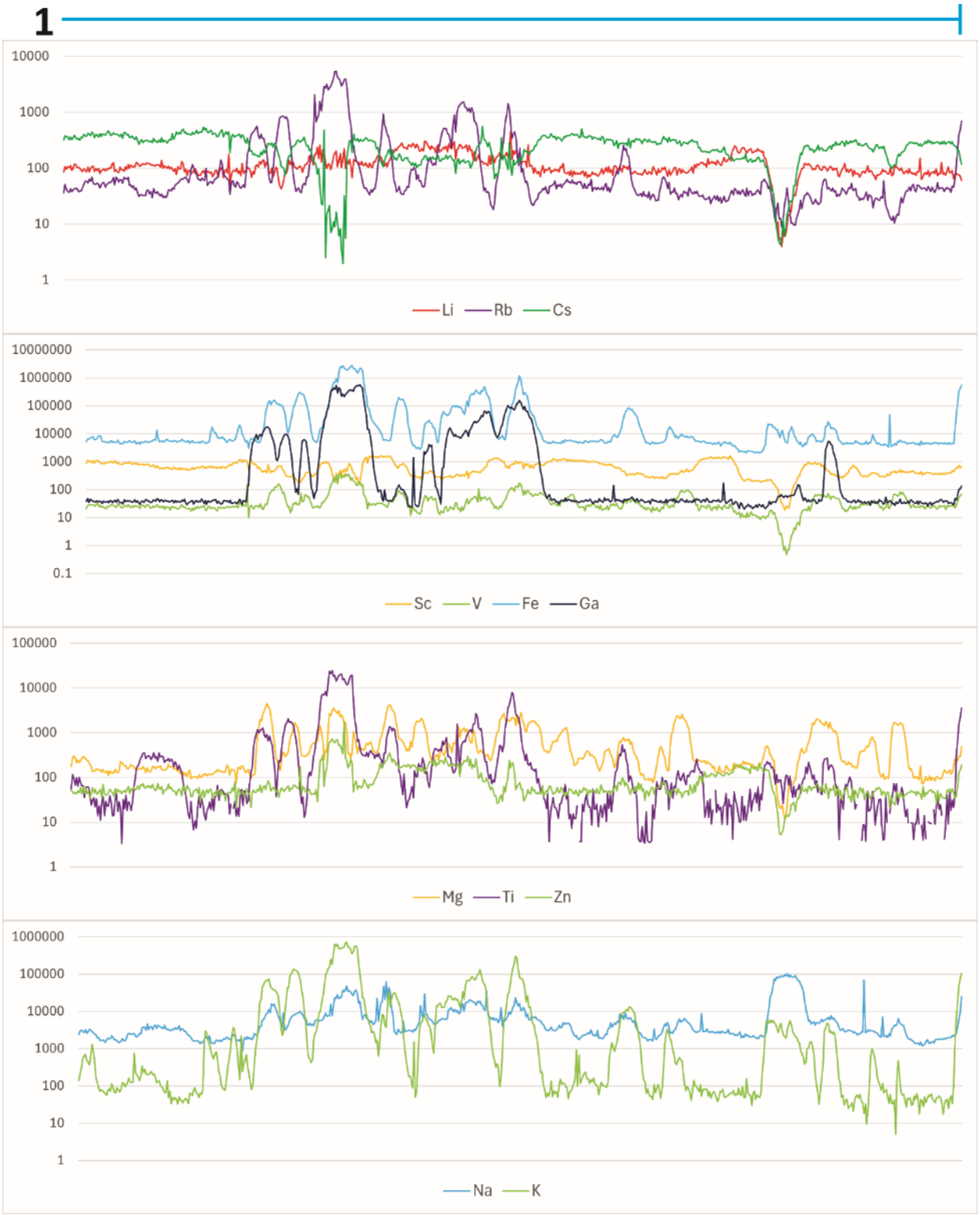
Appendix Figure 176: Concentrations (ppm) versus transect length. Sample LE25-9-1.13 is a beryl transect from pegmatite LE25-9.



Appendix Figure 177: Concentrations (ppm) versus transect length. Sample LE25-9-1.14 is a beryl transect from pegmatite LE25-9.



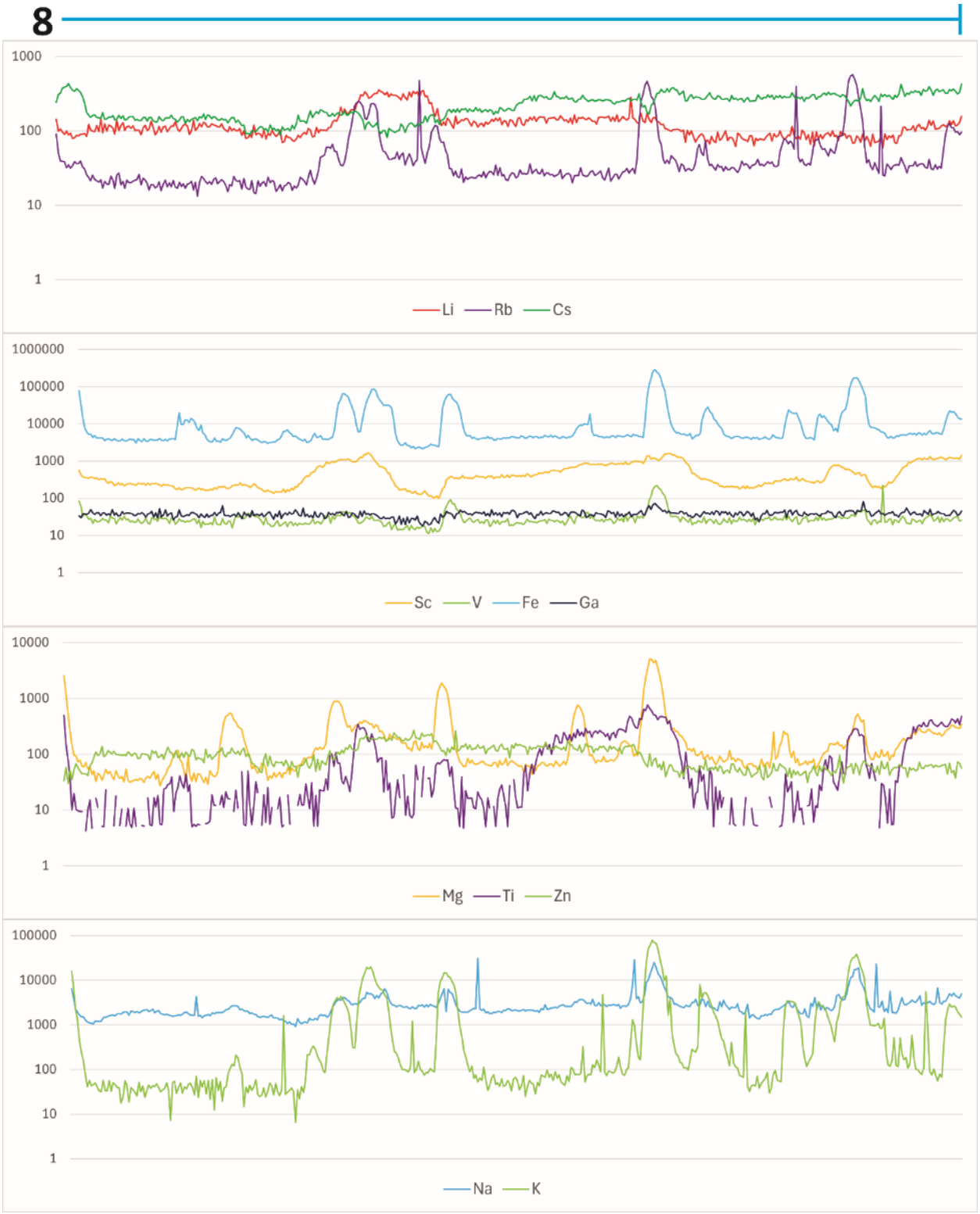
Appendix Figure 178: Sample LE25-9-2, 100 micron double polished thick section of pegmatite LE25-9 core zone. Blue (beryl transect) lines and numbers correspond to LA-ICP-MS transect lines (e.g., LE25-9-2.1 is the blue line labelled 1).



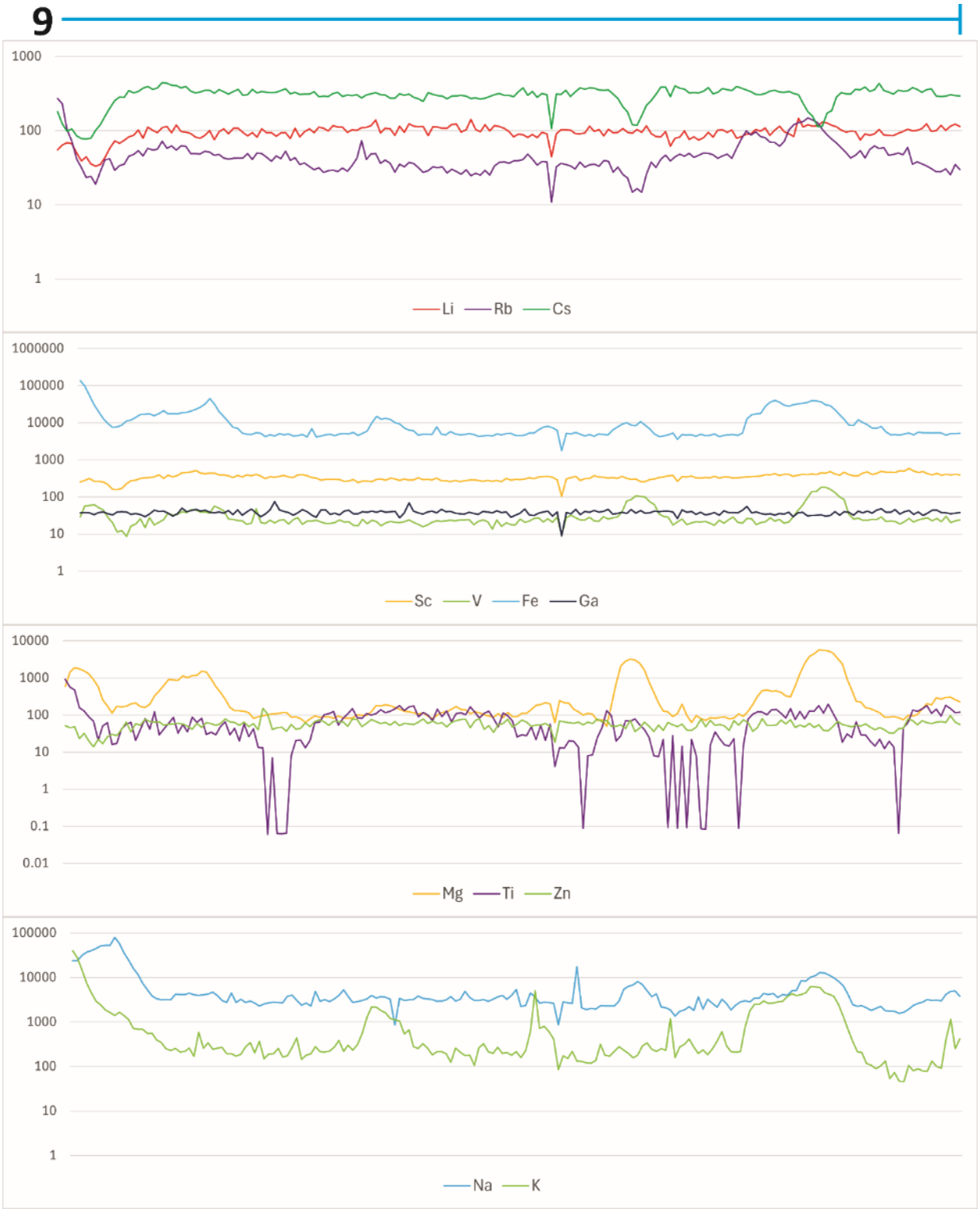
Appendix Figure 179: Concentrations (ppm) versus transect length. Sample LE25-9-2.1 is a beryl transect from pegmatite LE25-9.



Appendix Figure 180: Concentrations (ppm) versus transect length. Sample LE25-9-2.5 is a beryl transect from pegmatite LE25-9.



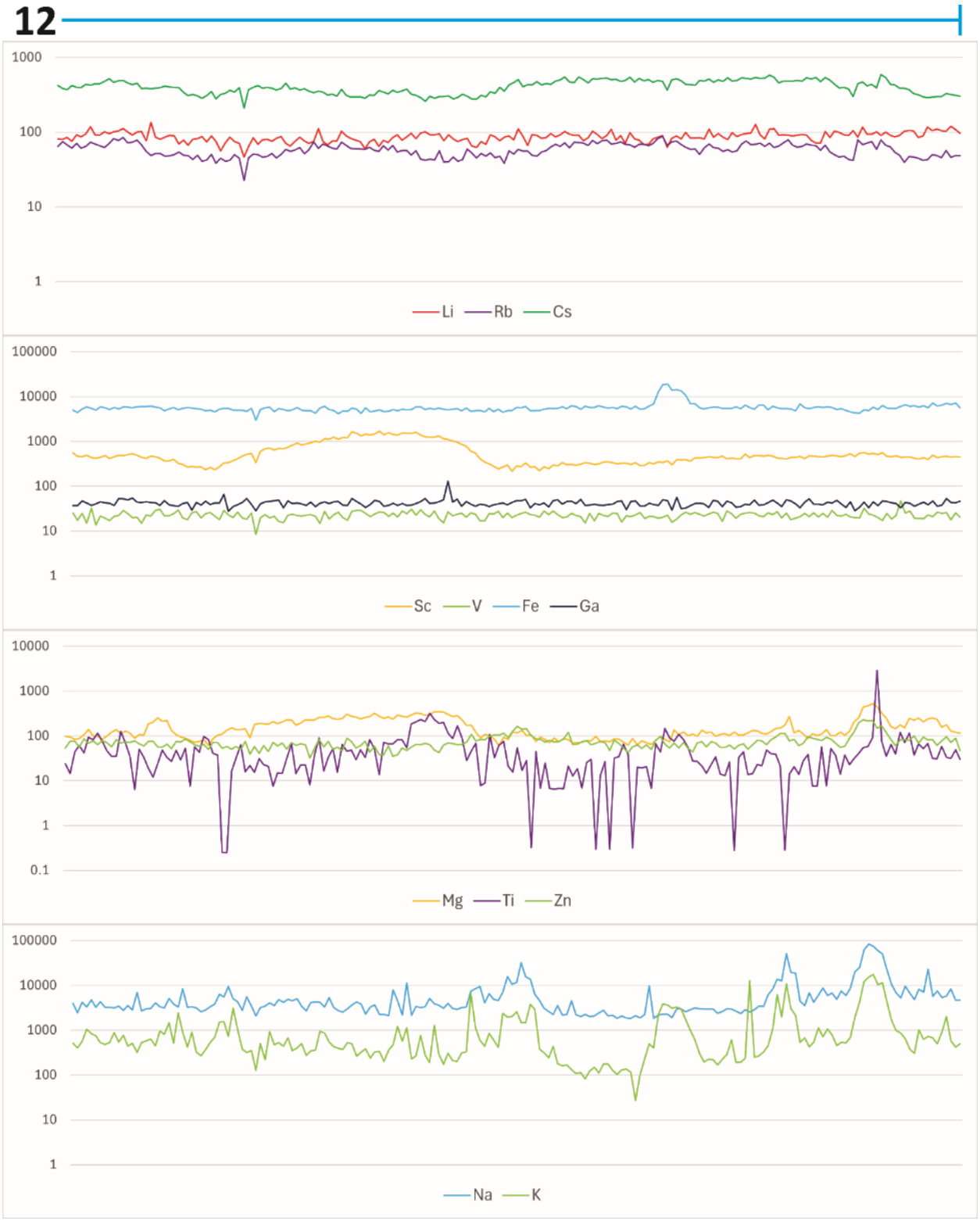
Appendix Figure 181: Concentrations (ppm) versus transect length. Sample LE25-9-2.8 is a beryl transect from pegmatite LE25-9.



Appendix Figure 182: Concentrations (ppm) versus transect length. Sample LE25-9-2.9 is a beryl transect from pegmatite LE25-9.



Appendix Figure 183: Concentrations (ppm) versus transect length. Sample LE25-9-2.10 is a beryl transect from pegmatite LE25-9.

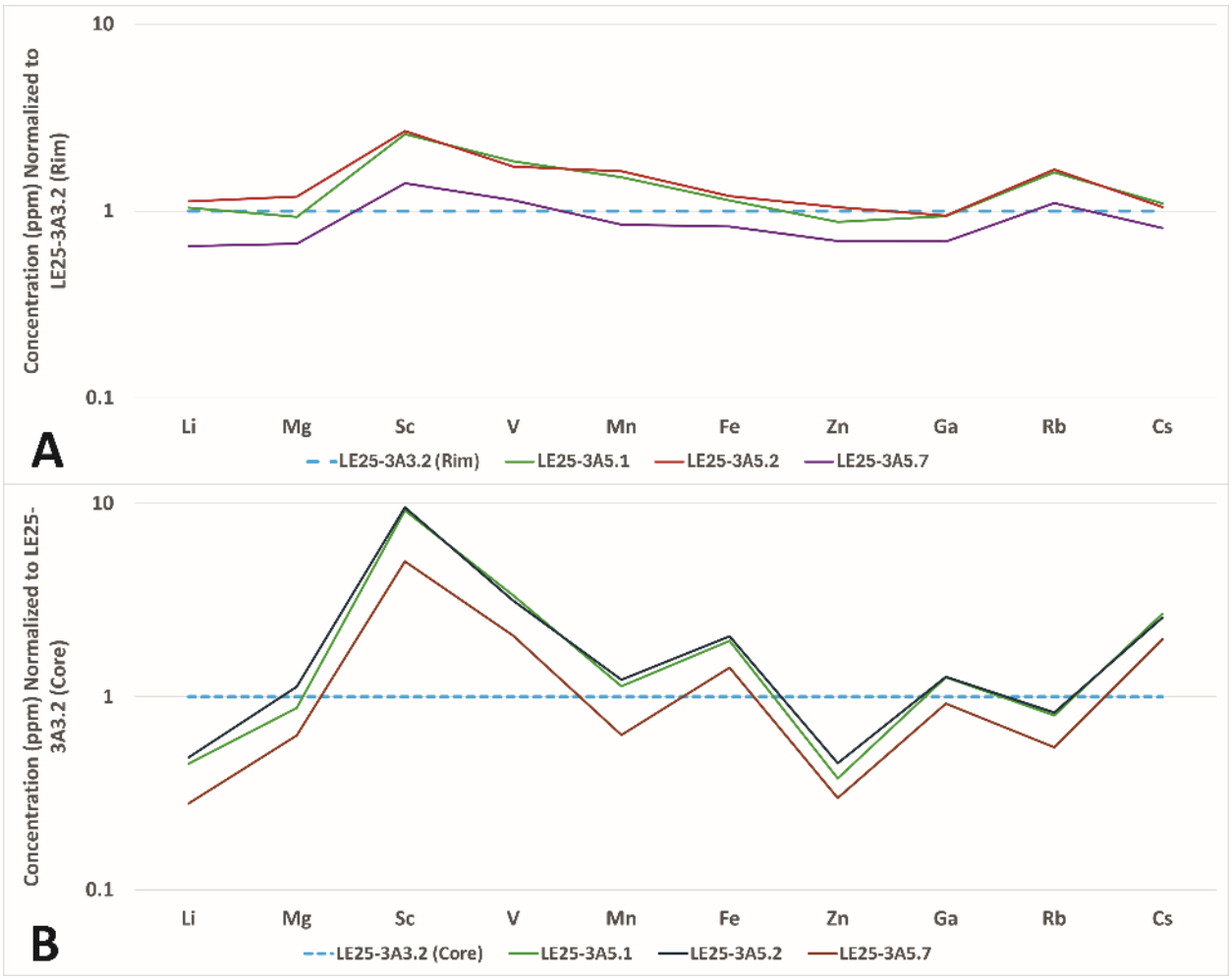


Appendix Figure 184: Concentrations (ppm) versus transect length. Sample LE25-9-2.12 is a beryl transect from pegmatite LE25-9.

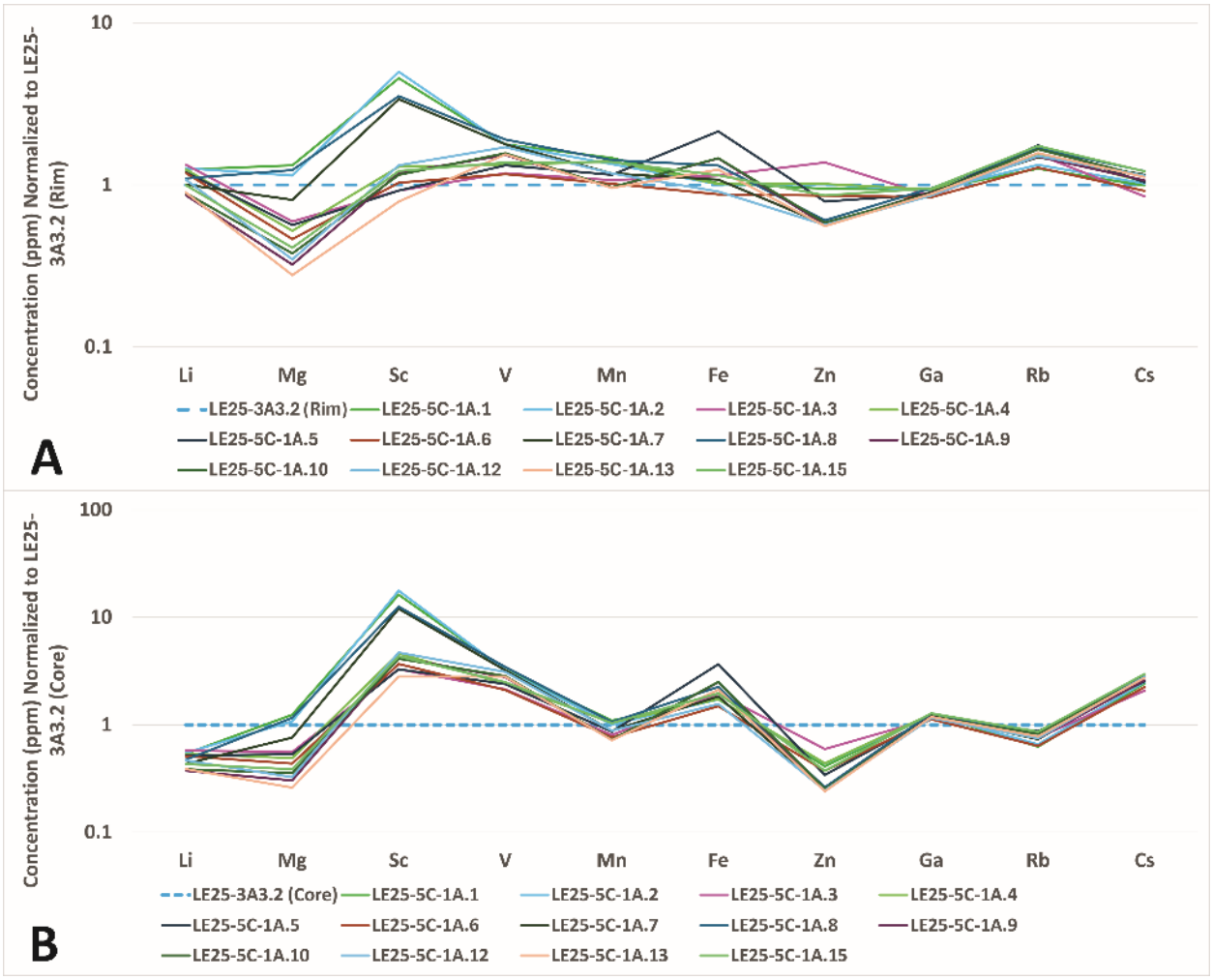
Appendix B - Pegmatite Beryl Comparison Graphs



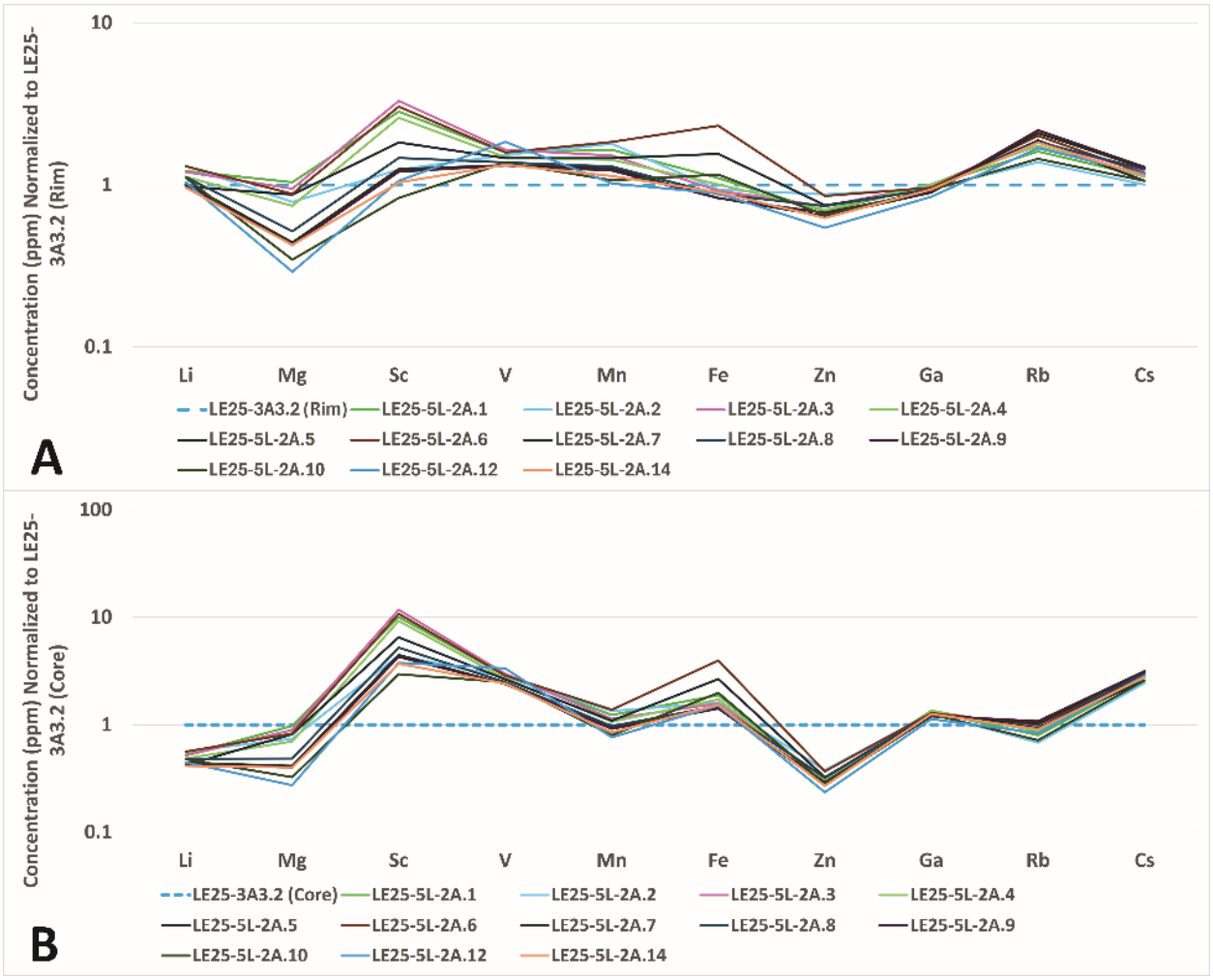
Appendix Figure 185: Beryl concentrations from LE25-3A3 normalized to the rim (A) and core (B) of euhedral beryl LE25-3A3.2.



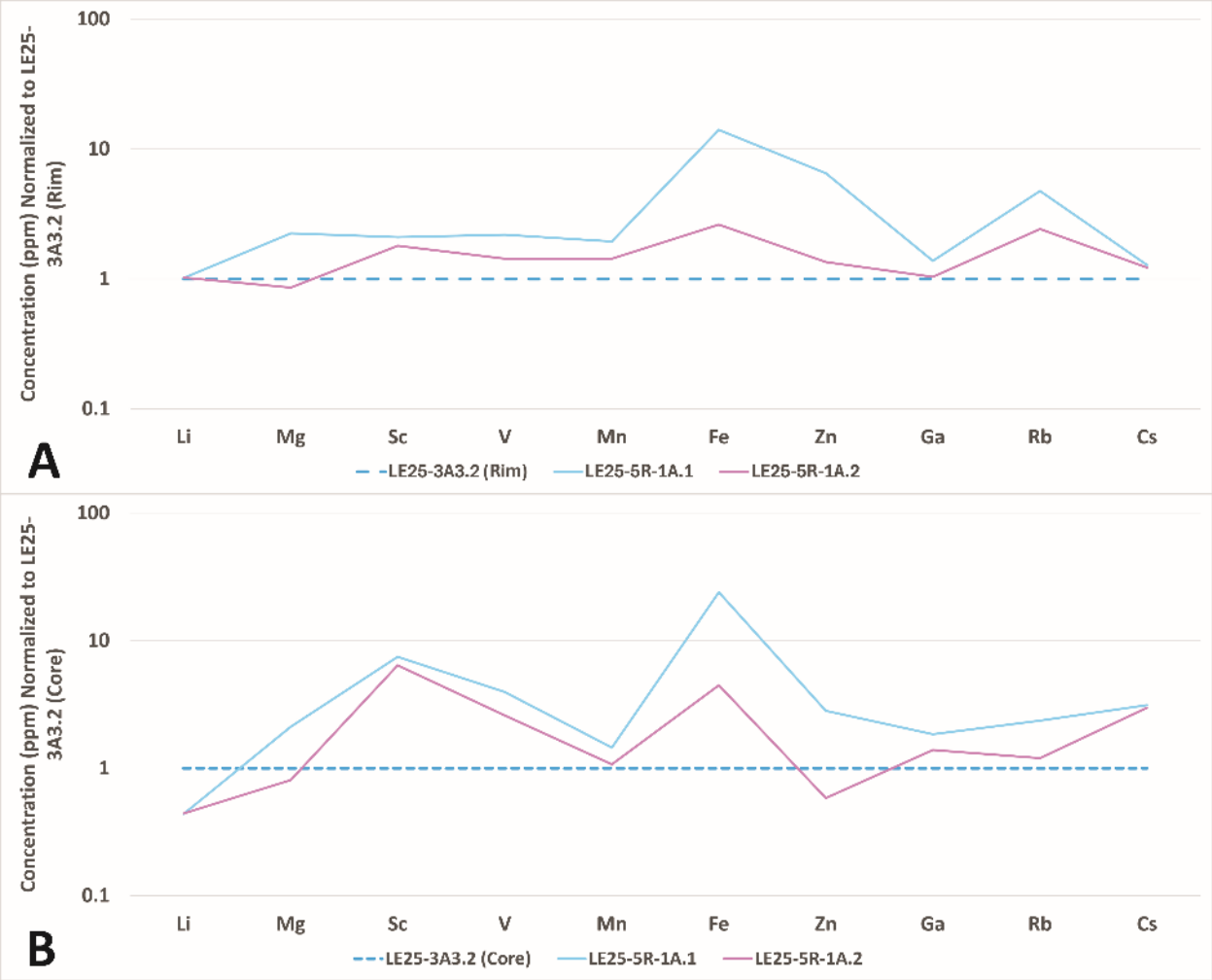
Appendix Figure 186: Beryl concentrations from LE25-3A5 normalized to the rim (A) and core (B) of euhedral beryl LE25-3A3.2.



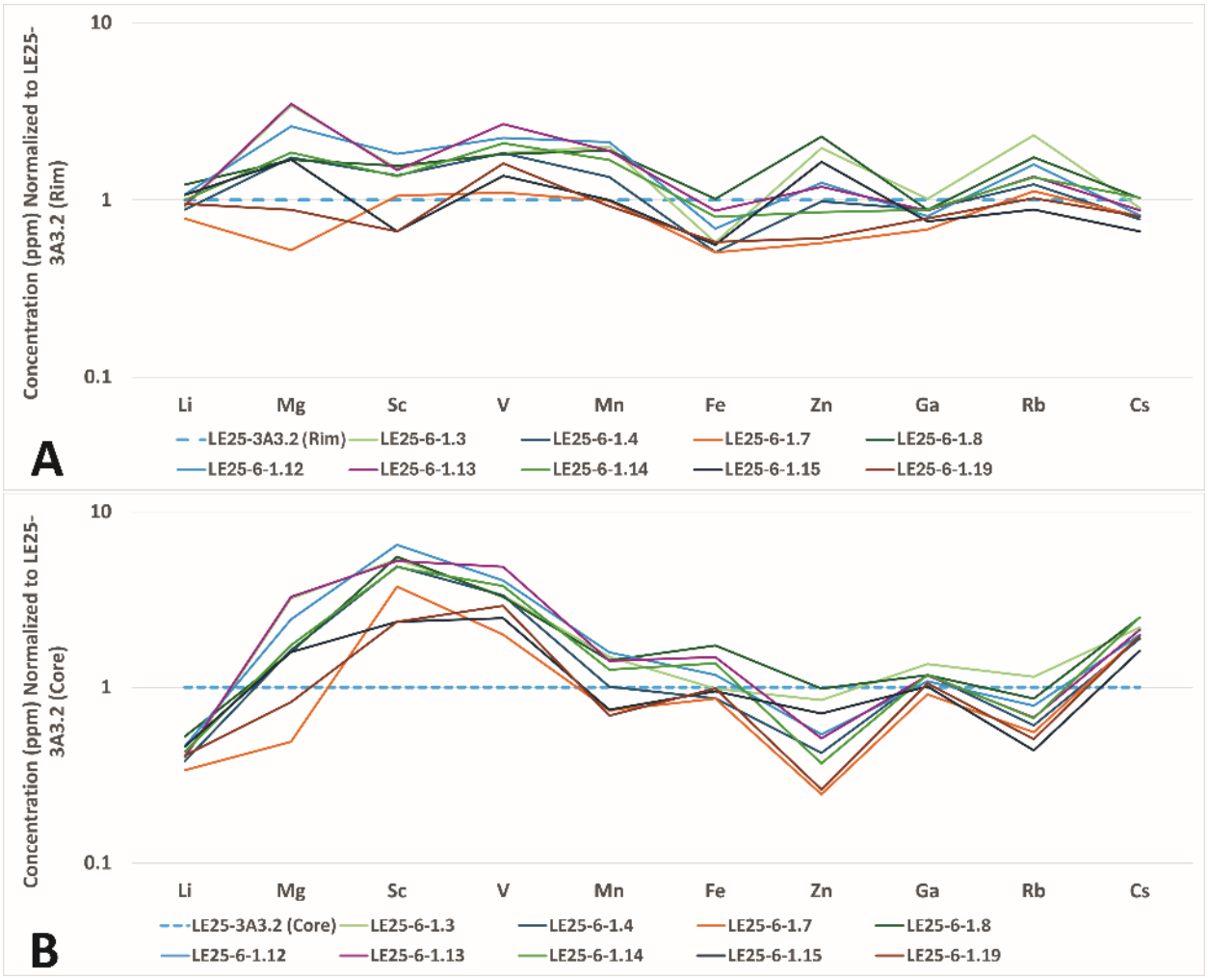
Appendix Figure 187: Beryl concentrations from LE25-5C-1A normalized to the rim (A) and core (B) of euhedral beryl LE25-3A3.2.



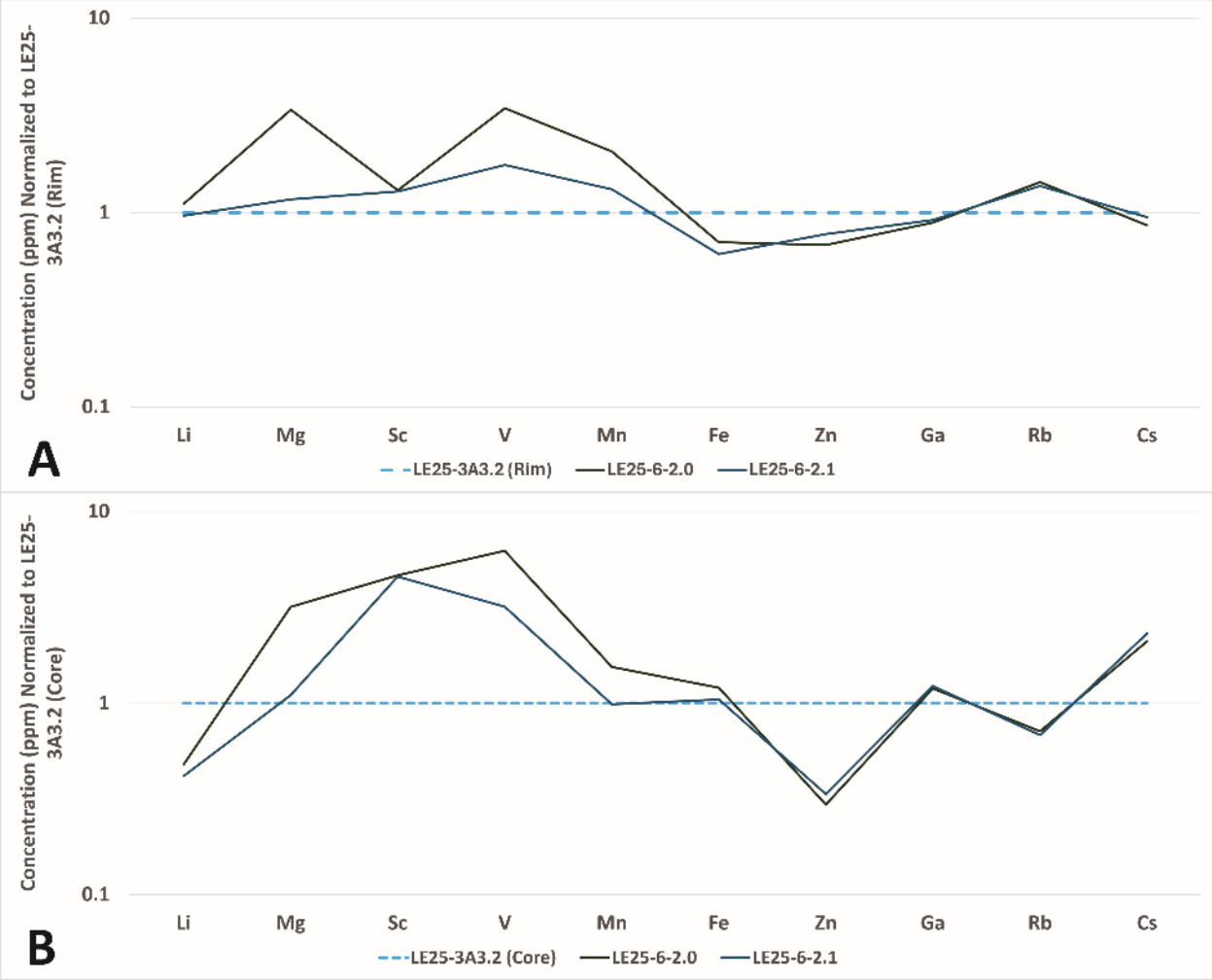
Appendix Figure 188: Beryl concentrations from LE25-5L-2A normalized to the rim (A) and core (B) of euhedral beryl LE25-3A3.2.



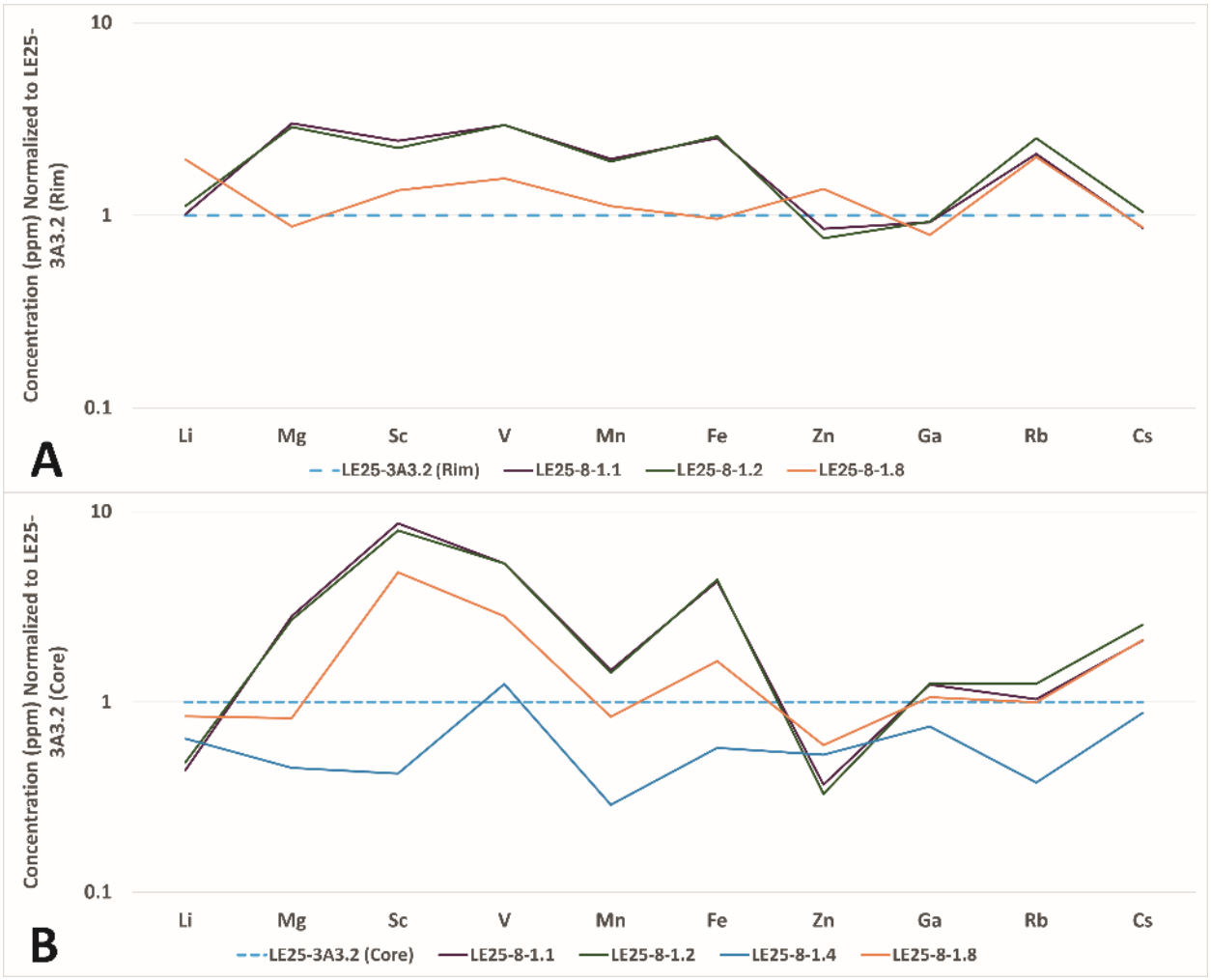
Appendix Figure 189: Beryl concentrations from LE25-5R-1A normalized to the rim (A) and core (B) of euhedral beryl LE25-3A3.2.



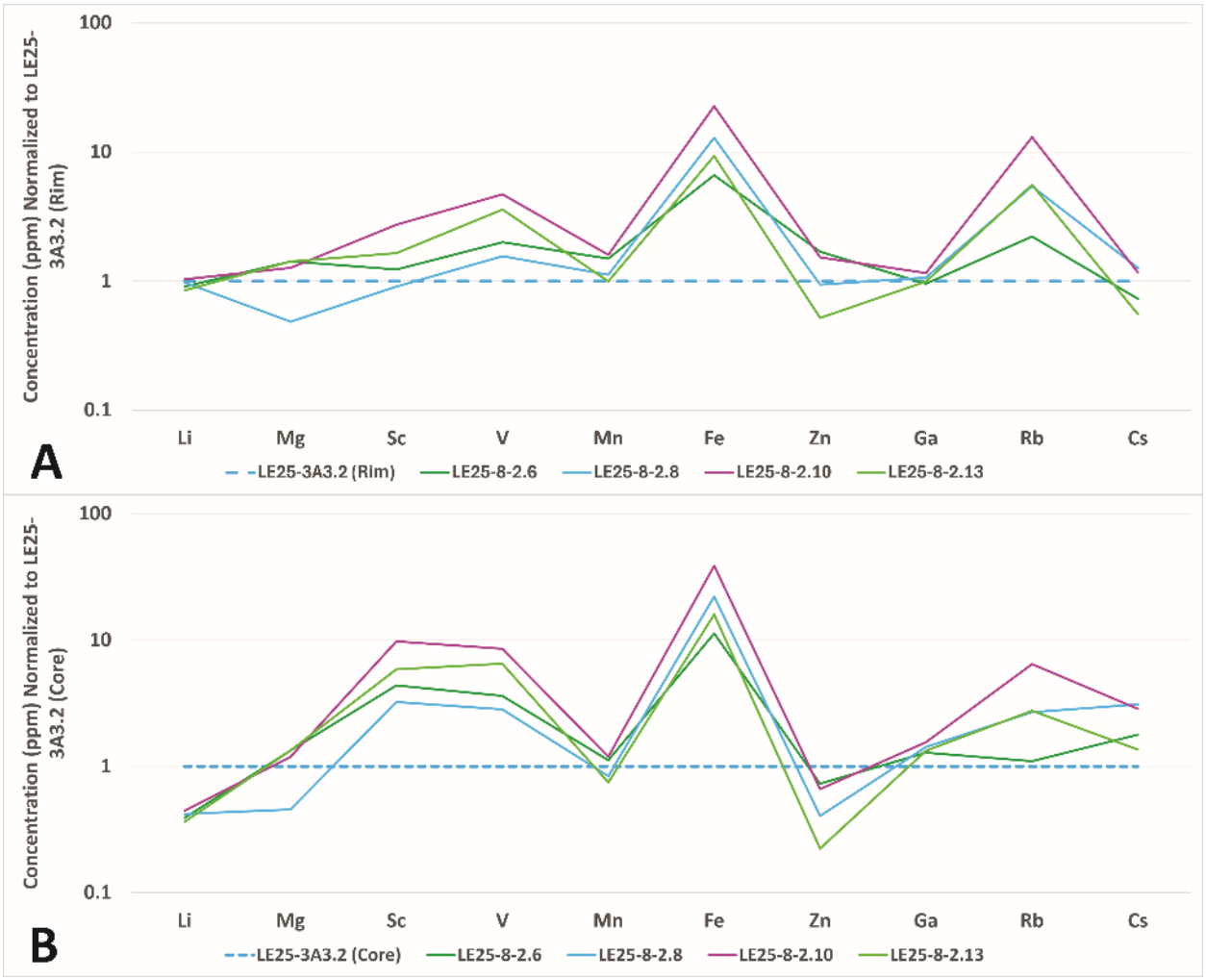
Appendix Figure 190: Beryl concentrations from LE25-6-1 normalized to the rim (A) and core (B) of euhedral beryl LE25-3A3.2.



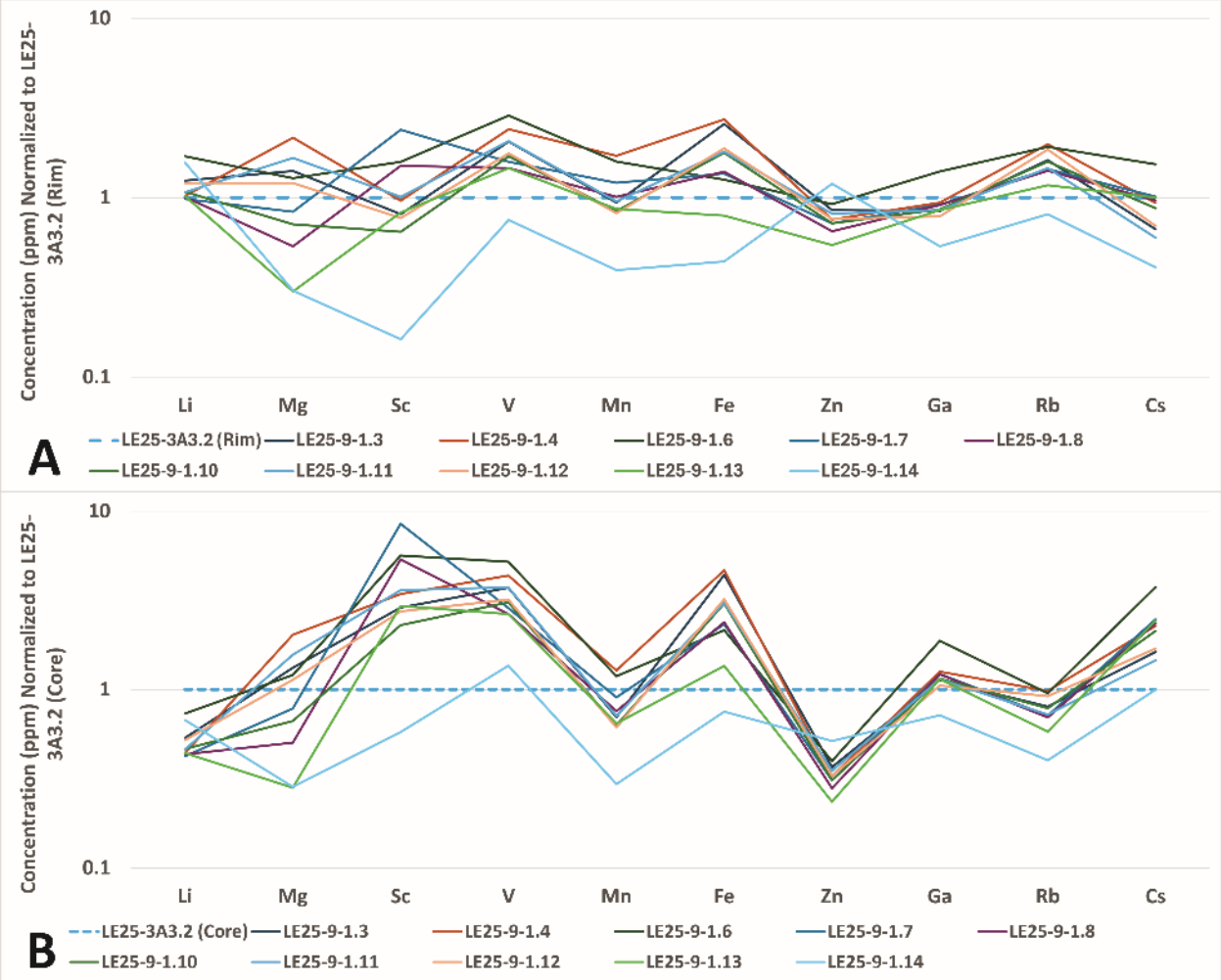
Appendix Figure 191: Beryl concentrations from LE25-6-2 normalized to the rim (A) and core (B) of euhedral beryl LE25-3A3.2.



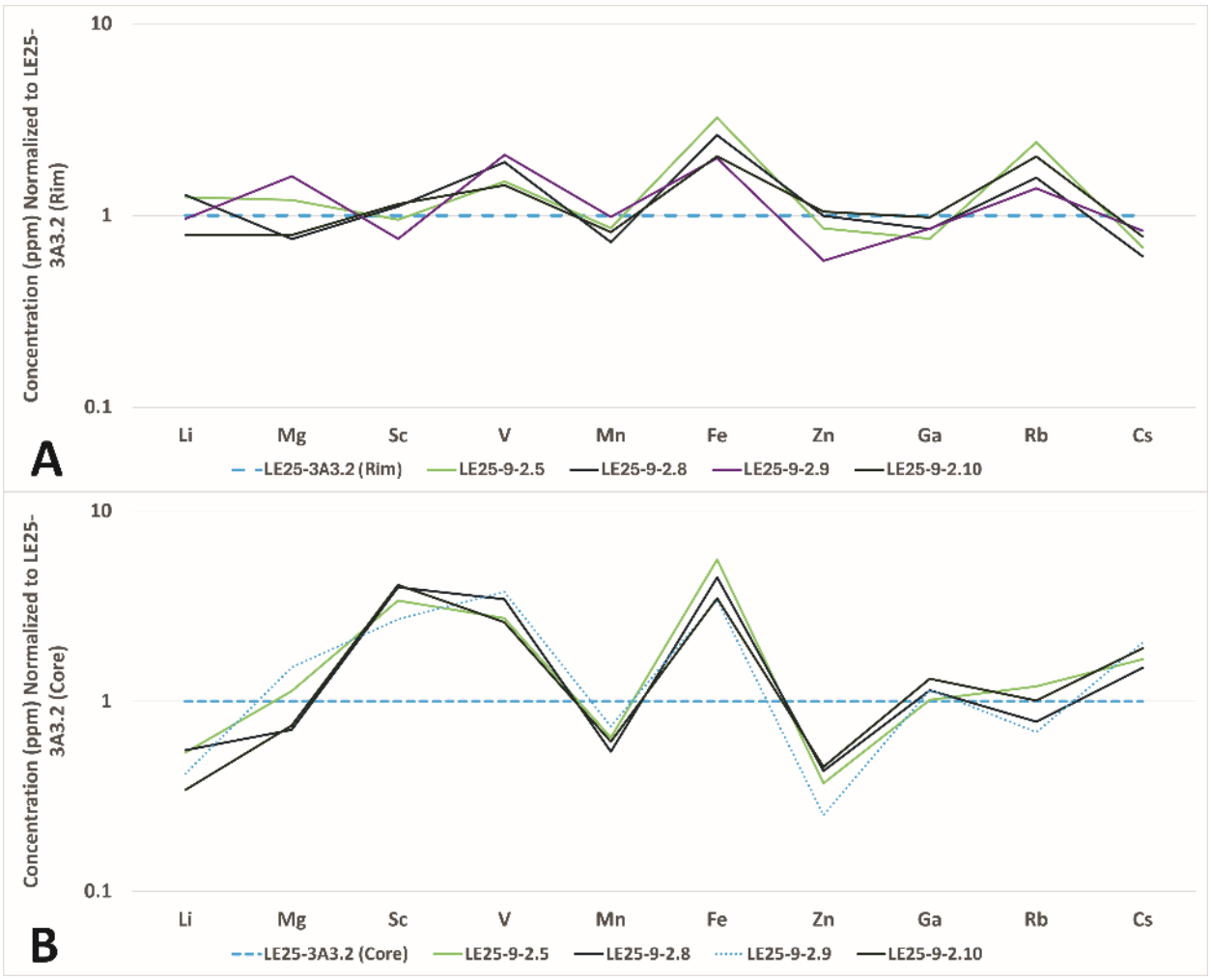
Appendix Figure 192: Beryl concentrations from LE25-8-1 normalized to the rim (A) and core (B) of euhedral beryl LE25-3A3.2.



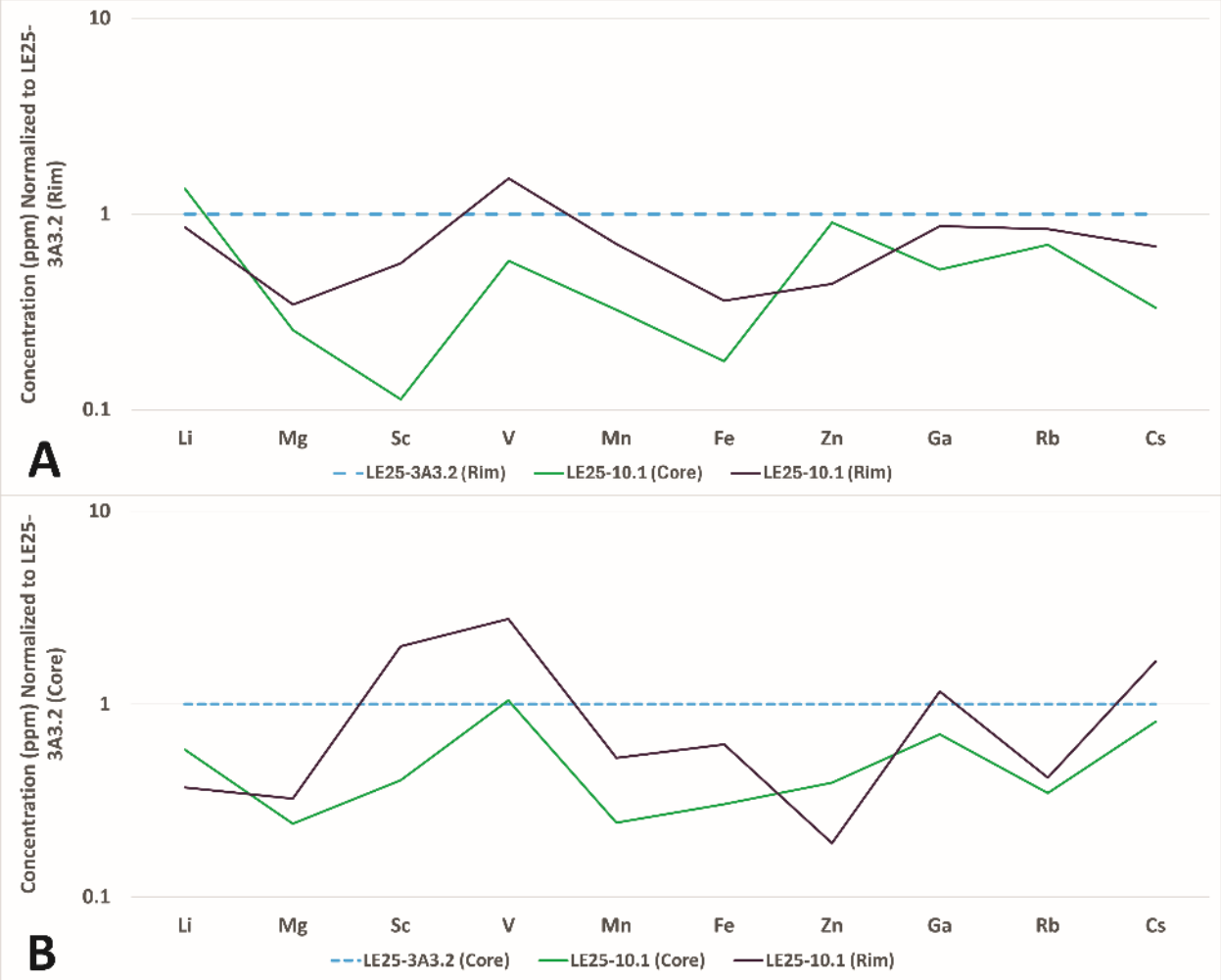
Appendix Figure 193: Beryl concentrations from LE25-8-2 normalized to the rim (A) and core (B) of euhedral beryl LE25-3A3.2.



Appendix Figure 194: Beryl concentrations from LE25-9-1 normalized to the rim (A) and core (B) of euhedral beryl LE25-3A3.2.

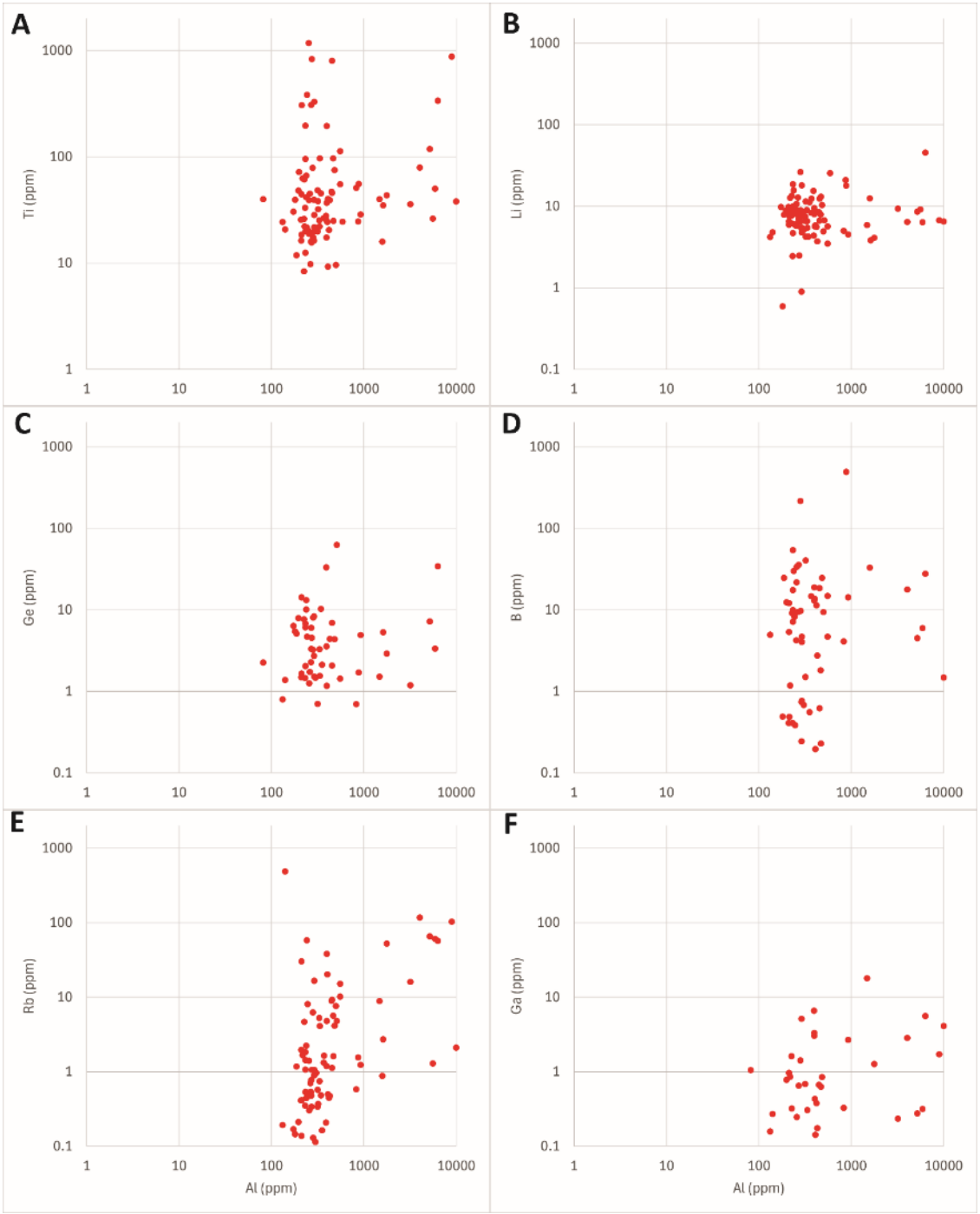


Appendix Figure 195: Beryl concentrations from LE25-9-2 normalized to the rim (A) and core (B) of euhedral beryl LE25-3A3.2.

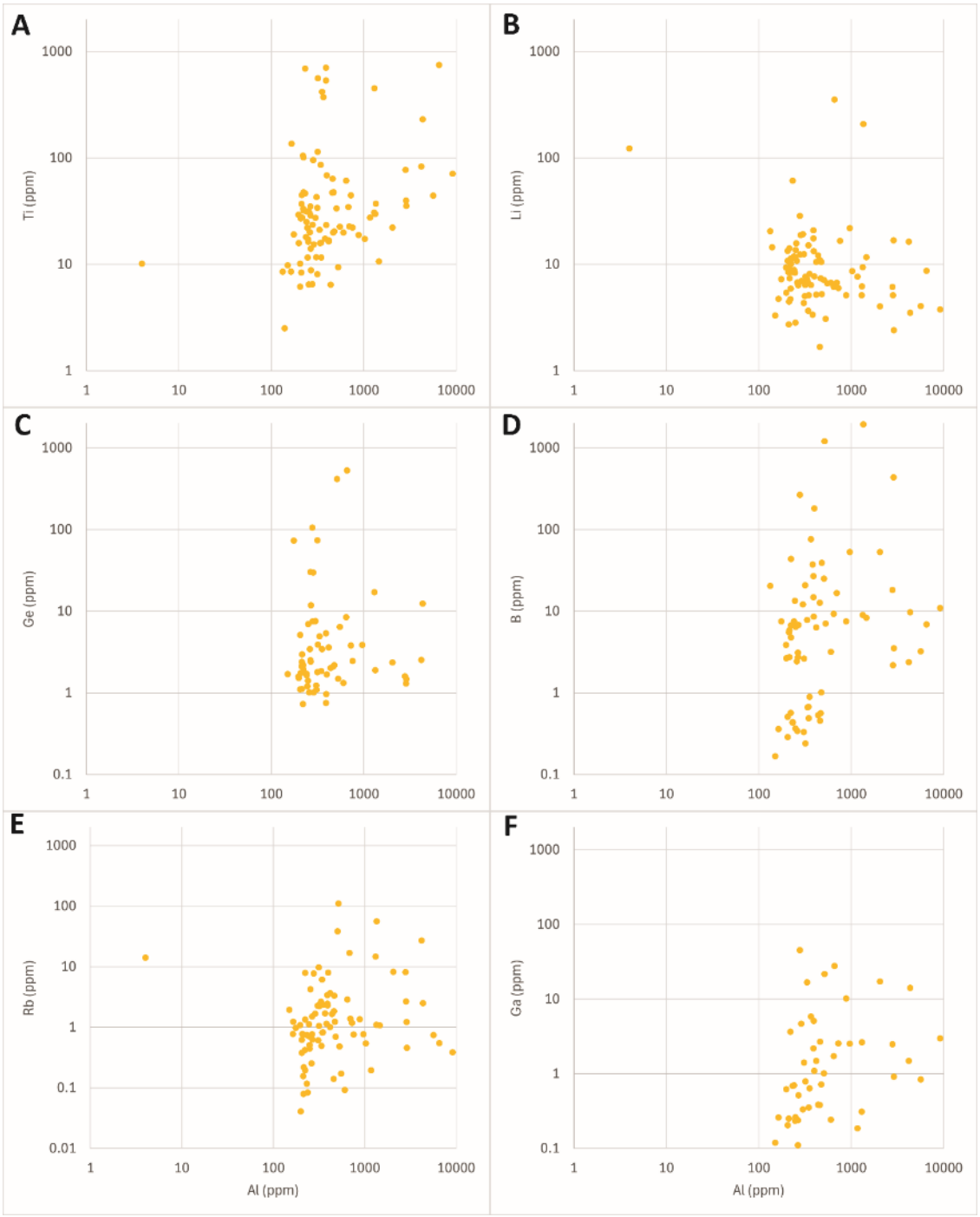


Appendix Figure 196: Beryl concentrations from LE25-10 normalized to the rim (A) and core (B) of euhedral beryl LE25-3A3.2.

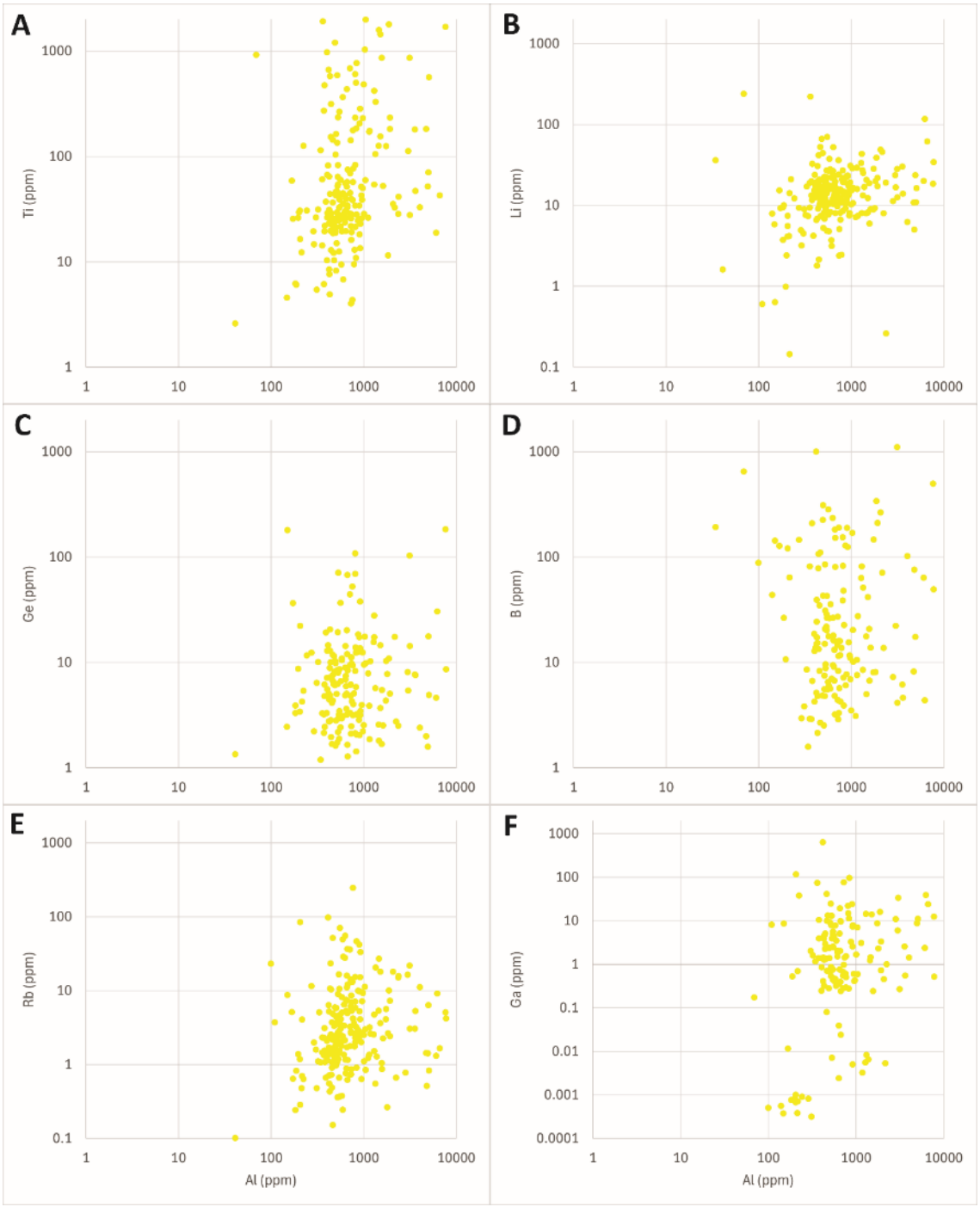
Appendix C - Quartz Bivariate Graphs



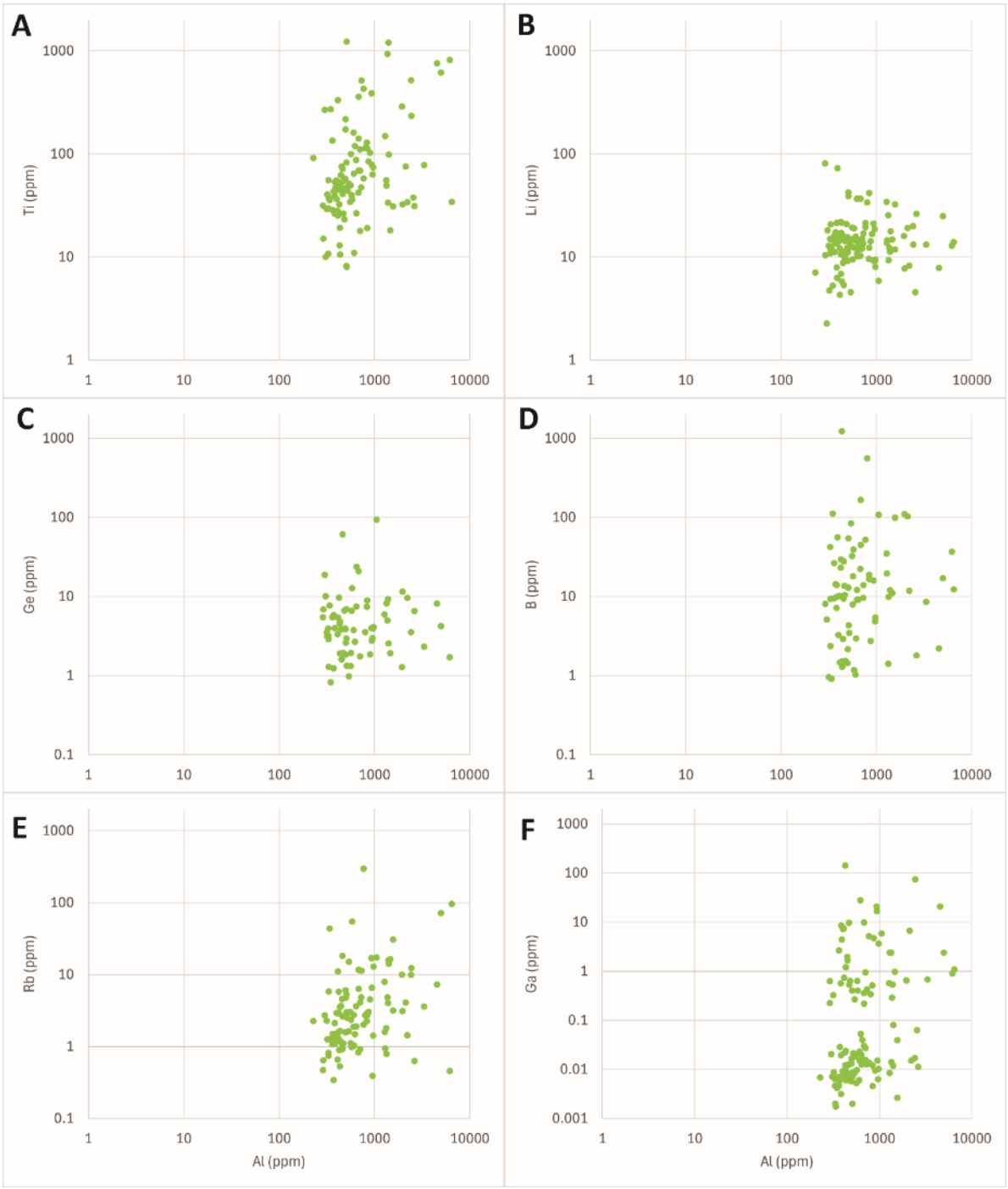
Appendix Figure 197: Bivariate plots for trace element concentrations from Mt. Antero quartz crystal LE25-3A1.6 (n=101). A) Al versus Ti; B) Al versus Li; C) Al versus Ge; D) Al versus B; E) Al versus Ga; F) Al versus Rb.



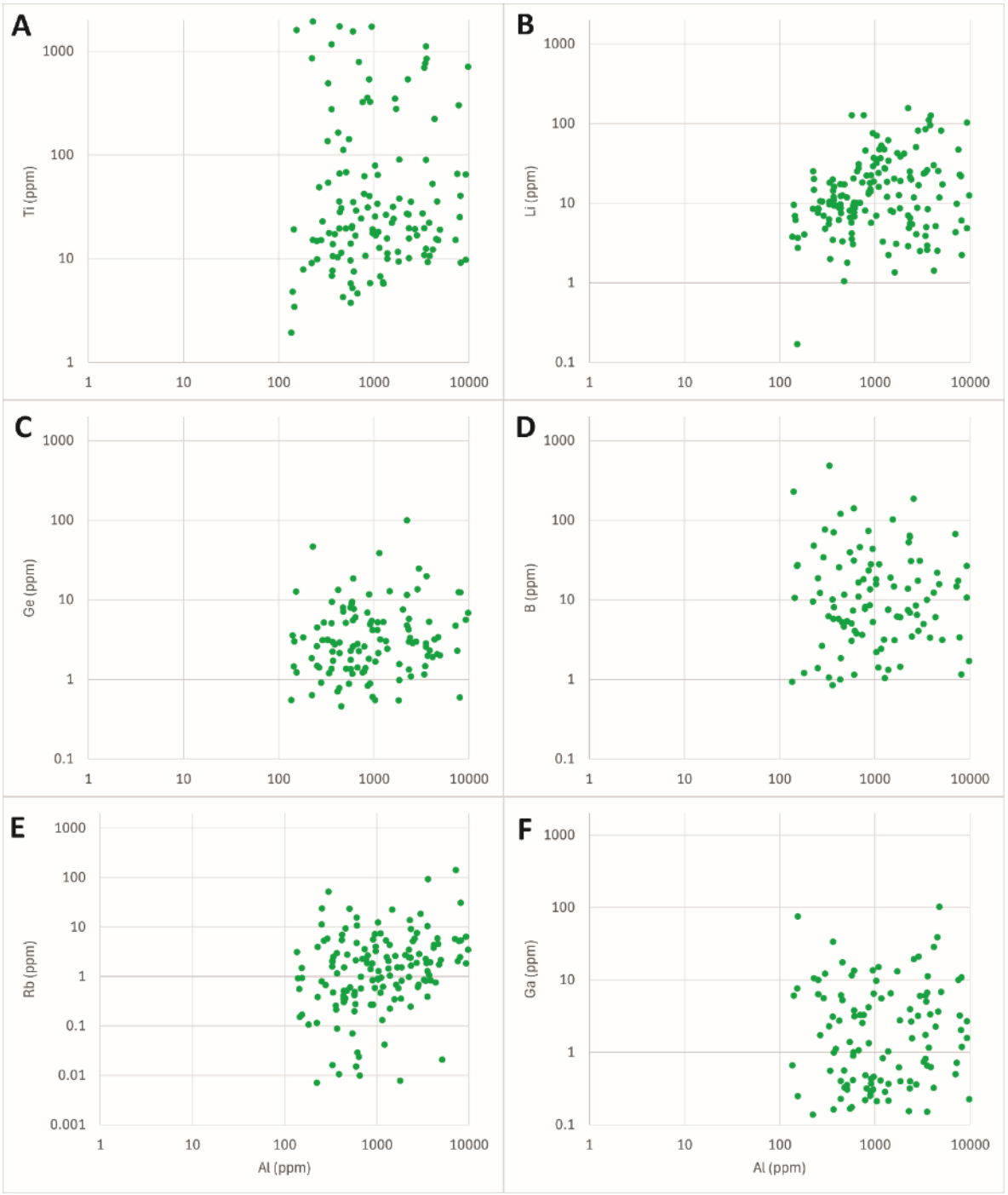
Appendix Figure 198: Bivariate plots for trace element concentrations from Mt. Antero quartz crystal LE25-3A1.17 (n=110). A) Al versus Ti; B) Al versus Li; C) Al versus Ge; D) Al versus B; E) Al versus Ga; F) Al versus Rb.



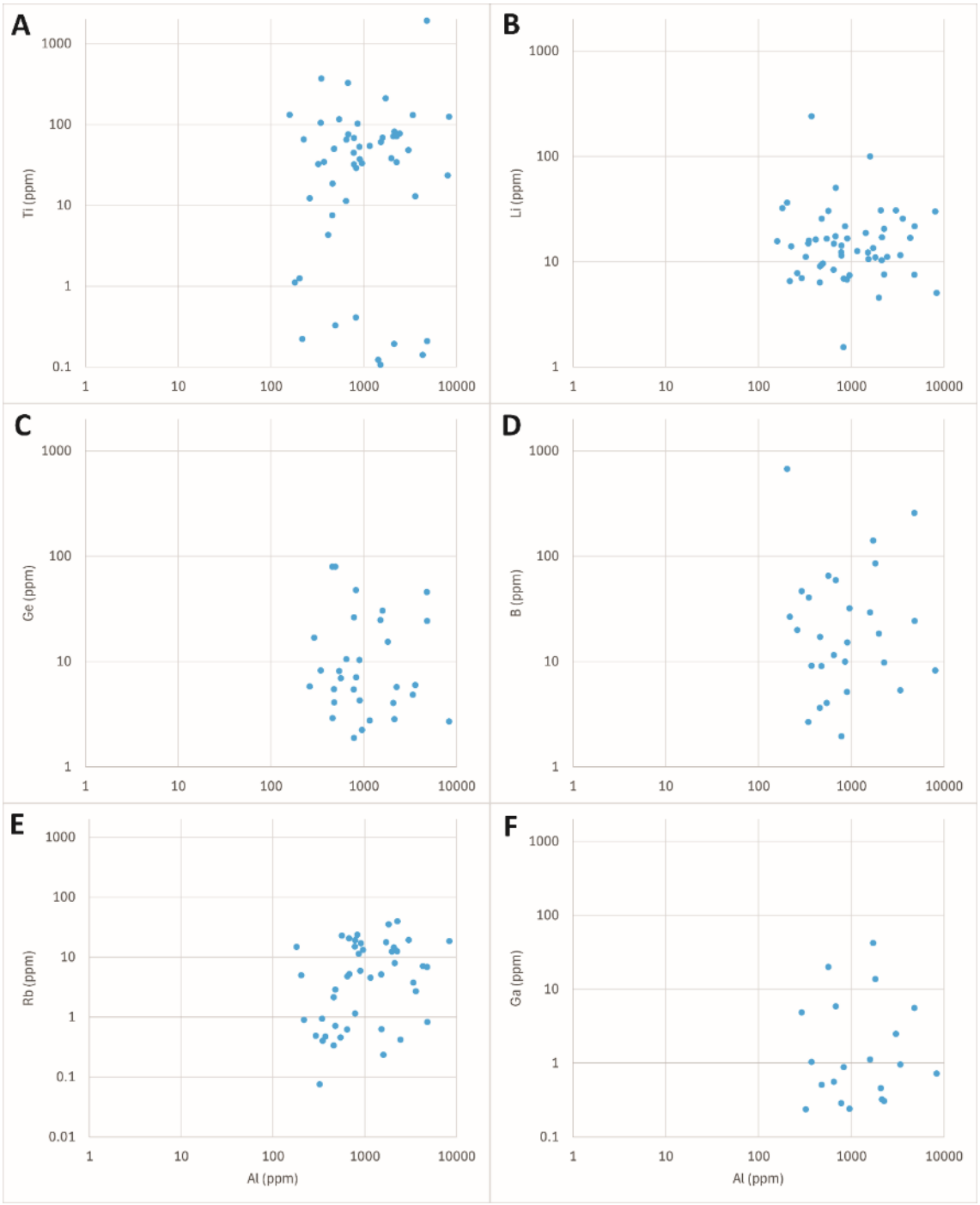
Appendix Figure 199: Bivariate plots for trace element concentrations from Mt. Antero quartz crystal LE25-5C-1A.17 (n=166). A) Al versus Ti; B) Al versus Li; C) Al versus Ge; D) Al versus B; E) Al versus Ga; F) Al versus Rb.



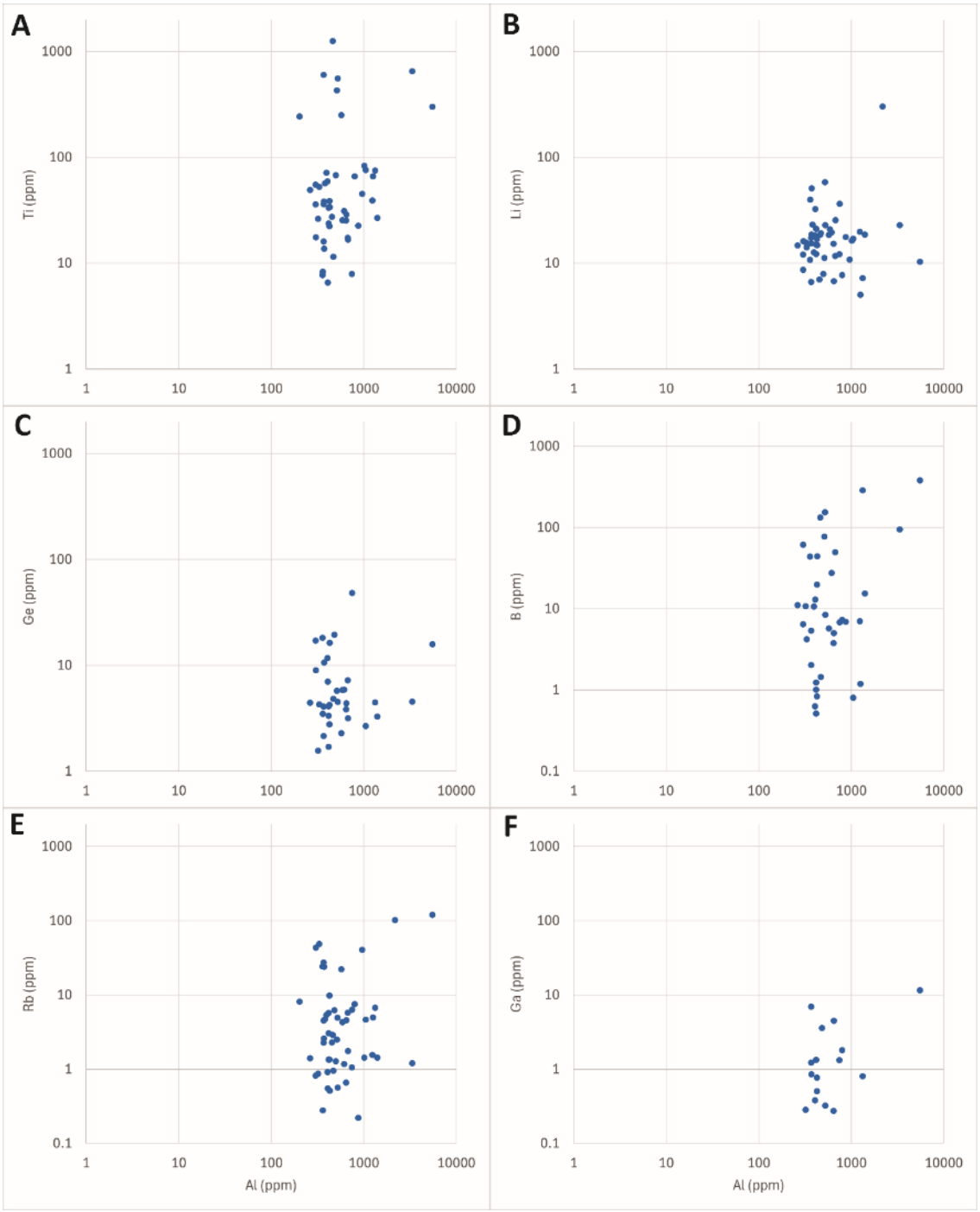
Appendix Figure 200: Bivariate plots for trace element concentrations from Mt. Antero quartz crystals LE25-5C-1B.14 (n=120). A) Al versus Ti; B) Al versus Li; C) Al versus Ge; D) Al versus B; E) Al versus Ga; F) Al versus Rb.



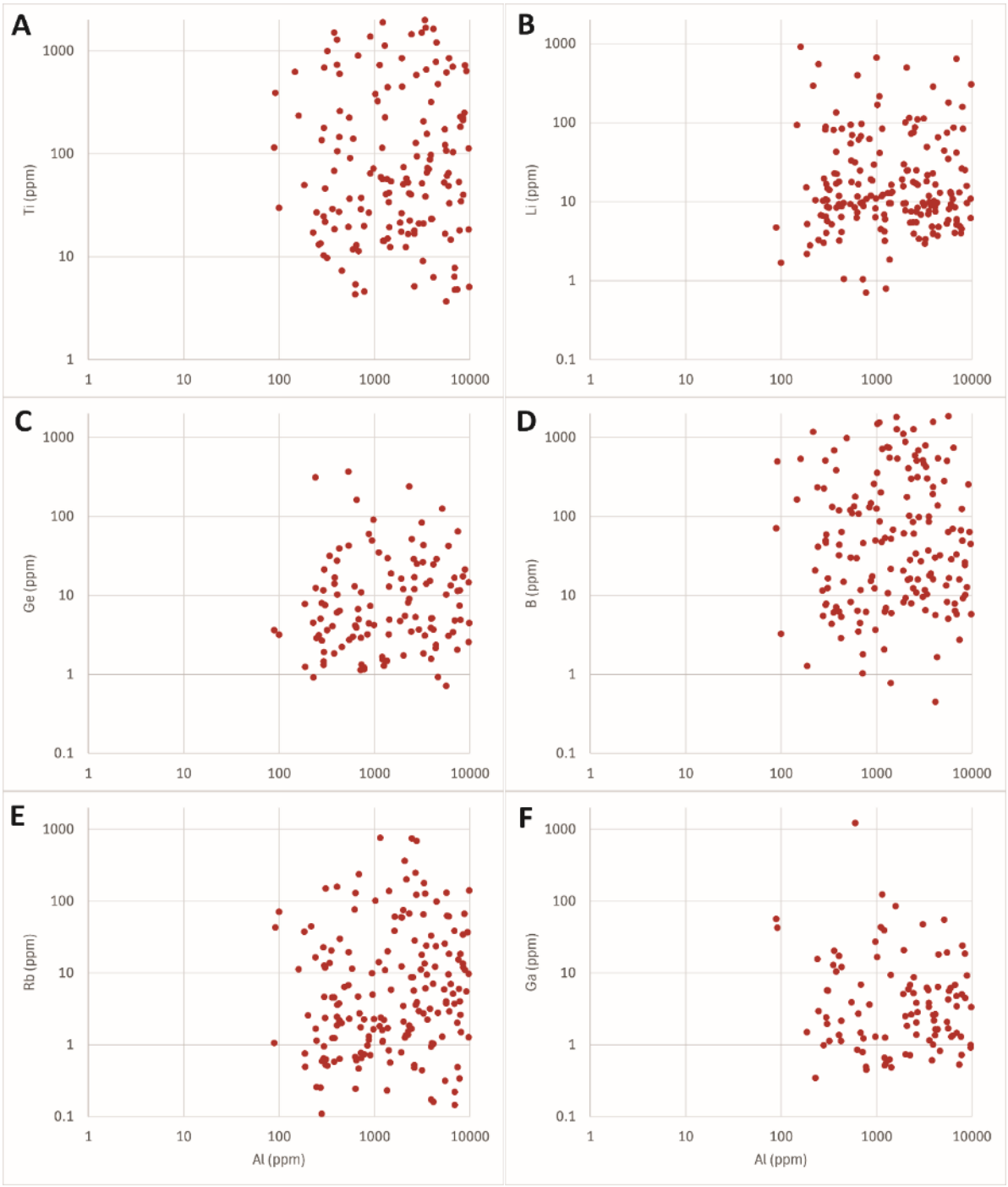
Appendix Figure 201: Bivariate plots for trace element concentrations from Mt. Antero quartz crystal LE25-5L-1B.4 (n=174). A) Al versus Ti; B) Al versus Li; C) Al versus Ge; D) Al versus B; E) Al versus Ga; F) Al versus Rb.



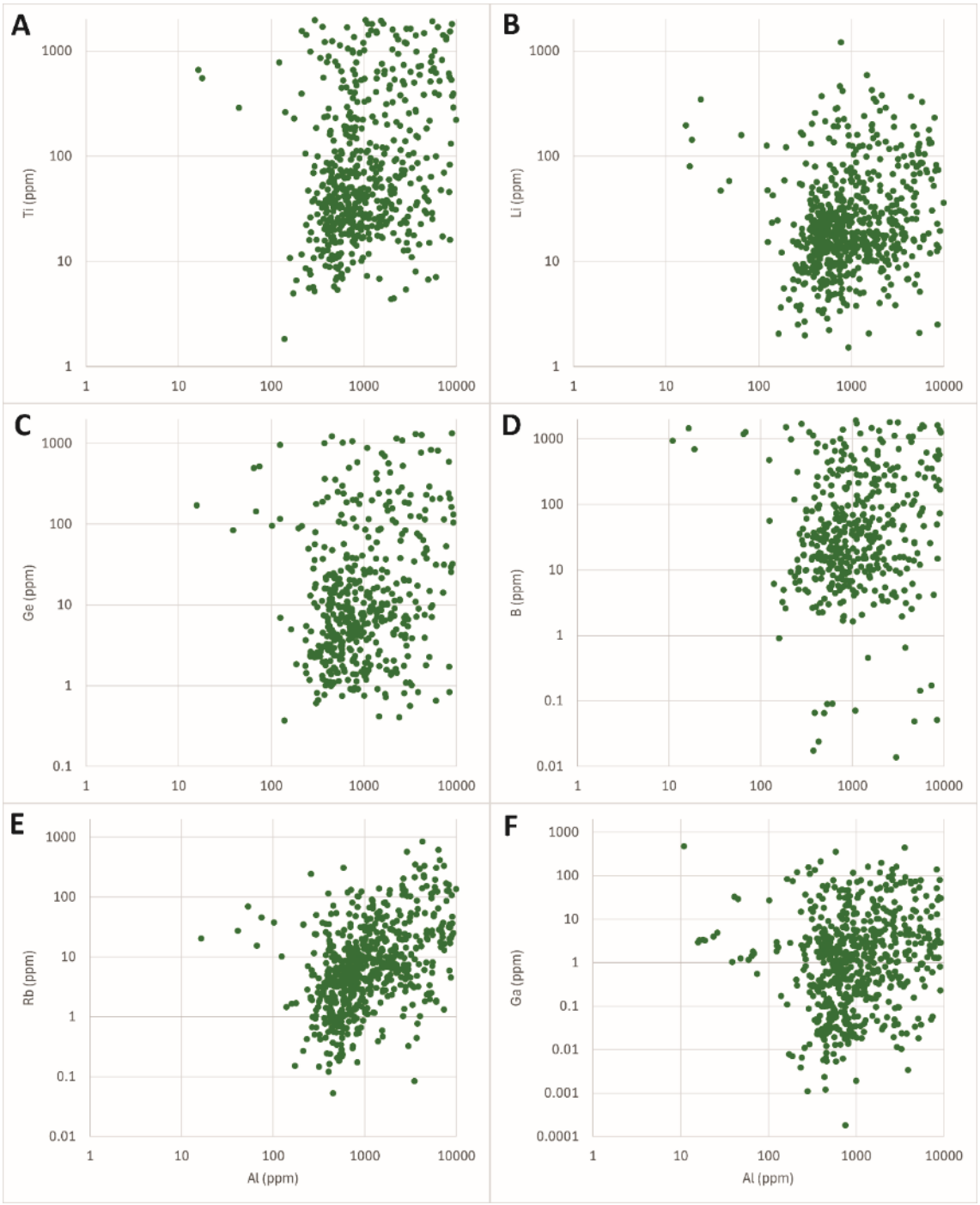
Appendix Figure 202: Bivariate plots for trace element concentrations from Mt. Antero quartz crystal LE25-5R-1A.7 (n=55). A) Al versus Ti; B) Al versus Li; C) Al versus Ge; D) Al versus B; E) Al versus Ga; F) Al versus Rb.



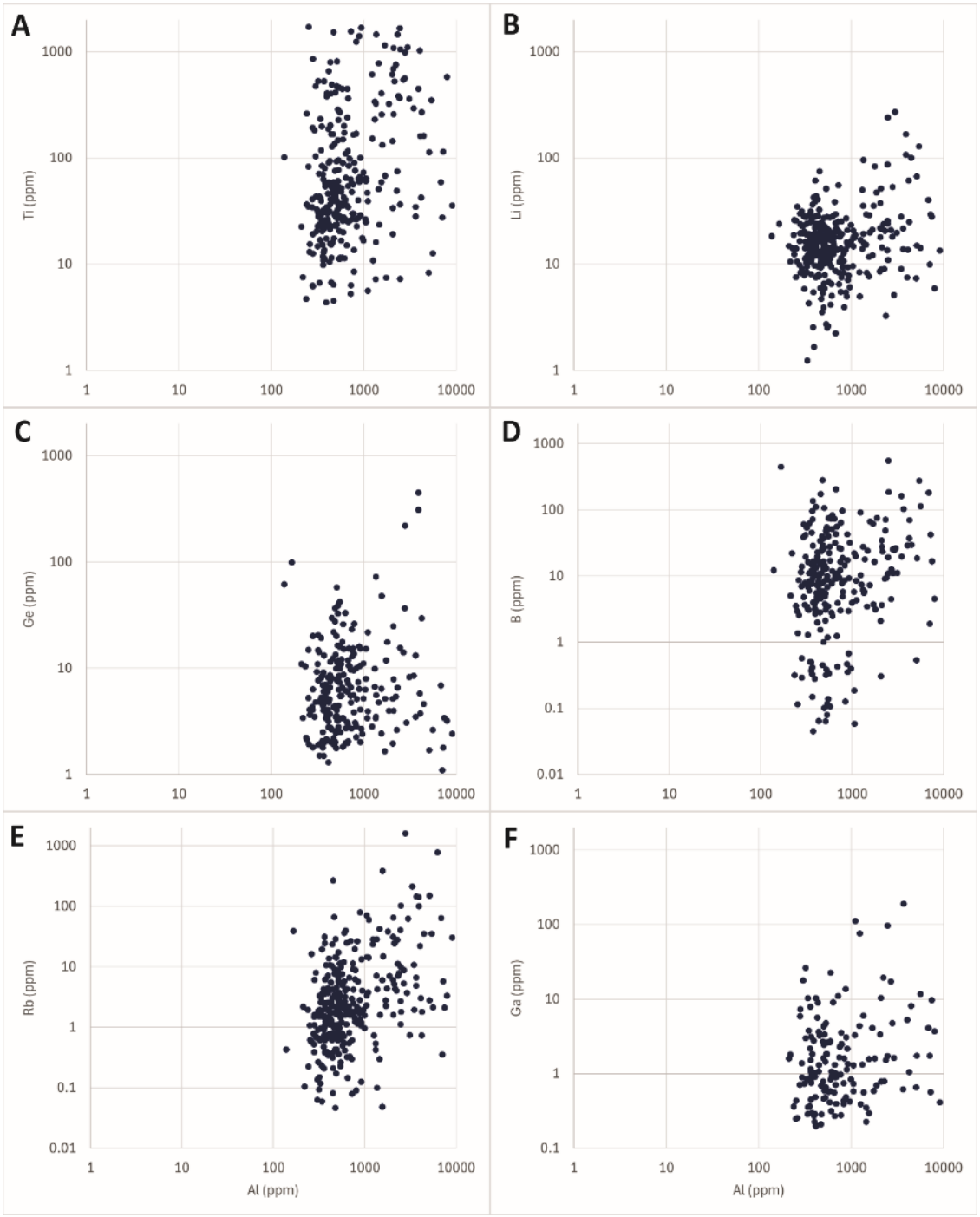
Appendix Figure 203: Bivariate plots for trace element concentrations from Mt. Antero quartz crystal LE25-5R-1B.7 (n=55). A) Al versus Ti; B) Al versus Li; C) Al versus Ge; D) Al versus B; E) Al versus Ga; F) Al versus Rb.



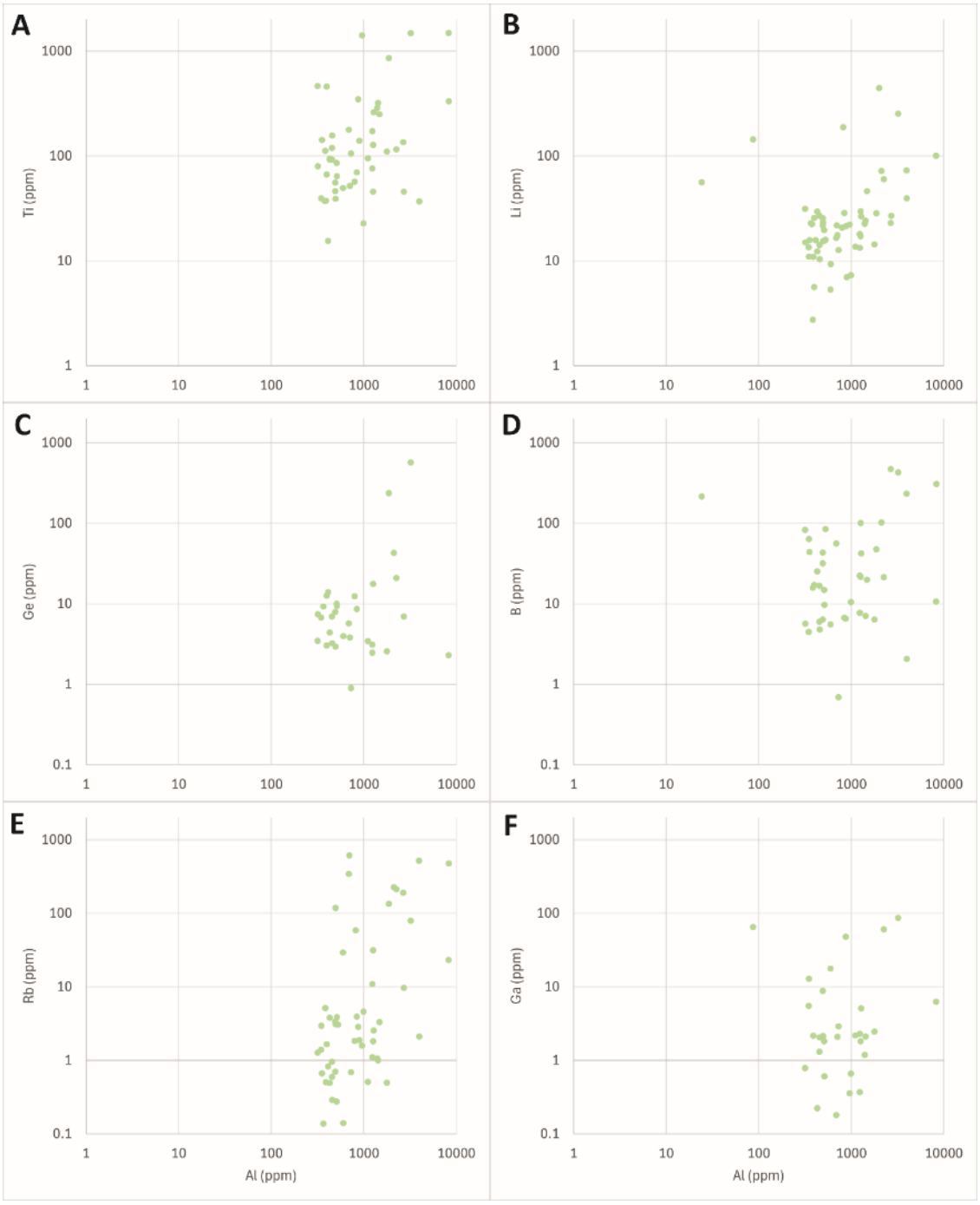
Appendix Figure 204: Bivariate plots for trace element concentrations from Mt. Antero quartz crystal LE25-6-1.19 (n=427). A) Al versus Ti; B) Al versus Li; C) Al versus Ge; D) Al versus B; E) Al versus Ga; F) Al versus Rb.



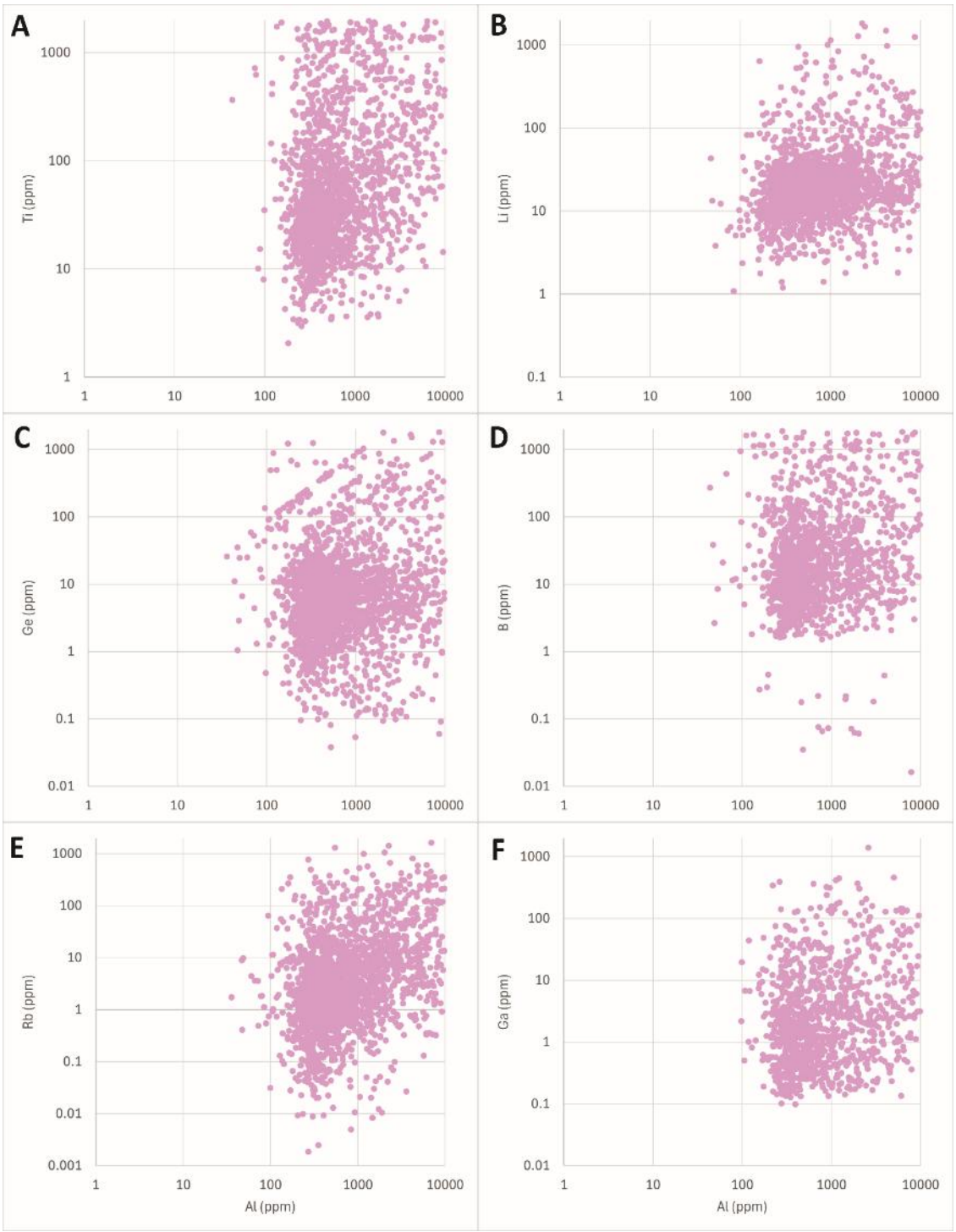
Appendix Figure 205: Bivariate plots for trace element concentrations from Mt. Antero quartz crystal LE25-6-2.3 (n=910). A) Al versus Ti; B) Al versus Li; C) Al versus Ge; D) Al versus B; E) Al versus Ga; F) Al versus Rb.



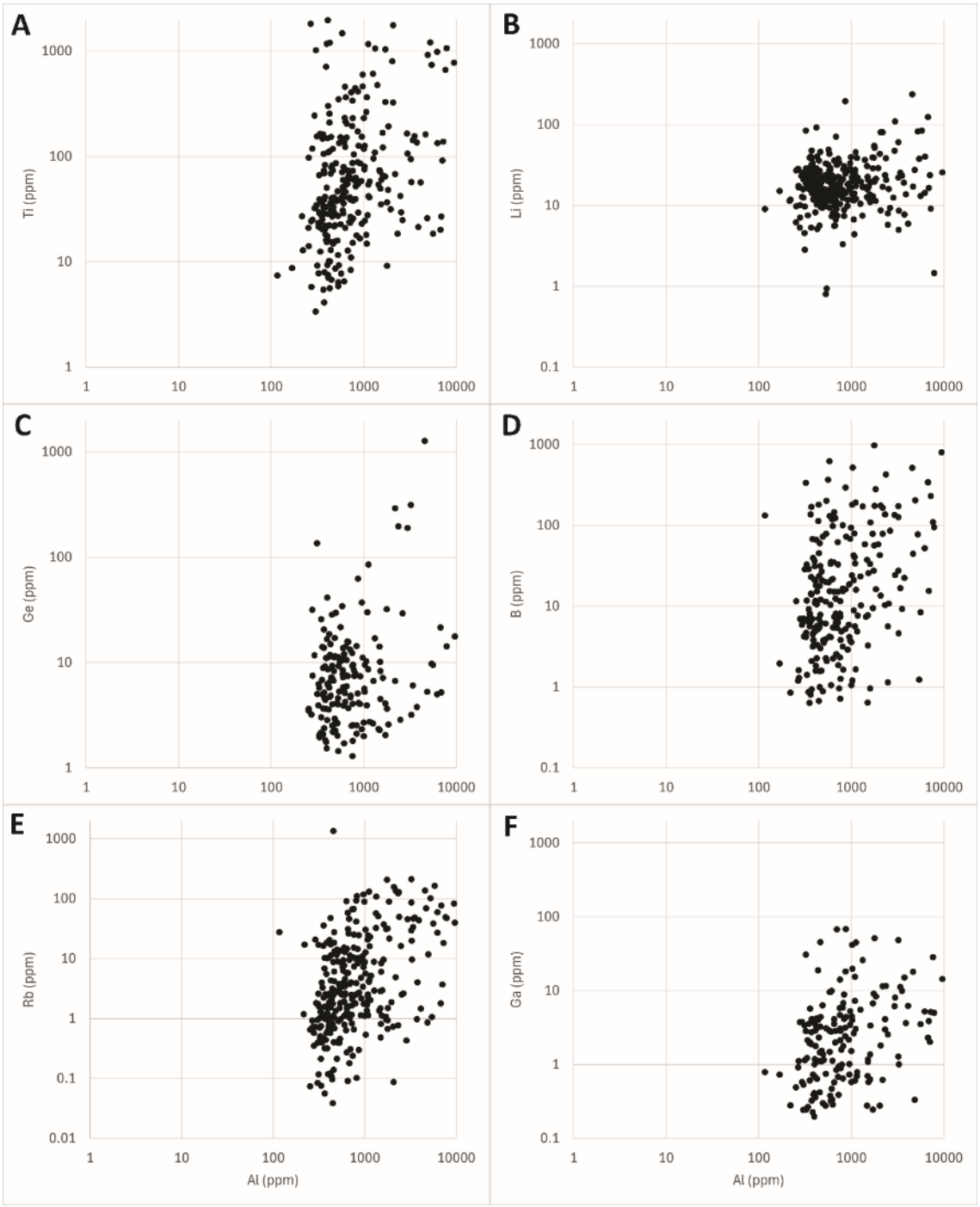
Appendix Figure 206: Bivariate plots for trace element concentrations from Mt. Antero quartz crystal LE25-7-1A.11 (n=345). A) Al versus Ti; B) Al versus Li; C) Al versus Ge; D) Al versus B; E) Al versus Ga; F) Al versus Rb.



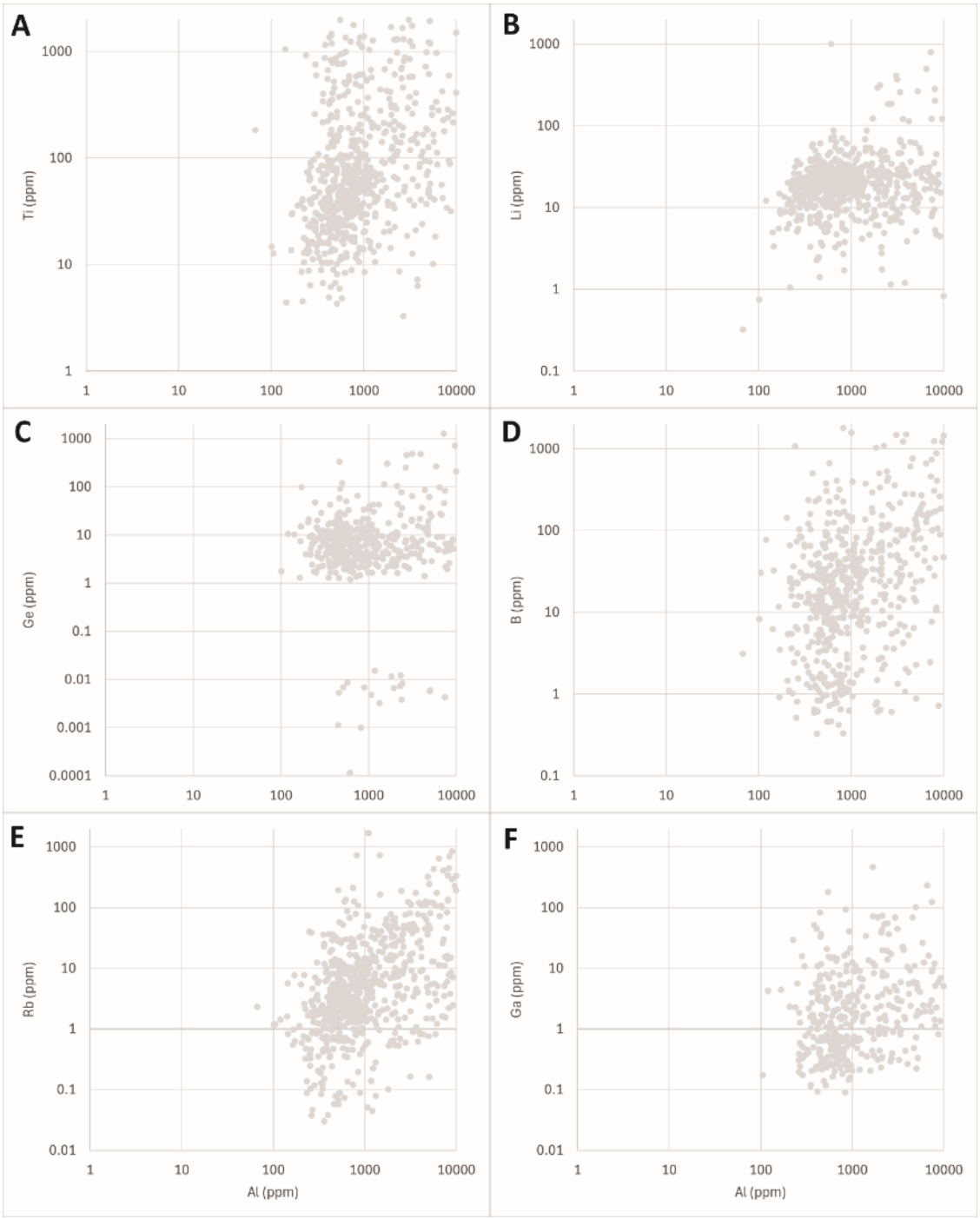
Appendix Figure 207: Bivariate plots for trace element concentrations from Mt. Antero quartz crystal LE25-7-1B.1 (n=67). A) Al versus Ti; B) Al versus Li; C) Al versus Ge; D) Al versus B; E) Al versus Ga; F) Al versus Rb.



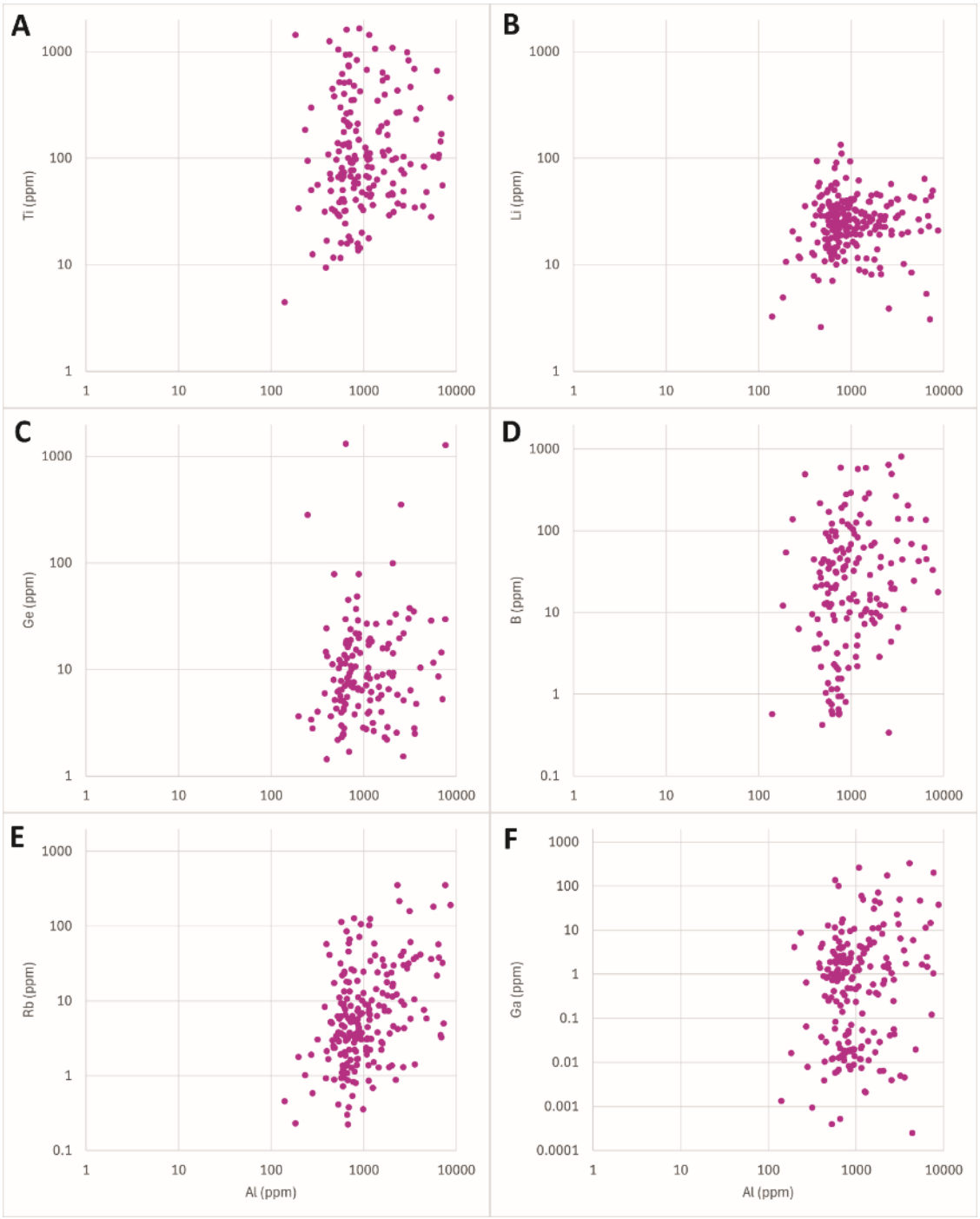
Appendix Figure 208: Bivariate plots for trace element concentrations from Mt. Antero quartz crystal LE25-7-2A.1 (n=2,755). A) Al versus Ti; B) Al versus Li; C) Al versus Ge; D) Al versus B; E) Al versus Ga; F) Al versus Rb.



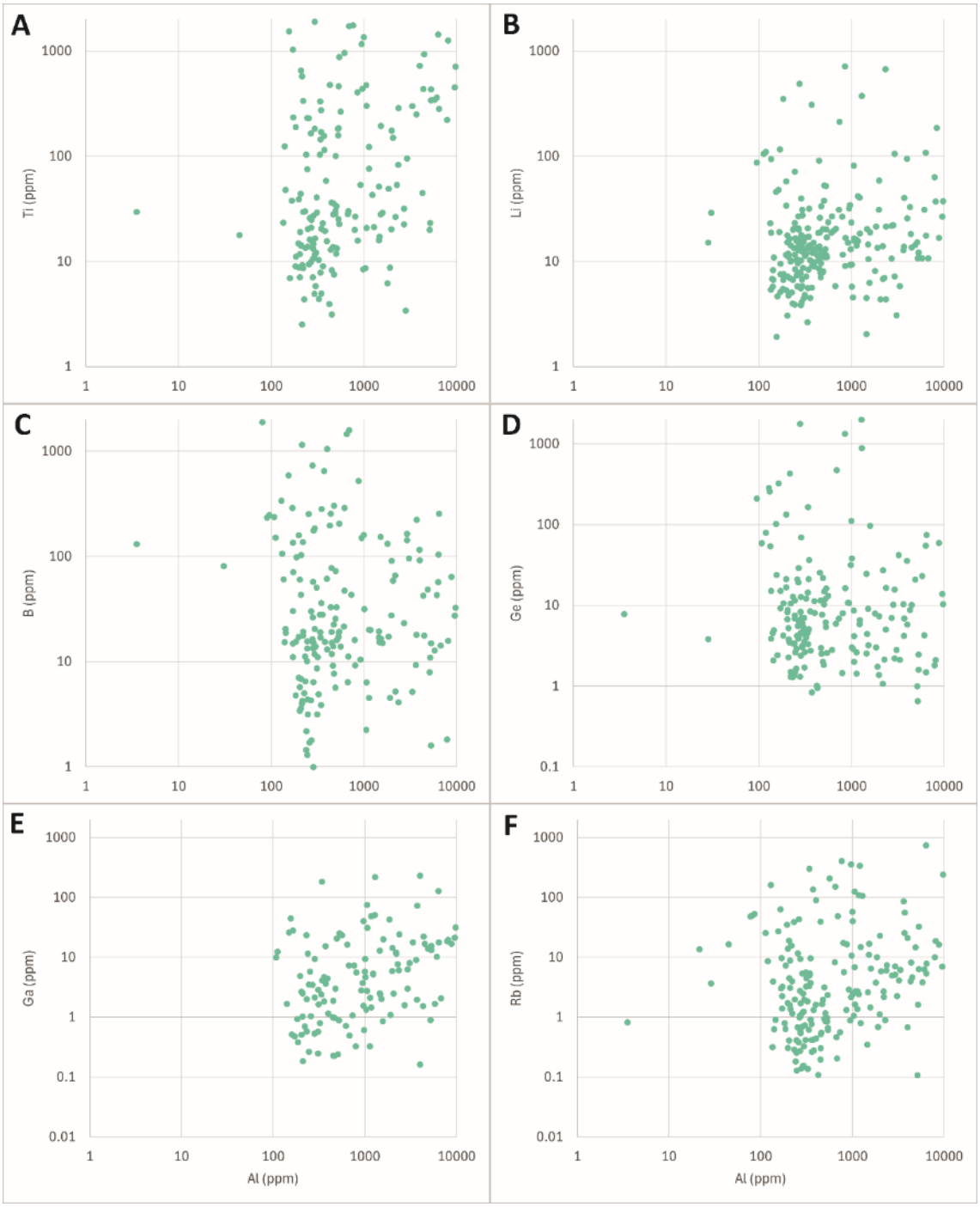
Appendix Figure 209: Bivariate plots for trace element concentrations from Mt. Antero quartz crystal LE25-7-2A.15 (n=340). A) Al versus Ti; B) Al versus Li; C) Al versus Ge; D) Al versus B; E) Al versus Ga; F) Al versus Rb.



Appendix Figure 210: Bivariate plots for trace element concentrations from Mt. Antero quartz crystal LE25-7-2B.1 (n=827). A) Al versus Ti; B) Al versus Li; C) Al versus Ge; D) Al versus B; E) Al versus Ga; F) Al versus Rb.



Appendix Figure 211: Bivariate plots for trace element concentrations from Mt. Antero quartz crystal LE25-7-2B.10 (n=249). A) Al versus Ti; B) Al versus Li; C) Al versus Ge; D) Al versus B; E) Al versus Ga; F) Al versus Rb.



Appendix Figure 212: Bivariate plots for trace element concentrations from Mt. Antero quartz crystal LE25-8-2.5 (n=337). A) Al versus Ti; B) Al versus Li; C) Al versus Ge; D) Al versus B; E) Al versus Ga; F) Al versus Rb.